

MITOCHONDRIAL FUNCTION DOES NOT LIMIT AEROBIC
METABOLISM IN TYPE 2 DIABETES: MAGNETIC RESONANCE
STUDIES IN THE GOTO-KAKIZAKI RAT

By

Matthew T. Lewis

A DISSERTATION

Submitted to
Michigan State University
in partial fulfillment of the requirements
for the degree of

Physiology – Doctor of Philosophy

2019

ABSTRACT

MITOCHONDRIAL FUNCTION DOES NOT LIMIT AEROBIC METABOLISM IN TYPE 2 DIABETES: MAGNETIC RESONANCE STUDIES IN THE GOTO-KAKIZAKI RAT

By

Matthew T. Lewis

Type 2 diabetes (T2D) is a growing health concern with nearly 400 million affected worldwide as of 2014 (418). T2D presents with hyperglycemia and insulin resistance resulting in increased risk for blindness, renal failure, nerve damage and premature death (10). Skeletal muscle is a major site for insulin resistance and is responsible for up to 80% of glucose uptake during euglycemic hyperinsulinemic clamps (89). Glucose uptake in skeletal muscle is driven by mitochondrial oxidative phosphorylation (MOP) and for this reason mitochondrial dysfunction has been implicated in T2D (225). Mitochondrial function in this sense is defined as the capacity for skeletal muscle mitochondria to produce ATP. In the present document, skeletal muscle mitochondrial function and its limitations were studied utilizing the Goto-Kakizaki (GK) rat model of type 2 diabetes. Mitochondrial function was defined computationally demonstrating the relationship between the drivers of ATP production (ADP, Pi) and ATP production itself. Computational depiction of MOP allowed for a functional understanding of any changes in mitochondrial function. Quantification of mitochondrial function demonstrated deficits during high metabolic workloads in the GK rat. However, upon closer analysis utilizing both computational and *in vitro* techniques results suggested that metabolic deficits were due to limitations separate from mitochondrial dysfunction. Since MOP ATP production requires oxygen utilization by the mitochondria and oxygen supply to the mitochondria, oxygen deficits may present in the same fashion as dysfunctional mitochondria and thus

the most logical explanation to target for dysregulation was a limitation in oxygen supply. For this reason, cardiovascular function was measured in the conscious GK rat utilizing an array of challenges. Results showed no deficits in skeletal muscle performance at low workloads consistent with measures of normal mitochondrial function. However, measures indicated a harder working heart along with cardiovascular disease risk factors that may cause blood flow limitations during high intensity workloads. Quantification of blood flow using the identical setup that measured mitochondrial function during hindlimb contraction showed reductions in blood flow that could limit MOP during high intensity workloads in the diabetic GK rat. Taken together this culmination of works suggests that mitochondrial dysfunction is not inherent to type 2 diabetes, but rather muscle metabolic deficits manifest from blunted oxygen supply. This result is crucial to advance therapeutic interventions in type 2 diabetes and similar experiments in humans may direct drug therapies away from targeting skeletal muscle mitochondria and towards improving skeletal muscle blood flow.

ACKNOWLEDGEMENTS

I would first like to thank my mentor, Dr. Robert Wiseman, for guiding me along my journey to a PhD. He has taught me countless things in science and life along the way especially with challenging me to question everything until I prove it to myself. I would also like to thank my lab members while at Michigan State including Dr. Jonathan Kasper and Dr. Anne Tonson that taught me a lot of the skills I've developed, were along my side for many experiments, and were good friends as well.

I would also like to thank members of my committee including Dr. Jason Bazil, Dr. Greg Fink, Dr. Ron Meyer, Dr. Karl Olson, and Dr. Jill Slade. Each of them helped guide me along the way and provided valuable insight into my project each from a unique perspective. Their doors were always open to not only chat about my thesis work but to offer advice in many aspects of life. I would also like to thank Dr. Steve DiCarlo and Dr. Heidi Lujan. I spent several months working on a part of this project with their help and learned many valuable lessons while interacting with each of them. They were always looking out for me and great sources of advice/motivation to not only be a better scientist but a better person. I would also like to thank Dr. Jeff Frisbee who was a close collaborator for several of our studies. Jeff's insight and contribution to our productivity was integral in furthering my understanding of vascular regulation and academic career and provided some much-needed humor along the way.

I would also like to thank my family including Mom, Dad, Mike, Amanda, Dr. Johnathan, Stephanie, Nicholas, Kelly, Daniel, and Grace. They have always been in my

corner and a strong supporting cast for my academic career, whether I kept them up to date on what I was actually doing or not, and I could not have done it without them. Last but not least, I would like to thank my wife Shelby and her family. She has been my biggest supporter and by my side since joining the Wiseman Lab. Shelby always found a way to keep me upbeat and moving forward along the way and I could not have done it without her.

TABLE OF CONTENTS

LIST OF TABLES	x
LIST OF FIGURES.....	xi
KEY TO ABBREVIATIONS	xviii
CHAPTER 1: QUANTIFICATION OF MITOCHONDRIAL OXIDATIVE PHOSPHORYLATION IN METABOLIC DISEASE: APPLICATION TO TYPE 2 DIABETES	1
1.1 DEFINITIONS.....	2
1.2 INTRODUCTION	5
1.3 MITOCHONDRIAL OXIDATIVE PHOSPHORYLATION (MOP)	6
1.3.1 Tricarboxylic Acid Cycle.....	8
1.3.2 Electron Transport System	9
1.4 MEASUREMENT OF MITOCHONDRIAL FUNCTION	11
1.4.1 Mitochondrial Function Quantified in vitro	12
1.4.2 Mitochondrial Function Quantified in vivo	15
1.5 OBESITY, PHYSICAL INACTIVITY AND MOP CAPACITY	18
1.5.1 Obesity effect on MOP capacity.....	19
1.5.2 Physical activity and MOP capacity	20
1.5.3 Summary	24
1.6 HUMAN TYPE 2 DIABETES MITOCHONDRIAL FUNCTION.....	24
1.6.1 Human type 2 diabetes mitochondrial function in vitro.....	25
1.6.2 Human type 2 diabetes mitochondrial function in vivo	27
1.6.3 What is missing?.....	29
1.7 RAT MODELS OF TYPE 2 DIABETES	29
1.7.1 Zucker Diabetic Fatty (ZDF) Rat	32
1.7.2 Goto-Kakizaki (GK) Rat	35
1.8 Summary	38
CHAPTER 2: RESEARCH AIMS AND HYPOTHESES.....	39
2.1 Research Goals.....	40
2.2 Central Hypothesis	41
2.3 Specific Aims	41
2.3.1 Define mitochondrial function computationally:.....	41
2.3.2 Quantify mitochondrial function within the Goto-Kakizaki rat model of type 2 diabetes:	41
2.3.3 Determine if blood flow delivery could limit mitochondrial respiration in the Goto-Kakizaki rat model of type 2 diabetes:.....	42

CHAPTER 3: TOP-DOWN MODELING OF ENERGY METABOLISM PREDICTS SUBSTRATE UTILIZATION IN SKELETAL MUSCLE MITOCHONDRIA	43
3.1 Summary	44
3.2 Introduction	45
3.3 Methods.....	47
3.3.1 Model Development	47
3.3.2 ³¹ Phosphorus Magnetic Resonance Spectroscopy (³¹ PMRS).....	53
3.3.3 Model Simulations.....	55
3.3.4 Altering relative energetic demand: in vivo	56
3.4 Results.....	56
3.4.1 Activation of PDH Predicts Reduced PCr Hydrolysis and Greater Reliance on Carbohydrates	57
3.4.2 Reducing Aerobic Capacity Predicts Increased Carbohydrate Oxidation.....	60
3.4.3 Model Sensitivity Analysis.....	68
3.4.4 Model Application to Prior Studies Explains Differences in Aerobic Capacity.....	70
3.5 Discussion	73
3.5.1 Computational simulations accurately predict ³¹ PMRS data	74
3.5.2 Substrate shift towards carbohydrate utilization improves muscle energetics	74
3.5.3 NADH feedback explains carbohydrate inhibition of fat oxidation ...	76
3.5.4 ADP + Pi feedback is dependent on muscle aerobic capacity	77
3.5.5 Summary	79

CHAPTER 4: SKELETAL MUSCLE ENERGETICS ARE COMPROMISED ONLY DURING HIGH INTENSITY CONTRACTIONS IN THE GOTO-KAKIZAKI RAT MODEL OF TYPE 2 DIABETES.....	81
4.1 Abstract	82
4.2 Introduction.....	83
4.3 Methods.....	86
4.3.1 Animals	86
4.3.2 Oral Glucose Tolerance Test	86
4.3.3 Phosphorus Magnetic Resonance Spectroscopy (³¹ PMRS)	87
4.3.4 Mitochondrial Content and Metabolite Quantification.....	89
4.3.5 High-Resolution Respirometry	89
4.3.6 Calculations	91
4.3.7 Statistics	92
4.4 Results.....	92
4.4.1 Animal Characteristics	92
4.4.2 Resting Metabolites, pH, Free Energy	94
4.4.3 Mitochondrial Function in vivo at High Intensity	95
4.4.4 Mitochondrial Content and Function in vitro	98

4.4.5 Mitochondrial Function in vivo at Low Intensity	101
4.4.6 Quantification of ATP Production and Free ADP	103
4.5 Discussion	105
4.5.1 Perspectives and Significance	111

CHAPTER 5: OBESITY AND INACTIVITY, NOT HYPERGLYCEMIA, CAUSE EXERCISE INTOLERANCE IN INDIVIDUALS WITH TYPE 2 DIABETES: SOLVING THE OBESITY AND INACTIVITY VERSUS HYPERGLYCEMIA CAUSALITY

DILEMMA	112
5.1 Abstract	113
5.2 Introduction: Background to the Hypothesis	114
5.2.1 Exercise intolerance associated with type 2 diabetes	114
5.2.2 Tests of exercise tolerance	114
5.2.3 An analysis of the literature	115
5.2.4 Solving the obesity and inactivity versus hyperglycemia causality dilemma; “Which came first: the chicken or the egg?”	117
5.2.5 Statement of the Hypothesis	117
5.3 Methods and Results	118
5.3.1 Animals	118
5.3.2 Activity levels of Wistar control and GK type 2 diabetic rats	118
5.3.3 Test of exercise tolerance: time to exhaustion at a fixed submaximal workload	119
5.4 Discussion: Significance of the Hypothesis	121

CHAPTER 6: THE HYPERTENSION ADVANTAGE AND NATURAL SELECTION: SINCE TYPE 2 DIABETES ASSOCIATES WITH CO-MORBIDITIES AND PREMATURE DEATH, WHY HAVE THE GENETIC VARIANTS REMAINED IN THE HUMAN GENOME?

125	
6.1 Abstract	126
6.2 Introduction: Background to the Hypothesis	127
6.2.1 Type 2 diabetes is destructive to health	127
6.2.2 The “thrifty genotype” and “carnivore connection” hypotheses	127
6.2.3 The hypertension hypothesis	128
6.2.4 Hypertension enhances exercise tolerance	129
6.2.5 Statement of the Hypothesis	132
6.3 Methods and Results	134
6.3.1 Animals	134
6.3.2 Advantage during hunting and gathering; test of exercise tolerance	134
6.3.3 Benefits of hypertension during exercise	135
6.3.4 Parasympathetic hyperactivity	137
6.3.5 Costs of hypertension during exercise	140

6.3.6 Additional negative consequences of the “hypertension advantage”	141
6.4 Discussion: Significance of the Hypothesis	144
6.4.1 Phenotypic similarities of the genetic GK type 2 diabetic rats and exercise training.....	144
6.4.2 Cardiac vagal activity is strongly associated with exercise capacity	146
6.4.3 Genetic determinants of cardiac vagal tone	147
6.4.4 Summary	148
CHAPTER 7: REDUCED SKELETAL MUSCLE BLOOD FLOW MEASURED BY MR ANGIOGRAPHY IN THE GOTO-KAKIZAKI RAT MODEL OF TYPE 2 DIABETES ..	149
7.1 Abstract	150
7.2 Introduction.....	151
7.3 Methods.....	153
7.3.1 Animals	153
7.3.2 Experimental Setup.....	154
7.3.3 T1 Flash Sequence.....	155
7.3.4 Phase Contrast Angiography	156
7.3.5 Data Analysis.....	158
7.3.6 Statistics	158
7.4 Results.....	159
7.4.1 Animal Characteristics	159
7.4.2 Muscle Performance	161
7.4.3 Blood Flow Response to Contractions	163
7.5 Discussion	166
7.5.1 Conclusions	171
CHAPTER 8: GENERAL SUMMARIES/CONCLUSIONS AND DISCUSSION	173
8.1 Summary	174
8.2 Future Applications.....	177
8.3 Final Conclusions	185
REFERENCES.....	187

LIST OF TABLES

Table 1. Underlying assumptions for using the PCr recovery time constant to infer mitochondrial function (283).....	17
Table 2. Summary of diabetic animal models re-summarized from Srinivasan et al. 2007	31
Table 3. Adjustable Model Parameters	49
Table 4. <i>Animal Characteristics describing Wistar and GK rats used in the present study</i>	93
Table 5. <i>Resting Metabolites, pH, Free Energy</i>	95
Table 6. <i>Muscle Twitch Characteristics</i>	97
Table 7. Animal characteristics describing Wistar control and diabetic GK rats used in the present study.....	159
Table 8. Muscle twitch performance	162
Table 9. Post-contractile Recovery	164

LIST OF FIGURES

Figure 1. Mitochondrial Oxidative Phosphorylation. Mitochondria produce reducing equivalents through the TCA cycle within the mitochondrial matrix. Reducing equivalents (NADH, FADH₂) contribute to the electron transport system at complex I and II, respectively. Donation of electrons provides the energy to pump protons to generate the proton motive force (pmf). This pmf is utilized by the F₁F₀ ATP synthase in the production of ATP which is translocated to the intermembrane space through the adenine nucleotide translocase (ANT). The proton pumping stoichiometries are given as “effective” protons per pair of electrons. Created with Biorender.com..... 7

Figure 2. Mitochondrial oxidative phosphorylation capacity is comprised of both number and function that can be measured in vivo or in vitro. Mitochondria within skeletal muscle measured in vivo can be measured via phosphorus magnetic resonance spectroscopy (³¹PMRS). ³¹PMRS infers function from measures of MOP capacity, that when paired with V_{MITO} quantitatively describes function. Mitochondrial function in vitro can be measured via high-resolution respirometry following isolation of the organelle from the tissue. Created with Biorender.com. 12

Figure 3. Role of inactivity on mitochondrial fractional volume adapted from Morrison et al. 1987. Rat quadriceps muscles were immobilized by cast for 7 days and mitochondrial fractional volume determined from cytochrome c content. Measures were taken from muscle samples before immobilization and at time points 0-, 0.25-, 2-, and 4-days following cast-removal..... 23

Figure 4. Summary of human mitochondrial (dys)function in diabetes. Data of reported mitochondrial (dys)function was compiled from the literature and presented relative to respective control subjects. Control (white circles) is always equal to 1 and diabetics (black triangles) presented as a fraction of that determined from the reported measures of function. This was determined for (A) in vitro and (B) in vivo studies where both deficits and no deficits in mitochondrial function have been reported. A) Kelley 2002; B) Mogensen 2007; C) Phielix 2008; D) Ritov 2005; E) Abdul-Ghani 2009; F) Boushel 2007; G) Hey-Mogensen 2010; H) Meex 2010; I) Scheuermann-Freestone 2003; J) Schrauwen-Hinderling 2007; K) De Feyter 2008; L) Praet 2006; M) van Tienen 2012. 25

Figure 5. Model schematic and representative PMRS data. A simplified representation of the skeletal muscle model diagram that incorporates separate carbohydrate (CARB) and fatty acid (FAT) contributions is shown (A). The model output for phosphocreatine (PCr) was used to compare with the skeletal muscle experimental studies. The model input is ATPase rate calculated from the initial PCr decline during twitch contractions in vivo. A representative stack plot of high energy phosphates in gastrocnemius muscle before, during, and after electrically stimulated twitch contractions at 0.5 Hz (B). During contraction PCr is hydrolyzed and [ATP] stays constant via the near equilibrium CK reaction. 52

Figure 6. DCA treatment increases PCr levels during twitch contractions by increasing carbohydrate oxidation. The model was used to simulate the experimental protocol for 0.35, 0.50, and 0.75 Hz twitch contractions. With the DCA treatment, the PCr level does not decline as much as the control condition (A). For these simulations, the ATPase rate was set to 0.095 mM/sec, 0.162 mM/sec, and 0.253 mM/sec for twitch frequencies of 0.35 Hz, 0.50 Hz, and 0.75 Hz, respectively. Data shown as +/- SD (n=6-7). As ATP demand increases, muscle switches its fuel source from fatty acids to carbohydrates (B). At approximately 60% J_{O_2} max, the oxygen consumption rates from fatty acids (red) and carbohydrates (blue) are nearly equal. Model simulations are represented as lines and data are given as symbols (175). The model predicts that DCA treatment (dashed lines) shifts the crossover point to approximately 30% J_{O_2} max. Carbohydrate J_{O_2} was computed from Eq. 3 and assuming 5/2 O_2 consumed per reducing equivalents generated. Fatty acid J_{O_2} was computed from Eq. 4 and assuming 6/2 O_2 consumed per reducing equivalents generated. Substrate specific oxygen consumption at a given total ATP demand shifts from control (solid lines), in DCA, and 4-week treated MMI (dotted lines) conditions (C). ATP demand is represented as total tissue oxygen consumption rate. DCA treatment causes carbohydrate flux to increase and fatty acid flux to decrease at any given ATP demand. This leads to the crossover point shifting to the left. MMI treatment cuts the maximum tissue oxygen consumption rate in half and causes the crossover point to shift further to the left. 59

Figure 7. Model predictions of PCr dynamics in 4-week MMI treated muscle (A). Stimulation frequencies greater than 0.50 Hz exceed the aerobic capacity and leads to a significant ATP contribution by glycolysis. The muscle also begins to fatigue. Thus, the model results for the 0.75 Hz condition are expected as it does not include glycolysis or fatigue. Model predictions of the ATP hydrolysis products Pi (B) and ADP (C) dynamics match the increase observed during twitch contractions. As explained in Panel A, the model simulations for the 0.75 Hz condition are expected due to the absence of fatigue and glycolysis. Data shown as +/- SD (n=6-7). 63

Figure 8. Model prediction of carbohydrate (A) and fatty acid (B) fluxes for control (blue), DCA (red), and 4-week MMI treated (yellow) conditions at the different twitch stimulation frequencies. DCA treatment causes an increase in carbohydrate flux which in turn suppresses fatty acid oxidation rates relative to the control. In contrast, MMI treatment causes an increase in both carbohydrate and fatty acid oxidation rates relative to control. However, as ATP hydrolysis products accumulate during the twitch contractions, fatty acid metabolism is decreased due to accumulation of mitochondrial NADH. Mitochondrial NADH dynamics during twitch contractions reveal complex dynamics (C). Control and DCA treated mitochondria burn oxygen at the same rate for a given stimulation frequency (D); however, MMI treated mitochondria increase their respiratory activity per mitochondrion to compensate for the lower mitochondrial content. 65

Figure 9. Cytoplasmic ADP concentrations needed to match ATP demand are a function of Pi and mitochondrial function. 3D plot of steady-state ADP and Pi concentrations for a given rate of oxidative phosphorylation for the control, DCA, and 4-

week treated MMI conditions (A). Grey lines are 2D projections of the 3D plot on each axis. Mitochondrial volume fraction is the most sensitive parameter with respect to PCr dynamics calculated at 0.5 Hz stimulation frequency (B). DCA treatment decreases the importance of the volume fraction due to an increase in intrinsic metabolic activity per mitochondrion. However, the volume fraction is extremely important in the MMI condition as this stimulation frequency exceeds the aerobic capacity for this treatment. Local sensitivities computed with respect to PCr dynamics of carbohydrate (C) and fatty acid (D) related kinetic parameters elucidates the mechanism responsible for substrate selection in exercising muscle for the 0.5 Hz stimulation frequency. Carbohydrate metabolism is more important than fatty acid metabolism during ATP demand. In contrast, fatty acid metabolism is important for energy metabolism at rest. DCA treatment decreases the reliance on fatty acid metabolism, while all pathways become critical to sustain energy metabolism after MMI treatment. The sensitivity coefficient trends are similar for 0.35 Hz and 0.75 Hz stimulation frequencies. 67

Figure 10. Model simulations of PCr recovery time constant (τ) as a function of mitochondrial content. Model simulations were compared to the stepwise change in mitochondrial content (A), as well as, literature data for both rats (circles) and humans (squares) (B). Data that fall far below the line depict metabolic limitations (e.g., oxygen). This is explicitly shown by PAD patient data. With vascular therapy (PAD-T), the PCr recovery time constant decreases resulting in an upward shift relative to the PAD control. Values are means \pm SE. 72

Figure 11. Mean \pm SE blood glucose measures following OGTT at 2 g/kg glucose/body weight in Wistar (white circles, n=3) and GK (black triangles, n=5) rats at 0, 5, 15, 30, 60, 90, and 120 minutes following gavage (Panel A) and the resultant area under the curve (AUC) during testing (Panel B). Blood glucose was significantly higher in GK rats at every time point measured ($*=p<0.001$ Tukey test). AUC was significantly increased in GK rats ($*=p<0.001$ two-tailed t-test). Dashed lines indicate one or more measures were beyond limit of detection and capped at 600 mg/dL. 94

Figure 12. Representative ^{31}P MRS spectra and 10 second sample of force recording for Wistar control (Panels A and C) and diabetic GK rats (Panels B and D) during 1 Hz stimulation in gastrocnemius muscle. 96

Figure 13. Mean \pm SE values for phosphocreatine (PCr) during rest, contraction, and recovery at 2 (Panel A) and 4 Hz (Panel B) intensities of stimulation for GK (black triangles, n=7) and Wistar controls (WC, white circles, n=8). 98

Figure 14. Mean \pm SE measures of mitochondrial function *in vitro* including mitochondrial content (Panel A), respiration during leak state (Panel B), respiration during maximal ADP-stimulated state (Panel C), and respiratory control ratio (Panel D). No difference was seen between GK (black bars, n=7) and Wistar controls (white bars, n=8) in mitochondrial content in white (WG) nor red (RG) gastrocnemius muscle (Panel A). Mitochondrial respiratory capacity (Panels B-D) was not different using pyruvate and

malate (PM) as substrate but increased when using palmitoyl-carnitine and malate (PCM) in GK (n=5) versus Wistar controls (n=5). (*= $p \leq 0.01$ two-tailed t-test). 100

Figure 15. Representative oxygen consumption rates for Wistar control (WC) and GK rats while respiring in the presence of pyruvate and L-malate (P + M, Panel A) or palmitoyl-carnitine and L-malate (PC + M, Panel B). Leak state (LS) was measured during the steady-state before ADP stimulation while maximal ADP-stimulated state (ADP) was measured by averaging over the peak designated by the shaded boxes. AUC (P:O ratio) were not different between groups for either P + M or PC + M. 101

Figure 16. Mean \pm SE values for phosphocreatine (PCr) during rest, contraction, and recovery at 0.25 (Panel A), 0.5 (Panel B), 0.75 (Panel C), and 1 Hz (Panel D) intensities of stimulation for GK (black triangles, n=7) and Wistar controls (WC, white circles, n=8). 102

Figure 17. Markers of mitochondrial function measured *in vivo* by ^{31}P PMRS presented by mean \pm SE phosphocreatine (PCr) level as a percent of initial at energetic steady-state for Wistar control (white bars, n=8) and GK rats (black bars, n=7) during stimulation at 0.25, 0.5, 0.75, 1, and 2 Hz (Panel A) and PCr recovery time constant following stimulation below 1 Hz (Panel B). Since no energetic steady-state was achieved at 4 Hz it was not included. Significantly more PCr was hydrolyzed at 2 Hz (*= $p < 0.02$ two tailed t-test) in the GK rat but no difference for 0.25 – 1 Hz nor PCr recovery time constant. 103

Figure 18. Mean \pm SE ATP hydrolysis rate (J_{ATPase} , Panel A), glycolytic ATP production rate (J_{GLY} , Panel B), and mitochondrial oxidative phosphorylation ATP production rate (J_{MOP} , Panel C) during stimulation intensities of 0.25, 0.5, 0.75, 1 and 2 Hz for Wistar control (WC, white circles, n=8) and GK (black triangles, n=7) rats. Linear regressions are depicted for each relationship from 0.25 - 1 Hz and in Panels B and C 2 Hz did not fall on the regression line since contractions could no longer be sustained aerobically. No difference was seen for any source of ATP production between WC and GK rats. 104

Figure 19. Mean \pm SE concentrations of phosphocreatine (PCr) versus inorganic phosphate (Pi) in Wistar control (WC, white circles, n=8) and GK (black triangles, n=7) rats during energetic steady-states at stimulation frequencies of 0.25, 0.5, 0.75, 1 and 2 Hz (Panel A). Stoichiometric changes were demonstrated by a slope of -1.06 and R^2 value of 0.99 indicating no changes in the phosphate pool size. J_{MOP} versus ADP (apparent ADP sensitivity, Panel B) indicated a rightward shift with more ADP present for a given MOP at 0.75 and 1 Hz stimulation frequencies. 2 Hz stimulation frequency was not included in apparent ADP sensitivity since the muscle fatigued. (*= $p < 0.05$ two-tailed t-test). 106

Figure 20. Day/night activity counts averaged over 8 consecutive days. No difference was observed in locomotor activity between GK and Wistar control rats. Values are mean \pm SE, (* $P < 0.05$, two-tailed t-test). 119

Figure 21. Submaximal workload performance as determined by time to exhaustion (A), distance to exhaustion (B), vertical work performed per gram muscle mass (C), and absolute vertical work performed (D). Values represent Mean \pm SE. GK rats ran significantly longer and farther and performed more vertical work per gram muscle mass. (*P<0.05, two-tailed t-test). 120

Figure 22. Day/night systolic and diastolic arterial pressure (A) and pulse pressure (B) averaged over 8 consecutive days. GK systolic pressure and pulse pressure were significantly higher than Wistar controls during both day and night while no difference was seen in diastolic pressure. Values are mean \pm SE, (*P<0.05, two-tailed t-test). .. 123

Figure 23. Schematic representation of the presented hypothesis. Insulin resistance directly stimulates sympathetic hyperactivity, resulting in cardiovascular adaptations that are consistent with and contribute to increased exercise tolerance..... 133

Figure 24. Voluntary treadmill running performance presented as time to exhaustion (A), distance to exhaustion (B), vertical work performed per gram muscle mass (C), and absolute vertical work performed (D). Values represent Mean \pm SE. Genetic GK type 2 diabetic rats ran significantly longer and farther and performed more vertical work per gram muscle mass. (*P<0.05, two-tailed t-test)..... 135

Figure 25. Mean \pm SE mean arterial pressure (A), heart rate (B), triceps surae blood flow (C), and triceps surae vascular resistance (D) for Wistar and GK rats during running to exhaustion. MAP, HR, and triceps surae blood flow were each significantly higher in GK rats while triceps surae vascular resistance was significantly reduced. [*P<0.05, one-tailed t-test (A,B); two-tailed t-test (C,D)]...... 137

Figure 26. Mean \pm SE mean arterial pressure (A), heart rate (B), triceps surae blood flow (C), and triceps surae vascular resistance (D) during rest and graded exercise at 5, 10, and 15 m/min. Arterial pressure was increased in GK rats and heart rate showed a group x treadmill speed interaction (*P<0.05, group difference two-way repeated measures ANOVA; #P<0.05, group x treadmill speed interaction two-way repeated measures ANOVA)..... 138

Figure 27. Markers for vagal activity: Mean \pm SE resting parasympathetic tonus (A) and heart rate recovery (HRR) following exercise to exhaustion (B). Parasympathetic tonus was significantly elevated in GK rats compared to controls and HRR was significantly faster when measured at approximately 20 seconds and 3 minutes after exercise (*P<.05, one-tailed t-test). 139

Figure 28. Mean \pm SE rate pressure product for Wistar and GK rats. Rate pressure product was significantly elevated in GK rats during running to exhaustion (A) and graded exercise (B) but not different during stress test (C) (P=0.34). (*P<0.05, two-tailed t-test). 141

Figure 29. Mean \pm SE mean arterial pressure (A) and heart rate (B) for Wistar and genetic GK type 2 diabetic rats at rest and during restrainer stress challenge. Mean arterial pressure was significantly higher in GK rats (* $P < 0.05$, two-way repeated measures ANOVA)..... 142

Figure 30. Experimental Setup. A) T1 image demonstrating the tungsten pin passing through the head of the tibial bone. B) Rat leg fixed in place with knee posts and custom force transducer to permit measure of muscle function at Lo. 155

Figure 31. Representative images for the popliteal vessel angiogram and velocity map. A,B) High resolution time of flight images for Wistar control (WC) and Goto-Kakizaki (GK) rats depicting where the imaging acquisition plane (green rectangle) was placed for the velocity map (C,D) used for flow analysis. 157

Figure 32. Representative muscle cross-sectional areas (CSA) and muscle twitch force production. A,B) T1 Images for Wistar control (WC) and Goto-Kakizaki rat hindlimb and (C,D) respective force traces per cross sectional area..... 160

Figure 33. Muscle cross-sectional area demonstrated a direct relationship to muscle mass. Each individual rat was plotted for its respective muscle mass and cross-sectional area for the triceps surae muscle group alone (two left clusters) and entire hindlimb (two right clusters) and fit to a line of regression..... 160

Figure 34. Mean \pm SE muscle blood flow responses during and following contraction. Wistar controls (WC, white circles) demonstrated elevated blood flow compared to Goto-Kakizaki rats (GK, black triangles) during every contraction tested..... 163

Figure 35. Mean \pm SE maximal blood flow and total blood flow delivered during and post contraction. Maximal blood flow was higher in the Wistar controls (WC, white bars) versus Goto-Kakizaki (GK, black bars) rats for every stimulation intensity both during contraction (A) and immediately post-contraction (B). This coincided with increased total blood flow delivered (C). * $p < 0.05$ 165

Figure 36. Total flow delivered per work performed. Total flow was reduced in the GK rat for every metabolic demand tested. Lines of regression were fit from 0.25 – 1 Hz since 2 and 4 Hz were nonlinear due to muscle fatigue. This was expected since blood flow response is more closely related to metabolic demand than mechanical contraction (126) and metabolic demand declines during fatigue. Values are presented as Mean \pm SE. 166

Figure 37. Theoretical description of the critical point for limitations to mitochondrial respiration. Modified from Connett et al. (71) this qualitatively shows the limitations to mitochondrial respiration. The green “saturated” zone represents where oxygen is in excess and reductions at low workloads will not affect mitochondrial function. If oxygen supply is decreased into the “metabolic phenotype” zone, mitochondrial respiration will not decline but at the expense of increased oxygen extraction and decreased

phosphate potential. Finally, in the extreme or “O₂ limited” zone, oxygen supply will limit mitochondrial respiration and result in a first-order dependence on oxygen that could be misinterpreted as mitochondrial dysfunction. 179

Figure 38. The critical point that limits muscle aerobic respiration varies between metabolic conditions. Within the control condition, oxygen is not limiting until the aerobic capacity is nearly reached and glycolysis affects measures of MOP capacity inherent to mitochondrial function. As cardiovascular disease (CVD) develops such as in the GK rat presented herein, oxygen supply to muscle is reduced and results in a metabolic phenotype (reduced phosphate potential) at lower workloads that may develop into complete oxygen limitations in severe CVD. For simplicity here, severe CVD includes any disease presenting poor oxygen delivery including PAD, heart failure, COPD, and others. In contrast, exercise training increases mitochondrial fractional volume as well as oxygen delivering capacity and thus falls within a zone where oxygen saturation persists at higher workloads. 182

Figure 39. Experimental design measuring blood flow delivery and phosphorus energetics concurrently. As contractile intensity increases, blood flow to the muscle increases (A-C) and more PCr is hydrolyzed (D-F). 186

KEY TO ABBREVIATIONS

ATP – Adenosine triphosphate

PCr – Phosphocreatine

Pi – Inorganic Phosphate

CK – Creatine Kinase

³¹PMRS – Phosphorus magnetic resonance spectroscopy

ADP – Adenosine diphosphate

ΔG_{ATP} – Free energy of ATP hydrolysis

SERCA – Sarcoplasmic endoplasmic reticulum calcium ATPase

TCA – Tricarboxylic acid cycle

ETS – Electron transport system

MOP – Mitochondrial oxidative phosphorylation

Pmf – Proton motive force

ANT – Adenine nucleotide translocase

$\dot{Q}O_2$ – Oxygen delivery/supply

$\dot{V}O_2$ – Oxygen consumption rate

$\dot{V}O_{2Max}$ – Maximal oxygen consumption rate

NO – Nitric Oxide

WC – Wistar control

GK – Goto-Kakizaki

T2D – Type 2 diabetes

OGTT – Oral glucose tolerance test

**CHAPTER 1: QUANTIFICATION OF MITOCHONDRIAL OXIDATIVE
PHOSPHORYLATION IN METABOLIC DISEASE: APPLICATION TO
TYPE 2 DIABETES**

1.1 DEFINITIONS

A brief list of specific definitions is provided for clarity in conceptual aspects of this chapter. They are to be used in place of other meanings that may have several less stringent descriptions within the literature.

- Mitochondrial Respiratory Capacity (f_{MITO}) – *functional capacity inherent to the organelle. Equivalent to mitochondrial function.*
- Mitochondrial Function – *Mitochondrial function is the ability for mitochondria to sense and match the ATP demand (410). Increased function therefore means increased ATP production capacity per organelle and conversely decreased function means decreased ATP production capacity per organelle.*
- Mitochondrial Fractional Volume (V_{MITO}) – *An indicator for the amount of mitochondria within a tissue. V_{MITO} is the amount of volume mitochondria hold relative to the volume of the cell. This definition does not discriminate between hypotheses on mitochondrial networks or individual organelles. This measure is derived from estimates of mitochondrial protein, respiratory enzyme activity, and other biochemical determinations [see Larson et al. (210)]*

- Muscle Mitochondrial Oxidative Phosphorylation Capacity (MOP Capacity) –
Absolute capacity for muscle to produce ATP aerobically. This is a function of the V_{MITO} and f_{MITO} :

$$MOP\ capacity = V_{MITO} \times f_{MITO}$$

MOP capacity is often what is measured in vivo in whole tissue.

- Fasting Blood Glucose (FBG) – *Refers to 12-h fasting conditions.*
- Oral Glucose Tolerance Test (OGTT) – A large bolus of glucose is given and glucose regulation is determined from changes in plasma glucose with greater increases reflecting worsened glucose regulation.
- Insulin Clamp Techniques – Insulin clamps permit controlled infusion rates of varying levels of glucose or insulin to determine the body's ability to respond to changes in glucose or insulin and quantify glucose tolerance and insulin resistance.
- Nicotinamide adenine dinucleotide - *reduced form, NADH; oxidized form NAD⁺*
- Flavin adenine dinucleotide - *reduced form, FADH₂; oxidized form FAD*

- Phosphate potential – Defined by the free energy of ATP hydrolysis (ΔG_{ATP}) at 37°C, pH 7.0. Its magnitude increases further from equilibrium when the $\frac{[ADP][Pi]}{[ATP]}$ ratio decreases:

$$\Delta G_{ATP} = \Delta G_{ATP}^{\circ} + 2.58 \times \ln \left(\frac{[ADP][Pi]}{[ATP]} \right)$$

The more negative the ΔG_{ATP} (kJ/mol) the greater the phosphate potential and in healthy muscle cells at rest ranges from about -64 to -68 kJ/mol at rest and decreases with intense exercise but not below -48 kJ/mol where the energy required for calcium pumping by the sarcoplasmic reticulum can no longer be met resulting in fatigue (256).

- Redox potential – Determined from the reduction status of the pyridine pool the redox potential describes the energy contributed to the proton motive force from NADH oxidation at 37°C, pH 7.0:

$$\Delta G_{REDOX} = \Delta G_{REDOX}^{\circ} + 2.58 \times \ln \left(\frac{[NAD^+]}{[NADH]} \right)$$

The more negative ΔG_{REDOX} , the greater the redox potential and this value ranges from roughly -210 to -230 kJ/mol when near full oxidation or full reduction respectively. Note that up to three ATP are produced from the oxidation of one NADH molecule when optimally coupled.

1.2 INTRODUCTION

Metabolic diseases present with deficient handling of glucose and lipids and developing comorbidities that ultimately lead to premature death (111). The most common and well-studied example of metabolic disease is type 2 diabetes (T2D) which is a growing epidemic with 30.3 million patients in the US in 2015 (54) and is expected to exceed 54 million by 2030 (332). Type 2 diabetes is characterized by increased blood glucose, resistance to insulin action, and beta cell failure (10). This ultimately results in reduced net glucose disposal and increased risk for cardiovascular disease, blindness, renal failure, nerve damage, loss of limb, and other co-morbidities (46, 201). Exercise intolerance, defined as a susceptibility to fatigue or reduced exercise capacity ($\dot{V}O_{2\text{Max}}$), has also been a disputed co-morbidity of this disease (97, 152, 221, 296, 313, 314, 350, 388). Skeletal muscle accounts for ~80% of glucose uptake during an insulin clamp (89) and can increase from resting levels anywhere from 20-fold [~ 0.25 mM/min \rightarrow ~ 4 mM/min single leg (389)] to 50-fold (336) during exercise (320, 389, 395). This dynamic range for insulin-dependent and insulin-independent glucose uptake (137, 148, 320) has resulted in exercise therapies being touted as the most effective treatment strategies to combat the disease (152, 186, 217, 258, 362) and as a consequence skeletal muscle is a primary target in diabetic research.

Skeletal muscle mitochondria oxidize carbohydrates to support ATP production and fuel contracting muscle and as a consequence glucose uptake is largely driven by mitochondrial ATP production (253, 256, 410). Exercise training improves skeletal muscle MOP capacity (102, 147) with a concomitant increase in glucose tolerance (247). Meex and colleagues reported a reduction in MOP capacity in diabetic subjects compared with

healthy controls using phosphorus magnetic resonance spectroscopy ($^{31}\text{PMRS}$). Following a 12-week exercise training regimen, MOP capacity was restored, *and* glucose tolerance improved. The close association of MOP capacity and glucose tolerance has resulted in a glut of hypotheses involving mitochondrial dysfunction in the development of type 2 diabetes.

Skeletal muscle mitochondrial dysfunction in type 2 diabetes was suggested by Kelley and colleagues in 2002 after reporting reduced electron transport chain activity measured from NADH:O₂ oxidoreductase (179). This study also reported a reduction in mitochondrial fractional volume measured from electron microscopy and citrate synthase activity. Several years later Shulman (2005) expounded upon the observations of Kelley and other investigators arguing that mitochondrial dysfunction was not only present in type 2 diabetes, but a major contributor to the development of insulin resistance (225). Mitochondrial dysfunction in type 2 diabetes has gained widespread support since 2002 despite contradictory reports. This review summarizes the body of literature for both human and animal models and attempts a balanced summation of mitochondrial (dys)function in type 2 diabetes.

1.3 MITOCHONDRIAL OXIDATIVE PHOSPHORYLATION (MOP)

The primary function of mitochondria is to provide the cell with ATP. While this organelle plays other roles that may contribute to cell survival [e.g. ROS signaling, calcium toxicity, apoptosis, etc. (44)], here only ATP production is used to define function as a conceptual simplification. Mitochondria fuel oxidative phosphorylation by consuming

oxygen at cytochrome c oxidase (complex IV). This is a complex process that begins with fuel conversion by the tricarboxylic acid (TCA) cycle to NADH and FADH₂ to be used by the electron transport system (ETS) ultimately generating ATP (Figure 1) [for detailed description see Bioenergetics by Nicholls and Ferguson (276)].

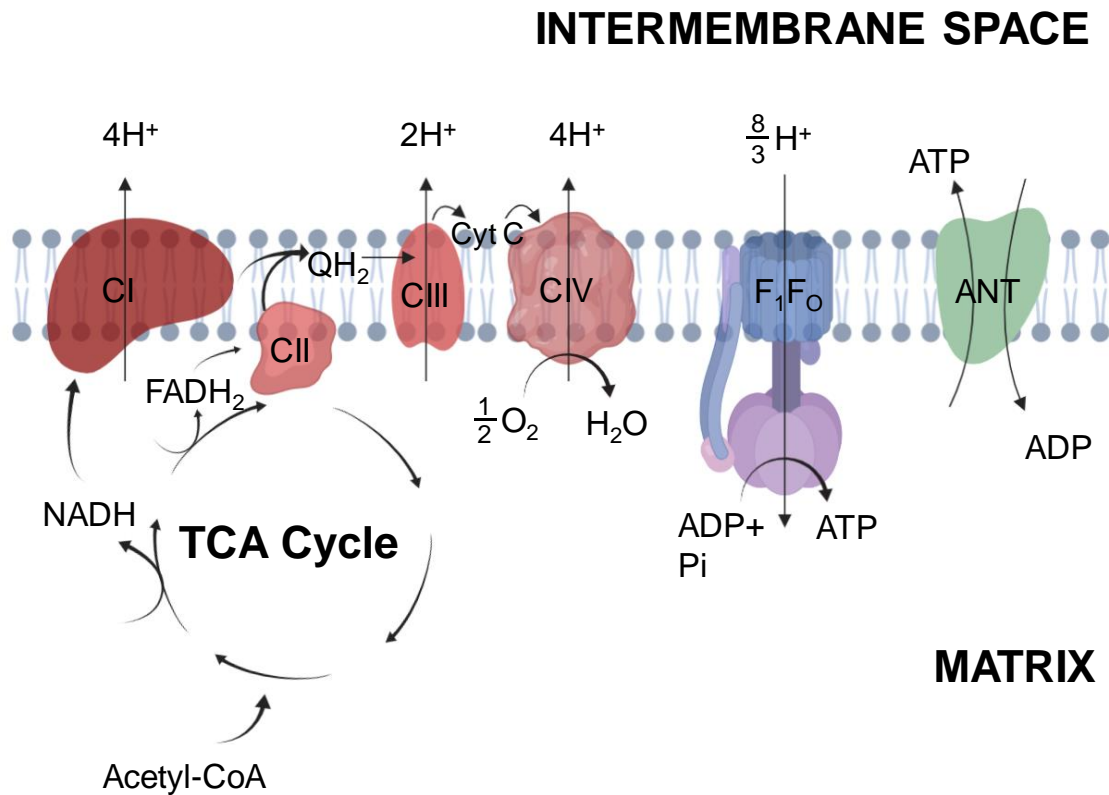


Figure 1. Mitochondrial Oxidative Phosphorylation. Mitochondria produce reducing equivalents through the TCA cycle within the mitochondrial matrix. Reducing equivalents (NADH, FADH₂) contribute to the electron transport system at complex I and II, respectively. Donation of electrons provides the energy to pump protons to generate the proton motive force (pmf). This pmf is utilized by the F₁F₀ ATP synthase in the production of ATP which is translocated to the intermembrane space through the adenine nucleotide translocase (ANT). The proton pumping stoichiometries are given as “effective” protons per pair of electrons. Created with Biorender.com.

1.3.1 Tricarboxylic Acid Cycle

The TCA cycle resides within the mitochondrial matrix and produces reducing equivalents for the ETS. Although the TCA cycle is complex, for brevity it will be described only in the production of reducing equivalents to permit ATP production and evaluate mitochondrial function (Figure 1). Composed of 9 enzymes, the cycle begins with citrate synthase catalyzing the condensation of acetyl-CoA with oxaloacetate and water to produce citrate. Acetyl-CoA is introduced from carbohydrate or fatty acid oxidation from pyruvate dehydrogenase (PDH) or 3-Ketoacyl-CoA thiolase reactions, respectively. Within the cycle these biochemical reactions produce reducing equivalents including NADH and FADH₂ for the use at complex I (CI) or complex II (CII) to produce ubiquinol. During the cycle three NAD⁺ are reduced to NADH; one each by isocitrate dehydrogenase, alpha-ketoglutarate dehydrogenase, and malate dehydrogenase and one FAD⁺ is utilized by succinate dehydrogenase to produce FADH₂ and subsequent QH₂. Oxidation of carbohydrates produces an extra NADH from the PDH reaction and fatty acid oxidation produces an additional NADH *and* FADH₂ from the 3-hydroxyacyl-CoA dehydrogenase reaction and Acyl-CoA dehydrogenase, respectively. This results in a total of 4:1 NADH:QH₂ produced per acetyl-CoA from pyruvate oxidization and 4:2 NADH:QH₂ per acetyl-CoA from fatty acids.

Flux through the TCA cycle is regulated in part by the redox potential and phosphate potential to maintain the energetic status of the cell. This regulation is described using a series of reservoirs as metaphors for the potential energy differences by Meyer and Wiseman (2011) (256) and demonstrate that metabolic flux is driven by the cytosolic ATP demand (i.e., increased $\frac{ADP+P_i}{ATP}$ and $\frac{NAD^+}{NADH}$). It follows that TCA cycle flux also

must increase with increasing ATP demand and this results in increased glucose oxidation to provide substrates to the TCA cycle. This fundamental principle of metabolism serving as a pull-through system was demonstrated by Jensen and colleagues showing a direct increase in glucose oxidation with increased rate of ATP consumption (ATPase rate). *Escherichia coli* were transfected with the F₁ portion of the membrane bound F₁F₀ ATPase to increase ATP consumption without affecting other aspects of metabolism. Glucose consumption through glycolysis directly increased with increased ATP consumption demonstrating the pull-through effect of ATP demand (188). The relationship between ATP demand and glucose oxidation perhaps explains at least a portion of the improved glucose handling in type 2 diabetes following exercise intervention.

1.3.2 Electron Transport System

Reducing equivalents feed into the ETS to support chemiosmotic ATP production. NADH and FADH₂ produced from the TCA cycle are incorporated into the ETS by the donation of electrons at NADH dehydrogenase (CI) or succinate dehydrogenase (CII), respectively. Donated electrons pass down an electrochemical gradient through membrane soluble carriers to complex III (CIII) and complex IV (CIV). The energy provided from donated electrons fuels proton pumping across the mitochondrial inner membrane and develops a proton motive force (Δp_{mf} , resting value 180 – 200 mV) that is a function of the membrane potential (~170 mV) and proton concentration gradient (10-30 mV) (Figure 1). This Δp_{mf} permits ATP production by ATP synthase (F₁F₀ ATP synthase) as originally described by Mitchell in his “chemiosmotic theory” (264). During

increased ATP demand imposed by exercise, the proton gradient is dissipated through the ATP synthase to produce ATP in a direct relationship with demand (256). ATP is transported from the matrix to the cytosol through adenine nucleotide translocase (ANT) and this transport is the accepted limitation to ADP sensitivity (170, 393). ANT activity directly influences the phosphate potential and reductions in activity are frequently suggested as the cause of impaired ATP production. However the precise mechanistic role of ANT in metabolic diseases including diabetes remains to be established empirically (131, 219, 226, 260).

Oxidation of NADH and transfer of electrons to CI provides the energy to pump 4 protons across the inner membrane contributing to the proton motive force. In contrast, CII oxidation of FADH₂ does not pump any protons but is used to produce QH₂ (276). The electrons produced at CI and CII transfer through the ETS via QH₂ to CIII which pumps 2 protons. Finally, electrons are transferred via cytochrome c to CIV where two molecules of cytochrome c are oxidized to reduce $\frac{1}{2}$ O₂ to water, and 4 protons are pumped across the inner membrane. Together, this results in a total of 10 protons pumped per NADH and 6 protons per FADH₂. The F₁F₀ ATP synthase utilizes this proton gradient by coupling the backflow of protons into mitochondrial matrix with the synthesis of ATP at the cost of 8/3 protons per ATP synthesized. The non-integer proton value originates from the fact that 8 c-subunit rings are associated with each ATP synthase molecule in mammals, and a complete 360° rotation of the F₁ catalytic head produces 3 ATP molecules (396). Accounting for an additional proton used for ATP and Pi translocation across the inner membrane by ANT and the inorganic phosphate carrier (PiC), respectively, this results in the calculated ATP:O ratios of 10/(8/3+1), or 2.73 for NADH and 6/(8/3+1), or 1.64 for

FADH₂. Thus, the amount of ATP produced per O₂ is dependent on which substrates are used to energize mitochondria.

Production of ATP through the ETS, like TCA cycle regulation, is driven by ATP consumption via feedback regulation of ADP, Pi, and ATP. Other controllers and influences on respiration have been proposed and suggested to alter metabolic flux (176, 367, 383), however none occur without ADP and Pi being the prominent controllers of respiration. The result of this tight regulation permits maintenance of the intracellular free energy of ATP hydrolysis that ultimately determines the energy released from ATP hydrolysis. This intricately linked system comprises the ATP production capacity or MOP capacity of the mitochondria that is routinely quantified experimentally.

1.4 MEASUREMENT OF MITOCHONDRIAL FUNCTION

MOP capacity is a combination of two factors: mitochondrial respiratory capacity; and the absolute fractional volume of mitochondria present within a given tissue. Therefore, before concluding mitochondria are either functional or dysfunctional both components must be known. V_{MITO} is routinely measured through biochemical assays of isolated tissue [see Larsen et al. (210)] and for this reason the present review will focus on measures of overall MOP capacity and inherent respiratory function. Mitochondrial

oxidative phosphorylation capacity involves ATP production from TCA cycle and ETS flux and is routinely measured both *in vitro* and *in vivo* (Figure 2).

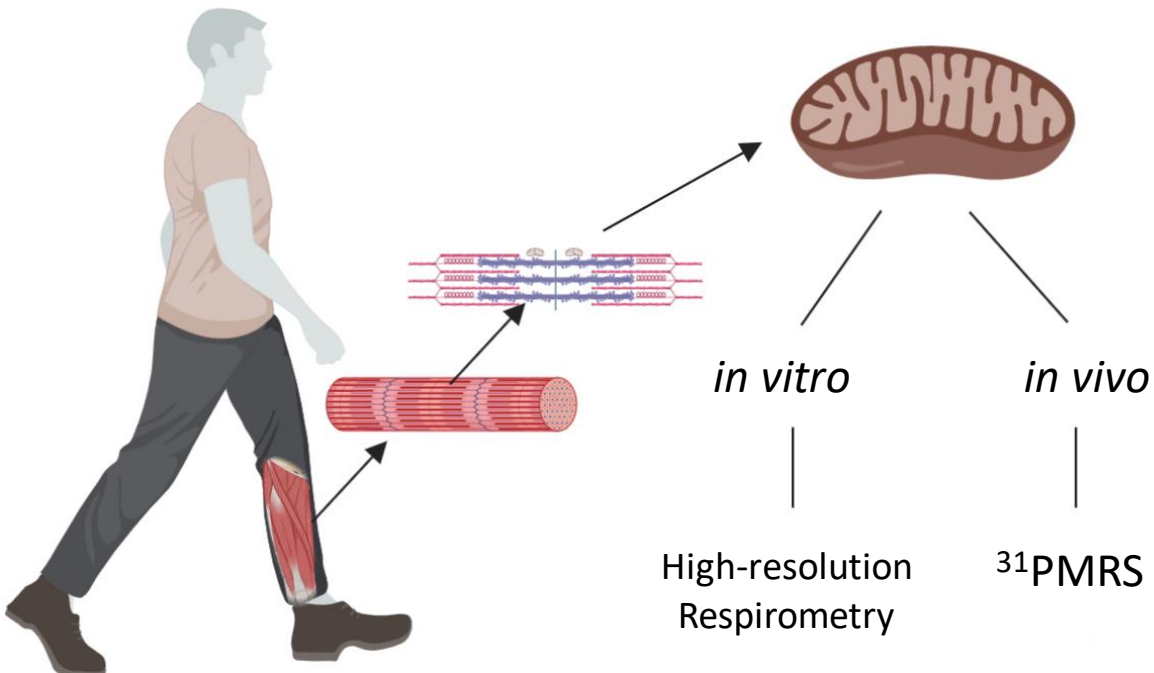


Figure 2. Mitochondrial oxidative phosphorylation capacity is comprised of both number and function that can be measured *in vivo* or *in vitro*. Mitochondria within skeletal muscle measured *in vivo* can be measured via phosphorus magnetic resonance spectroscopy (³¹PMRS). ³¹PMRS infers function from measures of MOP capacity, that when paired with V_{MITO} quantitatively describes function. Mitochondrial function *in vitro* can be measured via high-resolution respirometry following isolation of the organelle from the tissue. Created with Biorender.com.

1.4.1 Mitochondrial Function Quantified *in vitro*

Mitochondria isolated from skeletal muscle via centrifugation (383) allows study of the properties of the organelle in a well-controlled external environment (413). Controlling

in vitro conditions permits quantification of mitochondrial biochemical properties such as proton leak and the absolute maximal ATP production rates using non-physiological conditions that are never attained *in vivo* because the muscle fatigues long before this can occur. Isolated mitochondria studies can be particularly valuable in metabolic diseases where it may not be known how excess glucose, lipids, or altered blood flow affect mitochondrial respiration *in vivo*. Removing these factors by isolating the mitochondria permits direct quantification of mitochondrial respiratory capacity *in vitro* (42). Instruments used to measure respiration in isolated mitochondria primarily include Oroboros O2k (Oroboros Instruments) and Seahorse XF Analyzers (Agilent). In the present review, the Oroboros O2k will be primarily focused on due to its advantage in accuracy relative to Seahorse XF Analyzers which are designed for high-throughput qualitative measurements (287).

Mitochondrial function is quantitatively measured using high-resolution respirometry (Oroboros Instruments) to record changes in dissolved oxygen with a Clark-type oxygen electrode. These changes in dissolved oxygen are direct indicators of mitochondrial oxygen consumption at cytochrome c oxidase. Mitochondrial function is determined by a series of metabolic challenges to quantify the leak state, maximal-ADP stimulated state, and respiratory control ratio (RCR, $\left[\frac{\text{maximal ADP-stimulated state}}{\text{leak state}} \right]$). The leak state is attributed to dissipation of the proton gradient across the inner membrane *without* ATP production. The leak state is determined in the chamber by presence of only mitochondria and substrate *without* ADP. Substrates for these studies generally include either pyruvate for carbohydrates or palmitoyl-CoA for fats. The maximal ADP-stimulated state is an absolute measure of maximal mitochondrial ATP production rates. To measure

this a saturating bolus of ADP is added and all oxygen consumed is directly attributed to ATP produced. Taken alone the maximal ADP-stimulated state is used to indicate function; however, it does not account for mitochondrial volume within a sample. For this reason, a known quantity of mitochondria is typically loaded into the chamber as determined from mitochondrial protein quantification. The RCR is the most widely accepted measure for mitochondrial function since this relative measure will not change with differences in mitochondrial sample loading (42). There is not a set “standard” value for RCR however when comparing between animals *within the same muscle group* it permits direct comparison of mitochondrial efficiency to produce ATP from ADP. RCR comparisons must be from the same type of tissue and using the same substrate since different substrates or tissues will change both measures of leak and the maximal ADP-stimulated state. For example, RCR values using pyruvate-based substrate are >20 in skeletal muscle, >17 in cardiac muscle, and >3-4 in liver while fatty-acid based substrates produce values of >8, >10, and >2-3 respectively (172, 220, 413). In isolated mitochondria, measures of respiratory control are the most widely accepted indicators for mitochondrial function (42). If RCR values fall below the expected range, the mitochondrial preparation should not be used as the isolation process caused a portion of the mitochondria to lose the tight coupling required for proper function. For this reason, RCR should always be conducted at the start of this type of experiment to verify the integrity of the inner mitochondrial membrane.

Measures of isolated mitochondria are performed in non-physiological conditions using saturating substrate and O₂ but permit a direct comparison of mitochondrial respiratory capacity *ex vivo*. Maximal mitochondrial respiratory capacity measured *ex vivo*

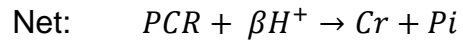
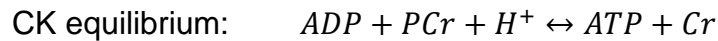
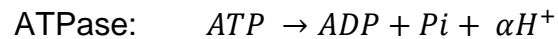
is well beyond the range of conditions that skeletal muscle mitochondria operate during normal duty cycles of contractile activity but is an important measure for objective quantification of mitochondrial function. Further measures to better understand *in vitro* respiration will not be covered here but are well described by Fisher-Wellman et al. (101).

1.4.2 Mitochondrial Function Quantified *in vivo*

Skeletal muscle permits quantification of MOP capacity because ATP demand can be controlled and quantified in discreet steps through graded exercise intensities. Since ATP production is driven by ATP consumption, measuring these together is crucial to determine how well the mitochondria respond to step changes in demand (e.g. changes in cytosolic [ADP]). The study of skeletal muscle metabolism is powerful because ATP synthesis is driven by ATP demand and metabolic demand is difficult to quantify in other tissues *in vivo*. MOP capacity is routinely assayed by near-infrared spectroscopy (NIRS) by measuring hemoglobin and myoglobin desaturation (62, 127, 189, 334) and by phosphorus magnetic resonance spectroscopy (³¹PMRS) measuring of phosphate metabolites (132, 169, 180, 252, 253, 329, 410). In the present review, ³¹PMRS will be the primary method discussed due to its quantitative advantage measuring metabolites inherent to mitochondrial respiration while NIRS quantification of oxygen dynamics is an indirect measure of mitochondrial function.

Using *in vivo* magnetic resonance MOP capacity is estimated by measuring the dynamics of the coupled metabolite phosphocreatine (PCr). Utilizing the creatine kinase

equilibrium, changes in PCr directly reflect changes in ATP consumption/production (4, 253, 255, 256, 410):



Where α (0.6) and β (0.4) represent partial protons produced as a function of environmental variables such as temperature, ionic strength, pH, and the differences in pK_a of substrate and product (213). MOP capacity *in vivo* is most commonly determined from measuring PCr recovery time following exercise. The veracity of this measure was illustrated by Paganini et al. (124) where the PCr recovery time constant was directly related to mitochondrial volume and hence MOP capacity. Following alteration of muscle MOP capacity by chemical treatment (reduce) or exercise training (increase) the PCr recovery time grew faster with increased MOP capacity (124). This technique has been broadly used in studies performed on human subjects and animal models and is a well-accepted measure of MOP capacity and by extension has been used to infer mitochondrial function (244, 283, 410). However, this measurement relies on several assumptions which are often ignored or ill-considered (Table 1):

Table 1. Underlying assumptions for using the PCr recovery time constant to infer mitochondrial function (283).	
<u>#</u>	<u>Assumptions</u>
1)	Equilibrium of the cytoplasmic creatine kinase reaction
2)	Oxygen and substrate supply are not limiting during recovery
3)	Glycolytic ATP production is negligible during recovery
4)	Mitochondrial ATP:O and basal muscle oxygen consumption ($\dot{V}O_2$) are each constant
5)	PCr resynthesis accounts for all but a negligible fraction of the extra ATP consumed during recovery
6)	Similar mitochondrial fractional volumes within the measured tissues

Ascribing PCr recovery to mitochondrial function is no longer valid if any of the assumptions in Table 1 do not hold true (105, 130, 174, 215, 245, 375, 391, 392). For example, in the case of peripheral arterial disease (PAD), blood flow to peripheral muscles is reduced depending on disease progression and can limit oxygen delivery to working muscles (280). Therefore, it is likely that oxygen is limiting mitochondrial respiration in individuals with PAD, violating assumption #2 and making interpretation of PCr recovery in relation to mitochondrial function equivocal. Likewise if oxygen becomes limiting, assumption #3 would likely be violated since the muscle would become acidic and directly reduce muscle mitochondrial ATP production (130, 174, 215, 391, 392). Perhaps most often violated, assumption #3 requires interventions to be within the aerobic range where glycolytic ATP production is not significant. For example, during high

intensity contractions above the lactate threshold (122) glycolytic ATP production is apparent and makes interpretation of the PCr recovery time constant no longer a valid measure of MOP capacity.

³¹PMRS can quantitatively determine mitochondrial function from several other perspectives [for review see Wiseman et al. 2008 (410)]. Skeletal muscle experiments performed at multiple workloads where MOP ATP production can match ATP consumption permits quantification of apparent ADP sensitivity, free energy of ATP (ΔG_{ATP}), ATPase rates from initial rate of PCr hydrolysis, glycolytic ATP production, and others [see (410)]. For quantification of each of these components in skeletal muscle, experiments should include several work intensities within the sustainable range that an energetic steady state can be reached and abide by each of the assumptions outlined in Table 1. Results are no longer related to solely mitochondrial function if the assumptions are not valid and therefore these must be known especially in cases of metabolic disease where oxygen or substrate limitations have been suggested (82, 108, 111, 132, 134, 209, 388, 406).

1.5 OBESITY, PHYSICAL INACTIVITY AND MOP CAPACITY

MOP capacity can be altered by changes in f_{MITO} , V_{MITO} , or both. Mitochondrial fractional volume within skeletal muscle is highly plastic and sensitive to the effects of lifestyle including obesity and physical activity. Obesity and physical activity independently affect MOP capacity, through changes in mitochondrial volume (V_{MITO}) but with some reports of reduced respiration per organelle (f_{MITO})(38, 141, 147, 372). This is

particularly important in metabolic diseases, often termed “lifestyle diseases”, because over-nutrition and inactivity can play a role in their development. In fact, reduction in weight and increased physical activity vastly reduces diabetes risk both independently and in conjunction with one another (128) and exercise continues to be the most effective treatment combatting type 2 diabetes (186).

1.5.1 Obesity effect on MOP capacity

Obesity affects MOP capacity as demonstrated in several models of murine species and in human subjects as well. In a detailed study by Turner et al. (2007) increased mitochondrial volume in mice and rats subjected to elevated fat intake were reported. C5BL/6J mice were acquired at 8 weeks of age and subjected to a high-fat diet for 20 weeks. Mice were sacrificed at 5 and 20 weeks of age and assayed for markers of mitochondrial volume including citrate synthase (mitochondrial matrix enzyme) and β -hydroxyacyl CoA dehydrogenase (β -HAD, enzyme of fatty acid oxidation). Feeding a high fat diet resulted in increased fat mass to obese levels and mitochondrial volume was elevated in quadriceps muscles by 20% at 5 weeks and 57% at 20 weeks. This result was also shown in the same study in Wistar rats subjected to 4 weeks of HFD, the chronically obese Zucker rat, and db/db mouse showing 14% 36%, and 17% increased mitochondrial volume. Taken together, these observations show that increased fat composition leading to obesity can directly alter mitochondrial volume and by extension the MOP capacity across species (372).

The inherent effect of obesity on MOP likely depends on the stage of its progression since many other studies of obesity report contradictory effects on MOP capacity (141). Mice subjected to a high fat and high sucrose diet for 16 weeks demonstrated reduced mitochondrial volume and maximal ADP-stimulated respiration (36). Sprague Dawley rats subjected to a high fat diet for 3 weeks demonstrated increased ROS production and reduced maximal ADP-stimulated respiration (12). The effect of obesity on MOP capacity also translates to humans where obese women demonstrated reduced mitochondrial function measured by reduced maximal ADP-stimulated respiration and reduced RCR in mitochondria isolated from vastus lateralis muscle (191). Clearly, obesity can have a direct effect on MOP capacity, but the magnitude and direction of its effect are variable and thus requires careful matching for lean body mass in studies of type 2 diabetes.

1.5.2 Physical activity and MOP capacity

Physical activity level directly influences skeletal muscle MOP capacity as shown by the late Dr. John Holloszy and colleagues in over 50 years of work studying exercise training (79, 102, 137, 147–152, 163). In 1967, Holloszy reported a two-fold increase in mitochondrial fractional volume in rat muscles following a 12-week training regimen measured by the changes in cytochrome oxidase and succinate oxidase activities. Increased mitochondrial volume resulted in a two-fold increase in oxidative capacity measured from rat gastrocnemius and soleus muscles (147). This was one of the first reports to demonstrate increased mitochondrial volume and muscle oxidative capacity together and was foundational to future exercise physiology studies. Among these

adaptations, Holloszy hypothesized that increased MOP capacity from increased mitochondrial volume would increase the sensitivity of ADP feedback regulation (102). In other words, less ADP would be required for ATP production as muscle mitochondrial volume increases. Thus, a given workload would disrupt homeostasis less since ADP sensitivity is increased and increase muscle performance including less glycogen consumed and more work performed. This concept was subsequently supported in work by Chance and colleagues (56) and demonstrated by Terjung and Dudley (93). Following alteration of muscle mitochondrial volume by exercise training (increase) or chemical treatment (decrease), Dudley et al. (1987) demonstrated that sensitivity to metabolic feedback is increased with increasing mitochondrial volume (93). This higher ADP sensitivity enhances maximal exercise performance (increased ATP production capacity) and endurance exercise performance [glycogen sparing (102)] a concept crucial to understanding muscle oxidative phosphorylation measured *in vivo* (249, 250, 283, 410). Since these early works, the relationship between training, mitochondrial volume, and MOP capacity has been well characterized in both the adaptable range of mitochondrial volume and its effect on MOP capacity (140, 283).

More recently, studies have focused on a direct effect of sedentary behavior or physical *inactivity* on health and development of disease pathology. Inactivity is strongly related to development of obesity and insulin resistance (177). In fact, sitting for more than $\frac{3}{4}$ of a day increases mortality risk by ~30% even in physically active individuals (greater than 7.5 METs per hour per week) (178). The role of inactivity on disease progression in type 2 diabetes impacts several aspects of metabolism important in

glucose handling and delivery (80, 315, 386). After a brief period of inactivity (<5,000 steps per day for 5 days) insulin sensitivity was reduced in healthy subjects measured from Matsuda index during an OGTT however there was with no change in delivery or blood flow response (315). Using the same model of inactivity, during an OGTT arterial compliance was decreased and stiffness increased suggesting an effect of inactivity on vascular function contributing to insulin responsiveness also without reported changes in blood flow (80). Finally, after comparable periods of inactivity reduced microvascular function was reported but without larger vessel dysfunction. This suggests that there is nearly immediate onset of microvascular dysfunction and insulin resistance with a sedentary lifestyle (386). The impact of reduced microvascular function in progression of the disease particularly with respect to mitochondrial function and muscle performance have recently been suggested (111).

Sedentary lifestyle is directly related to a reduction in skeletal muscle MOP capacity. Booth and colleagues (1987) demonstrated 25% reduced MOP capacity after merely 7 days of sudden inactivity in rat quadriceps muscle (271). Both hindlimbs of female Sprague-Dawley rats (200-300 grams) were immobilized by cast and muscle mitochondrial fractional volume was quantified from cytochrome c concentration after 7 days of immobilization. Subsequently, separate groups were immobilized for 7 days and casts removed to allow recovery from immobilization for 6 hours, 2 and 4 days to directly relate results to sudden inactivity. Mitochondrial fractional volume measured by cytochrome c content gradually recovered reaching levels 94% of control in merely 4 days (271). Taken together, these results [Figure 3, adapted from Morrison et al (1987)]

demonstrate the direct effects of inactivity alone on mitochondrial fractional volume and MOP capacity.

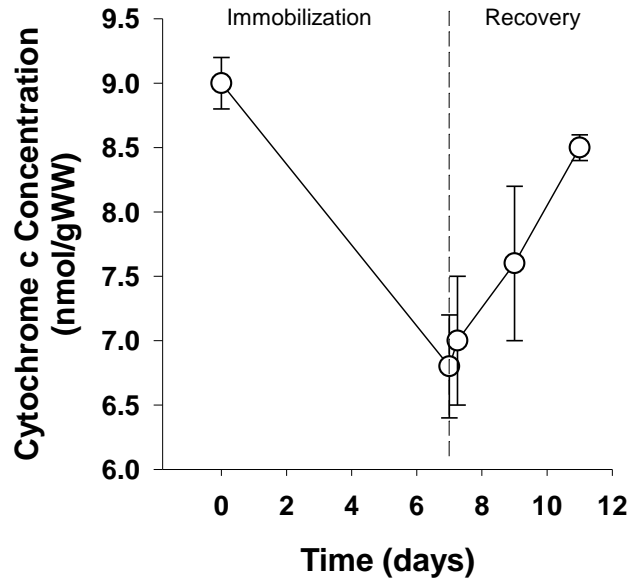


Figure 3. Role of inactivity on mitochondrial fractional volume adapted from Morrison et al. 1987. Rat quadriceps muscles were immobilized by cast for 7 days and mitochondrial fractional volume determined from cytochrome c content. Measures were taken from muscle samples before immobilization and at time points 0-, 0.25-, 2-, and 4-days following cast-removal.

The direct role of inactivity on MOP capacity also translates to human subjects (25). Berg et al. (1993) showed 18% reduced mitochondrial volume in muscle biopsies from vastus lateralis muscle following 4 weeks of immobilization. A single hindlimb was immobilized by suspension with a harness and custom shoe for contralateral limb to ensure weight-bearing was null in harnessed limb. After 4 weeks of immobilization, mitochondrial fractional volume measured by citrate synthase activity was reduced (Pre: 40.2 ± 7.2 versus Post: 32.9 ± 4.9 $\mu\text{mol/g/min}$) with no change in the contralateral limb (Pre: 39.0 ± 4.7 versus Post: 37.1 ± 3.3 $\mu\text{mol/g/min}$) (25). Berg et al (1993) concluded that inactivity alone reduced mitochondrial volume and thus MOP capacity and similar

results have been demonstrated following bedrest (143, 181). It is evident that inactivity by itself has a direct effect on MOP capacity and must be considered in metabolic disease especially those presenting comorbidities linked with inactivity (37, 38, 205, 378). In contrast, increasing activity vastly increases the quality of life in diseased individuals belabored by exercise intolerance (53, 152) and suggests a direct role of activity on MOP capacity and disease progression. Future experiments must carefully match subjects for daily activity perhaps through questionnaires or wearing accelerometers although neither are perfect (265).

1.5.3 Summary

Obesity and inactivity each can independently influence skeletal muscle MOP capacity. Therefore, these variables must be controlled for especially in studies of “lifestyle diseases” including obesity, peripheral arterial disease, type 2 diabetes, or chronic obstructive pulmonary disorder. The role of further sequelae of obesity, inactivity and metabolic syndrome that may alter apparent mitochondrial function including substrate and oxygen availability must also be weighed in the measure of MOP capacity and mitochondrial function (Table 1) but for brevity are not discussed here.

1.6 HUMAN TYPE 2 DIABETES MITOCHONDRIAL FUNCTION

Mitochondrial function has been widely studied in human T2D since the early works by Kelley and Shulman (179, 288) proposed disruption of aerobic metabolism as a consequence of this disease. Many studies are contradictory in the literature (Figure 4)

and a study that tests across a range of contractile intensities within the MOP capacity has not been performed. Despite this, the dogmatic view that mitochondrial dysfunction plays a role in the development of type 2 diabetes is still widely accepted (98, 121, 269). This section carefully reviews the main body of literature related to mitochondrial (dys)function in type 2 diabetes and concludes that many of these reported deficits are likely more related to obesity and sedentary lifestyles than the disease itself.

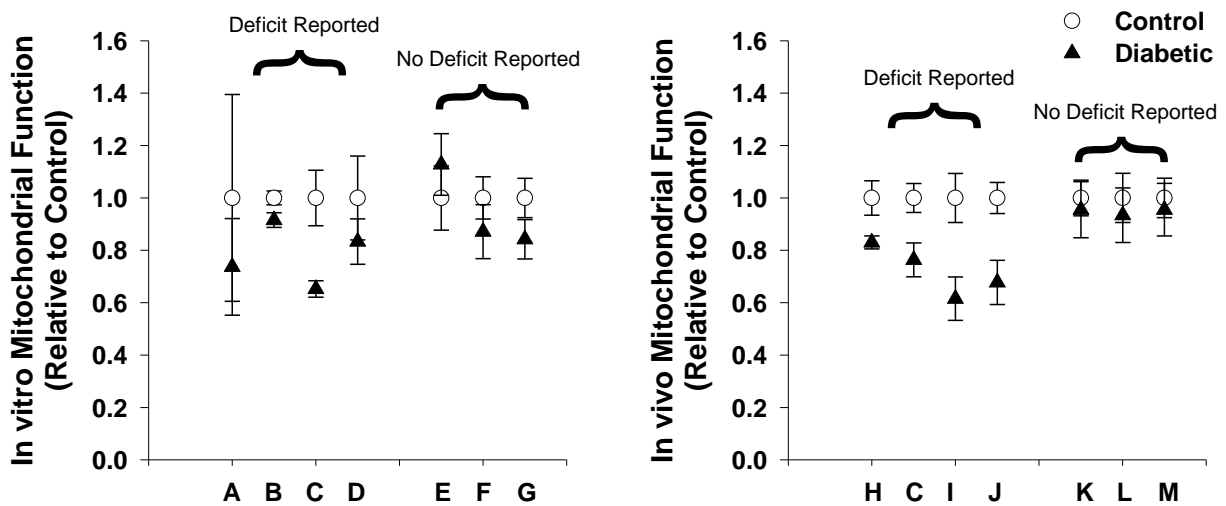


Figure 4. Summary of human mitochondrial (dys)function in diabetes. Data of reported mitochondrial (dys)function was compiled from the literature and presented relative to respective control subjects. Control (white circles) is always equal to 1 and diabetics (black triangles) presented as a fraction of that determined from the reported measures of function. This was determined for (A) *in vitro* and (B) *in vivo* studies where both deficits and no deficits in mitochondrial function have been reported. A) Kelley 2002; B) Mogensen 2007; C) Pielix 2008; D) Ritov 2005; E) Abdul-Ghani 2009; F) Boushel 2007; G) Hey-Mogensen 2010; H) Meex 2010; I) Scheuermann-Freestone 2003; J) Schrauwen-Hinderling 2007; K) De Feyter 2008; L) Praet 2006; M) van Tienen 2012.

1.6.1 Human type 2 diabetes mitochondrial function *in vitro*

Mitochondrial function *in vitro* is routinely measured in mitochondria isolated from skeletal muscle biopsies of individuals with type 2 diabetes. Several studies report

reduced mitochondrial function (179, 266, 291, 321) while others demonstrate no difference in function (2, 40, 142) when comparing obese controls with diabetic patients. Mogensen and colleagues (2007) reached the conclusion of mitochondrial dysfunction when mitochondria were isolated from vastus lateralis muscle of individuals with type 2 diabetes and their BMI-matched controls (266). Oxygen consumption recorded polarographically (DW1 oxygraph) showed reduced maximal ADP-stimulated oxygen consumption rates when respiring in the presence of pyruvate and malate and no difference in presence of palmitoyl-carnitine and malate. However, neither daily activity nor muscle aerobic capacity were measured in these individuals (266), a limitation acknowledged by the authors in later publication (142). Ritov et al. (2005) also reported mitochondrial dysfunction measuring 17% reduced ETS activity in diabetic patients compared to obese controls from vastus lateralis isolated mitochondria determined by succinate oxidase activity (321). However, this was presented without accounting for the reported 27% reduction in mitochondrial fractional volume.

In contrast, normal mitochondrial function in muscle from individuals with diabetes compared to BMI-matched controls has been shown (2, 142). Hey-Mogensen and colleagues (2010) demonstrated nearly identical respiration in mitochondria isolated from vastus lateralis muscle of individuals with diabetes versus control subjects matched for age, physical activity and BMI. Respiration was comparable in the presence of both pyruvate and malate as well as palmitoyl-carnitine and malate during the mitochondrial leak state and maximal ADP-stimulated state (142). In a similar study, Abdul-Ghani and colleagues (2009) showed no difference between individuals with diabetes and BMI-matched controls. ATP production rates of isolated mitochondria were not different in the

presence of either glutamate and malate or succinate and rotenone (2). Taken together, evidence suggests that mitochondrial function is not reduced when isolated from diabetic patients *and* controlling for fractional volume, and further suggests no apparent link to the metabolic condition itself.

1.6.2 Human type 2 diabetes mitochondrial function in vivo

Studies in type 2 diabetes have also reported mixed results when determining skeletal muscle mitochondrial function *in vivo*. Many investigators have suggested mitochondrial dysfunction (247, 291, 338, 340) while others suggest none (86, 304, 378) when determined from PCr recovery time following exercise. Inspection of the results from these studies suggests differences are not inherent deficiencies of the mitochondrial organelle itself but rather deficiencies in study design.

Scheurmann-Freestone and colleagues (2003) demonstrated slowed PCr recovery in individuals with type 2 diabetes and concluded that MOP capacity was reduced due to mitochondrial dysfunction in type 2 diabetes (338). In this study, individuals with type 2 diabetes were compared to healthy controls but factors including age, physical activity, and body mass index (BMI) were not weighed. Aging is frequently reported to independently contribute to reduced MOP capacity (43, 205) and control subjects were ~10% younger than diabetic subjects. Further, type 2 diabetes frequently presents with obesity [87.5% of diabetic patients report overweight or obese (54)] and reduced physical activity [40.8% achieve less than 10 minutes of moderate physical activity per week (54)]. The potential variability in mitochondrial function between subject

populations is highlighted in work by Praet et al. (2006) (304). In this work, PCr recovery times were measured in individuals with type 2 diabetes following exercise in the vastus lateralis muscle. Results demonstrated similar PCr recovery time constants to control subjects in the Scheurmann-Freestone (2003) study and the authors concluded no deficit in MOP capacity or mitochondrial function (304).

Subsequent studies also concluded mitochondrial dysfunction in type 2 diabetes from reduced PCr recovery time and controlled for obesity by BMI matching controls and diabetic subjects (247, 340). However, in each of these works physical activity levels were not quantified or compared between subjects and their respective mitochondrial fractional volumes were not measured. This leaves the possibility that the result could be explained by reduced MOP capacity due to sedentary lifestyle rather than the diabetes itself. Further, it is important to note that the BMI descriptor for obesity has recently been challenged (379, 394, 405). When age, obesity, and activity levels were carefully controlled for no difference was measured in PCr recovery rates with the conclusion of normal mitochondrial function in type 2 diabetes (87, 378). De Feyter et al. (87) recruited patients based on age, similar BMI and activity levels. Diabetics presented 200% higher fasting glucose and nearly 50% higher HbA_{1c}. Despite pronounced type 2 diabetes, no differences were measured in PCr recovery after contracting at workloads where muscle acidity remained negligible. This work by De Feyter et al. suggests that *in vivo* dysfunction reported in type 2 diabetes is likely a result of age, obesity, and/or physical activity and not the disease itself (87).

1.6.3 What is missing?

Contradictory evidence appears to leave the question of mitochondrial dysfunction in type 2 diabetes unanswered. However, the literature *suggests* that conflicting reports of mitochondrial function in type 2 diabetes are the result of subject variability and not the disease itself. To correct this shortcoming, studies that report changes in mitochondrial function *in vivo* should also have mitochondrial function evaluated *in vitro* in the same subject. Further, studies must expand upon work by De Feyter et al. performing on well-controlled subjects matching for physical activity, obesity, and abiding by the assumptions in Table 1 by measuring pH, oxygen supply, and others across several contractile intensities. Variability in lifestyles within human populations proves difficult for such experimental design and thus studies rely on animal models of type 2 diabetes that provide cogent control of lifestyle variants before carefully translating to human populations.

1.7 RAT MODELS OF TYPE 2 DIABETES

Muscle metabolism has been extensively studied in rat models (55, 63, 115, 176, 218, 220, 252) that allow for precise control of experiments and closely resemble human muscle metabolism and composition (339). For example, studies in human subjects rely on maximum voluntary contraction of the muscle which can be difficult to interpret due to inconsistencies in muscle recruitment (363). In contrast, the use of rodents provides the advantage of simultaneous recruitment of all hindlimb muscle fibers via electrical pacing of the sciatic nerve. Further, maximal recruitment in the hindlimb together with

simultaneous force recording of muscle contraction permits measures to be performed at the optimal length of the muscle (L_0 , determined from the length tension relationship at which the maximal force is obtained). L_0 is crucial in studies of muscle metabolism since any deviation can vastly influence metabolic demand (8). Quantification of muscle metabolism in rat models that present with the type 2 diabetic metabolic condition can be used to determine its role on mitochondrial function.

Many animal models of type 2 diabetes are used to study various organ systems and their link to the disease. For the purposes of brevity in this review focused on type 2 diabetes skeletal muscle mitochondrial function, studies discussed are confined to two of the most commonly used models including the Zucker Diabetic Fatty (ZDF) and Goto-Kakizaki (GK) rat models. For reference, Table 2 [adapted from work by Srinivasan et al. (2007)] presents a summary of further animal models used in the study of type 2 diabetes and how they relate to the human condition in presentation of the disease. While rat models do not directly recapitulate the progression of type 2 diabetes in humans, studies within similar metabolic conditions (hyperglycemia, insulin resistance) can provide needed insight into skeletal muscle mitochondrial function in type 2 diabetes.

Table 2. Summary of diabetic animal models re-summarized from Srinivasan et al. 2007

	<u>Model</u>	<u>Summary</u>
<u>Genetically developed diabetic animals:</u>		
<i>Obese:</i>	ob/ob mouse	<p>Pros: Develop resembling severe insulin resistance and type 2 diabetes in humans, homogeneous genetic background reduces variability.</p> <p>Cons: Highly genetic-determined diagnosis unlike mostly lifestyle disease in humans, limited and expensive, substantial maintenance often due to disease severity.</p>
	db/db mouse	
	Obese Zucker rat	
	ZDF rat	
	OLETF rat	
	Obese rhesus monkey	
<i>Nonobese:</i>	Cohen diabetic rat	
	GK rat	
	Akita mouse	
<u>Diet induced diabetic animals:</u>		
<i>Obese:</i>	Sand rat	<p>Pros: Diabetes progression similar to diabetes in obese populations overnutrition, toxicity from chemical induction avoided.</p> <p>Cons: Generally, take a long time for development, frank hyperglycemia only apparent in certain animal models and therefore confounds development factors.</p>
	C57/BL 6J mouse	
	spiny mouse	
<u>Chemical, surgical induced diabetic animals:</u>		
<i>Non-obese:</i>	HFD, low dose STZ	<p>Pros: Controlled onset of diabetic progression, residual insulin secretion better maintains health, inexpensive, recapitulates human with reduced beta cell mass.</p> <p>Cons: Hyperglycemia results mostly due to cytotoxic effect on beta cells versus initial insulin resistance, difficult for long term experiments due to beta cell regeneration, toxic actions on other organ systems.</p>
	Neonatal STZ rat	
	Partial pancreatectomized	
<u>Myriad transgenic murine models targeting insulin receptors, glucose transporters, etc.</u>		
		<p>Pros: Effect of single gene, better understanding of genetic contribution to type 2 diabetes.</p> <p>Cons: Highly expensive, translation to human population unclear.</p>

1.7.1 Zucker Diabetic Fatty (ZDF) Rat

The Zucker diabetic fatty (ZDF) rat is perhaps the most widely used rat model for the study of the impact of type 2 diabetes. ZDF rats were developed through selective breeding of Obese Zucker rats (OZR) showing the greatest increase in the severity of insulin resistance and poor glycemic control with time (289). OZR manifest a dysfunctional (based in a coding error) leptin receptor and resulting in a severe leptin resistance, and the ensuing hyperphagia, obesity, and insulin resistance. However, due to insulin overproduction, most OZR do not present with severe fasting hyperglycemia until they become significantly older than matched ZDF (348). It is important to note that OZR and ZDF rats are not equivalent animal strains and thus cannot be interchanged when comparing either existing studies or in experimental design and data interpretation for ongoing studies.

The OZR develop metabolic disease along a very predictable time course spanning many weeks. It begins with rapid increases in body mass until they are overweight/obese and gradually worsening glycemic control culminating in the development of a moderate level of hypertension (109) and the other systemic pathologies of “metabolic syndrome” (24). Animals are exposed to these conditions over protracted periods of time prior to the overt development of end-organ damage and the consequences of long-term loss of glycemic control. In contrast, the ZDF rat model demonstrates a modest development of obesity, but a rapidly accelerated progression through insulin resistance to severe type 2 diabetes. Associated with this development, the ZDF exhibit a rapid progression of end-organ damage including early pancreatic and renal failure. Based on the dramatic differences in the physiology of these animal models

caution should be exercised when interpreting the results of experiments using the different animal strains particularly regarding age, severity of metabolic dysfunction, and the potential influence of untoward pathology not part of the specific study. Mitochondrial function has been measured in the ZDF rat both *in vitro* and *in vivo* to determine whether (dys)function is present in T2D.

1.7.1.1 Mitochondrial function *in vitro*

Skeletal muscle mitochondrial function quantified *in vitro* in the ZDF rat shows no difference in mitochondrial function. Mitochondria have been isolated from the skeletal muscles of ZDF rat tibialis anterior (153, 218, 399, 400) and gastrocnemius muscles (35, 354, 374). To date published results reveal no detectable deficiencies in mitochondrial respiratory capacity utilizing either carbohydrate (pyruvate and malate) (218, 374, 399, 400) or fatty acids (palmitate or palmitoyl-carnitine and malate) (218, 354, 374) as substrate. However, Lenaers et al. reported reduced fat respiratory capacity at 6 weeks of age with no difference seen at 12 or 19 weeks (218). Many other studies report an increase in fat respiratory capacity in ZDF compared with lean controls (35, 153, 399, 400). Wessels et al. (2014, 2015) reported no differences in isolated mitochondria but from animals that already had evidence of mitochondrial dysfunction measured *in vivo* by ³¹PMRS (399, 400). Taken together the results from the *in vitro* ZDF literature suggest that apparent mitochondrial dysfunction *in vivo* (if any) is likely a result of substrate or oxygen limitations or reduced mitochondrial volume fraction since mitochondrial respiratory capacity is unaltered when studied in isolation.

1.7.1.2 Mitochondrial function *in vivo*

ZDF rat mitochondrial function *in vivo* studies have reported inconsistent results. Wessels et al. (2014, 2015) described slowed skeletal muscle PCr recovery rates compared to age matched lean controls and reported mitochondrial dysfunction in two separate studies (399, 400). Measurements were obtained from the tibialis anterior muscle following tetanic contractions (80Hz, 100ms, 1/s) that were designed to drive PCr concentration down to ~50% of resting levels (2-minute stimulation). However, experiments performed with the same experimental protocol previously resulted in no difference in PCr recovery rates in ZDF rats and lean controls suggesting mitochondrial function is normal at ages 6, 12, and 18 weeks (87). Differences in results likely arise from the protocol using 1 tetanic contraction per second which elicits a very intense metabolic demand nearly double the reported MOP capacity of the rat hindlimb of ~0.5 tetani/s twitch stimulation (155). Interpretation of PCr kinetics beyond MOP capacity is arbitrary since oxygen delivery and pH changes are likely altered (105, 155, 168) and assumptions (2) and (3) from Table 1 are violated. Increased muscle acidity is directly proportionate to lactate production from glyco(geno)lysis (256, 303, 326, 409) and PCr kinetics are no longer related to MOP capacity when the muscle becomes acidic (105, 375, 392). Forbes et al. (2009) demonstrated a nearly twofold slowing in PCr recovery time constant in rat gastrocnemius muscle measured at low intensity (0.75 Hz, 48 ± 3 seconds) and high intensity (5 Hz, 89 ± 8 seconds) twitch stimulation where acidosis was apparent and directly slowed PCr recovery in agreement with previous studies (130, 174). Taken together, the literature in ZDF rat skeletal muscle mitochondrial function *in vivo* is equivocal especially when performed at high intensities. Future experiments in these rats

should include metabolic challenges across a broader dynamic range but within the MOP capacity ($\sim < 1$ Hz twitch contractions).

1.7.2 Goto-Kakizaki (GK) Rat

The Goto-Kakizaki (GK) rat is the most widely used non-obese model of type 2 diabetes (6). The spontaneously diabetic GK rat was developed through selective breeding of Wistar control (WC) rats. Oral glucose tolerance tests (OGTT) were performed on WC rats and the minority that demonstrated reduced glycemic control were inbred and this process was repeated over many generations resulting in the hyperglycemic and insulin resistant GK rat (123). Primarily male rats are used for studies since females do not consistently develop T2D due to estrogen-protecting effects (91). At a very young age, GK rats first present diabetic symptoms at around 3 weeks of age with hyperglycemia due to impaired beta cell insulin secretion (261). Progression develops towards peripheral insulin resistance (277), hepatic glucose overproduction (345), and frank type 2 diabetes between 14-17 weeks of age (220, 302). GK rats demonstrate many of the comorbidities seen in human type 2 diabetes and thus are beneficial in application to human diabetes [for review, see (6, 302)]. Major advantages in studying the GK rat versus ZDF and others is this model presents without obesity (6) and is physically active (7, 221). This isolates the type 2 metabolic condition and permits a direct relationship between mitochondrial function and the type 2 diabetic metabolic condition itself.

1.7.2.1 Mitochondrial function *in vitro*

Mitochondrial function *in vitro* in GK rat skeletal muscle shows findings consistent with both human T2D and ZDF rat literature and shows no evidence of mitochondrial dysfunction. Skeletal muscle isolated mitochondria in the GK rat include data from both quadriceps muscles (172, 203) and triceps surae (gastrocnemius, plantaris soleus) muscles (220). These studies all report no deficit in skeletal muscle mitochondrial function measured by maximal ADP-stimulated respiration in the presence of varying substrates. Jørgensen et al. (2012) measured mitochondrial respiration in the presence of pyruvate and malate, palmitoyl carnitine and malate, and pyruvate, palmitoyl carnitine, and malate all together. Results showed no deficit in maximal ADP-stimulated respiration and an increase in capacity for 6 and 16 week old GK rats compared to 16 week old Wistar controls (172). Similarly, Lai et al. (2017) detected no differences in GK rat skeletal muscle mitochondria when maximally ADP-stimulated at either 18 or 28 weeks in presence of glutamate (203). Taken together, the body of literature for GK rat studies show no evidence of mitochondrial dysfunction *ex vivo*.

1.7.2.2 Mitochondrial function *in vivo*

Skeletal muscle mitochondrial function *in vivo* has been measured by ³¹PMRS in the GK rat with the qualitatively consistent conclusion that mitochondrial function is not impaired (223, 233). Liu et al. (2016) report normal mitochondrial function in the GK rat from similar PCr recovery time compared to Wistar controls (223). In this study the rat hindlimb was occluded by an inflatable cuff to cause ischemic depletion of PCr, and upon

releasing the cuff PCr recovery time was measured. Although no differences were observed, PCr recovery following ischemia occurs in a very acidic environment violating a primary assumption regarding the utility of PCr kinetics and mitochondrial function (Table 1) (105, 375, 392). This is demonstrated in Figure 3 of Liu et al. (2016) showing pH dropping to about 6.7 during ischemia and the authors acknowledging that this may influence the result (223).

In an elegant experiment, Macia and colleagues (2015) reported normal mitochondrial function in the GK rat with similar PCr contractile steady states and recovery time constants compared to Wistar controls (233). Rats were stimulated at 3.3 Hz and ³¹PMRS was measured from the gastrocnemius muscle using a custom built NMR probe (115). PCr kinetics were not different between groups during contraction despite reduced force production in the GK rat. The authors acknowledged this by stating that although force production was different, ATP cost per contraction was not different between groups and allowed direct comparison. These measures together are crucial for accurate quantification of mitochondrial function using ³¹PMRS and are often not an integral part of the experimental protocols. Although no differences were seen, 3.3 Hz is well beyond the MOP capacity of the hindlimb for twitch stimulation [reported as 1 Hz (155)] and makes interpretation of PCr recovery time constants for inferring mitochondrial function debatable (105, 375). To this point, PCr hydrolysis reached >80% of the resting concentration, pH dropped from ~7.1 to 6.2 - 6.4 and PCr recovery times were nearly 3X previously reported values even in controls (176, 220, 252, 283) suggesting that this experimental system causes an occlusion of blood flow and therefore inadequate oxygen delivery.

1.8 Summary

Taken together, evidence in the literature in both human type 2 diabetes and rat models of type 2 diabetes questions skeletal muscle mitochondrial dysfunction that is dogmatically thought to be inherently linked to the type 2 diabetic metabolic condition. When isolated from cellular conditions and quantified via high-resolution respirometry the literature suggests MOP capacity is not reduced in type 2 diabetes and mitochondrial function is intact. Further, when accounting for the effects of mitochondrial content, obesity, and physical activity mitochondrial function *in vivo* appears to be normal. Vascular limitations are apparent in type 2 diabetes (108, 110, 111, 217, 222, 316, 406) and sufficient oxygen supply is necessary for mitochondrial respiration (71, 111, 208, 283). MOP measured *in vivo* will be limited if oxygen supply is significantly reduced and could be falsely interpreted as mitochondrial dysfunction. The complete experiment that takes each of these variables into account has not been performed.

CHAPTER 2: RESEARCH AIMS AND HYPOTHESES

2.1 Research Goals

The goal of this research was to determine the limitation to skeletal muscle mitochondrial oxidative phosphorylation in the type 2 diabetic metabolic condition. Skeletal muscle can account for up to 80% of glucose uptake (89) and mitochondrial respiration is the driving force for glucose disposal in muscle. As such, the role of mitochondrial function on insulin resistance and hyperglycemia has been questioned (183, 225, 290, 349) and its understanding is imperative to develop effective therapeutic treatments combatting the disease.

In this study, mitochondrial function was first defined computationally utilizing a mathematical model to understand how mitochondrial alterations would present bioenergetically. Mitochondrial function was then quantified in skeletal muscle of the non-obese, non-sedentary Goto-Kakizaki rat model of type 2 diabetes. Mitochondrial function was determined both *in vivo* using ^{31}P MRS techniques and *in vitro* using high-resolution respirometry. Finally, cardiovascular function, muscle blood flow, and muscle performance were quantified to determine if impaired oxygen supply limits muscle metabolism in the diabetic GK rat.

Ultimately the present work aimed to make clear the obfuscated literature of mitochondrial function in type 2 diabetes. By carefully controlling for experimental conditions and variability between animals we believe the current work will better contribute to the understanding of skeletal muscle metabolic performance in patients with type 2 diabetes.

2.2 Central Hypothesis

The central hypothesis for the present work is that mitochondrial dysfunction is not inherently linked to the type 2 diabetic metabolic condition and that any muscle metabolic dysfunction is the result of limitations in oxygen supply to the mitochondria.

2.3 Specific Aims

2.3.1 *Define mitochondrial function computationally:*

Mitochondrial function will first be described by computational modeling to understand how alterations impact muscle bioenergetics. This understanding is crucial for determining any deficits within type 2 diabetes.

2.3.2 *Quantify mitochondrial function within the Goto-Kakizaki rat model of type 2 diabetes:*

Skeletal muscle mitochondrial function will be quantified in the Goto-Kakizaki rat model of type 2 diabetes and its Wistar control. Function will be determined *in vivo* by phosphorus magnetic resonance spectroscopy and *in vitro* by high-resolution respirometry across a broad range of challenges to determine any mitochondrial and/or metabolic limitations.

2.3.3 Determine if blood flow delivery could limit mitochondrial respiration in the Goto-Kakizaki rat model of type 2 diabetes:

Rats will be chronically instrumented for measures including blood pressure and heart rate using intra-arterial telemetry placed within the descending aorta and tested consciously for cardiovascular and muscle performance. Further, animals will be tested for blood flow delivery during identical experimental parameters that mitochondrial function was quantified to determine if reduced blood flow could limit respiration.

**CHAPTER 3: TOP-DOWN MODELING OF ENERGY METABOLISM
PREDICTS SUBSTRATE UTILIZATION IN SKELETAL MUSCLE
MITOCHONDRIA**

3.1 Summary

Skeletal muscle mitochondrial ATP homeostasis involves feedback regulation from the drivers of respiration (ADP, Pi) and modulation by pyridine nucleotides (NADH/NAD⁺) to sustain metabolic workloads. This coincides with a shift in substrate utilization from fat-towards carbohydrate-oxidation as metabolic workloads increase; however, the driving force for this shift is not as well understood. In this study, muscle energetics were quantitatively described from ATP hydrolysis products and NADH/NAD⁺ and the mechanism for substrate selection was explained through a combination of computational and experimental approaches. Computational analysis demonstrates that pyruvate dehydrogenase activation causes an increase in NADH/NAD⁺ which subsequently causes partial inhibition of beta-oxidation. In two independent experiments, this mechanism was tested by chemically activating carbohydrate oxidation and pharmacologically manipulating muscle mitochondrial content. This computational model quantitatively predicts mitochondrial substrate selection and provides crucial insight into diseases involving mitochondrial dysfunction and by extension a firm rationale for design of mitochondrial therapeutics.

3.2 Introduction

Muscle-specific aerobic capacity is the maximal ATP demand that can be supported by aerobic respiration and is dictated by the capacity for mitochondrial oxidative phosphorylation (MOP) (102, 140, 283). MOP capacity in skeletal muscle is a function of both the content (number or volume) of mitochondria and the inherent capacity per organelle and thus can be altered by changes in mitochondrial content or organelle function. This can be appreciated from studies involving athletic training where MOP capacity is improved by increasing mitochondrial content (102, 147, 149, 157). Conversely, inactivity decreases MOP capacity by reducing mitochondrial content (25, 143, 271, 366). Likewise, a reduction in mitochondrial function is directly related to reduced MOP activity as shown by titrated inhibition of mitochondrial complex III (243). In skeletal muscle, MOP capacity is routinely determined utilizing the creatine kinase (CK) equilibrium and measuring phosphorylation rates in response to varied contractile intensities via phosphorus magnetic resonance spectroscopy (³¹PMRS). For example, the time constant for phosphocreatine (PCr) recovery post-contraction and amount of PCr hydrolyzed during contraction are inversely proportional to MOP capacity (169, 249, 256, 283). For a given work intensity, ADP phosphorylation rates critically depend on adequate substrate utilization to support flux through the tri-carboxylic acid (TCA) cycle and oxygen supply to the electron transport system (ETS) (149, 198). If either of these factors become limiting, ADP phosphorylation rates will slow and sustainable muscle force will decline.

Skeletal muscle primarily oxidizes fatty acids and carbohydrates to fuel the TCA cycle. In resting muscle, fatty acids are the primary substrate utilized but as contractile intensity is increased this shifts towards carbohydrate (150, 389). Pyruvate

dehydrogenase (PDH) plays a direct role in this shift since its activity is linearly related to contractile intensity (159, 377) leading to an increase in carbohydrate utilization (51, 158, 242, 328, 367). In the absence of a shift towards carbohydrate utilization, high workloads are not sustainable by fat oxidation alone. The direct impact of substrate utilization on muscle energetics was quantified with ^{31}P MRS following chemical activation of PDH (176). Activated PDH resulted in less PCr hydrolysis and an increase in the magnitude of the free energy of ATP hydrolysis (ΔG_{ATP}) during contraction despite similar ATP demands. This was attributed to increased NADH/NAD⁺ and proton motive force (pmf) from increased carbohydrate utilization (176). These results suggested a quantitative relationship between substrate utilization and muscle energetics; however, the precise interplay between substrate utilization and muscle energetics during exercise at the cellular level is difficult to measure directly and has eluded a comprehensive understanding. To accomplish this a top down mathematical model linking energy demand with supply in skeletal muscle mitochondria was developed and experimentally verified.

A computational model describing the regulation of oxidative metabolism has been developed for cardiac muscle (21, 235) incorporating a lumped TCA cycle module that includes two non-linear Hill functions for metabolite and redox feedback. Assuming this type of feedback regulation of energy metabolism is conserved across striated muscle (70), this approach was used to develop insight into mechanisms of substrate utilization in skeletal muscle during increases in ATP demand. This new model of skeletal muscle energetics includes carbohydrate and beta-oxidation contributions to mitochondrial ATP production calibrated with published observations (175, 176). Parameters were optimized

using ^{31}P MRS data on PCr and inorganic phosphate (Pi) dynamics during twitch contractions (176) and data on relative rates of carbohydrate and fat driven oxygen consumption (175). The model was then used to simulate carbohydrate and fat metabolism, muscle energetics, and oxygen consumption with fully activated PDH. Finally, predictions were made on how these bioenergetic variables are affected following a reduction in aerobic capacity. Model analysis reveals that when muscle aerobic capacity is decreased, there is a shift in substrate utilization towards carbohydrates at lower absolute ATP demands. Taken together, the current work demonstrates the interdependence between substrate utilization and metabolic demand in muscle. The understanding of this relationship is crucial in its application to the study of metabolic diseases associated with reduced muscle aerobic capacity or mitochondrial function including diabetes (311–313), COPD (3, 53), and heart failure (301).

3.3 Methods

3.3.1 Model Development

The model of oxidative phosphorylation by Malyala et al. (235) was updated to incorporate separate carbohydrate and fatty acid TCA cycle flux contributions. For simplicity, pyruvate is represented in the model as the carbohydrate source, and palmitate is represented as the fatty acid source. As pyruvate and palmitate oxidation consume different amounts of oxygen per carbon skeleton, they differ in their contribution toward pmf generation. Specifically, complete oxidation of acetyl-CoA from pyruvate produces 4 NADH and 1 ubiquinol (QH_2) while each acetyl-CoA from palmitate produces 4 NADH

and 2 QH₂. Thus, the oxidation of fatty acids cost more oxygen per acetyl-CoA. To account for these production differences of redox equivalents, the differential equations for NADH and QH₂ concentrations in the Malyala et al. model were modified as shown in Eqs. 1 and 2. NAD⁺ and Q concentrations were solved for algebraically using a total nicotinamide adenine nucleotide pool of 3 mM and a quinone pool of 20 mM, as described in Malyala et al.

$$\frac{d[NADH]}{dt} = (4J_{carb} + 4J_{fat} - J_{CI}) / V_{mito} \quad (1)$$

$$\frac{d[QH_2]}{dt} = (J_{CI} + 1J_{carb} + 2J_{fat} - J_{CIII}) / V_{mito} \quad (2)$$

The fluxes J_{carb} , J_{fat} , J_{CI} , and J_{CIII} represent the NADH and QH₂ production rates from carbohydrate oxidation, NADH and QH₂ production rate from fatty acid oxidation, and NADH consumption and QH₂ production rate from complex I, and QH₂ consumption rate from complex III, respectively. The parameter, V_{mito} , is mitochondrial matrix water space per mg mitochondria (1 μl/mg). The rate expressions for complexes I and III are as given in Malyala et al. (235). The fluxes for carbohydrate and fatty acid consumption rates are given in Eqs. 3 and 4.

$$J_{carb} = X_{carb} \frac{Q^{n_{carb}}}{Q^{n_{carb}} + K_{Qcarb}^{n_{carb}}} \frac{[NAD^+]}{[NAD^+] + K_{Ncarb}[NADH]} \quad (3)$$

$$J_{fat} = X_{fat} \frac{Q^{n_{fat}}}{Q^{n_{fat}} + K_{Qfat}^{n_{fat}}} \frac{[NAD^+]}{[NAD^+] + K_{Nfat}[NADH]} \quad (4)$$

In these expressions, Q is the mass action term for ATP hydrolysis ($[ADP]_m[Pi]_m/[ATP]_m$) in the mitochondrial matrix, and X 's, K 's, and n 's are the carbohydrate and beta-oxidation specific parameters governing the metabolic and redox regulation of each pathway. The value of these adjustable parameters and their definitions are given in Table 3.

Table 3. Adjustable Model Parameters			
Parameter	Description	Value	Units
X_{carb}	carbohydrate dehydrogenase activity	261.7	nmol/mg/min
K_{Ncarb}	carbohydrate redox feedback constant	0.1	-
K_{Qcarb}	carbohydrate metabolite feedback constant	0.08	M
n_{carb}	carbohydrate metabolite Hill function constant	2	-
X_{fat}	fatty acid dehydrogenase activity	99.4	nmol/mg/min
K_{Nfat}	fatty acid redox feedback constant	1.96	-
K_{Qfat}	fatty acid metabolite feedback constant	0.003	M
n_{fat}	fatty acid metabolite Hill function constant	1.26	-
$K_{Qcarb,DCA}$	DCA-activated carbohydrate metabolite feedback constant	0.045	M
ρ_{mito}	mitochondrial volume fraction	3.1	%

High energy phosphate pools and initial conditions for skeletal muscle were determined from work performed by Kasper et al. (176). In addition, modifications to the model were performed to allow for the simulation of skeletal muscle energetics as measured directly by ^{31}P MRS. Specifically, the creatine kinase and myosin ATPase reactions were added to the model. PCr dynamics measured by ^{31}P MRS are directly related to ATP via the creatine kinase equilibrium (253, 255). These reactions are listed in Eqs. 5-7. The stoichiometric coefficient α represents the fractional proton uptake or

release by the net reaction and depends on temperature, ionic strength, and available metabolites.



The myosin ATPase rates were obtained from reported values calculated from the initial decline in PCr ³¹PMRS data (176). Equation 8 was used in the model where X_{ATPase} is the rate of ATP hydrolysis quantified from the data and dependent on the stimulation frequency, and R_{ATPase} is a feedback constant equal to 32.9 M⁻¹. This value was adjusted from Wu et al. (417) so that ATP hydrolysis products do not significantly lower the ATPase rate during twitch contractions.

$$J_{ATPase} = X_{ATPase} / (1 + R_{ATPase} [ATP] / [ADP] / [Pi]) \quad (8)$$

The overall model diagram is presented in Figure 5A. The model was numerically integrated using MATLAB (R2019a) and the stiff ode solver ode15s using a relative error tolerance of 10⁻⁴ and an absolute error tolerance and 10⁻⁹. Backward differentiation formulas were used to solve the system. Parameter optimization was done using a

desktop PC (64-bit operating system and x64-based processor Intel1core™ i7-7700 CPU @3.60GHz and 16 GB RAM) using the Parallel Computing Toolbox. A custom global optimization algorithm followed by the gradient-based optimization algorithm, fmincon, was used to identify the model parameters. The cost function used to fit the data was:

$$f = \frac{1}{N_D} \sum_i ((y_i - d_i) / \sigma_i)^2$$
 where N_D is the total number of data points, y_i is the model

output corresponding to data d_i , and σ_i is the standard deviation for data d_i . Local sensitivity analyses were also performed to determine model output sensitivities to the adjustable parameters. These values were computed using the complex method (357) as described in Bazil et al. (235).

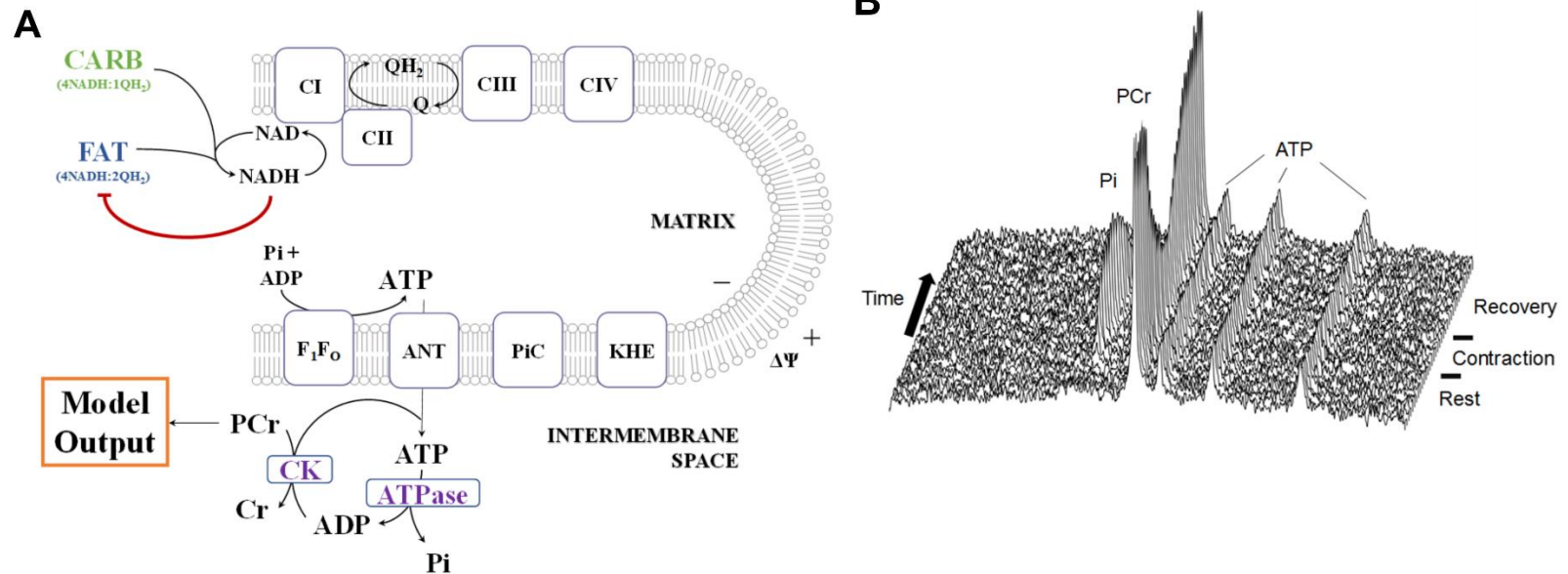


Figure 5. Model schematic and representative PMRS data. A simplified representation of the skeletal muscle model diagram that incorporates separate carbohydrate (CARB) and fatty acid (FAT) contributions is shown (A). The model output for phosphocreatine (PCr) was used to compare with the skeletal muscle experimental studies. The model input is ATPase rate calculated from the initial PCr decline during twitch contractions in vivo. A representative stack plot of high energy phosphates in gastrocnemius muscle before, during, and after electrically stimulated twitch contractions at 0.5 Hz (B). During contraction PCr is hydrolyzed and [ATP] stays constant via the near equilibrium CK reaction.

3.3.2 ³¹Phosphorus Magnetic Resonance Spectroscopy (³¹PMRS)

Animals were fasted 12 hours overnight and on the day of experiment were anesthetized at 5% Isoflurane in 100% O₂ for three minutes and maintained at 1-2% throughout experimentation. Animals were weighed and their blood glucose was measured before being prepared for *in situ* stimulation of the triceps surae (gastrocnemius, plantaris, soleus) muscle group within a ³¹PMRS surface coil probe as described previously (176, 220, 251). In brief, the hindlimb was secured in a custom-built NMR probe to a brass knee post via a tungsten pin inserted through the head of the femur, and the Achilles tendon was tied to an isometric force transducer. This orientation positioned the superficial gastrocnemius muscle over a 1.7 cm diameter surface coil wound from two turns of copper wire. The muscle was passively stretched to its optimal length (L₀) to give maximum peak tension in response to supramaximal stimulus (2-10 V, 2 ms duration) applied via bipolar platinum electrodes placed on the sciatic nerve. This protocol for stimulation ensures all muscle fibers are stimulated in the limb (8, 360) and avoids force summation which can confound interpretation and reduces the dynamic range for study. Respiration and rectal temperature were monitored and maintained between 45-60 breaths per minute and 36-37 °C, respectively.

Phosphorus NMR spectra of the superficial gastrocnemius muscles were acquired in the Fourier transform mode at 161.8 MHz on a Bruker AM400 wide-bore spectrometer (9.4 T, 7.4 cm vertical bore magnet) housed in the Department of Physiology. The surface coil was tuned for phosphorus (161.8 MHz at 9.4T) with the animal in place and the field was shimmed using the proton signal from muscle water. For phosphorus spectra, the pulse width (10 μs) was chosen to optimize signal-to-noise ratio in this study at a repetition

time of 3.25 s. Prior to stimulation, two high-resolution phosphorus spectra were acquired with 128 averages. One spectrum allowed complete T_1 relaxation (interpulse interval 15 s) and one at time optimized for during contraction (3.25 s). Spectra were directly compared to calculate saturation factors based on ratios of fully relaxed integrals with 3.25 s TR intervals. During experimental acquisition, phosphorus spectra were continuously acquired over 26 s intervals (sweep width 8012 Hz, 4096 data points, interpulse interval 3.25 s, 16 averages) during 2 min 36 s of resting muscle, 5 min 12 s of isometric twitch stimulation, and 7 min 48 s of recovery. A representative stackplot of PCr during experimental acquisition is presented in Figure 5B. Twitch stimulations were performed in random order for 0.35, 0.5, and 0.75 Hz frequencies. After acquiring recovery spectra for each stimulation, animals recovered for ten extra minutes and resting metabolites and pH were verified before subsequent stimulation. Following this series of stimulations dichloroacetate (DCA), a potent activator of PDH, was administered intraperitoneally (150 mg/kg) and allowed to incubate for 1 h (176). Subsequently, each frequency of stimulation was identically performed as previously to determine the effect of DCA on muscle energetics. A representative stack plot (Figure 5) shows data collected from a non-DCA treated animal during the experimental protocol.

The summed free-induction decays were multiplied by a 30 Hz exponential line broadening before Fourier transformation. Phosphorus signal integrals were computed using jMRUI AMARES fitting software (380). For each stimulation, results were expressed as metabolite concentrations after normalizing to total phosphate integral (196) and determined from resting phosphocreatine concentrations reported by Kasper et al. (176).

3.3.3 Model Simulations

Computational simulations of the substrate utilization data and DCA treated muscle energetics were performed to match *in vivo* experimental conditions as close as possible. The kinetic parameters for carbohydrate and fatty acid oxidation rates (Eqs. 3 and 4) along with the mitochondrial volume fraction (ρ_{mito}) were adjusted to fit the experimental data. These values are given in Table 3. Three phases of metabolic activity were simulated: 2 min 36 s of rest, 5 min 12 s of stimulation, and 7 min 48 s of recovery. Model simulations were performed using a resting ATPase rate of 0.008 mM/s (169, 410) and contractile ATPase rates (Eq. 8) calculated experimentally from 0.35, 0.5, and 0.75 Hz stimulation frequencies. These frequencies of stimulation were chosen such that glycolytic contributions to ATP production are negligible (155, 220). At this time, the model does not include glycolysis and is strictly based on MOP. Furthermore, anaerobic ATP production by glycolysis beyond the aerobic range can significantly influence PCr dynamics and confound interpretation of PCr recovery rates (105, 215, 392).

Once the model was calibrated using the substrate utilization and DCA data, it was used to predict how changes in relative energetic demand influence substrate utilization and energetics. We define relative energetic demand as the ATP demand (ATPase rate) relative to the maximal capacity for MOP. The maximal capacity for MOP is a function of the mitochondrial volume fraction and intrinsic metabolic activity of the mitochondria. To lower the maximal MOP capacity, we reduced the mitochondrial volume fraction by 50% and simulated the model at various ATP demands. All other parameters were unchanged from the control. In these simulations, we assumed the intrinsic metabolic activity is unchanged (i.e., protein and lipid composition are not significantly altered). With a

decrease in ρ_{mito} , the relative energetic demand will increase. However, how this change impacts substrate utilization and energetics is unknown. We then tested the model predictions on mitochondrial function and PCr dynamics when MOP capacity is reduced.

3.3.4 Altering relative energetic demand: in vivo

Mitochondrial content was altered in 4 groups of rats using methimazole (MMI) administered in drinking water (0.025% w/v) for 2, 4, 6, and 8 weeks of treatment. MMI is a thyroid synthase inhibitor that results in reduced muscle mitochondrial content in a direct relation with duration of treatment. Energetic measures were acquired as described above using ^{31}P MRS at a range of intensities (0.35 – 0.75 Hz) to determine apparent aerobic capacity from contractile energetic steady-states and PCr recovery time constants. For each group of MMI-treated animals plus a control group, mitochondrial content was determined by citrate synthase assay described by Srere et al. (358). Relative changes in citrate synthase activity compared to control were used to determine percent change in mitochondrial content to directly compare with computational simulations of energetics.

3.4 Results

The list of adjustable parameters for this model include the activities of carbohydrate- and fatty acid-dependent catabolic pathways in mitochondria along with the associated regulatory redox and metabolite parameters (Table 3). Mitochondrial volume fraction was optimized for skeletal muscle and is within the expected range of 1-

5% for the fiber types included in the experimental analysis (398). Relative to carbohydrate metabolism, the fatty acid catabolic pathway shows greater inhibition at any given redox state. In contrast, carbohydrate metabolism responds to metabolite feedback to a greater extent than fatty acid metabolism. Treatment with DCA shifts the carbohydrate metabolite feedback so that this pathway is activated at lower levels of metabolic demand. Using these parameters, the present model simulates control and DCA data with remarkable accuracy. In addition, the model makes several predictions on the nature of substrate selection and the metabolic consequences of exceeding aerobic capacity in skeletal muscle.

3.4.1 Activation of PDH Predicts Reduced PCr Hydrolysis and Greater Reliance on Carbohydrates

Model simulations of intramuscular PCr concentrations for control and DCA treated muscle during rest, contraction, and recovery for 0.35, 0.5, and 0.75 Hz twitch frequencies are presented in Figure 6A. These simulations highlight the model's ability to capture *in vivo* phosphoenergetics during ATP utilization and recovery phases in skeletal muscle in both control and DCA treated muscle. At the beginning of twitch contractions, the rate of ATP hydrolysis increases through activation of contractile ATPases (myosin, SERCA) but ATP content is predominantly buffered by PCr by the near equilibrium CK reaction (253, 256, 410). As contraction continues, the products of ATP hydrolysis (ADP and Pi) increase and stimulate mitochondrial ATP synthesis until ATP demand is matched. This results in a gradual decline in PCr until a steady state is reached a few minutes after the twitch contractions begin. During recovery, PCr resynthesis leads to a dramatic shift in

high energy phosphates back to resting conditions (low ADP and Pi). During this entire sequence, the CK reaction maintains ATP at near constant levels. DCA treatment increases PDH activity and shifts substrate utilization towards carbohydrates (176). As a result, less PCr is hydrolyzed and PCr levels are higher for a given metabolic load. To account for the effect of DCA on PDH, the model parameter K_{Qc} was lowered so that the activity of PDH at a given metabolic load increases. This results in an increase in the magnitude of ΔG_{ATP} (ATP hydrolysis potential), less PCr hydrolyzed during contractions, and a minimal change in PCr levels at rest.

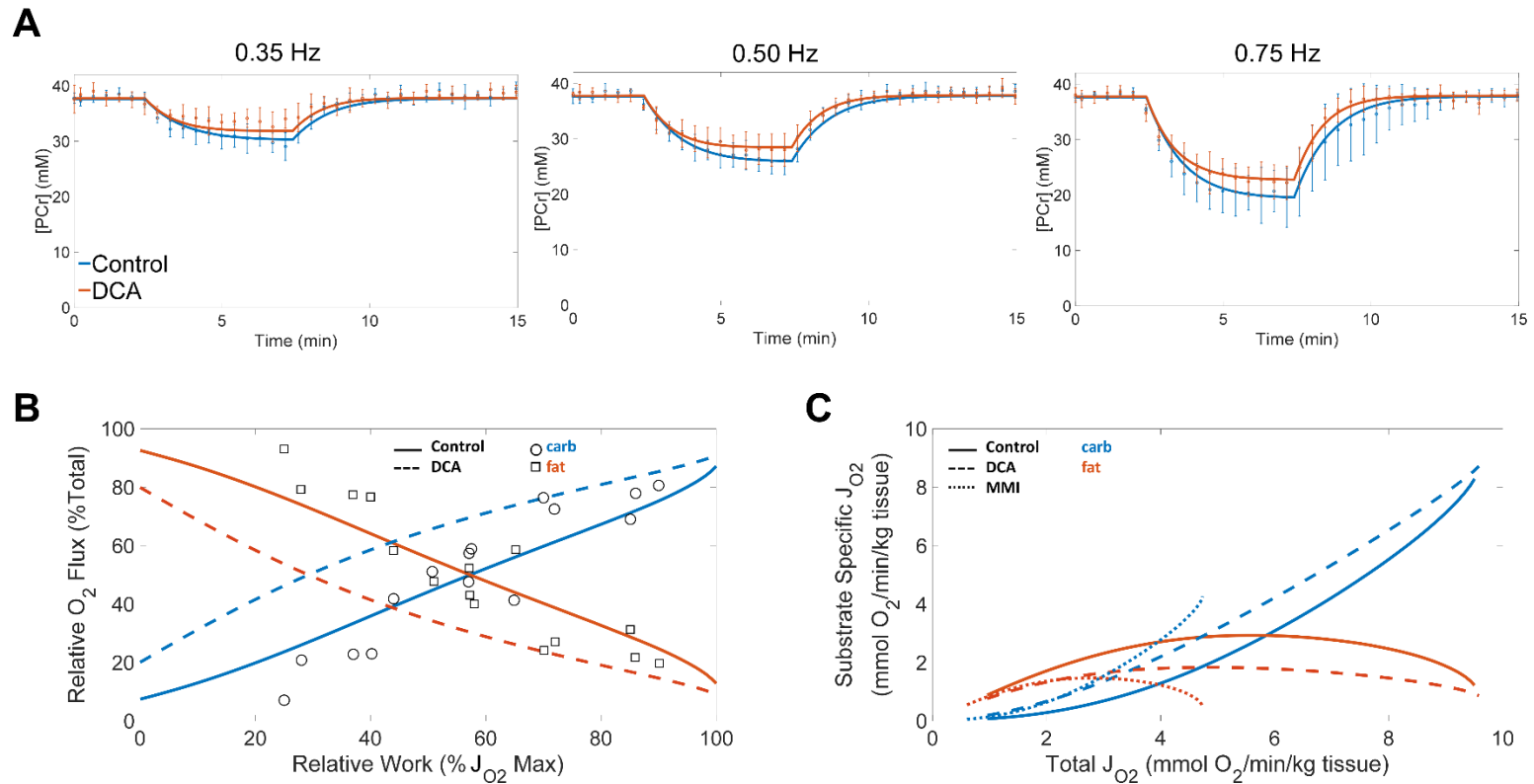


Figure 6. DCA treatment increases PCr levels during twitch contractions by increasing carbohydrate oxidation. The model was used to simulate the experimental protocol for 0.35, 0.50, and 0.75 Hz twitch contractions. With the DCA treatment, the PCr level does not decline as much as the control condition (A). For these simulations, the ATPase rate was set to 0.095 mM/sec, 0.162 mM/sec, and 0.253 mM/sec for twitch frequencies of 0.35 Hz, 0.50 Hz, and 0.75 Hz, respectively. Data shown as \pm SD ($n=6-7$). As ATP demand increases, muscle switches its fuel source from fatty acids to carbohydrates (B). At approximately 60% J_{O_2} max, the oxygen consumption rates from fatty acids (red) and carbohydrates (blue) are nearly equal. Model simulations are represented as lines and data are given as symbols (175). The model predicts that DCA treatment (dashed lines) shifts the crossover point to approximately 30% J_{O_2} max. Carbohydrate J_{O_2} was computed from Eq. 3 and assuming 5/2 O_2 consumed per reducing equivalents generated. Fatty acid J_{O_2} was computed from Eq. 4 and assuming 6/2 O_2 consumed per reducing equivalents generated. Substrate specific oxygen consumption at a given total ATP demand shifts from control (solid lines), in DCA, and 4-week treated MMI (dotted lines) conditions (C). ATP demand is represented as total tissue oxygen consumption rate. DCA treatment causes carbohydrate flux to increase and fatty acid flux to decrease at any given ATP demand. This leads to the crossover point shifting to the left. MMI treatment cuts the maximum tissue oxygen consumption rate in half and causes the crossover point to shift further to the left.

At rest, fatty acids comprise over 90% of the oxygen consumption as shown in Figure 6B. As the relative workload increases, relative oxygen consumption from carbohydrates begins to rise, and the oxygen consumption from fatty acids reciprocally drops. At around a 60% relative workload, the oxygen consumption from carbohydrates and fatty acids are equal. This is known as the crossover concept of substrate utilization (45). When the workload approaches 100% of maximum oxygen consumption, carbohydrate oxidation makes up nearly 100% of substrate utilized. However, DCA treatment shifts the crossover point to the left to approximately 30% of maximum oxygen consumption according to model predictions. In addition, the relative resting oxygen consumption rate due to carbohydrates increases from 10% to 20%. Prior studies have shown that activation of PDH and ensuing shift towards carbohydrate utilization *in vivo* results in reduced PCr hydrolysis during contraction in both human subjects (328) and rats (176). Model predictions are congruent with these studies.

3.4.2 Reducing Aerobic Capacity Predicts Increased Carbohydrate Oxidation

Metabolic and redox feedback are essential to maintain energy homeostasis in muscle. The magnitude of the feedback signals required to maintain this homeostasis is critically dependent on the mitochondrial content within the tissue. Therefore, the computer model was used to predict how a large reduction (50%) in the mitochondrial volume effects energetics and substrate utilization. To test model predictions, rats were treated with MMI administered in drinking water for 2, 4, 6, and 8 weeks. This treatment lowered the muscle-specific aerobic capacity inferred by citrate synthase activity and PCr recovery time constants. Citrate synthase activity was 12.11 ± 1.45 , 8.7 ± 0.62 , $6.57 \pm$

1.35, 5.45 ± 1.35 , and 3.60 ± 1.84 $\mu\text{mol}/\text{min}/\text{g}$ and PCr recovery time constants were 61 ± 14 , 100 ± 21 , 116 ± 16 , 123 ± 12 , and 169 ± 41 s for 0 (n=3), 2 (n=3), 4 (n=3), 6 (n=3), and 8 (n=2) weeks of treatment respectively. At 4 weeks of treatment, muscle aerobic capacity was ~50% of controls and used to compare with computational predictions. All data is presented as mean \pm SD.

The absolute flux of substrate utilization for control, DCA, and 4-week MMI treated tissue for a given workload is shown in Figure 6C. When comparing substrate consumption at a given absolute workload, more carbohydrate utilization is required in the MMI condition to maintain tissue energetics versus fatty acids for lower workloads. This causes the crossover point to shift far to the left. However, when accounting for the aerobic capacity being reduced by 50%, the carbohydrate and fatty acid utilization rates relative to the 4-week treated MMI aerobic capacity are identical to the control condition. In the DCA treated tissue, carbohydrate flux is increased relative to control in conjunction with a reciprocal drop in fatty acid flux. These results reinforce the relationship between substrate utilization and the workload relative to aerobic capacity described above and by Brooks et al. (45).

Model predictions compared to experimental data of PCr dynamics in 4-week MMI treated animals are shown in Figure 7A. Nearly twice as much PCr is hydrolyzed for a given workload compared to controls, and the PCr recovery time constant is doubled. These results corroborate the computational predictions. The slight deviation between computational simulations and experimental data at 0.5 Hz stimulation frequency is due to a glycolytic contribution to ATP production. At this stimulation intensity, the aerobic capacity is nearly exceeded. At 0.75 Hz, the ATP demand far exceeds the aerobic

capacity, and the muscles begin to heavily rely on glycolysis for ATP, the muscles fatigue, and ATP demand drops experimentally. The deviation between computational and experimental 0.75 Hz thus is expected since neither fatigue nor glycolytic contribution are present in the computational model.

Model predictions of Pi and ADP dynamics for the control, DCA, and 4-week treated MMI conditions for each stimulation frequency are given in Figure 7B and Figure 7C. As the stimulation intensity increases, both Pi and ADP levels increase. In DCA treated tissue, this increase is not as much as the control; conversely, Pi and ADP increase more in the MMI treated tissue. At the highest simulation intensity, the mitochondria from the MMI treated tissue are unable to match the ATP demand. This result is expected as mentioned above.

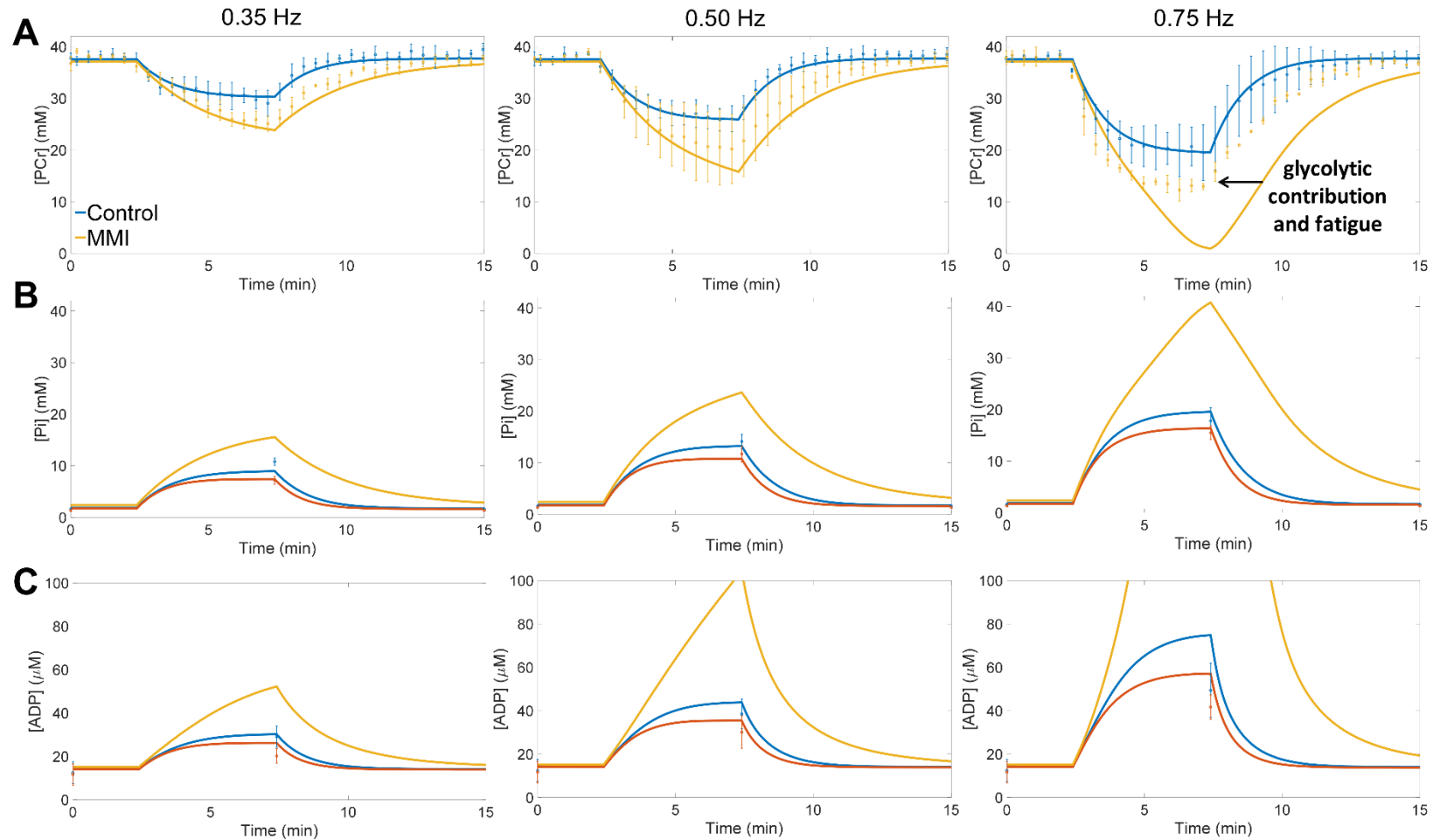


Figure 7. Model predictions of PCr dynamics in 4-week MMI treated muscle (A). Stimulation frequencies greater than 0.50 Hz exceed the aerobic capacity and leads to a significant ATP contribution by glycolysis. The muscle also begins to fatigue. Thus, the model results for the 0.75 Hz condition are expected as it does not include glycolysis or fatigue. Model predictions of the ATP hydrolysis products Pi (B) and ADP (C) dynamics match the increase observed during twitch contractions. As explained in Panel A, the model simulations for the 0.75 Hz condition are expected due to the absence of fatigue and glycolysis. Data shown as +/- SD (n=6-7).

The model predictions for the control, DCA, and 4-week treated MMI conditions for carbohydrate and fatty acid oxidation rates for each stimulation frequency are shown in Figure 8A and Figure 8B. In all conditions, the twitch contractions cause a rise in the rate of carbohydrate oxidation. However, DCA treatment leads to a higher rate than control, and MMI treatment causes even greater stimulation of carbohydrate metabolism. At the extreme end of ATP demand relative to the aerobic capacity, fatty acid metabolism drops to very low levels compared to carbohydrates. As a result, carbohydrates make up nearly all substrate being consumed. This is most apparent when the twitch stimulation frequency was 0.75 Hz for the MMI treated tissue. These results are a direct consequence of the interaction between carbohydrate and fatty acid metabolism (see Discussion section “*NADH feedback explains carbohydrate inhibition of fat oxidation*”).

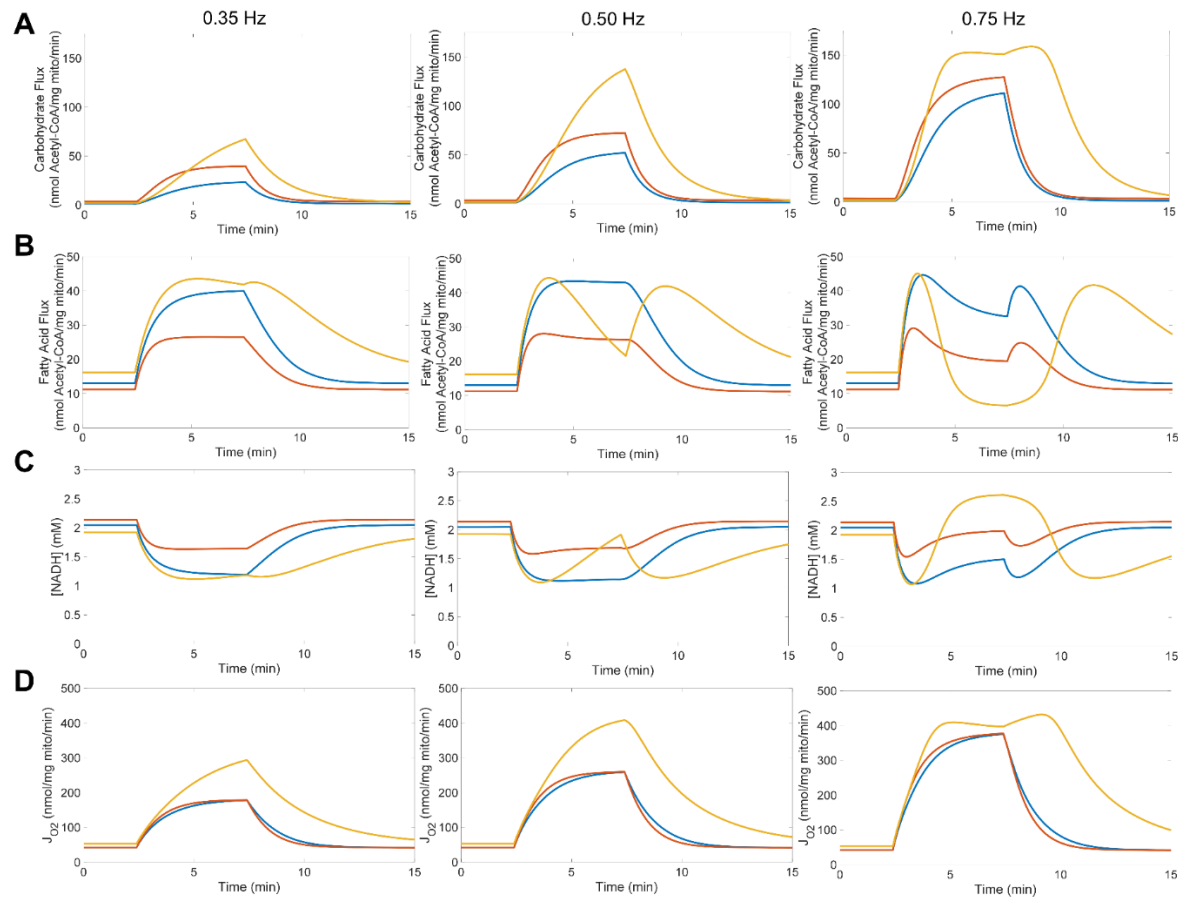


Figure 8. Model prediction of carbohydrate (A) and fatty acid (B) fluxes for control (blue), DCA (red), and 4-week MMI treated (yellow) conditions at the different twitch stimulation frequencies. DCA treatment causes an increase in carbohydrate flux which in turn suppresses fatty acid oxidation rates relative to the control. In contrast, MMI treatment causes an increase in both carbohydrate and fatty acid oxidation rates relative to control. However, as ATP hydrolysis products accumulate during the twitch contractions, fatty acid metabolism is decreased due to accumulation of mitochondrial NADH. Mitochondrial NADH dynamics during twitch contractions reveal complex dynamics (C). Control and DCA treated mitochondria burn oxygen at the same rate for a given stimulation frequency (D); however, MMI treated mitochondria increase their respiratory activity per mitochondrion to compensate for the lower mitochondrial content.

Model predictions of mitochondrial NADH and J_{O_2} dynamics for control, DCA, and 4-week treated MMI conditions are given in Figure 8C and Figure 8D. At low intensities, a mismatch between NADH production and consumption leads to a net decrease in NADH levels. This trend continues for 0.5 Hz for the control and DCA conditions. For the MMI condition at this stimulation frequency, ATP hydrolysis products accumulate to levels that activate the carbohydrate oxidation pathway, and NADH levels begin to rise. This increase leads to a decrease in fatty acid oxidation rates because the fatty acid NADH/NAD⁺ feedback parameter is larger than the feedback parameter for carbohydrates. Thus, fatty acid metabolism is inhibited when the NADH/NAD⁺ levels are high, but carbohydrate metabolism is less affected. At the highest stimulation frequency, the control and DCA condition behave in a similar manner. Computational simulations of oxygen consumption show no differences between control and DCA treated mitochondria. In contrast, MMI treated mitochondria must increase their respiratory activity per mitochondrion to compensate for the lower mitochondrial content. ATP demand at the highest stimulation frequency exceeds the aerobic capacity of the MMI treated condition due to reduced mitochondrial content.

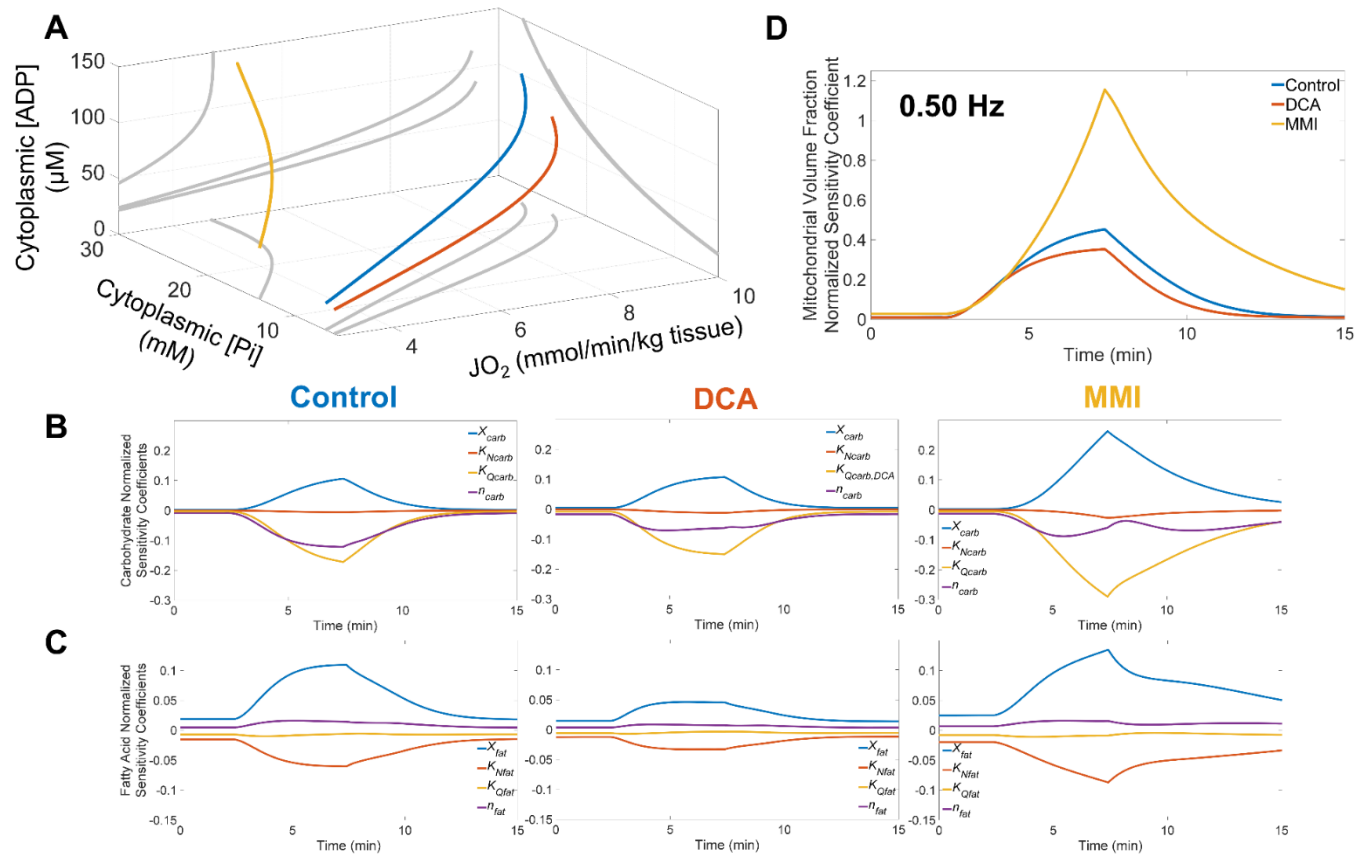


Figure 9. Cytoplasmic ADP concentrations needed to match ATP demand are a function of Pi and mitochondrial function. 3D plot of steady-state ADP and Pi concentrations for a given rate of oxidative phosphorylation for the control, DCA, and 4-week treated MMI conditions (A). Grey lines are 2D projections of the 3D plot on each axis. Mitochondrial volume fraction is the most sensitive parameter with respect to PCr dynamics calculated at 0.5 Hz stimulation frequency (B). DCA treatment decreases the importance of the volume fraction due to an increase in intrinsic metabolic activity per mitochondrion. However, the volume fraction is extremely important in the MMI condition as this stimulation frequency exceeds the aerobic capacity for this treatment. Local sensitivities computed with respect to PCr dynamics of carbohydrate (C) and fatty acid (D) related kinetic parameters elucidates the mechanism responsible for substrate selection in exercising muscle for the 0.5 Hz stimulation frequency. Carbohydrate metabolism is more important than fatty acid metabolism during ATP demand. In contrast, fatty acid metabolism is important for energy metabolism at rest. DCA treatment decreases the reliance on fatty acid metabolism, while all pathways become critical to sustain energy metabolism after MMI treatment. The sensitivity coefficient trends are similar for 0.35 Hz and 0.75 Hz stimulation frequencies.

Steady-state ADP and Pi concentrations at a given rate of oxidative phosphorylation for the control, DCA, and MMI conditions is shown in Figure 9A. As the ATP hydrolysis products (ADP and Pi) accumulate, they stimulate both the carbohydrate and fatty acid metabolic pathways in mitochondria. However, at high workloads, NADH builds up due to carbohydrate oxidation and inhibits fatty acid oxidation. Since carbohydrates are a more efficient fuel with respect to ATP production and oxygen consumption, DCA treatment leads to both lower ADP and Pi concentrations for a given rate of respiration. In contrast, metabolites must reach significantly higher levels to stimulate oxidative phosphorylation to meet the tissue ATP demand when mitochondrial content is reduced in MMI-treated animals.

3.4.3 Model Sensitivity Analysis

Sensitivity coefficients of the model parameters indicate how a small change in the parameter changes a given model output. A parameter is deemed important with respect to a model output if its normalized sensitivity coefficient is large. For example, a value of 0.1 means that an increase in the parameter value by 10% will result in the model output increasing by 1%. In Figure 9B and Figure 9C, the normalized local sensitivity coefficients for the 0.50 Hz stimulation frequency condition are shown. These sensitivity coefficients are with respect to the concentration of myoplasmic PCr and include carbohydrate and fatty acid metabolism parameters for each treatment condition. These results do not qualitatively change at other stimulation frequencies to a significant degree. Activity parameters all have a positive effect on PCr dynamics however, their biggest effect occurs during twitch stimulation. In contrast, an increase in the metabolite feedback

constants ($K_{Q_{carb}}$ and $K_{Q_{fat}}$) do not have the same effect. For the carbohydrate pathway, increasing $K_{Q_{carb}}$ leads to a relatively large decrease in overall carbohydrate metabolism. This is because a right-shift in the metabolite feedback constant yields a lower metabolite activation value. In contrast, the fatty acid metabolite feedback constant has only a minimal effect on fatty acid fluxes because its value (as given in Table 3) is too low with respect to the range of values the feedback factor Q ($[ADP]_m[Pi]_m/[ATP]_m$) takes on during the twitch stimulations. Therefore, the metabolite feedback function for fatty acids is close to the maximum value in nearly all conditions. Consequently, the carbohydrate metabolic pathway is much more sensitive to metabolic feedback than the fatty acid pathway. The sensitivity coefficients for the metabolite feedback Hill coefficients for carbohydrate metabolism follow similar trends to its respective metabolite feedback constant. This is because the carbohydrate metabolite feedback constant lies within the operating range of the feedback factor, Q . Thus, an increase in the corresponding Hill coefficient will decrease the metabolite feedback strength similarly to how an increase in the metabolite feedback constant decreases feedback. As with the fatty acid metabolic feedback constant, an increase in the Hill coefficient for fatty acid metabolism has a weak, positive effect on PCr concentrations. In contrast, an increase in the fatty acid redox feedback constant has a large, negative effect on the PCr concentrations. The PCr concentration is not very sensitive to changes in the carbohydrate redox feedback constant. This means that the carbohydrate pathway is not as affected by the redox status as the fatty acid pathway. Altogether, these results demonstrate how and why the model predicts substrate switching between fatty acids at rest and carbohydrates during increases in ATP demand.

Of all the adjustable model parameters, the mitochondrial volume fraction is the most sensitive as shown in Figure 9D. As with Figure 9B and Figure 9C, the sensitivity values are computed with respect to PCr concentrations at 0.50 Hz stimulation frequency. For all treatment conditions, this parameter is most sensitive during twitch stimulations. Interestingly, DCA treatment leads to a decrease in sensitivity with respect to the mitochondrial volume fraction. This is because DCA treatment results in increased intrinsic metabolic activity per mitochondrion; therefore, fewer mitochondria are required to sustain a metabolic load below the aerobic threshold. In contrast, the sensitivity of this parameter is the highest with MMI treatment. This is because MMI treatment causes a decrease in the volume fraction and results in the largest impact on PCr levels. At a given ATPase rate, the PCr concentration is dependent on the rate of oxidative phosphorylation. The rate of oxidative phosphorylation is directly proportional to the amount of mitochondria, therefore it's not surprising that the mitochondrial volume fraction is the most sensitive among all the other adjustable parameters.

3.4.4 Model Application to Prior Studies Explains Differences in Aerobic Capacity

The PCr recovery time constant is perhaps the most widely used indicator for muscle aerobic capacity measured *in vivo* and is a function of mitochondrial content and of total creatine content (249, 283). For this reason, the model was tested across a dynamic range of mitochondrial content using data from MMI treated muscle and compared with data from the literature. Relative values for mitochondrial content were used to reproduce a figure presented by Paganini et al. in Figure 10. Model simulations were performed across a range of mitochondrial contents and designated by the solid

line. Subsequently, MMI data and literature values were used to populate the plots using merely reported values of mitochondrial content and τ . The model accurately describes changes in mitochondrial content in the present work (triangles, Figure 10A), rat literature values (circles, Figure 10B), and human literature values (squares, Figure 10B). Human data selected included controls compared with diabetics (288) and patients with peripheral arterial disease [PAD, (401)]. Data that fall below the predictive line cannot be explained by model predictions of mitochondrial changes and therefore are likely limited by oxygen or substrate supply. This is highlighted by the PAD patients that fall drastically below the line due to blood flow limitations. After vascular therapy increased blood flow, the PCr recovery time constant decreased and results in an upward shift towards the predicted line. Likewise, reduced τ in type 2 diabetes is mostly explained by changes in mitochondrial content but falls slightly below the line suggesting limited substrate or oxygen supply. Mitochondrial content for West et al. (401) was determined from Pipinos et al. (294) while content for Peterson et al. (288) was determined from Kelley et al. (179) and ATP synthesis rates converted to τ (378). Total creatine content was determined from Mogensen et al. (267).

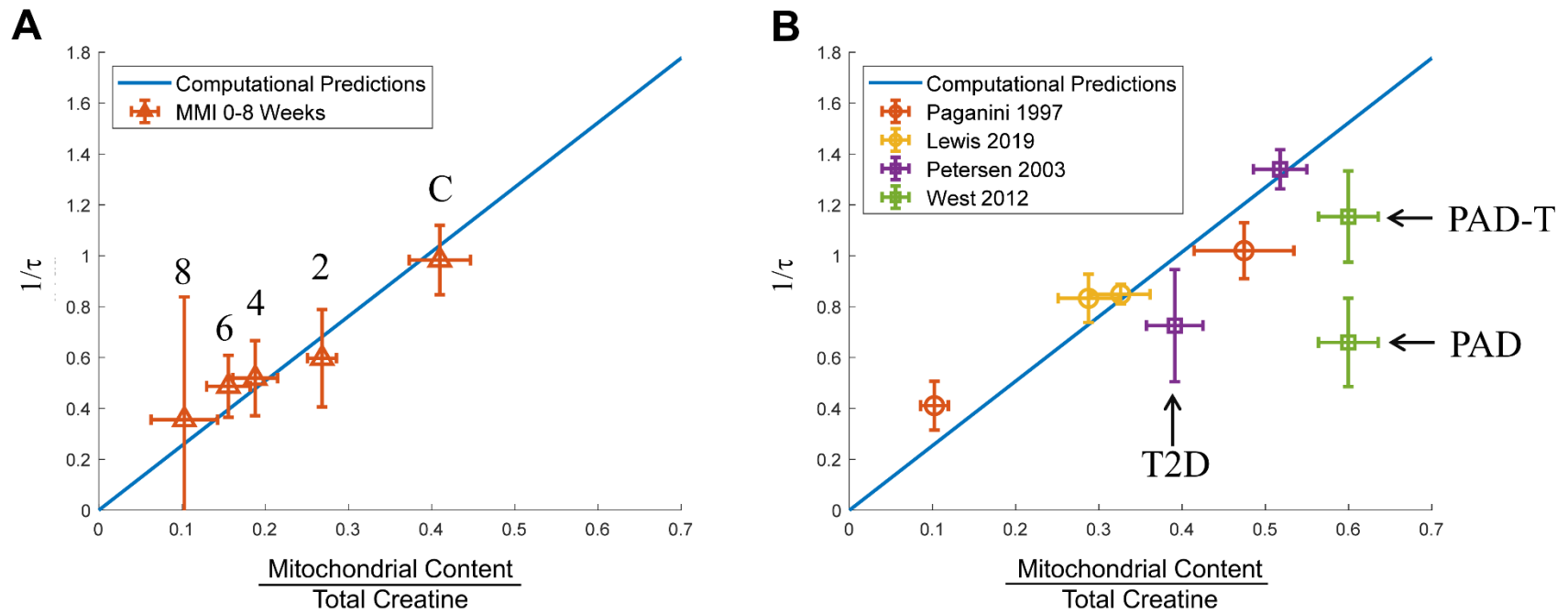


Figure 10. Model simulations of PCr recovery time constant (τ) as a function of mitochondrial content. Model simulations were compared to the stepwise change in mitochondrial content (A), as well as, literature data for both rats (circles) and humans (squares) (B). Data that fall far below the line depict metabolic limitations (e.g., oxygen). This is explicitly shown by PAD patient data. With vascular therapy (PAD-T), the PCr recovery time constant decreases resulting in an upward shift relative to the PAD control. Values are means \pm SE.

3.5 Discussion

The current study defines the quantitative relationship between skeletal muscle energetics and substrate utilization using a combined computational and experimental approach. The computational model accurately describes PCr dynamics across a wide range of contractile intensities, in addition to, substrate utilization rates relative to workload. Computer simulations predicted that when PDH was activated less PCr was hydrolyzed due to increased carbohydrate utilization. The computer model was then validated by testing its predictions on tissue energetics after a decrease in aerobic capacity. Specifically, the model predicted increased PCr hydrolysis during contraction and slowed PCr recovery times post-contraction. These predictions were experimentally confirmed *in vivo* after reducing muscle aerobic capacity with MMI treatment. Furthermore, the computational model predicts that a shift in substrate utilization towards carbohydrate in lower aerobic capacity muscle is necessary to sustain workloads similar to controls. Together these observations allow a quantitative understanding of the relationship between substrate utilization and tissue energetics. Specifically, the model predicts that ATP hydrolysis products activate PDH and PDH activation increases NADH/NAD⁺ to inhibit fatty acid oxidation. It is important to note that this mechanism is not mutually exclusive with additional control mechanisms that include CoA competition (190, 257), Ca²⁺ activation of dehydrogenases (117), and accumulation of fatty acid intermediates at high workloads (376).

3.5.1 Computational simulations accurately predict ³¹PMRS data

The primary controller for aerobic respiration is [ADP] and the apparent sensitivity to [ADP] is directly increased with increasing [Pi] (31, 170, 382). At the onset of muscle contraction, [ADP] and [Pi] are low and ATP resynthesis initially occurs through the CK reaction. During sustained workloads, [ADP] and [Pi] accumulate and increase mitochondrial respiration until ATP production via MOP matches muscle ATP consumption resulting in a PCr contractile steady-state (~3-5 minutes during isometric twitch contractions). While many have argued for a kinetic or “inertial” limitation to mitochondrial respiration (192, 322, 367), the present study explains these data without an inertial component in agreement with earlier studies (250, 256, 319, 325). The absence of mitochondrial “inertia” is perhaps best demonstrated experimentally by partially or fully removing the CK equilibrium and measuring the response time for MOP. If mitochondrial “inertia” were present, a reduction in creatine content by β -GPA feeding (creatine analogue) or a CK knockout would not influence the rate of mitochondrial respiration response. However, results showed faster increases in MOP measured by PCr hydrolysis rate that were directly related with reductions in creatine content or CK KO demonstrating no inertial limitation to the response of MOP (250, 325).

3.5.2 Substrate shift towards carbohydrate utilization improves muscle energetics

Mitochondrial respiration and tissue energetics rely on sufficient substrate oxidation in support of TCA cycle and ETS flux, especially during high workloads such as intense contraction (256). In muscle, when there is an increase in workload, substrate

utilization shifts from primarily fat oxidation towards more efficient carbohydrate oxidation. Recently, Kasper et al. suggested that altered substrate utilization can improve tissue energetics in a feed-forward manner (176). This was demonstrated by measuring energetics and PDH activity before and after complete chemical activation of PDH. PDH activity is directly related to carbohydrate oxidation rates (51, 242) and was used as a marker for carbohydrate flux. Specifically, PDH activity was first measured in white gastrocnemius muscle of rats during rest and contraction to establish “normal” activity levels. In parallel, tissue energetics were measured before and after DCA administration to quantify both the change in PDH activity and the resultant effects on PCr dynamics. At lower workloads where “normal” PDH activity is low, DCA resulted in reduced PCr hydrolysis and increased magnitude of ΔG_{ATP} (176). This effect is encompassed in the present study both experimentally and computationally. However, the present study expands upon this by demonstrating that increased carbohydrate flux (as opposed to PDH activity alone) can entirely explain improvements in energetic efficiency. A future experiment with muscle energetics, direct measures of PDH activity, *and* substrate utilization will be required to confirm these predictions.

While not experimentally shown, a shift towards carbohydrate flux via chemical PDH activation appears to alter tissue energetics by increasing the NADH/NAD⁺ ratio. This would result in a greater pmf translating to higher ΔG_{ATP} in the cytoplasm (14, 176, 256). To test this hypothesis, a computational approach is necessary as the NADH/NAD⁺ ratio cannot be measured *in vivo* with the temporal and spatial resolution required. The model results bolster this argument and show that PDH activation leads to higher NADH/NAD⁺ ratios. These higher NADH/NAD⁺ ratios support higher pmf and thus higher

rates of MOP. In addition, the model predicts a shift towards carbohydrate utilization with PDH activation which is in agreement with several other studies (14, 176, 256). This finding highlights the importance of considering the effect of changes in substrate utilization on muscle energetics. For example, metabolic diseases such as type 2 diabetes report compromised muscle energetics concurrent with reduced carbohydrate utilization (76, 209, 247, 290). This would result in reductions in NADH/NAD⁺ ratio and lower pmf and could contribute to a deficient energetic status relative to controls. The quantitative relationship between substrate utilization and muscle energetics could be understood in future versions of this computational model by allowing controlled clamping of substrate utilization and observing the effect on muscle energetics.

3.5.3 NADH feedback explains carbohydrate inhibition of fat oxidation

Changes in substrate selection were initially proposed by Randle et al. to involve a direct interaction between carbohydrates and fatty acids with carbohydrate oxidation directly inhibiting fat oxidation and vice versa (161, 309). The present study is consistent with these studies in that an inhibition of fat oxidation by increased carbohydrate oxidation, however, the present work reaches this conclusion by explaining this substrate switch simply from the accumulation of NADH. The interaction between fatty acids and carbohydrate oxidation is evident from inspection of individual fluxes during elevated contractile intensities (~>60% aerobic max). As the aerobic capacity is approached, carbohydrate flux rises and reaches a point where it inhibits fat oxidation solely due to the accumulation of NADH. This results in an increase in oxygen consumption due to carbohydrate oxidation while oxygen consumption due to fat oxidation is reduced. At this

same time point, the redox poise of NADH shifts from oxidized to reduced caused by elevated carbohydrate flux. The inhibition of fat oxidation by NADH accumulation can perhaps be explained from the limitations to metabolite feedback. Fat oxidation feedback in control is near maximal at rest and quickly activated to maximum at low workloads due to high relative K_{Qfat} and this effect is pronounced in reduced aerobic capacity muscle. As workload is increased, carbohydrate flux takes over ($\sim >60\%$ of the aerobic capacity) due to higher maximal metabolite feedback (K_{Qcarb}). This shift in utilization is also described when quantifying absolute flux per substrate. Above 60% of the aerobic capacity, the carbohydrate oxidation continues to rise while fat oxidation plateaus and subsequently drops. When aerobic capacity is reduced or PDH is chemically activated, this shifts towards the left and again fat oxidation reaches its maximum and subsequent decline much earlier compared to control conditions.

3.5.4 ADP + Pi feedback is dependent on muscle aerobic capacity

The effect of mitochondrial content on muscle aerobic capacity and energetic performance is often ignored when comparing populations that likely have reduced mitochondrial content due to inactive lifestyles. The present work demonstrates the importance of accounting for mitochondrial content by predicting the effect of reductions on tissue energetics both computationally and experimentally. Reductions in muscle aerobic capacity result in more PCr hydrolysis at a given workload and a slower PCr recovery time constant, but at the same relative workload (e.g., 50% of max) amount of PCr hydrolyzed is the same (283). Further, the model demonstrates increased [ADP] for a given stimulation in reduced aerobic capacity muscle despite similar oxygen flux.

Increased ADP for a given JO_2 indicates a reduced ADP sensitivity and this has been shown experimentally in reduced aerobic capacity muscle (93, 249, 283). For example, Dudley et al. (1987) showed that much more [ADP] is present despite similar JO_2 (93). As described above, this results in slowed JO_2 kinetics (319) and increased PCr hydrolysis (249, 283) due to prolonged accumulation of [ADP]. The same analysis performed by Dudley et al. is applied in the current work demonstrating model predictions of altered [ADP] and [Pi] for the same JO_2 in differing metabolic conditions. In reduced aerobic capacity muscle, [ADP] and [Pi] are increased for a given JO_2 and rise accordingly with increased JO_2 . In contrast, DCA treated conditions present with less [ADP] and [Pi] for a given JO_2 indicating an increased sensitivity due to increased NADH and pmf. Taken together, experimental data and computational predictions support changes in muscle energetics can be directly explained by the feedback of ADP + Pi relative to substrate utilization and/or muscle aerobic capacity.

The direct relationship between aerobic capacity and apparent ADP sensitivity was first proposed by Holloszy in 1967 (147). Holloszy suggested that a larger disruption from homeostasis is required for lower aerobic capacities to match ATP demand after altering muscle aerobic capacity via exercise training in rats. Rats with lower aerobic capacity imposed higher energetic loads per mitochondria and ultimately led to larger disruptions from homeostasis. This necessitated more [ADP] to accumulate concomitant with more carbohydrate utilization to support ETS flux (147). Altered aerobic capacity via mitochondrial content is often overlooked for its effect on substrate utilization and/or tissue energetics in diseased subjects. For example, in type 2 diabetes reduced muscle aerobic capacity is often attributed to mitochondrial dysfunction without quantifying the

effect of reduced mitochondrial content (247, 340). Interestingly, when accounting for a change in mitochondrial content, model predictions demonstrated that changes in energetics reported in human type 2 diabetes can be largely explained by a difference in the amount of mitochondria rather than the dogmatic view of mitochondrial dysfunction. Data that do not fall along the predicted line from computational simulations must result from factors separate mitochondrial function. Specifically, data reported in PAD patients that have reduced muscle oxygen supply demonstrate that slowed τ is not described by mitochondrial limitations since data are not described by the predictive line. This highlights the importance of accounting for both mitochondrial content and extra-mitochondrial limitations before concluding mitochondrial dysfunction in disease conditions.

3.5.5 Summary

The current work demonstrates the synergistic relationship between control of oxidative phosphorylation and substrate utilization for a range of workloads both experimentally and computationally. To do this, a computational model of skeletal muscle mitochondrial energetics and substrate utilization was developed, validated, and analyzed. Importantly, each of these components are profoundly influenced by muscle aerobic capacity and proper feedback regulation. The model was used to show how alterations in muscle aerobic capacity are expected to influence PCr dynamics and substrate utilization. Future applications particularly in disease states plagued by muscle energetic deficiencies and altered substrate utilization will allow for cogent understanding

of muscle metabolic limitations and guide therapeutic intervention in diseases such as type 2 diabetes and metabolic syndrome.

**CHAPTER 4: SKELETAL MUSCLE ENERGETICS ARE COMPROMISED
ONLY DURING HIGH INTENSITY CONTRACTIONS IN THE GOTO-
KAKIZAKI RAT MODEL OF TYPE 2 DIABETES**

4.1 Abstract

Type 2 diabetes (T2D) presents with hyperglycemia and insulin resistance affecting over 30 million people in the US alone. Previous work has hypothesized that mitochondria are dysfunctional in T2D and results in both reduced ATP production and glucose disposal. However, a direct link between mitochondrial function and T2D has not been determined. In the current study, the Goto-Kakizaki (GK) rat model of T2D was used to quantify mitochondrial function *in vitro* and *in vivo* over a broad range of contraction-induced metabolic workloads. During high frequency sciatic nerve stimulation hindlimb muscle contractions at 2 and 4 Hz intensities the GK rat failed to maintain similar bioenergetic steady-states to Wistar controls (WC) measured by phosphorus magnetic resonance spectroscopy despite similar force production. Differences were not due to changes in mitochondrial content in red (RG) or white gastrocnemius (WG) muscles (cytochrome c oxidase, RG: 22.2 ± 1.6 versus 23.3 ± 1.7 U/gWW, WG: 10.8 ± 1.1 versus 12.1 ± 0.9 U/gWW; GK versus WC, respectively). Mitochondria isolated from muscles of GK and WC rats also showed no difference in mitochondrial ATP production capacity *in vitro* measured by high-resolution respirometry. At lower intensities (0.25-1 Hz) there were no detectable differences between GK and WC rats in sustained energy balance. There were similar phosphocreatine concentrations during steady-state contraction and post-contraction recovery ($\tau=72 \pm 6$ GK vs. 71 ± 2 s WC). Taken together these results suggest that deficiencies in skeletal muscle energetics seen at higher intensities are not due to mitochondrial dysfunction in the Goto-Kakizaki rat.

4.2 Introduction

Type 2 diabetes presents with hyperglycemia and insulin resistance that can cause co-morbidities and premature death resulting in medical costs of greater than \$245 billion each year (54). Skeletal muscle insulin resistance plays a primary role in diabetes since skeletal muscle can account for up to 80% of glucose uptake demonstrated during euglycemic hyperinsulinemic clamps (89). Insulin resistance is believed by some to contribute to skeletal muscle mitochondrial dysfunction (225, 247, 290) and argued to constitute an important part in development of the disease (1, 183, 225). Here mitochondrial dysfunction is defined as the inability of mitochondria to sense and match ATP demand and is governed by the maximum rate of ATP synthesis, or the mitochondrial oxidative phosphorylation (MOP) capacity. MOP capacity is dependent on both mitochondrial content (or number) within the muscle and the inherent function per mitochondrion. Glucose oxidation in skeletal muscle is driven by ATP demand and thus dysfunctional mitochondria could result in both reduced ATP production capacity and altered glycaemic control.

Skeletal muscle mitochondrial function can be non-invasively quantified *in vivo* utilizing phosphorus magnetic resonance spectroscopy (³¹PMRS) providing the assumptions that neither metabolic fuel nor oxygen limitations occur (256, 410). These assumptions are valid in non-trained healthy human subjects during single-limb contractions (11, 116, 135, 318, 356). Utilizing *in vivo* ³¹PMRS in insulin-resistant elderly patients, a reduced MOP capacity and mitochondrial dysfunction were concluded from the observation of a 40% reduction in mitochondrial ATP synthesis rates (288). This finding led to the hypothesis that mitochondrial dysfunction in type 2 diabetes results in

increased fatty acid metabolites that disrupt insulin signaling (225). This hypothesis was further supported by findings of decreased expression of the mitochondrial biogenesis regulators PGC-1 α , PGC-1 β , and NRF-1 (270, 284) and reduced mitochondrial enzymes including citrate synthase and NADH oxidoreductase in some studies of diabetic human subjects (179, 384). Despite this evidence, age, BMI and physical activity can independently influence MOP capacity separate from the effects of hyperglycemia and insulin resistance and likely resulted in a misinterpretation of the data in direct relation to diabetes (43, 141, 148). For example, De Feyter et al. (2008) concluded no mitochondrial dysfunction *in vivo* when carefully matching diabetics to controls in age, BMI, and physical activity, demonstrating no difference in MOP capacity from similar phosphocreatine (PCr) recovery rates measured by ³¹PMRS (87). This finding raises serious questions on whether changes in mitochondrial function reported in type 2 diabetes are directly linked with the disease itself or a result of lifestyle factors such as obesity and/or reduced physical activity typically associated with the disease (179, 207, 225, 248, 349, 368).

Diabetic patients subjected to a moderate exercise regimen showed a slight reduction in BMI and a dramatic improvement in MOP capacity measured by increased rates of PCr recovery through ³¹PMRS (247, 378). These observations suggest increased physical activity and reduced BMI alone can alleviate and even reverse *apparent* mitochondrial dysfunction in diabetic patients. Nonetheless, the high degree of variability in body mass indices [87.5% of diabetic patients report overweight or obese (54)] and activity levels [40.8% of diabetics get less than 10 minutes of moderate physical activity per week (54)] continues to contribute to conflicting observations in the literature (205, 378). Resolution of whether mitochondrial dysfunction is directly linked with type 2

diabetes or not will require rigorously controlled experiments that are difficult to perform in human subjects given variability in lifestyles.

There are several accepted animal models of type 2 diabetes that recapitulate the human condition in both insulin resistance and hyperglycemia, and permit well-controlled, quantitative experiments (359). The spontaneously diabetic Goto-Kakizaki (GK) rat is a hyperglycemic and insulin resistant model of type 2 diabetes developed from selective breeding of Wistar rats (6). GK rats develop type 2 diabetes initially (~3 weeks of age) due to hyperglycemia and impaired beta cell insulin secretion (261). This is followed by peripheral insulin resistance (277) and hepatic glucose overproduction (345), which results in frank type 2 diabetes by 16 weeks of age. This inbred animal model of type 2 diabetes is nonobese (6) and physically active (7, 221). Since MOP capacity is directly influenced by both obesity and activity levels (38, 141, 148), the GK rat permits clear interpretation of type 2 diabetic skeletal muscle mitochondrial function *in vivo* without these confounding influences.

The present study is a quantitative investigation of skeletal muscle mitochondrial function in type 2 diabetes utilizing both *in vivo* and *in vitro* measurements in the GK rat model of type 2 diabetes. Mitochondrial function was quantified *in vivo* using ³¹PMRS to measure the bioenergetic response to muscle contraction. Phosphorus metabolites (PCr, Pi, ATP) were quantified in real time while muscles were electrically paced over a broad range of contractile workloads where force output was simultaneously recorded and quantified. Mitochondria isolated from these muscles were evaluated by high-resolution respirometry and mitochondrial content was quantified biochemically. Concurrent quantification of mitochondrial function *in vivo* and comparisons with *in vitro* assays in GK

rat skeletal muscle tested the hypothesis that mitochondria are inherently dysfunctional in type 2 diabetes.

4.3 Methods

4.3.1 Animals

Type 2 diabetic male Goto-Kakizaki Rats (n=7) studied at 15-17 weeks of age were obtained from Taconic Farm (Taconic Farm, Germantown, NY). Male Wistar rats (n=8) from Charles River Laboratories (Wilmington, MA) were used as age-matched controls. Animals were housed three per cage in a temperature-controlled room and provided food (NIH-31M: 23% calories from protein, 18% calories from fat, 59% calories from carbohydrate) and water ad libitum. Animals were maintained on a 12:12-h light-dark cycle. All procedures were approved by the Michigan State University Institutional Animal Care and Use Committee and complied with The American Physiological Society's "Guiding Principles in the Care and Use of Animals".

4.3.2 Oral Glucose Tolerance Test

A week before terminal experimentation, rats were given an oral glucose tolerance test (OGTT) by oral gavage of 2 g glucose per kg body weight dissolved in double distilled water following 12 h overnight fast. Blood glucose was measured in the conscious animal via tail vein puncture before gavage (time zero) and at time points 5, 15, 30, 60, 90, and 120 minutes post-gavage. Total area under the curve was determined by trapezoidal numerical integration (MATLAB) from time 0 to 120 minutes.

4.3.3 Phosphorus Magnetic Resonance Spectroscopy (^{31}P MRS)

Animals were fasted 12 hours overnight and on the day of experiment were anesthetized at 3-5% Isoflurane in 100% O₂ and maintained at 1-2% throughout experimentation. Animals were weighed and their blood glucose was measured before being prepared for *in situ* stimulation of the triceps surae (gastrocnemius, plantaris, soleus) muscle group within a ^{31}P MRS surface coil probe as described previously (176, 251). In brief, the hindlimb was secured in a custom-built NMR probe to a brass knee post via a tungsten pin inserted through the head of the femur, and the Achilles tendon was tied to an isometric force transducer. This orientation positioned the superficial gastrocnemius muscle over a 1.7 cm diameter surface coil wound from two turns of copper wire. The muscle was passively stretched to its optimal length (L_0) to give maximum peak tension in response to supramaximal stimulus (2-10 V, 2 ms duration) applied via bipolar platinum electrodes placed on the sciatic nerve. This protocol for stimulation ensures all muscle fibers are stimulated in the limb (8, 360) and avoids force summation which can confound interpretation and reduces the dynamic range for study. Respiration and rectal temperature were monitored and maintained between 45-60 breaths per minute and 36-37 °C respectively.

Phosphorus NMR spectra of the superficial gastrocnemius muscles were acquired in the Fourier transform mode at 161.8 MHz on a Bruker AM400 wide-bore spectrometer (9.4 T, 7.4 cm vertical bore magnet) housed in the Department of Physiology. The surface coil was tuned with the animal in place and the field shimmed using the available proton signal from muscle water. For phosphorus spectra, the pulse width (4.5 μs) was chosen to optimize the signal-to-noise ratio at a repetition time (TR) of 1.5 s. Spectra were

continuously acquired over 24 s intervals (sweep width 8012 Hz, 4096 complex points, interpulse interval 1.5 s, 16 averages) during 2 min 24 s of muscle at rest (6 spectra), 4 min 48 s of isometric twitch contraction (12 spectra), and 7 min 12 s of recovery (18 spectra). Twitch stimulations were performed in random order for 0.25, 0.5, 0.75, 1, 2 and 4 Hz frequencies. High intensity frequencies (2,4 Hz) were selected to permit direct comparisons with previous studies in the literature (55, 233, 399, 400) while the remaining lower frequencies were used to challenge within the sustainable range of MOP capacity (155, 168, 170, 410). Between contractile bouts animals received an extra ten minutes of recovery and resting metabolites and pH were verified before subsequent stimulation was imposed. The NMR signal was corrected for partial saturation by acquiring 64 FIDs prior to stimulation under the experimental conditions and a second at $5 \cdot T_1$ for PCr at 9.4 T (TR = 15 s).

The summed free-induction decays were multiplied by a 30 Hz exponential line broadening before Fourier transformation. Phosphorus signal integrals were computed using jMRUI AMARES fitting software (380). For each stimulation, initial phosphocreatine (PCr) levels were determined from resting spectra and during contraction from the average of the final minute of stimulation (~3 data points). Results were expressed as metabolite concentrations determined from PCr:ATP ratios after normalizing to total phosphate integral and normalized to absolute chemical content by HPLC determined ATP and creatine contents as previously described (196, 411). Mono-exponential time constants for PCr recovery dynamics were computed by least squares regression algorithm using MATLAB curve fitting toolbox (Mathworks). The rates of ATP hydrolysis during contraction (J_{ATPase}) were determined from the initial slope (linear regression) of

PCr hydrolysis during stimulation (169). During steady-state contractions, the ATP consumption rate is equal to the ATP production rate ($J_{\text{ATPase}} = J_{\text{ATP}}$).

4.3.4 Mitochondrial Content and Metabolite Quantification

Red and white gastrocnemius muscles from the stimulated leg were separately excised, weighed, and immediately freeze clamped in liquid nitrogen using homemade steel tongs. The samples were stored at -80 °C until powdered under liquid nitrogen for biochemical analysis. Cytochrome c oxidase was used as a marker of mitochondrial content and measured spectrophotometrically at 37 °C as previously described (355). HPLC analysis was performed for measurement of ATP and total creatine content following perchloric acid extraction as described previously (197, 412).

4.3.5 High-Resolution Respirometry

Triceps surae muscles from non-stimulated legs were excised and prepared for mitochondrial isolation as described previously (5, 383, 413). Briefly, muscle was mechanically minced and homogenized in ice cold isolation buffer (200 mM mannitol, 50 mM sucrose, 5 mM K_2HPO_4 , 5 mM MOPS, 1 mM EGTA, 0.1% (w/v) BSA, pH 7.15) with 0.5 units/mL of protease (*Bacillus licheniformis*). Subsequently, the homogenate was centrifuged twice at 8000 x g for ten minutes to wash the protease and the supernatant discarded. The pellet was then resuspended and centrifuged at 700 x g for ten minutes. The supernatant containing the mitochondria-rich fraction was collected and centrifuged at 8000 x g for ten minutes. The remaining pellet was resuspended in isolation buffer at

a concentration of 20 mg/ml and kept on ice for the duration of the experiments. Mitochondrial protein content was determined by the Bradford protein assay using BSA standards.

Following isolation, mitochondrial oxygen consumption was measured at 37 °C using an Oroboros Oxygraph 2K high-resolution respirometer (Oroboros Instruments, Innsbruck, Austria). Respiratory analysis was performed by loading 0.1 mg/ml mitochondrial protein in respiration buffer (110 mM sucrose, 60 mM potassium lactobionate, 20 mM taurine, 10 mM KH_2PO_4 , 3 mM MgCl_2 , 20 mM HEPES, 1 mM EGTA, and 0.1% (w/v) BSA at pH 7.1 at 37 °C) with either pyruvate (5 mM) and L-malate (1 mM) or palmitoyl-carnitine (50 μM) and L-malate (2 mM) as indicators of carbohydrate and fatty-acid oxidative flux, respectively (413). Respiratory rate was analyzed during two different states: 1) leak state, where mitochondrial respiration in the absence of ADP occurs due to proton leak, and 2) maximal ADP-stimulated state, where mitochondria are respiring in the presence of saturating concentration of ADP (0.5 mM). Oxygen consumption rates were determined averaging the 5 minutes prior to ADP-stimulation for the leak-state and averaging across the peak oxygen consumption rate for maximal ADP-stimulated state. The respiratory control ratio (RCR), an indicator for mitochondria quality, was calculated from the quotient of maximal ADP-stimulated state to the leak state (42). High RCR values represent well-coupled mitochondria with a high capacity for ATP turnover and low proton leak. All studies performed had a steady-state leak state and high RCR values (>20).

4.3.6 Calculations

HOMA-IR (240) was calculated from values of fasting blood glucose (mM) and insulin [mIU/L, using a value of 44.45 µg/IU insulin for unit conversion (277)] according to:

$$HOMA\ IR = \frac{glucose \times insulin}{22.5}$$

Intracellular pH was estimated from the chemical shift of inorganic phosphate (Pi) relative to PCr (ΔPPM) (410):

$$pH = 6.75 + \log \left(\frac{3.37 - \Delta PPM}{\Delta PPM - 5.63} \right)$$

Glycolytic ATP synthesis rate (J_{GLY} : in mM/s) was estimated by measuring the linear rate of acidification during stimulation post PCr-induced alkalization (linear region ranged 3-8 data points). Muscle buffer capacity (β) is assumed to be 27 slykes (4), 1.5 represents the proton/ATP stoichiometry, and the exchange of acid with the extracellular environment is assumed negligible (33, 34, 409):

$$J_{GLY} = 1.5 \times \beta \times \left(\frac{dpH_i}{dt} \right)$$

Since J_{ATP} (mM/s) is comprised of J_{GLY} and mitochondrial oxidative phosphorylation rate (J_{MOP}), J_{MOP} (mM/s) was determined by subtracting glycolytic flux from J_{ATP} :

$$J_{MOP} = J_{ATP} - J_{GLY}$$

Free ADP was calculated by rearrangement of the creatine kinase equilibrium using the equilibrium constant of $1.66 \times 10^9 \text{ M}^{-1}$ (213):

$$free\ ADP = \frac{[ATP][Cr]}{[PCr]K_{eq}[H^+]}$$

Free Energy of ATP hydrolysis (ΔG_{ATP}) was calculated with standard free energy = -32 kJ/mol assuming 37 °C and pH 7.0:

$$\Delta G_{ATP} = \Delta G^{\circ}_{ATP} + 2.58 \times \ln \left(\frac{[ADP][Pi]}{[ATP]} \right)$$

4.3.7 Statistics

All data are presented as Mean \pm SE. Comparison of group means was performed using SigmaPlot by Student's t-test for all comparisons except for OGTT (Figure 11A, Tukey's procedure) at the $p < 0.05$ level of significance. Two-tailed tests were used for all comparisons except HOMA-IR since GK rats were expected to have elevated insulin resistance. Linear regressions were fit using SigmaPlot and evaluated for differences in slope.

4.4 Results

4.4.1 Animal Characteristics

GK rats had elevated fasting blood glucose and free fatty acids and insulin concentration was higher compared to Wistar controls (Table 4). HOMA-IR index calculated from fasting glucose and insulin values suggests greater insulin resistance in GK versus Wistar control rats. Body mass and triceps surae muscle mass were each

decreased in GK versus Wistar rats. When normalizing muscle mass to body mass however, triceps surae relative mass was slightly increased in GK versus Wistar rats (Table 4).

Table 4. Animal Characteristics describing Wistar and GK rats used in the present study.		
	Wistar	GK
<i>FBG (mg/dL)</i>	114 ± 6	193 ± 19 [#]
<i>FFA (mM)</i>	0.97 ± 0.08	1.29 ± 0.1*
<i>Insulin (ng/mL)</i>	0.75 ± 0.1	1.42 ± 0.4
<i>HOMA-IR</i>	4.6 ± 1.0	16.0 ± 5.0*
<i>Body Mass (g)</i>	461 ± 5	325 ± 7 [#]
<i>Muscle Mass (g)</i>	2.86 ± 0.06	1.84 ± 0.04 [#]
<i>MM/BM*100</i>	0.57 ± 0.02	0.62 ± 0.01*
Values are mean ± SE. *= <i>p</i> < 0.05; #= <i>p</i> < 0.01. FBG, fasting blood glucose; FFA, free fatty acids; MM, muscle mass; BM, body mass.		

Differences in blood glucose levels during the OGTT between GK and Wistar controls are presented in Figure 11. The GK rat was hyperglycemic and displayed elevations in blood glucose throughout the OGTT challenge compared to Wistar controls. A two-way analysis of variances revealed a significant group, time, and group x time interaction for blood glucose at different time points post-gavage demonstrating that blood glucose was significantly elevated in GK versus Wistar controls. Post-Hoc Tukey test revealed increased blood glucose in GK rats compared to Wistar controls at every time point measured. Peak blood glucose was ~300% higher in GK rats at 30 minutes post-gavage and failed to significantly recover 2 hours post-gavage compared to Wistar controls. Increased fasting blood glucose and failure to recover 2 hours post oral gavage

both meet criterion for establishing type 2 diabetes as outlined by the American Diabetes Association (10).

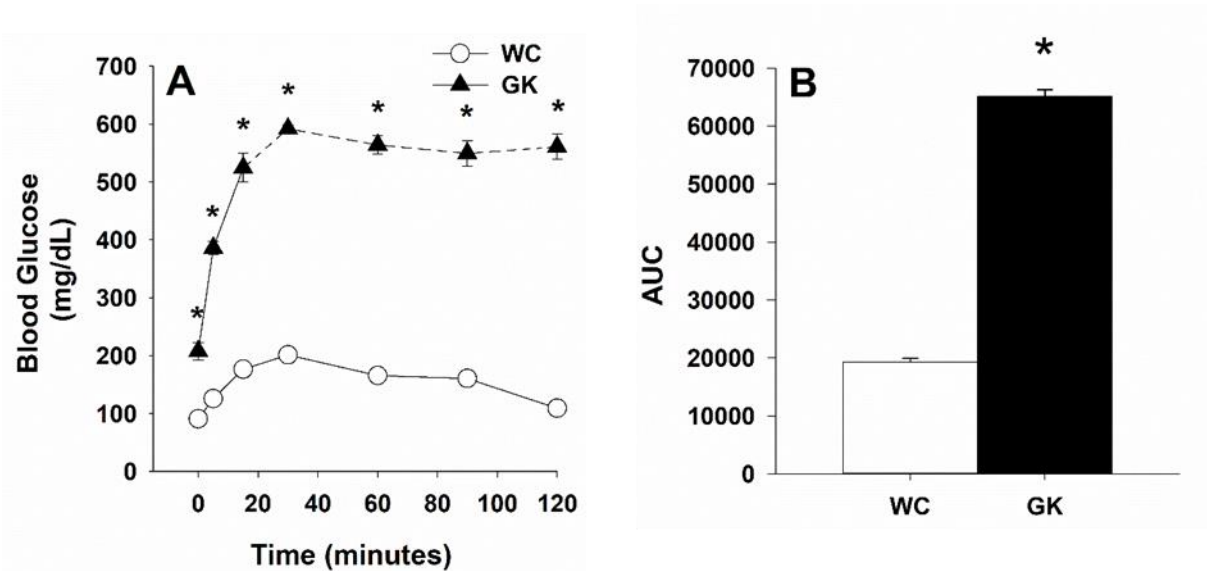


Figure 11. Mean \pm SE blood glucose measures following OGTT at 2 g/kg glucose/body weight in Wistar (white circles, n=3) and GK (black triangles, n=5) rats at 0, 5, 15, 30, 60, 90, and 120 minutes following gavage (Panel A) and the resultant area under the curve (AUC) during testing (Panel B). Blood glucose was significantly higher in GK rats at every time point measured (*=p<0.001 Tukey test). AUC was significantly increased in GK rats (*=p<0.001 two-tailed t-test). Dashed lines indicate one or more measures were beyond limit of detection and capped at 600 mg/dL.

4.4.2 Resting Metabolites, pH, Free Energy

Resting metabolites for GK and Wistar rat gastrocnemius muscle measured biochemically *in vitro* and *in vivo* by ^{31}P PMRS are summarized in Table 5. No differences were seen in either total creatine or ATP measured by HPLC. Quantification of resting ^{31}P PMRS from measured ATP concentrations showed no differences in resting PCr, Pi, pH, ADP, or free energy of ATP in GK versus Wistar control rats.

Table 5. Resting Metabolites, pH, Free Energy		
	Wistar	GK
<i>Pi</i> (mM)	3.71 ± 0.23	3.23 ± 0.18
<i>PCr</i> (mM)	38.1 ± 1.4	37.9 ± 1.3
<i>Cr_{tot}</i> (mM)	45.7 ± 1.6	47.5 ± 1.8
<i>ATP</i> (mM)	10.4 ± 0.2	10.6 ± 0.4
<i>ADP</i> (μM)	12.5 ± 2.4	19.4 ± 3.1
<i>PCr/ATP</i>	3.67 ± 0.1	3.58 ± 0.08
<i>pH</i>	6.96 ± 0.05	7.07 ± 0.03
ΔG_{ATP}	-64.51 ± 0.62	-62.97 ± 0.53
Values are mean ± SE. Pi, inorganic phosphate; PCr, phosphocreatine; Cr _{tot} , total creatine.		

4.4.3 Mitochondrial Function in vivo at High Intensity

Representative spectra and their corresponding mechanical recordings are presented in Figure 12 from Wistar control (Panels A, C) and diabetic GK (Panels B, D) rats. Simultaneous recording of twitch force output demonstrates force production between GK and Wistar controls per gram muscle were similar (Figure 12 B,D). This was further supported by detailed analysis of individual twitch characteristics which showed no differences in force produced or rate of fatigue between GK and Wistar controls (Table 6).

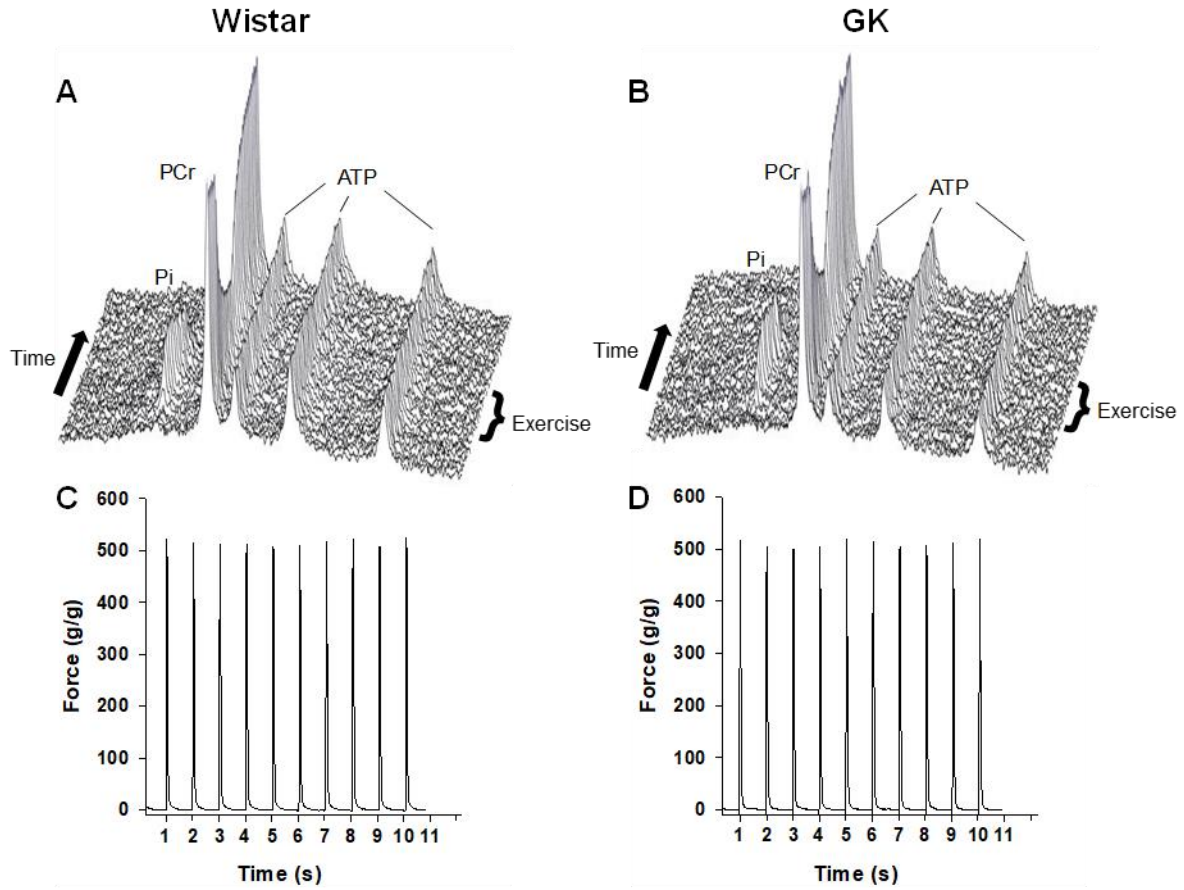


Figure 12. Representative ^{31}P MRS spectra and 10 second sample of force recording for Wistar control (Panels A and C) and diabetic GK rats (Panels B and D) during 1 Hz stimulation in gastrocnemius muscle.

Table 6. Muscle Twitch Characteristics							
		Stimulation Frequency (Hz)					
		0.25	0.5	0.75	1.0	2.0	4.0
Max Twitch (g/g)	<i>Wistar</i>	544 ± 62	558 ± 67	544 ± 67	526 ± 62	483 ± 55	512 ± 62
	<i>GK</i>	449 ± 46	458 ± 53	506 ± 31	502 ± 44	538 ± 64	487 ± 52
End Twitch (g/g)	<i>Wistar</i>	530 ± 61	545 ± 66	498 ± 50	480 ± 52	331 ± 28	219 ± 15
	<i>GK</i>	437 ± 45	442 ± 51	475 ± 34	420 ± 54	330 ± 33	212 ± 38
%Max	<i>Wistar</i>	97.4 ± 1.4	97.4 ± 0.9	93.2 ± 3.0	91.9 ± 2	65.4 ± 5	47.5 ± 4
	<i>GK</i>	97.2 ± 0.4	96.5 ± 0.6	93.8 ± 3.1	84.7 ± 8	70.5 ± 6	41.9 ± 7
Rise Time (ms)	<i>Wistar</i>	36.3 ± 0.8	36.0 ± 1.3	34.3 ± 1.3	36.1 ± 1.7	35.8 ± 1.8	37.8 ± 2.1
	<i>GK</i>	37.0 ± 1.3	38.0 ± 1.0	36.4 ± 1.1	36.5 ± 1.7	35.7 ± 1.6	41.1 ± 2.4
1/2 Relaxation (ms)	<i>Wistar</i>	22.6 ± 0.6	22.9 ± 0.8	24.0 ± 1.2	26.5 ± 1.2	30.4 ± 2.9	34.8 ± 2.6
	<i>GK</i>	24.0 ± 1.2	26.3 ± 1.6	23.1 ± 1.1	27.7 ± 2.6	30.4 ± 3.1	45.6 ± 2.9*
TTI (g*s/g)	<i>Wistar</i>	42.0 ± 4.4	46.5 ± 5.1	33.0 ± 4.4	35.8 ± 4.3	31.5 ± 3.5	28.1 ± 3.2
	<i>GK</i>	35.2 ± 0.3	37.0 ± 4.5	31.2 ± 3.2	34.6 ± 5.0	33.5 ± 5.7	36.1 ± 4.0
Values are mean ± SE. *= $p < 0.05$ versus Wistar control. g/g, gram per gram muscle.							

PCr content during rest, contraction and recovery during 2 Hz (Panel A) and 4 Hz (Panel B) twitch frequencies are presented in Figure 13. At each frequency, the PCr transients diverge and more PCr is hydrolyzed during contraction in the GK rats than in their Wistar controls consistent with other rodent studies in diabetes (55, 399, 400).

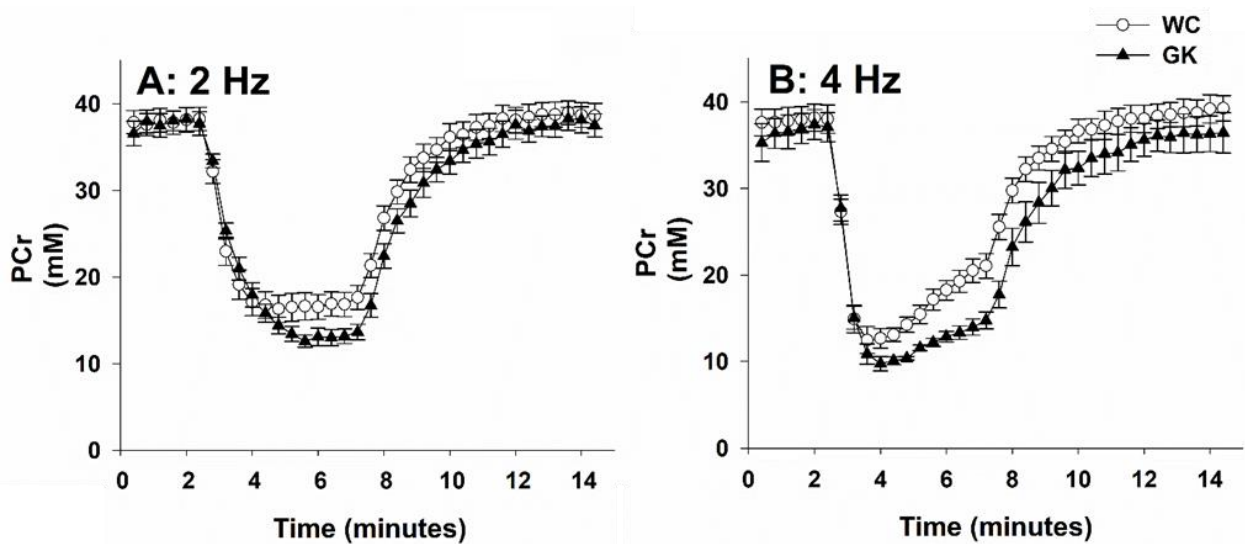


Figure 13. Mean \pm SE values for phosphocreatine (PCr) during rest, contraction, and recovery at 2 (Panel A) and 4 Hz (Panel B) intensities of stimulation for GK (black triangles, n=7) and Wistar controls (WC, white circles, n=8).

4.4.4 Mitochondrial Content and Function *in vitro*

Cytochrome c oxidase activities in red and white gastrocnemius muscles are presented in Figure 14A. Enzyme activities were significantly different in red vs. white gastrocnemius muscles consistent with known differences in mitochondrial content in these muscle types (90). However, there was no difference in white nor red gastrocnemius muscle mitochondrial content between GK and Wistar control rats. Oxygen consumption in isolated mitochondria from triceps surae muscle in the presence of pyruvate and L-malate (PM) or palmitoyl-carnitine and L-malate (PCM) is presented in

Figure 14B-D. Representative traces demonstrating the high quality of the respirometry data are presented in Figure 15. Respiration was slower when mitochondria were respiring in presence of PCM for Wistar controls but area under the curve (describing P:O ratio) was not different between Wistar and GK rats. Mitochondrial leak state was not different between GK and Wistar rats using PM or PCM (Figure 14B). When subjected to maximal ADP-stimulation, mitochondrial oxygen consumption rate was not different between GK and Wistar controls with PM but elevated 27% with PCM in GK versus Wistar respectively (Figure 14C). RCR values demonstrated well-coupled mitochondria and no difference between GK and Wistar controls in the presence of PM but was elevated 12% in presence of PCM for GK versus Wistar controls (Figure 14D).

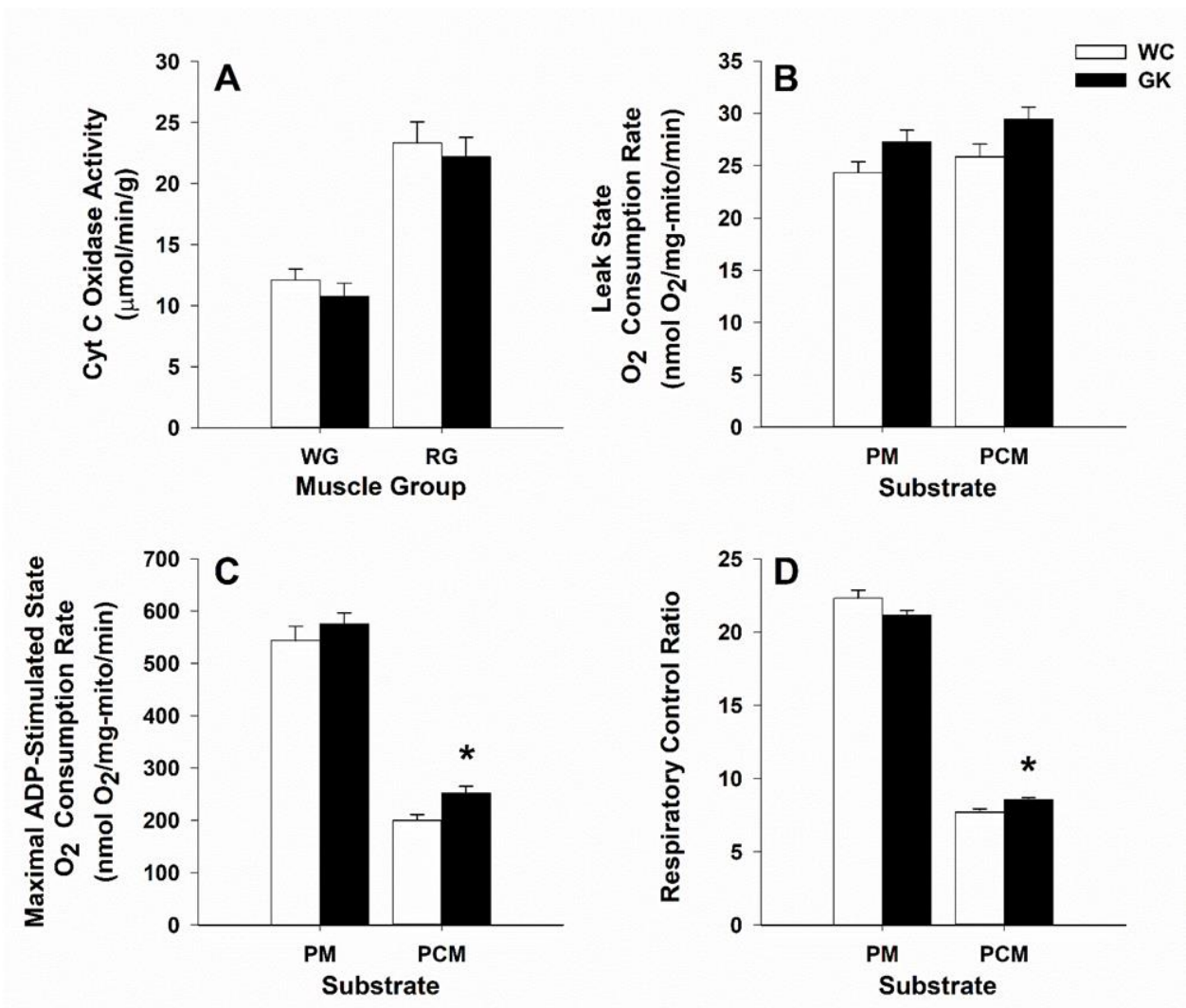


Figure 14. Mean \pm SE measures of mitochondrial function *in vitro* including mitochondrial content (Panel A), respiration during leak state (Panel B), respiration during maximal ADP-stimulated state (Panel C), and respiratory control ratio (Panel D). No difference was seen between GK (black bars, n=7) and Wistar controls (white bars, n=8) in mitochondrial content in white (WG) nor red (RG) gastrocnemius muscle (Panel A). Mitochondrial respiratory capacity (Panels B-D) was not different using pyruvate and malate (PM) as substrate but increased when using palmitoyl-carnitine and malate (PCM) in GK (n=5) versus Wistar controls (n=5). (*= $p \leq 0.01$ two-tailed t-test).

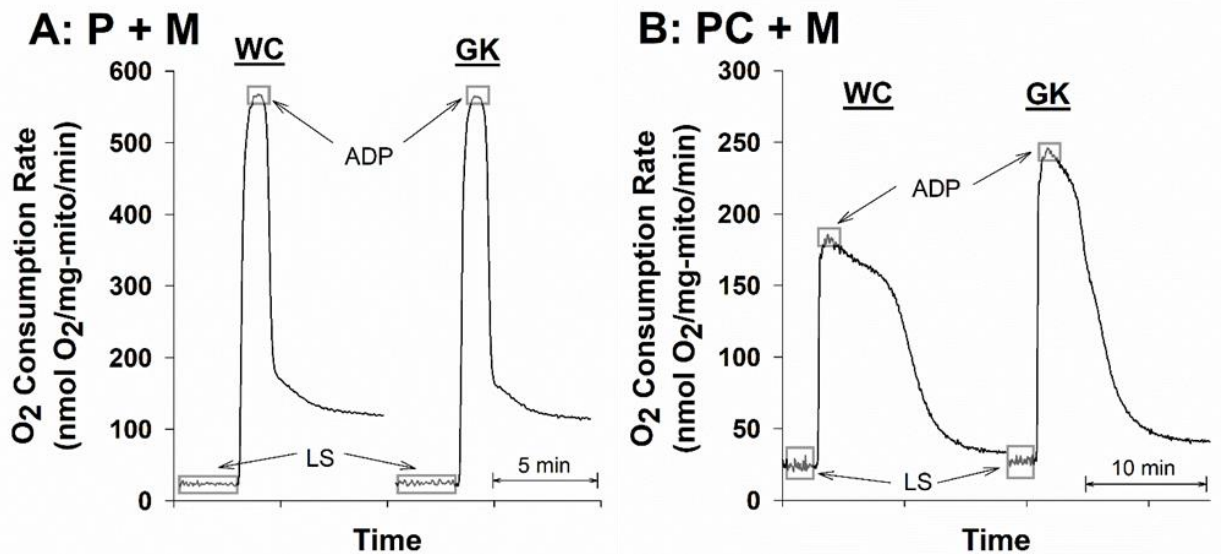


Figure 15. Representative oxygen consumption rates for Wistar control (WC) and GK rats while respiring in the presence of pyruvate and L-malate (P + M, Panel A) or palmitoyl-carnitine and L-malate (PC + M, Panel B). Leak state (LS) was measured during the steady-state before ADP stimulation while maximal ADP-stimulated state (ADP) was measured by averaging over the peak designated by the shaded boxes. AUC (P:O ratio) were not different between groups for either P + M or PC + M.

4.4.5 Mitochondrial Function *in vivo* at Low Intensity

PCr content during rest, contraction, and recovery during 0.25 Hz (Panel A), 0.5 Hz (Panel B), 0.75 Hz (Panel C), and 1 Hz (Panel D) twitch frequencies are presented in Figure 16. The PCr dynamics are indistinguishable between Wistar and GK rats at contraction rates of 1 Hz and below. *In vivo* measures of mitochondrial function including PCr contractile steady-state calculated from the last minute of stimulation (Panel A) and recovery time constant (Panel B) are presented in Figure 17. The PCr level during steady-state contraction was not different at or below 1 Hz intensity of stimulation for both the GK and Wistar rats (Figure 17A). At 2 Hz the PCr levels during steady-state contractions were 8% lower in GK rats compared to Wistar controls. No energetic steady-state was

attained during 4 Hz twitch frequency and was not included in the chart. Since the PCr recovery time constant is independent of workload within the submaximal range (249), PCr recovery kinetics post-stimulation were fit to a mono-exponential function for 0.25, 0.5, 0.75, and 1 Hz twitch frequencies and presented as the average. There was no difference between GK and Wistar control recovery time constants (Figure 17B).

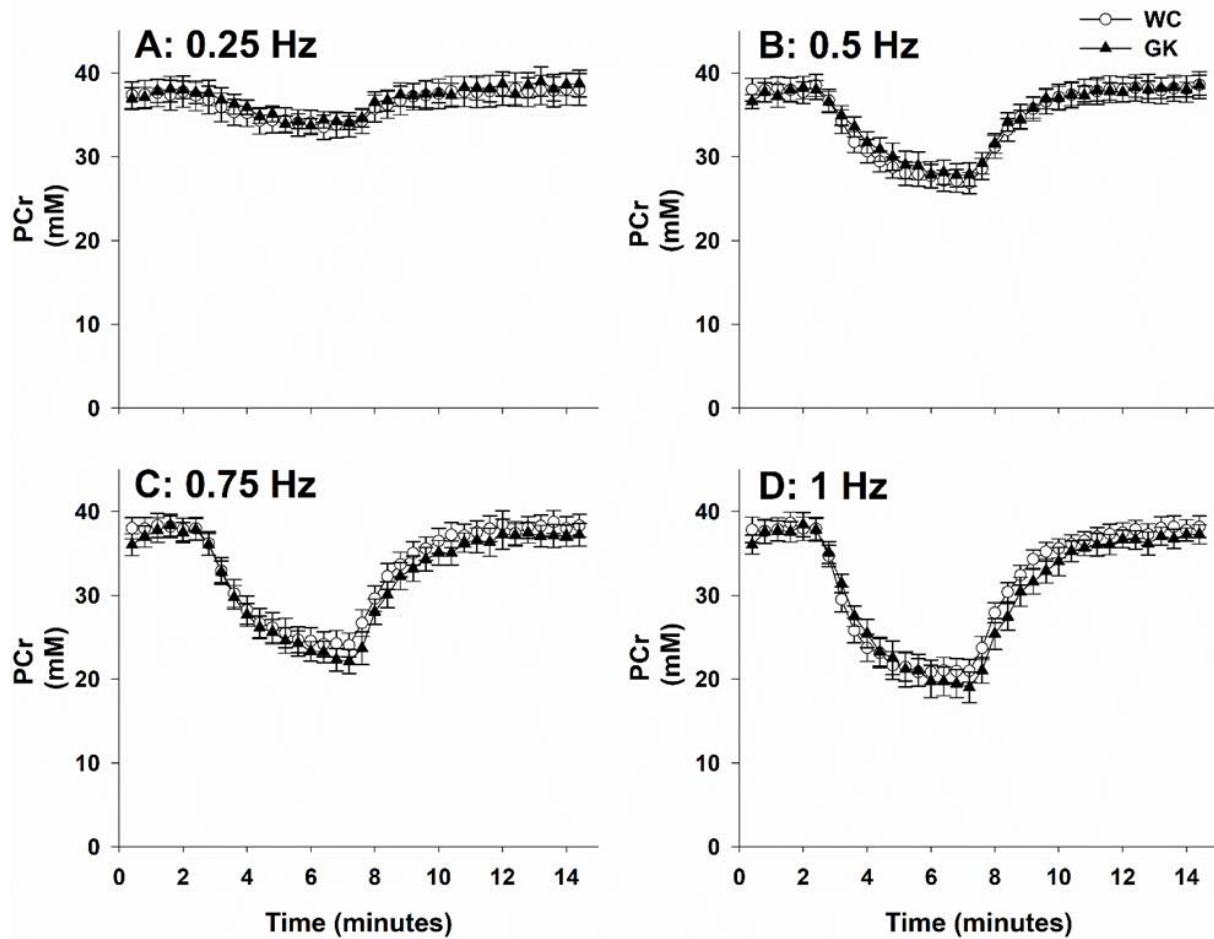


Figure 16. Mean \pm SE values for phosphocreatine (PCr) during rest, contraction, and recovery at 0.25 (Panel A), 0.5 (Panel B), 0.75 (Panel C), and 1 Hz (Panel D) intensities of stimulation for GK (black triangles, n=7) and Wistar controls (WC, white circles, n=8).

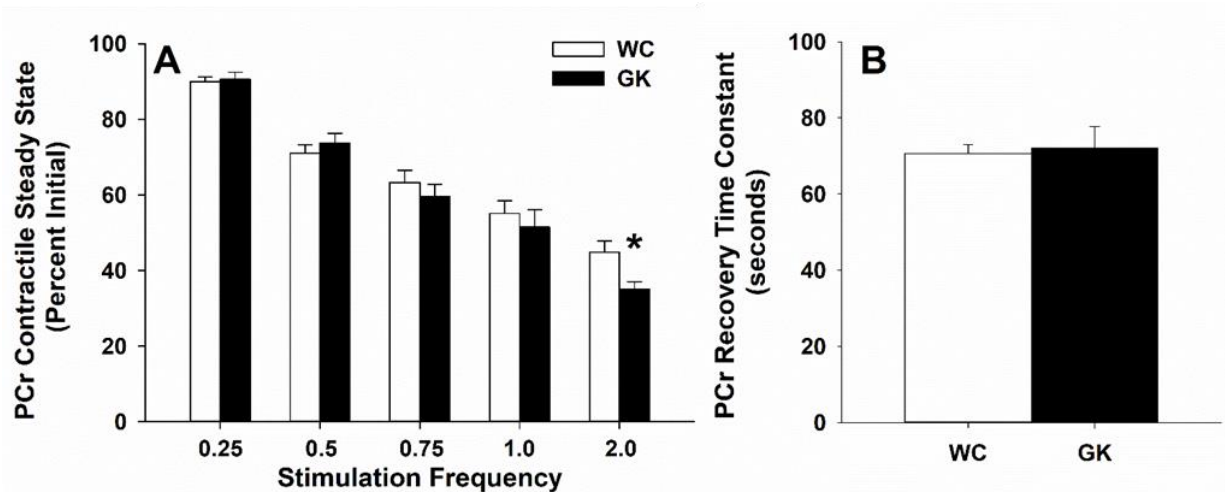


Figure 17. Markers of mitochondrial function measured *in vivo* by ^{31}P PMRS presented by mean \pm SE phosphocreatine (PCr) level as a percent of initial at energetic steady-state for Wistar control (white bars, $n=8$) and GK rats (black bars, $n=7$) during stimulation at 0.25, 0.5, 0.75, 1, and 2 Hz (Panel A) and PCr recovery time constant following stimulation below 1 Hz (Panel B). Since no energetic steady-state was achieved at 4 Hz it was not included. Significantly more PCr was hydrolyzed at 2 Hz ($*=p<0.02$ two tailed t-test) in the GK rat but no difference for 0.25 – 1 Hz nor PCr recovery time constant.

4.4.6 Quantification of ATP Production and Free ADP

The ATP cost of contraction (J_{ATPase}) was not different between GK and Wistar rats at any frequency of stimulation (Figure 18A). Glycolytic ATP flux (J_{GLY}) was also not different between GK and Wistar control rats at any frequency measured (Figure 18B). Thus, the calculated ATP produced from mitochondrial oxidative phosphorylation ($J_{\text{MOP}} = J_{\text{ATP}} - J_{\text{GLY}}$) was not different between GK and Wistar control rats at any stimulation frequency (Figure 18C). Further, at 2 Hz intensity of stimulation neither J_{GLY} nor J_{MOP} were described by the regression line (Figure 18B,C) illustrating that the MOP maximum fluxes were exceeded.

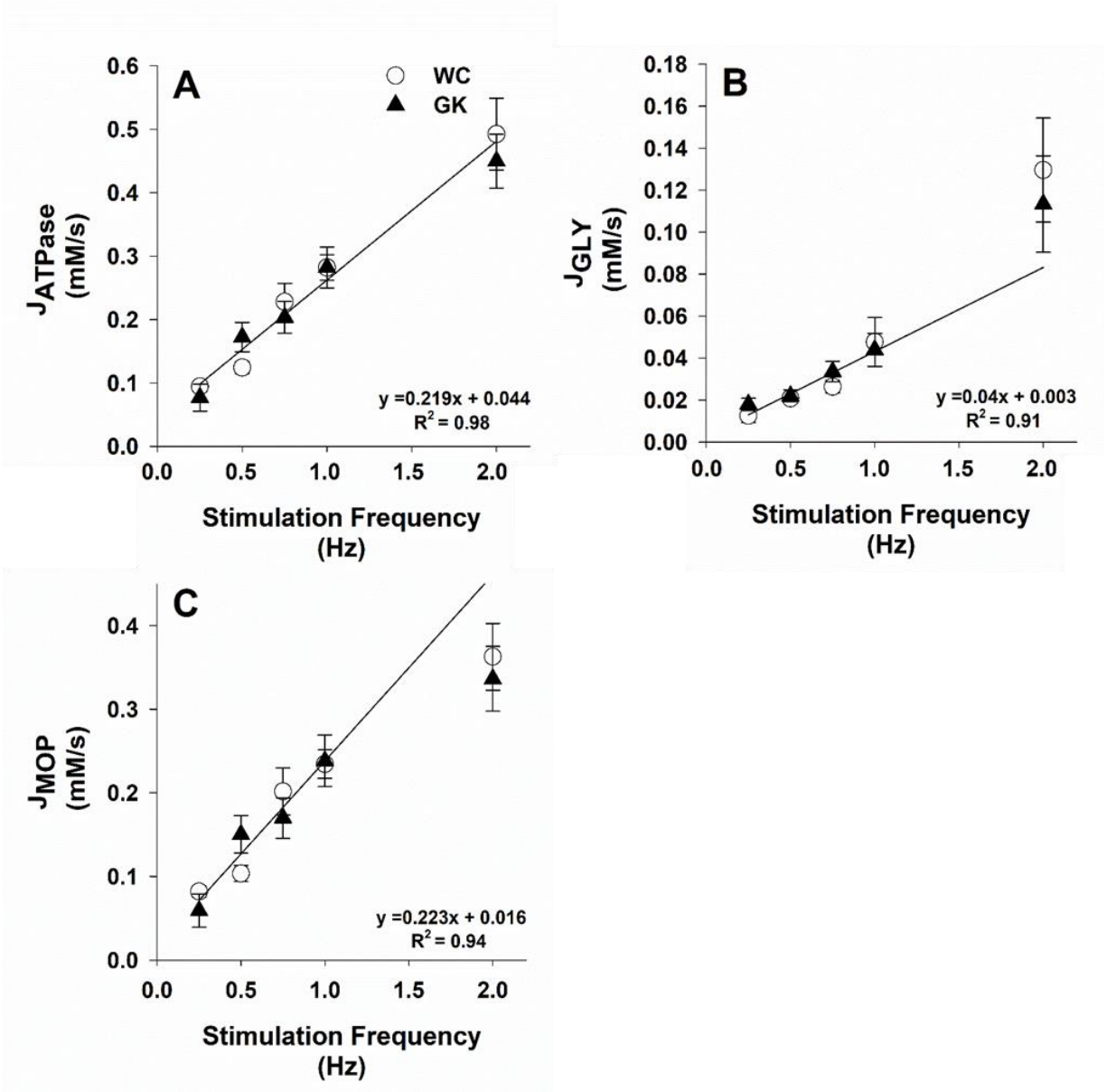


Figure 18. Mean \pm SE ATP hydrolysis rate (J_{ATPase} , Panel A), glycolytic ATP production rate (J_{GLY} , Panel B), and mitochondrial oxidative phosphorylation ATP production rate (J_{MOP} , Panel C) during stimulation intensities of 0.25, 0.5, 0.75, 1 and 2 Hz for Wistar control (WC, white circles, $n=8$) and GK (black triangles, $n=7$) rats. Linear regressions are depicted for each relationship from 0.25 - 1 Hz and in Panels B and C 2 Hz did not fall on the regression line since contractions could no longer be sustained aerobically. No difference was seen for any source of ATP production between WC and GK rats.

The quantification of metabolites during contractile steady-states are summarized in Figure 19. PCr during contractile steady-states decreased linearly with a corresponding stoichiometric increase in inorganic phosphate (Pi). The plot of PCr against Pi fit a linear regression with a slope of -1.06 confirming quantification of the phosphate pool dynamics (Figure 19A). The relationship between J_{MOP} and ADP concentration during any contractile steady-state is an index of *apparent* ADP sensitivity (56, 410). There was no difference in apparent ADP sensitivity between GK and Wistar rats based on similar slopes between groups (Figure 19B, $p=0.59$). However, as contractile intensity increases, significantly more ADP is present in GK versus Wistar controls at 0.75 and 1 Hz frequencies of stimulation despite similar J_{MOP} (Figure 19B).

4.5 Discussion

The current study quantified the *in vivo* muscle energetics during contraction in the GK rat model of type 2 diabetes and their Wistar controls concurrent with measures of muscle force production. The *apparent* dysfunction observed *in vivo* at higher intensities (2, 4 Hz; Figure 13) was not supported by direct measures of MOP capacity *in vitro*. When mitochondria were isolated and assayed by high-resolution respirometry there were no differences in maximal ADP stimulation and mitochondria were well-coupled in both groups (Figure 14B-D). The disparity between the *in vivo* results at highest stimulation rates and *in vitro* results could not be explained by differences in mitochondrial content nor ATP demand. Cytochrome c oxidase activities indicated mitochondrial content

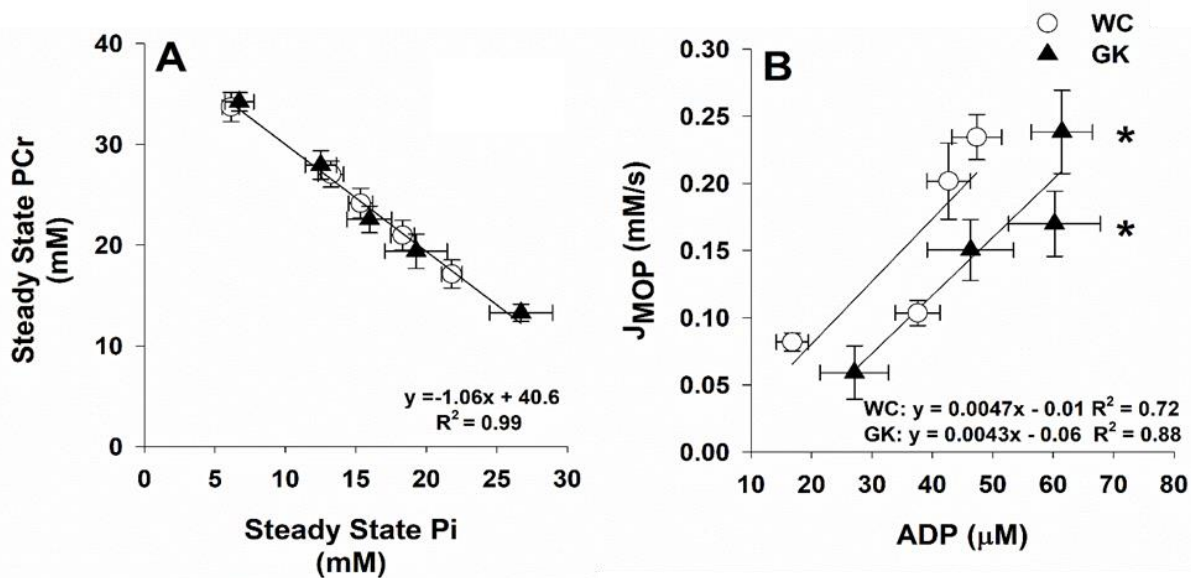


Figure 19. Mean \pm SE concentrations of phosphocreatine (PCr) versus inorganic phosphate (Pi) in Wistar control (WC, white circles, n=8) and GK (black triangles, n=7) rats during energetic steady-states at stimulation frequencies of 0.25, 0.5, 0.75, 1 and 2 Hz (Panel A). Stoichiometric changes were demonstrated by a slope of -1.06 and R^2 value of 0.99 indicating no changes in the phosphate pool size. J_{MOP} versus ADP (apparent ADP sensitivity, Panel B) indicated a rightward shift with more ADP present for a given MOP at 0.75 and 1 Hz stimulation frequencies. 2 Hz stimulation frequency was not included in apparent ADP sensitivity since the muscle fatigued. (*= $p < 0.05$ two-tailed t-test).

was the same for both diabetic and control muscles (Figure 14A) as was ATP-dependent force production (Table 6). Furthermore, when these same animals were paced at lower stimulation frequencies (0.25-1 Hz; Figure 16) both the GK diabetic animals and their Wistar controls had no differences in their bioenergetic performance or force output (Figure 16, Figure 17; Table 6). Together these observations suggest that mitochondria are not dysfunctional in type 2 diabetes, and *apparent* mitochondrial dysfunction at higher workloads is likely the result of extra-mitochondrial factors.

The *apparent* metabolic dysfunction observed in this study at the higher intensities (2, 4 Hz) is also seen in other studies in type 2 diabetic rat models (399, 400) but not in the GK strain (233). Although these higher intensity stimulations (2, 4 Hz) are beyond

what is aerobically sustainable (Figure 18B), their use permits direct comparison to previous studies (55, 233, 399). However, one must exercise caution when ascribing overall metabolic dysfunction specifically to mitochondrial dysfunction at stimulation intensities performed above the sustainable range of MOP capacity. When comparing sciatic nerve stimulation in healthy rodents PCr kinetics following high-intensity contractions recovered significantly slower than at low intensities (105). The lengthening in PCr recovery time was attributed to increased acidification from lactate production which has been previously shown to reduce mitochondrial ATP production and slow PCr dynamics (283, 375, 392). Thus, *apparent* mitochondrial dysfunction during high intensity contraction is no longer solely determined by the organelle itself because control over cellular energetics also becomes dependent on delivery of sufficient metabolic fuels and oxygen (105, 155, 168, 243, 283).

Previous work in the GK rat reports no mitochondrial nor metabolic dysfunction based on a lack of divergence in the energetic profiles measured by ³¹PMRS when stimulated at a frequency intermediate to the 2 and 4Hz data from the present study [3.3Hz, (233)]. The disparity in results is likely due to an inherent oxygen limitation in previous work best illustrated by the dramatically increased recovery times for PCr which are 3-4X reported values in mammalian tissue [summarized in Meyer and Foley (252)] even in their control animals. A subsequent study utilizing this experimental setup supports the contention for an oxygen deficit since increased mitochondrial content from an exercise training regime did not improve PCr recovery times (211, 232, 244, 283).

Overall mitochondrial function (MOP capacity) is defined by both mitochondrial content (or number) and the function per mitochondrion. When mitochondria were

isolated from these animals, *in vitro* assays showed no dysfunction (Figure 14). There were no deficits in mitochondrial content, oxygen consumption during leak-state, maximal ADP-stimulated state, or RCR between diabetic GK and Wistar control rats. Measures of maximal respiratory capacity, albeit a non-physiological dose of ADP, permit the comparison of maximal aerobic function and is well accepted as the gold-standard for determining mitochondrial function *in vitro* (42). GK rat mitochondria have an enhanced capacity for fat oxidation relative to the Wistar controls when respiring on PCM (Figure 14D) and this result is in agreement with previous work in diabetic GK rats (172), the Zucker Diabetic Fatty (ZDF) rat model of type 2 diabetes (399, 400) and reports of human subjects with type 2 diabetes (2, 40, 142). The increased capacity for fat oxidation may be an adaptation resulting from an excess in fat availability in diabetes as suggested by work involving rats fed a high fat diet (372). Indeed, the present study reported elevated blood free fatty acid levels (Table 4) and this has also been reported previously in this same strain (110). Irrespective of modest differences in fat oxidative capacity there is no evidence of “dysfunction” in the isolated organelle.

Under the appropriate circumstances (i.e. within the sustainable range of MOP) measures of mitochondrial function *in vivo* and biochemical measures of mitochondrial function *in vitro* are in absolute agreement (206, 244). In the present study, contractile PCr steady-state levels and recovery time constants were similar between diabetic GK and Wistar control rats (Figure 16, Figure 17) at low metabolic workloads (0.25-1 Hz). Paganini et al. (1997) showed that the amount of PCr hydrolyzed during contraction and time for PCr recovery decreases with increased MOP capacity (283). This demonstrates the direct relationship of mitochondrial function with PCr kinetics and for this reason PCr

recovery is the most accepted indicator of mitochondrial function measured *in vivo* (42, 206, 244, 410). The results of the present study show nearly identical recovery time constants (Figure 17B) and agrees with similar mitochondrial content (Figure 14A) and inherent function per organelle measured (Figure 14B-D) *in vitro*. Taken together, these measures reflect normal skeletal muscle MOP capacity and thus no mitochondrial dysfunction in the diabetic GK rat and further suggests that divergence at higher intensities likely manifests from differences in either cytosolic composition or extracellular properties of the diabetic animal.

There are a number of factors that could present as divergent energetics when stimulating at high intensities including differences in metabolic workload, glycolytic activity, lipid content, and intramuscular PO₂. Metabolic workload is set by the contraction-induced ATP demand (104) reflected in muscle force output. Force production at any frequency was not different in diabetic GK or Wistar control muscles (Table 6) indicating the ATP costs were also identical between groups (Figure 18A). Likewise, non-mitochondrial ATP production through glycolysis can contribute to PCr dynamics however this is also not different between groups (Figure 18B) (169, 215, 410). Similar mitochondrial ATP production between diabetic GK and Wistar control rats (Figure 18C) is in agreement with conclusions from previous studies (223, 233). However, each of these previous studies performed metabolic challenges where tissue acidification and/or oxygen supply complicate the interpretation of energetic changes that may have been fortuitously ascribed to mitochondria (105, 215, 375, 392). Although not measured in the current study, divergence in energetic performance between Wistar control and diabetic GK rats during high intensity contractions might also be explained by increased

intramyocellular lipid (IMCL) content. Elevated IMCL content has been reported in type 2 diabetes and argued to directly reduce mitochondrial ATP production measured by ^{31}P MRS that is restored by pioglitazone treatment (13, 400). While these authors argue for the direct impact of drug treatment on IMCL content they neglect to consider that pioglitazone also directly improves vascular function (30). Reduced blood flow during leg isometric exercise has been reported in diabetic patients and could limit mitochondrial ATP production (82, 268, 337, 406). The restorative effects of pioglitazone raises the question of whether oxygen utilization by the mitochondria or oxygen delivery by the vasculature limits metabolic performance in diabetes (82, 111).

Limitations in blood flow in the diabetic GK rat have been reported in recent work by Frisbee et al. (2018) demonstrating reduced blood flow contributes to reduced oxygen uptake ($\dot{V}\text{O}_2$) during electrically invoked isometric twitch stimulation frequencies of 3 and 5 Hz (110). $\dot{V}\text{O}_2$ is driven by MOP and thus these results are consistent with limited mitochondrial ATP production at higher intensities observed in the present study. Poole and colleagues have also shown reduced $\dot{V}\text{O}_2$ and microvascular impairment in the GK rat during electrically-stimulated muscle contractions (282) but no deficit in blood flow during voluntary running at a fixed low intensity (75). The present study is consistent with adequate skeletal muscle blood flow during low intensity contractions in the diabetic GK rat but an imposed oxygen limitation at the higher intensities. In this context, the higher levels of ADP for a given J_{MOP} (Figure 19B) reflect reduced apparent ADP sensitivity which would result from reduced oxygen supply measured by ^{31}P MRS (136).

4.5.1 Perspectives and Significance

The current study demonstrates skeletal muscle mitochondrial function is not impaired in the Goto-Kakizaki rat model of type 2 diabetes over a broad range of contractile intensities. The implications of this work suggest that there is no relationship between mitochondrial dysfunction and the metabolic deficiencies of type 2 diabetes and this may likely extend to human populations. However, despite such evidence, mitochondrial dysfunction is still targeted for pharmacological development to combat insulin resistance (121, 269). The present work suggests research must take a different direction likely towards the microcirculation where exercise paired with short-term drug-treatment has been demonstrated to vastly improve diabetic muscle function (217).

**CHAPTER 5: OBESITY AND INACTIVITY, NOT HYPERGLYCEMIA,
CAUSE EXERCISE INTOLERANCE IN INDIVIDUALS WITH TYPE 2
DIABETES: SOLVING THE OBESITY AND INACTIVITY VERSUS
HYPERGLYCEMIA CAUSALITY DILEMMA**

5.1 Abstract

Obesity, a sedentary lifestyle and type 2 diabetes are intricately linked conditions contributing to reduced exercise tolerance, significant morbidity, and premature deaths. It is unknown whether the reported exercise intolerance associated with type 2 diabetes is a direct result of the hyperglycemia, the impact of a relatively sedentary lifestyle, or increased adiposity. We hypothesize that obesity and inactivity, not hyperglycemia, cause exercise intolerance in individuals with type 2 diabetes. An analysis of the literature and results from the Goto-Kakizaki (GK) rat model of type 2 diabetes strongly support this hypothesis. GK rats were not sedentary or obese when compared with Wistar control rats and did not have exercise intolerance. Specifically, despite being hyperglycemic, GK rats demonstrated a longer treadmill run time to exhaustion (150.6 ± 9.0 vs. 77.2 ± 12.9 minutes), further distance run ($1,506 \pm 90$ vs. 772 ± 129 meters), more work performed per gram muscle (44.0 ± 2.8 vs. 21.9 ± 3.8 kg*m/g) and a small increase in total vertical work performed when accounting for body mass (116.8 ± 6.3 versus 98.9 ± 15.2 kg*m). These results document preserved exercise tolerance in the non-obese, non-sedentary GK rat supporting the hypothesis that the reported exercise intolerance in models of type 2 diabetes is dependent on obesity and inactivity. Solving the obesity and inactivity versus hyperglycemia causality dilemma is important in understanding the development of type 2 diabetes and implications for future pharmacological and lifestyle interventions.

5.2 Introduction: Background to the Hypothesis

5.2.1 Exercise intolerance associated with type 2 diabetes

Type 2 diabetes has been associated with decreased exercise tolerance [for review, see Regensteiner (311)]. This is an important association because exercise intolerance is a cardiovascular disease risk factor (204, 272) and individuals with type 2 diabetes have an increased risk of cardiovascular disease (201, 344). Furthermore, exercise intolerance negatively impacts activities of daily living which limits performance at work, school and during recreational events. It is not clear if the exercise intolerance associated with type 2 diabetes is a direct result of the disease, the impact of a relatively sedentary lifestyle, increased adiposity (297) or a combination of these factors. This is because type 2 diabetes primarily occurs concurrently with obesity and physical inactivity (404) and can be prevented by maintaining a low body mass index and exercising regularly (186, 404).

5.2.2 Tests of exercise tolerance

Most investigators have employed a maximal exercise test to examine exercise tolerance in individuals and animals with type 2 diabetes (20, 152, 311–313). However it has recently been noted that time to exhaustion at a fixed submaximal work rate is more relevant for assessing exercise tolerance (122). This is suggested because maximum exercise may not accurately reflect activities of daily living since the mechanism of fatigue during maximum exercise may be related to limits of cardiac output, lactate tolerance, or mental fatigue whereas exhaustion during prolonged submaximal exercise may be

related to muscle soreness and substrate availability (19, 65, 78, 102, 147, 148, 300). Importantly, exercise tolerance assessed by time to exhaustion at a fixed submaximal work rate, a more clinically relevant test, has not been documented in individuals or animals with type 2 diabetes (297). We hypothesize that measuring time to exhaustion at a fixed submaximal work rate will help resolve the obesity and inactivity versus hyperglycemia causality dilemma.

5.2.3 An analysis of the literature

Investigators have controlled for activity and obesity when examining questions related to exercise tolerance associated with type 2 diabetes. For example, Fang and colleagues compared body mass index (BMI) and heart rate recovery (HRR, a surrogate for activity) in diabetic patients with normal and reduced exercise tolerance for age (97). Reduced HRR is associated with poor physical fitness (50, 224). In the study by Fang and colleagues, reduced exercise capacity was associated with increasing obesity and reduced activity as noted by HRR (97).

Similarly, Regensteiner and colleagues also controlled for BMI and physical activity as determined by self-reported activity questionnaires. In two initial studies, the investigators reported reduced maximum oxygen uptake ($\dot{V}O_2$ max) in individuals with type 2 diabetes (312, 313). $\dot{V}O_2$ max is a measure of exercise capacity (212, 323). More importantly, in a later study, the investigators did not find differences in $\dot{V}O_2$ max between individuals with type 2 diabetes and control subjects when the individuals with diabetes self-reported higher levels of physical activity (20). Taken together, the results by Regensteiner and colleagues document the importance of controlling for body weight and

physical activity when assessing exercise tolerance in individuals with diabetes since the reduced exercise tolerance appears to be directly related to these initiating conditions. Specifically, when the individuals with diabetes had higher activity levels and similar BMI they did not have exercise intolerance. These results suggest that activity levels may be responsible for the differences in exercise capacity reported in the earlier studies.

In recent work by Slade and colleagues, age, BMI, and activity were matched in control subjects and individuals with type 2 diabetes. In this carefully controlled study, the investigators reported no difference in microcirculatory response following muscle contraction between control and diabetic subjects (350). Microcirculatory response following muscle contraction is an indicator of exercise tolerance (297). Specifically, the investigators measured blood oxygen level dependent (BOLD) changes by MRI following maximal contraction in the dorsiflexors of the leg. Following contraction, both peak and time to peak BOLD response were unchanged in individuals with diabetes, indicating normal blood flow kinetics. The kinetic response of blood flow (and by extension $\dot{V}O_2$) is inversely related to oxygen debt and slowing kinetics contributes to early fatigue (300, 403). Thus, when considering blood flow kinetics as a measure of exercise tolerance, the work by Slade and colleagues suggests that individuals with diabetes have normal exercise tolerance when matched for BMI and activity.

Taken together, the works of Fang and colleagues (97), Regensteiner and colleagues (20, 312, 313), and Slade and colleagues (350) support the hypothesis that when body weight and activity levels are controlled, individuals with type 2 diabetes do not have reduced exercise tolerance.

5.2.4 Solving the obesity and inactivity versus hyperglycemia causality dilemma; “Which came first: the chicken or the egg?”

The critical issue of whether the exercise intolerance reported for individuals with type 2 diabetes is a direct result of the disease or the result of a sedentary lifestyle or increased adiposity can be assessed with the Goto-Kakizaki (GK) rat model of type 2 diabetes (6). The GK model is a hyperglycemic, nonobese rat strain (6) *without* physical inactivity (7). The GK rat model was developed by breeding glucose-intolerant Wistar rats (123). The advantage of this genetic animal model is its reproducibility and healthy Wistar rats are appropriate controls because they derive from the same original strain as the GK rat. The ability to dissociate obesity, inactivity and hyperglycemia is powerful as obesity contributes to both type 2 diabetes and cardiovascular disease (49, 248) and inactivity reduces endurance capacity (147, 149, 157).

5.2.5 Statement of the Hypothesis

We explored the obesity and sedentary lifestyle versus hyperglycemia causality dilemma and studied which causes exercise intolerance in a model of type 2 diabetes. Specifically, we tested the hypothesis that rats with type 2 diabetes, but without obesity or inactivity, have preserved exercise tolerance.

5.3 Methods and Results

5.3.1 Animals

Non-obese and non-sedentary type 2 diabetic male Goto-Kakizaki Rats (n=5, 8-10 months old) and age-matched Wistar control rats (n=3-4) were used to evaluate the initial hypothesis. All procedures were approved by the Michigan State University Institutional Animal Care and Use Committee and complied with The American Physiological Society's "Guiding Principles in the Care and Use of Animals".

5.3.2 Activity levels of Wistar control and GK type 2 diabetic rats

Twelve-hour daytime and twelve-hour nighttime mean activity values, measured via radio telemetry over 8 consecutive days, are shown in Figure 20. No difference was observed in locomotor activity between groups during the day or night cycles (P=0.65 Day; P=0.38 Night). Documentation of similar activity levels between Wistar control animals and GK rats with type 2 diabetes (7), along with the absence of obesity in the GK animals, allowed for testing the hypothesis that rats with type 2 diabetes, but without obesity or inactivity, have preserved exercise tolerance.

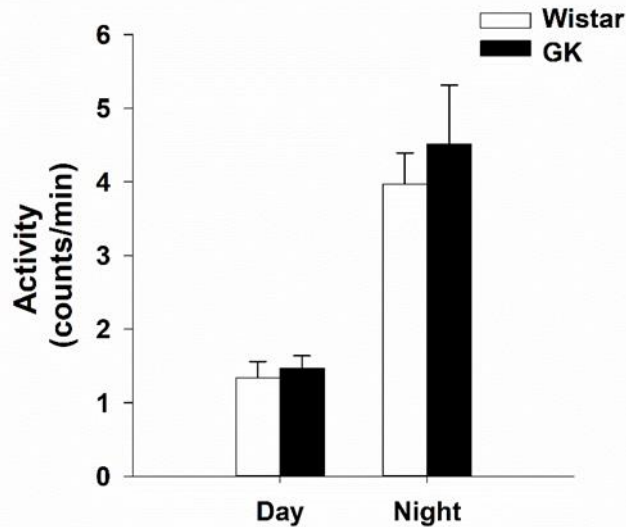


Figure 20. Day/night activity counts averaged over 8 consecutive days. No difference was observed in locomotor activity between GK and Wistar control rats. Values are mean \pm SE, (* P <0.05, two-tailed t-test).

5.3.3 Test of exercise tolerance: time to exhaustion at a fixed submaximal workload

As seen in Figure 21, when performing prolonged submaximal activity (~50-55% $\dot{V}O_2$ Max, which simulates activities of daily living) to exhaustion, GK type 2 diabetic animals ran significantly longer (Figure 21, Panel A), significantly farther (Figure 21, Panel B), performed more vertical work per gram muscle mass (Figure 21, Panel C) and performed similar absolute vertical work compared to their genetic controls (Figure 21, Panel D). Absolute vertical work (body mass x vertical distance) and vertical work per gram of muscle mass are important to consider when assessing exercise tolerance in different sized animals (187). These results support the hypothesis that when accounting for obesity and daily activity, exercise performance is preserved at submaximal workloads in a model of type 2 diabetes. This finding suggests that the cause of the purported

exercise intolerance in individuals with type 2 diabetes is due to obesity and sedentary lifestyle that precedes the disease. This is an important consideration because clinical and observational studies document that exercise tolerance is a strong predictor of cardiovascular and overall mortality (352).

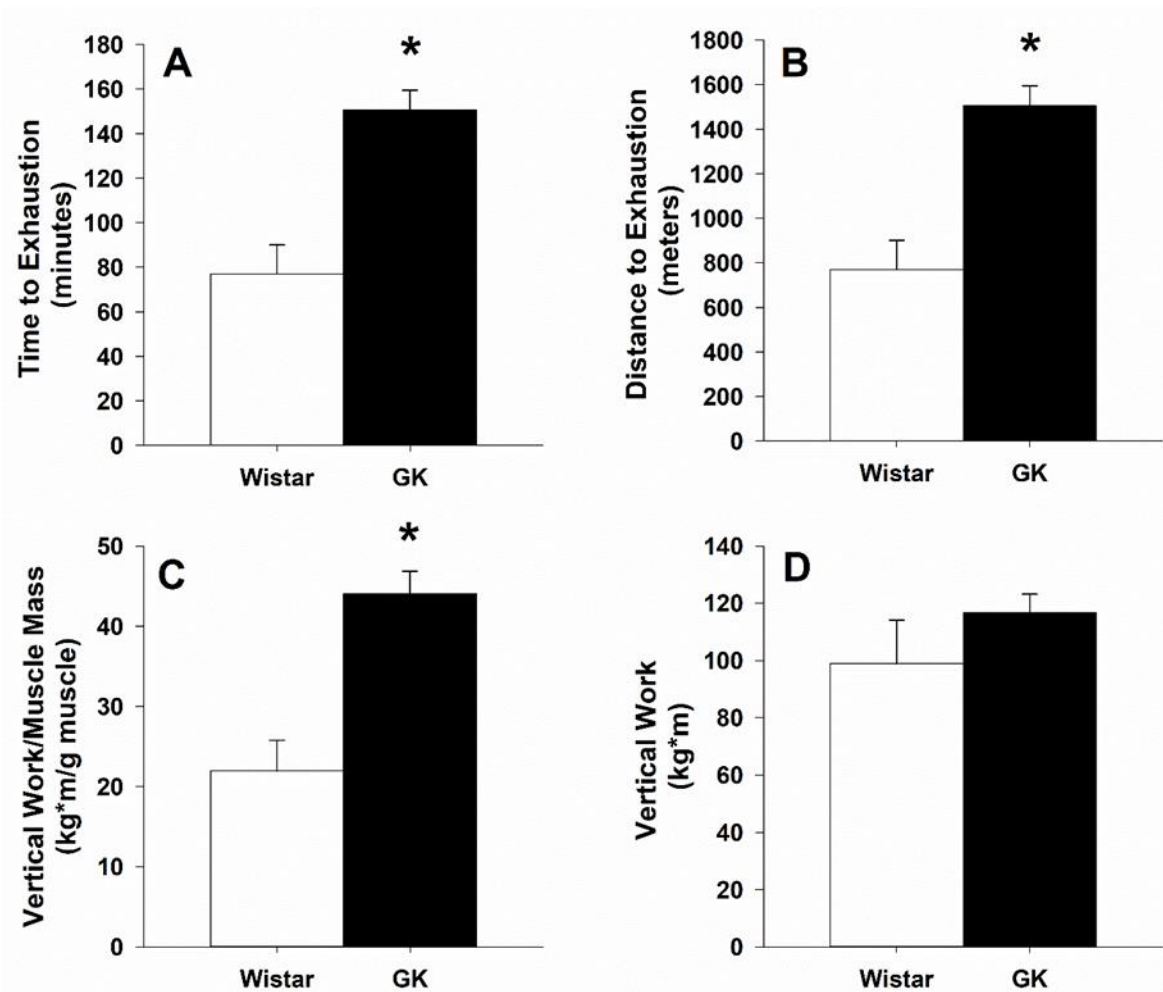


Figure 21. Submaximal workload performance as determined by time to exhaustion (A), distance to exhaustion (B), vertical work performed per gram muscle mass (C), and absolute vertical work performed (D). Values represent Mean \pm SE. GK rats ran significantly longer and farther and performed more vertical work per gram muscle mass. (* $P < 0.05$, two-tailed t-test).

5.4 Discussion: Significance of the Hypothesis

Type 2 diabetes constitutes approximately 90% of all diabetes cases and primarily occurs as a result of obesity and a sedentary lifestyle (404). In fact, the rates of type 2 diabetes have increased markedly since 1960 in parallel with obesity (370). As of 2015, approximately 392 million individuals currently live with type 2 diabetes compared with approximately 30 million in 1985 (351, 385).

According to the national institutes of health (NIH), treatment of type 2 diabetes includes exercise and weight reduction and the onset of type 2 diabetes can be delayed or prevented with regular exercise (186, 247, 279, 307). Importantly, the benefits of exercise to treat diabetes are independent from changes in body weight (307). However, weight loss surgery in those who are obese is also an effective measure to treat diabetes (293). Many individuals are able to maintain normal blood sugar levels with little or no medication following surgery (106) and long-term mortality is decreased (341).

Overweight and obese individuals have lower fitness levels due, in part, to being more sedentary than the general population (236) and having excess weight (373). Similarly, individuals with type 2 diabetes are also more likely to be overweight or obese and sedentary (373). Obesity and sedentary lifestyle are intricately linked conditions responsible for at least 300,000 premature deaths and significant morbidity (236). The results from this study and an analysis of the literature suggest that obesity and sedentary lifestyle, but not hyperglycemia, lead to exercise intolerance.

The mechanisms mediating the preserved exercise tolerance in GK rats are unknown but likely reflect increased substrate availability. In support of this concept,

fasting glucose, as expected, was higher in GK rats compared with Wistar control non-diabetic rats (242 ± 7 versus 154 ± 59 mg/dL, $P < 0.05$), perhaps providing enhanced glucose availability to working muscles. In work by Coggan and colleagues, endurance capacity of healthy individuals, as measured by time to exhaustion at a fixed submaximal work rate, was increased by more than 20% following carbohydrate ingestion after 2 hours of exercise. The authors concluded that increased plasma glucose availability delayed fatigue by increasing carbohydrate oxidation (65). Further, it has been shown that glucose oxidation during exercise is elevated in individuals with diabetes (239). Accordingly, elevated plasma glucose in GK rats may have enhanced endurance capacity at submaximal workloads by providing greater substrate availability.

Although hyperglycemia may have preserved exercise tolerance in the diabetic GK rats, it was also directly associated with increased cardiovascular disease (CVD) risk factors. Specifically, high fidelity recordings of intravascular arterial blood pressure obtained 20 seconds every minute via radio telemetry during eight consecutive days documented significant CVD risks in GK rats. GK rats had daily systolic hypertension without a difference in diastolic blood pressure (Figure 22, Panel A). Since systolic blood pressure was markedly elevated in GK rats and diastolic blood pressure was not different between GK and their genetic controls, pulse pressure (systolic minus diastolic arterial pressure) was also elevated in GK rats (Figure 22, Panel B). This is an important finding since systolic hypertension and elevated pulse pressure are powerful cardiovascular disease risk factors (278, 333, 347). Specifically, increased pulse pressure is consistent with CVD (278, 333, 347) and significant vascular dysfunction. Importantly, vascular dysfunction is consistently reported in individuals and animals with type 2 diabetes (58,

216, 282) and has been reported to be due to hyperglycemia-induced oxidative stress (165).

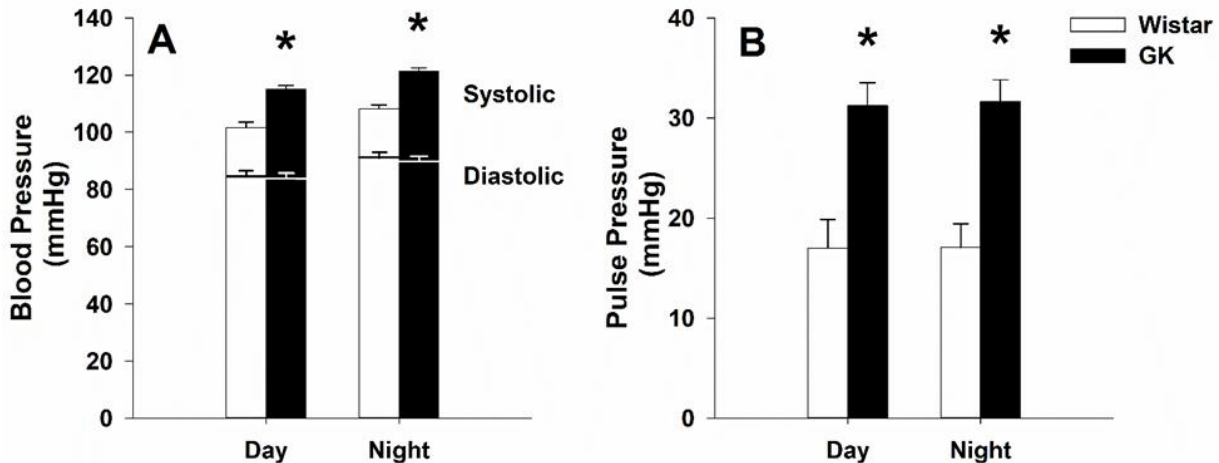


Figure 22. Day/night systolic and diastolic arterial pressure (A) and pulse pressure (B) averaged over 8 consecutive days. GK systolic pressure and pulse pressure were significantly higher than Wistar controls during both day and night while no difference was seen in diastolic pressure. Values are mean \pm SE, (* $P < 0.05$, two-tailed t-test).

Recent work supports the concept that hyperglycemia independently contributes to CVD risk factors (85, 199, 295). Specifically, individuals with impaired glucose tolerance have a two-fold increased risk of macrovascular disease (202, 305). Furthermore, hyperglycemia and CVD are tightly related such that there is an 18% greater risk for CVD per 1% increase in glycosylated hemoglobin (344) for individuals with either type 1 or 2 diabetes. The relationship between hyperglycemia and CVD is also supported by results obtained in individuals with pre-diabetes. Individuals with pre-diabetes do not exhibit elevated fasting blood glucose but following an oral glucose load, glucose levels remain elevated longer than healthy controls. These individuals have a 58% increase in CVD risk factors (77). Thus, even when frank diabetes is not present, CVD risk factors remain evident due to episodes of elevated glucose. Furthermore, intensive treatment of

hyperglycemia in individuals with type 2 diabetes has been shown to significantly reduce CVD risk factors, demonstrating that controlling glycemia alone can reduce risk (166). Thus, hyperglycemia, independent of obesity and sedentary lifestyle promotes cardiovascular disease.

In conclusion, the hypothesis that the reported exercise intolerance associated with type 2 diabetes is a result of obesity and sedentary lifestyle is supported by an analysis of the literature and the non-obese, non-sedentary GK rat model of type 2 diabetes. Specifically, the GK rat model of type 2 diabetes had preserved exercise tolerance when performing at a fixed submaximal work rate. Concomitantly, GK rats showed increased cardiovascular disease risk factors. Importantly, the use of the GK animal allows for the study of the type 2 diabetes hyperglycemic state without the confounding influence of obesity and inactivity.

**CHAPTER 6: THE HYPERTENSION ADVANTAGE AND NATURAL
SELECTION: SINCE TYPE 2 DIABETES ASSOCIATES WITH CO-
MORBIDITIES AND PREMATURE DEATH, WHY HAVE THE GENETIC
VARIANTS REMAINED IN THE HUMAN GENOME?**

6.1 Abstract

Type 2 diabetes is a major public health crisis around the world. It is estimated that more than 300 million people worldwide have type 2 diabetes. Furthermore, the World Health Organization estimates that deaths from the complications of diabetes will increase by two thirds between 2008 and 2030. Since type 2 diabetes is a major public health crisis, why have the genetic variants for diabetes not been removed from the genome by natural selection? We hypothesize that insulin resistance, a predisposition to type 2 diabetes, and the associated elevation in sympathetic nervous system activity and arterial blood pressure provided an advantage to humans who lived as hunter-gatherers. Specifically, sympathetic hyperactivity stimulates the renin-angiotensin aldosterone system, promotes sodium reabsorption, and increases blood volume, heart rate, stroke volume and peripheral vascular resistance, thus inducing hypertension. The hypertension in turn provides a hemodynamic advantage for hunter-gatherers. Specifically, sympathetic hyperactivity and increased blood pressure increases blood flow delivery to working muscles by increasing cardiac output and shunting blood from non-active tissue. This natural selection for hypertension occurred during the time in human evolutionary history when the lifespan of most individuals was probably 30–40 years, and morbidity and mortality from cardiovascular disorders was limited. Thus, the selection pressure for elevation in sympathetic nervous system activity and blood pressure provided an advantage for hunting and gathering that would be greater than the selection pressure exerted by the manifestations of cardiovascular disease in aged individuals.

6.2 Introduction: Background to the Hypothesis

6.2.1 *Type 2 diabetes is destructive to health*

Diabetes was the 7th leading cause of death in 2015 (54) and individuals with diabetes are at increased risk of blindness, renal failure, nerve damage (46), and cardiovascular disease (200, 201, 344). Diabetes mellitus is characterized by reduced glycemic control resulting in elevated glucose levels due to impaired insulin secretion and/or action and its etiology includes two main types: insulin dependent diabetes mellitus (Type 1) and non-insulin dependent diabetes mellitus (Type 2) (9). While type 1 diabetes is a result of complete beta-cell loss, type 2 diabetes arises from developed insulin resistance mostly concurrent with obesity (87.5% of diabetics are overweight or obese) and sedentary lifestyle (40.8% of diabetics get less than 10 minutes of moderate physical activity per week) (9, 54, 404). However, while commonly described as a lifestyle-disease, type 2 diabetes also involves a genetic component and occurs in select individuals without adiposity due to its genetic predisposition (18, 28, 343). The presence of a genetic contribution to type 2 diabetes suggests evolutionary conservation of genes contributing to insulin resistance. Importantly, preservation of these genes is not expected unless they provided a survival advantage. What is the survival advantage of type 2 diabetes?

6.2.2 *The “thrifty genotype” and “carnivore connection” hypotheses*

If diabetes is so destructive to health, shouldn't the genetic variants for diabetes have been removed from the genome by natural selection? The most well-accepted

hypothesis for the evolutionary conservation of genes resulting in diabetes was developed by University of Michigan geneticist James Neel in 1962. Neel described the evolutionary advantage of insulin resistance when humans were primarily hunters and gatherers (274, 275). His “thrifty-gene” hypothesis suggests that insulin resistance was important for efficient use of nutritional resources during periods when food was scarce, specifically conservation of glucose after a feast and prevention of hypoglycemia during periods of famine (274). Other hypotheses, e.g. the “carnivore connection,” suggest that insulin resistance developed due to the protein-rich diets in hunters and gatherers to accommodate low carbohydrate intake (66, 259). While these advantages may have ensured human survival as hunter-gatherers, continuation of this phenotype in modern societies may contribute to the epidemic of type 2 diabetes. The concept of evolutionarily conserved traits that can be disadvantageous in modern society is perhaps best illustrated by the sickle cell trait (274). The sickle cell trait is an evolutionary advantage selected for its nearly 10-fold reduction in severe cases of malaria in individuals heterozygous for the sickle cell gene (144). However, in modern societies where malaria is limited, mainly the negative aspects of sickle cell anemia remain.

6.2.3 The hypertension hypothesis

We hypothesize that insulin resistance, a predisposition to type 2 diabetes, and the associated elevation in sympathetic nervous system activity and arterial blood pressure provided an advantage to humans who lived as hunter-gatherers. Insulin resistance causes sympathetic hyperactivity (Figure 23). Sympathetic hyperactivity stimulates the renin-angiotensin aldosterone system, promotes sodium reabsorption, and

increases blood volume, heart rate, stroke volume and peripheral vascular resistance, thus inducing hypertension. The sympathetic hyperactivity and hypertension provide a hemodynamic advantage for hunter-gatherers by increasing cardiac output and shunting blood from non-active to active tissues thus increasing blood flow delivery to working muscles. This natural selection for hypertension occurred during the time in human evolutionary history when the lifespan of most individuals was probably 30–40 years, and morbidity and mortality from cardiovascular disorders would be limited because the impact of hypertension and related cardiovascular diseases are pathologies of old age (171). Moreover, since the detrimental effects of hypertension do not develop until after the reproductive years, the selection pressure for mechanisms that promote hunting and gathering would be greater than that exerted by the manifestations of cardiovascular disease in aged individuals (171).

6.2.4 Hypertension enhances exercise tolerance

An analysis of the literature supports the notion that inherited hypertension, resulting from exaggerated sympathetic activity at rest and during exercise, plays a beneficial role in exercise performance (Figure 23). Increased sympathetic activity during exercise is necessary to maintain arterial blood pressure and increase perfusion pressure to working skeletal muscle that results in increased blood flow delivery (61, 112). This response is mediated by increases in cardiac output and vasoconstriction to non-active tissue that redistribute blood flow towards exercising muscle (61, 330). The importance of elevated perfusion pressure on skeletal muscle performance is well-demonstrated by a series of innovative experiments by McCloskey and colleagues. Utilizing supramaximal

stimulation of the ulnar nerve via bipolar surface electrodes, isometric contractions were performed in the adductor pollicis muscle. During the exercising protocols, central blood pressure was measured and hydrostatic pressure was altered by positioning the hand above and below the heart. In one study, using this interesting technique, the authors demonstrated that the adductor pollicis muscle fatigued more quickly when the arm was elevated 45 centimeters and fatigued more slowly when lowered 45 centimeters (103). The change in muscle performance was attributed to the change in perfusion pressure resulting from raising and lowering the hand relative to heart level. In subsequent work, a similar experiment was completed with subjects performing voluntary adductor pollicis muscle exercise at and above heart level on two separate days (415). This exercise protocol involved 6 second sustained contractions at 50% of the maximum voluntary contraction (determined prior to protocol) with 4 seconds of rest between each contraction for a period of ten minutes. During the 4 second rest period, the ulnar nerve was stimulated to determine twitch strength and measure fatigue. The authors documented similar results of a reduced exercise performance when perfusion pressure was reduced by raising the hand above the heart compared to exercise performance when the hand was held at heart level. This study, using voluntary exercise, supports previous findings using electrically-induced contractions (415). Moreover, in a subsequent study the authors extended these findings, documenting that increasing systemic blood pressure increases exercise performance (416). Specifically, Wright and colleagues measured muscle fatigue in the adductor pollicis muscle at “normal” systemic blood pressure and demonstrated reduced fatigue after increasing systemic blood pressure by voluntary contraction of leg muscles. Contraction of this larger muscle mass increased sympathetic

activity and resulted in elevated systemic blood pressure (416). Taken together, the results from these studies document the critical role of perfusion pressure on muscle performance.

The critical role of perfusion pressure on exercise performance has also been demonstrated during dynamic treadmill running. In 1998, Barbato and colleagues tested 11 different inbred strains of rats for aerobic treadmill running capacity and found a continuum in capacity (16); the Dark Agouti (DA) strain of rats displayed the highest whereas the Copenhagen (COP) strain of rats displayed the lowest capacity for endurance running. Importantly, the DA rats had higher arterial pressure and heart rate during dynamic treadmill running. Furthermore, autonomic control of peripheral vascular function was also greater in the DA rats. Because endurance capacity is dependent on the exquisite matching of cardiac output and peripheral vascular tone, these phenotypic differences between DA and COP rats might be causative of the differences in aerobic capacity between the strains. The authors concluded that increased autonomic function and arterial blood pressure directly contributed to increased exercise performance (187).

Exercise performance is also enhanced in individuals with spinal cord injury by increasing arterial blood pressure. Specifically, cervical and thoracic spinal cord injury (SCI) causes loss of supraspinal control over sympathetic pre-ganglionic neurons. This leads to profoundly reduced sympathetic activity, hypotension, and a significantly reduced hemodynamic response to activities of daily living (ADL) as well as a reduced physical work capacity (PWC) (156, 194, 292). To overcome restrictions to activities of daily living and reduced physical work capacity, some individuals with SCI have resorted to the practice of “boosting”. Boosting involves the intentional induction of autonomic

dysreflexia (AD) (114, 397). Autonomic dysreflexia causes a profound increase in sympathetic activity and blood pressure (68, 69). AD-induced increases in sympathetic activity cause an increase in heart rate, blood pressure, cardiac output and oxygen transport to the working musculature thus increasing physical work capacity and delaying fatigue. Some paralympic athletes have also resorted to the banned practice of boosting to elevate arterial blood pressure and enhance (boost) exercise performance (26, 241). This example of boosting in individuals with spinal cord injuries further documents the profound benefits of elevated blood pressure on exercise performance.

6.2.5 Statement of the Hypothesis

We posit that type 2 diabetes, and the associated elevation in sympathetic nervous system activity and arterial blood pressure, provides an advantage to humans who lived as hunter-gatherers by increasing exercise tolerance. Specifically, insulin resistance causes sympathetic hyperactivity (Figure 23). Sympathetic hyperactivity stimulates the renin-angiotensin aldosterone system, promotes sodium reabsorption, and increases blood volume, heart rate, stroke volume and peripheral vascular resistance, thus inducing hypertension. The hypertension provides a hemodynamic advantage by increasing cardiac output, increasing blood flow delivery to working muscles and shunting blood from non-active tissue.

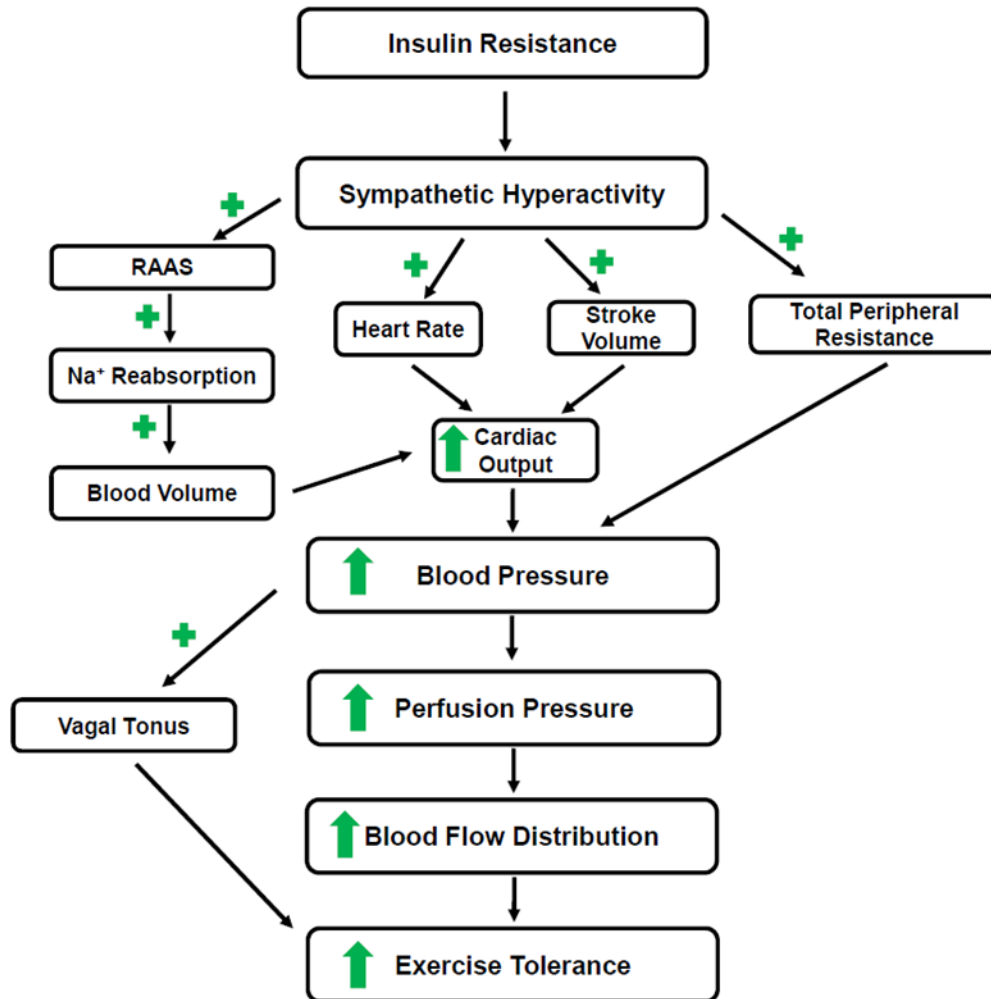


Figure 23. Schematic representation of the presented hypothesis. Insulin resistance directly stimulates sympathetic hyperactivity, resulting in cardiovascular adaptations that are consistent with and contribute to increased exercise tolerance.

6.3 Methods and Results

6.3.1 Animals

A non-obese and non-sedentary genetic model of type 2 diabetes, the Goto-Kakizaki (GK) Rat (male, 8-10 months old) and age and sex-matched Wistar control rats were used to evaluate the initial hypothesis. All procedures were approved by the Michigan State University Institutional Animal Care and Use Committee and complied with The American Physiological Society's "Guiding Principles in the Care and Use of Animals". In all procedures performed, rats were chronically instrumented with a radio telemeter device to record arterial blood pressure and heart rate and a Doppler ultra-sonic flow probe around the popliteal artery to record muscle blood flow (221).

6.3.2 Advantage during hunting and gathering; test of exercise tolerance

An exercise tolerance test determined by voluntary treadmill running, without aversive stimuli, at a fixed submaximal rate to exhaustion [10 m/min (221)] demonstrated that the genetic GK type 2 diabetic rats ran longer (Figure 24, Panel A), farther (Figure 24, Panel B) performed more vertical work per gram muscle mass (Figure 24, Panel C) and performed similar absolute vertical work compared to their genetic Wistar controls (Figure 24, Panel D). An increased endurance exercise performance would have been an advantage for the nomadic lifestyles of hunter-gatherers. Although increased substrate availability likely contributes to increased exercise performance in the genetic GK type 2 diabetic rats (221), we posit that an elevated arterial blood pressure during exercise (see below) is also a major contributing factor.

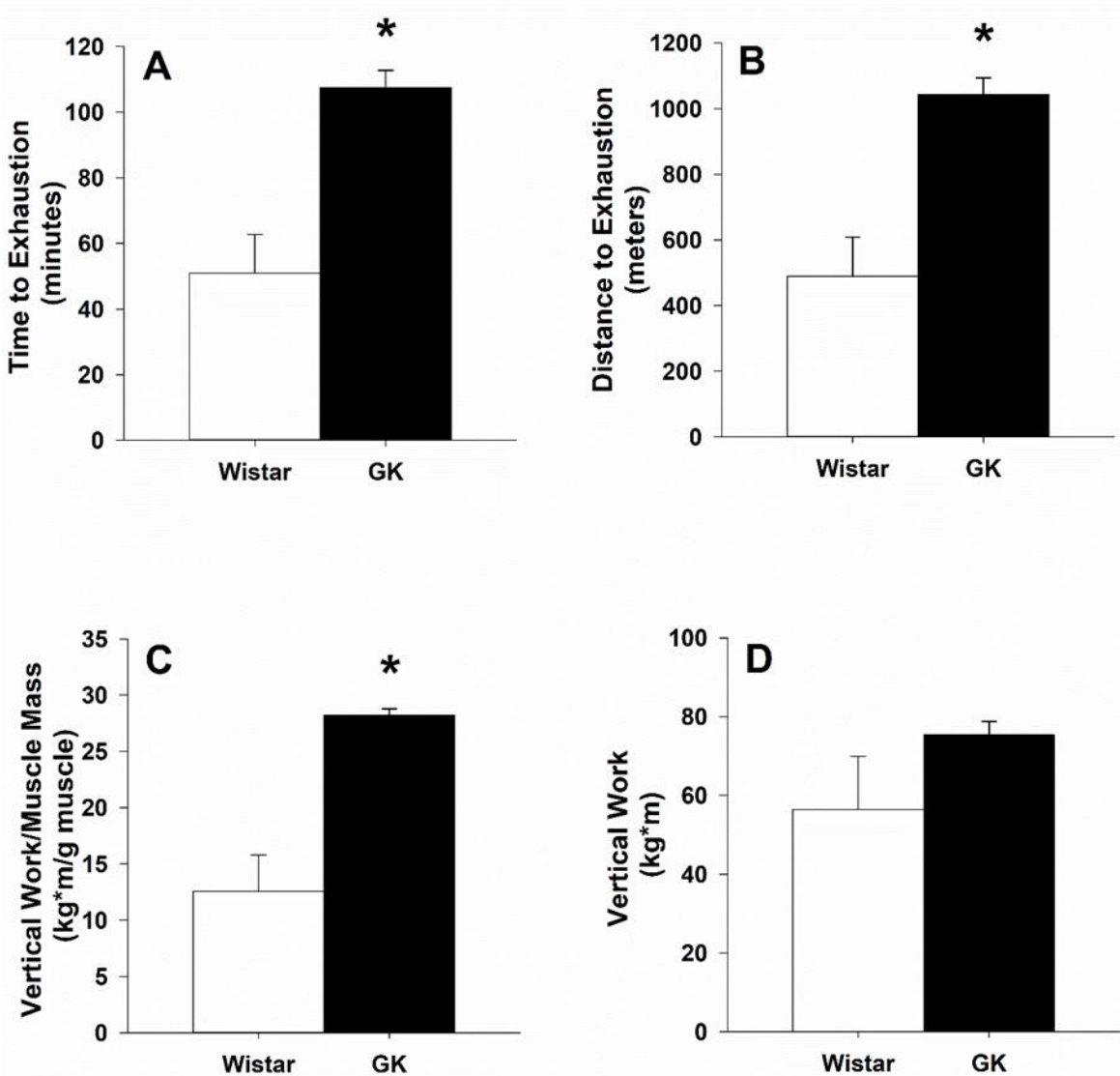


Figure 24. Voluntary treadmill running performance presented as time to exhaustion (A), distance to exhaustion (B), vertical work performed per gram muscle mass (C), and absolute vertical work performed (D). Values represent Mean \pm SE. Genetic GK type 2 diabetic rats ran significantly longer and farther and performed more vertical work per gram muscle mass. (* $P < 0.05$, two-tailed t-test).

6.3.3 Benefits of hypertension during exercise

Arterial blood pressure (Figure 25, Panel A) and heart rate (Figure 25, Panel B) were significantly higher during voluntary treadmill running at a fixed submaximal rate to

exhaustion in the genetic GK type 2 diabetic rats compared with their genetic control. The higher blood pressure and heart rate in the genetic GK type 2 diabetic rats was associated with a higher exercising muscle blood flow (Figure 25, Panel C) and lower exercising muscle vascular resistance (Figure 25, Panel D). These results suggest that sympathetic hyperactivity increases blood flow delivery to working muscles by increasing heart rate and cardiac output and shunting blood from non-active tissue to exercising muscle.

Similarly, arterial blood pressure (Figure 26, Panel A) and heart rate (Figure 26, Panel B) were significantly higher during a graded (5, 10 and 15 meters/min) exercise test in the genetic GK type 2 diabetic rats compared with their genetic control. The higher blood pressure and heart rate in the genetic GK type 2 diabetic rats was associated with a higher exercising muscle blood flow (Figure 26, Panel C). Again, these results suggest that sympathetic hyperactivity increases blood flow delivery to working muscles by increasing heart rate and cardiac output and shunting blood from non-active tissue to exercising muscle. These data support the hypothesis since increased tissue perfusion as a result of increased arterial blood pressure would have been an advantage for the nomadic lifestyles of hunter-gatherers (99, 133, 185).

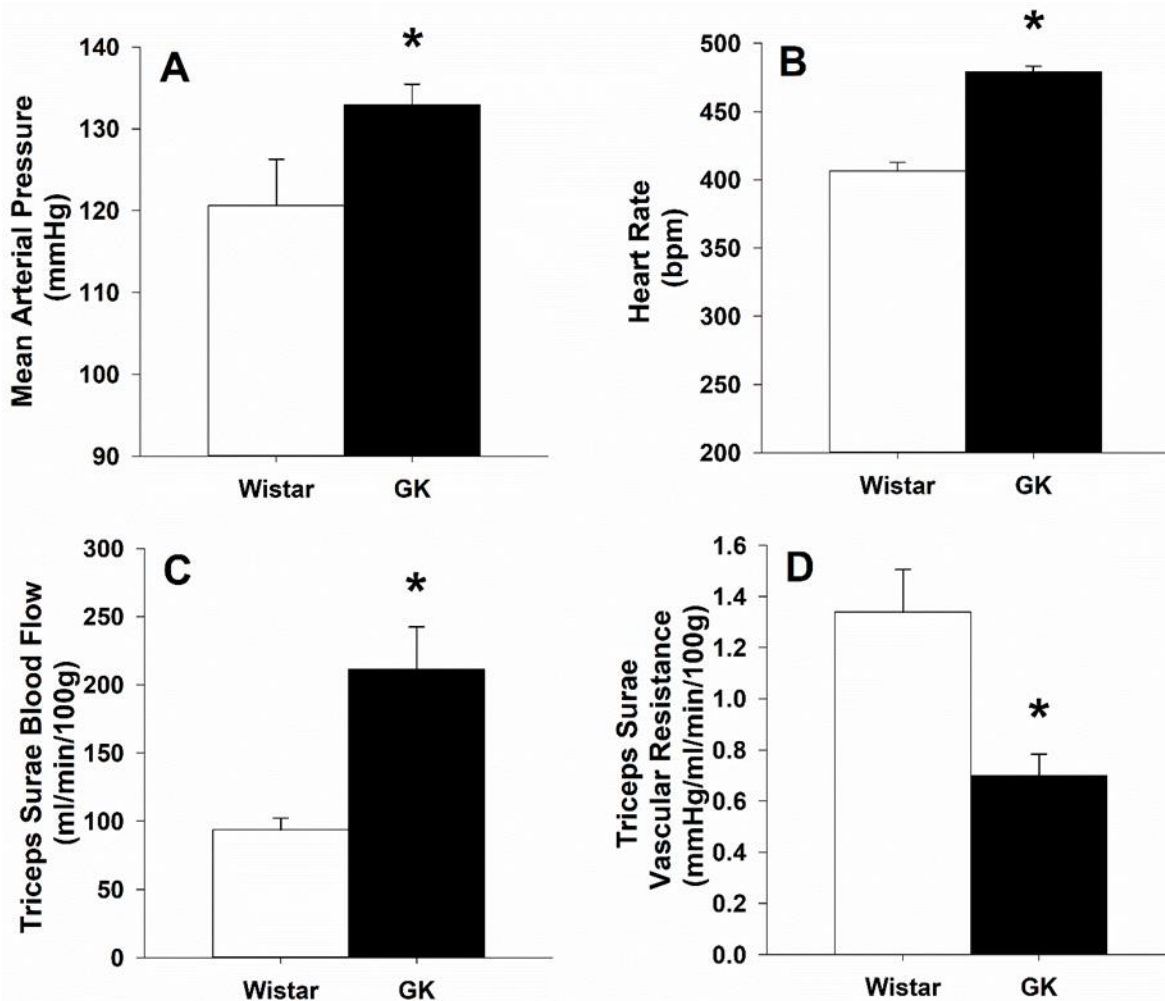


Figure 25. Mean \pm SE mean arterial pressure (A), heart rate (B), triceps surae blood flow (C), and triceps surae vascular resistance (D) for Wistar and GK rats during running to exhaustion. MAP, HR, and triceps surae blood flow were each significantly higher in GK rats while triceps surae vascular resistance was significantly reduced. [$*P < 0.05$, one-tailed t-test (A,B); two-tailed t-test (C,D)].

6.3.4 Parasympathetic hyperactivity

Lower resting heart rate and high autonomic vagal activity are strongly associated with increased exercise capacity. In fact, recent evidence suggests that the strength of cardiac vagal activity *causally* determines the ability to exercise (124, 231). A highly

reproducible measure of vagal activity is the speed of heart rate recovery (HRR) after exercise.

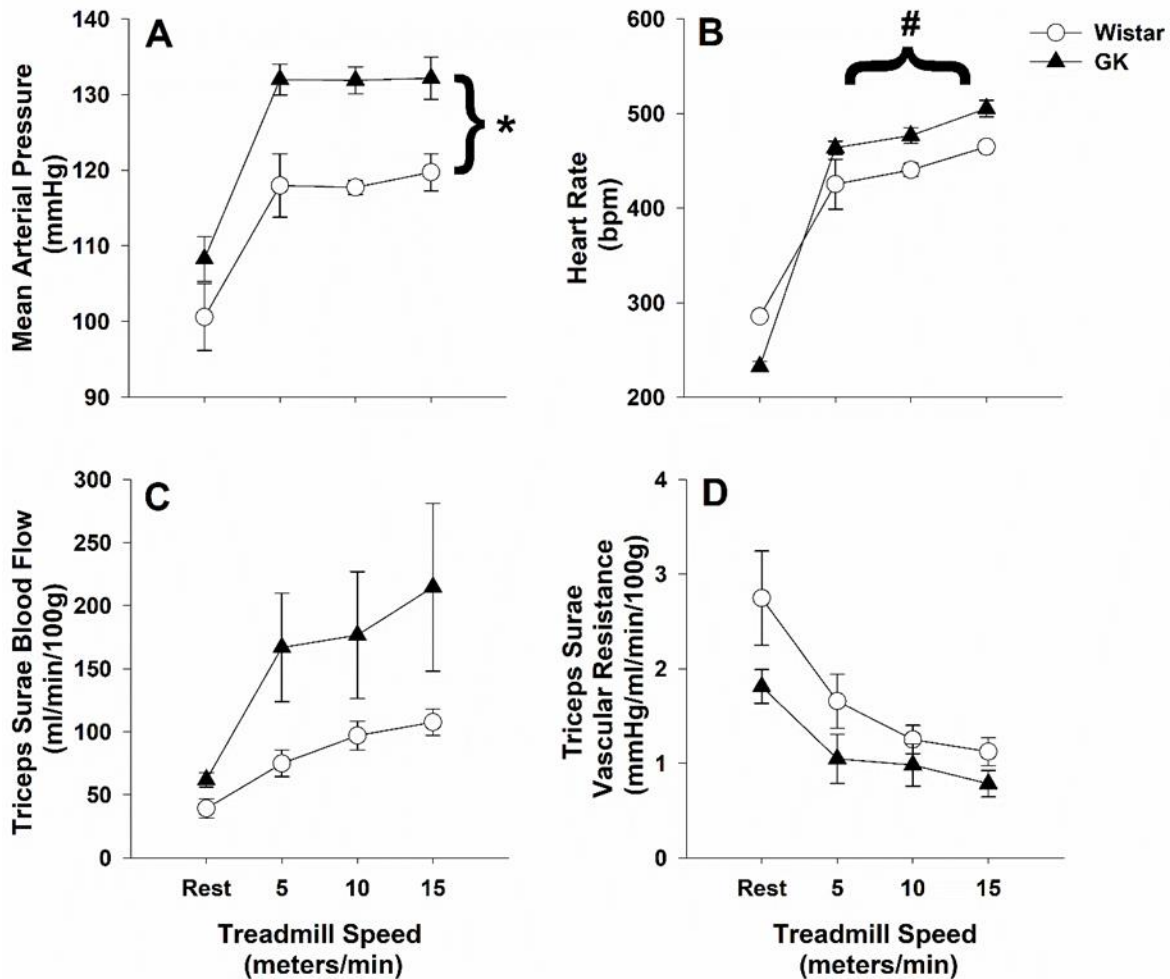


Figure 26. Mean \pm SE mean arterial pressure (A), heart rate (B), triceps surae blood flow (C), and triceps surae vascular resistance (D) during rest and graded exercise at 5, 10, and 15 m/min. Arterial pressure was increased in GK rats and heart rate showed a group x treadmill speed interaction (* $P < 0.05$, group difference two-way repeated measures ANOVA; # $P < 0.05$, group x treadmill speed interaction two-way repeated measures ANOVA).

There is a strong causal relationship between the rate of HRR and exercise capacity. As an example, there is a dramatic absolute difference in HRR between athletes and individuals with heart failure (231). The reduced resting heart rates in the GK animals (Figure 26, Panel B) suggest increased parasympathetic activation compared with their

genetic Wistar controls. In fact, the lower heart rate in the genetic GK type 2 diabetic rats compared with their genetic control was associated with a significantly enhanced parasympathetic tonus (Figure 27, Panel A) (57, 187, 227). In addition, HRR is mediated by the rate of vagal re-activation (74, 124). In agreement with the lower resting heart rate and higher parasympathetic tonus, HRR was faster in GK rats compared to genetic Wistar controls determined from change in heart rate during the first 20 seconds as well as during the first 3 minutes post-exercise cessation (Figure 27, Panel B). The increases in vagal tone in GK animals support the increased exercise tolerance (Figure 24) as increased vagal tone measured by HRR is documented to be the most effective predictor of exercise performance (124, 231).

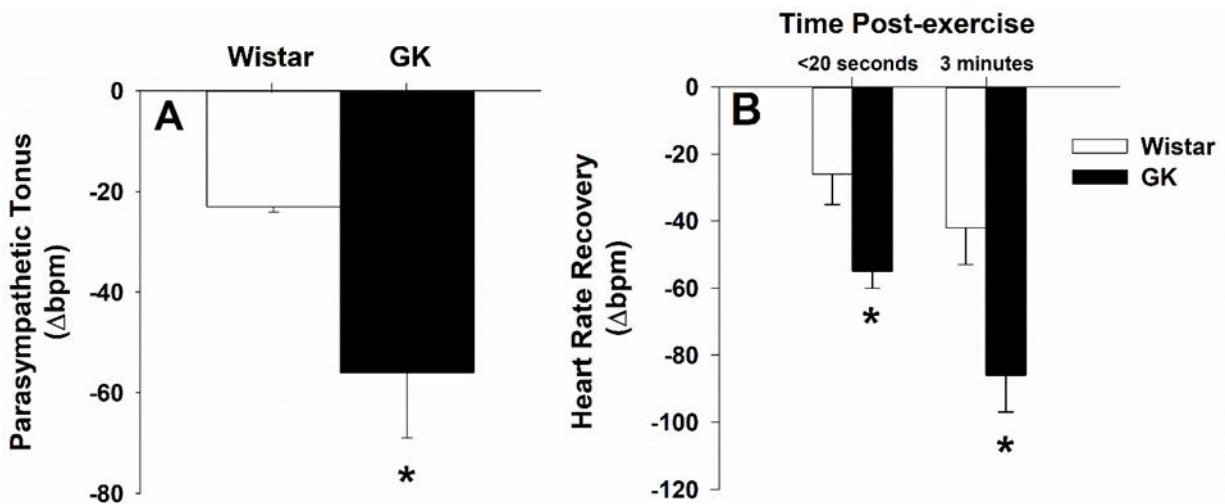


Figure 27. Markers for vagal activity: Mean +/- SE resting parasympathetic tonus (A) and heart rate recovery (HRR) following exercise to exhaustion (B). Parasympathetic tonus was significantly elevated in GK rats compared to controls and HRR was significantly faster when measured at approximately 20 seconds and 3 minutes after exercise (*P<.05, one-tailed t-test).

6.3.5 Costs of hypertension during exercise

The elevated blood pressure and heart rates during exercise caused a greater metabolic demand on the heart as measured by the rate pressure product (Figure 28, Panels A and B). Indirect indices of myocardial oxygen consumption (rate pressure product, tension-time index, double product, and triple product) are used in clinical and experimental studies (15). These indirect indices are highly correlated with direct measurements of myocardial oxygen consumption and energy demand of the heart (119). The cost of increased sympathetic activity elevating blood pressure, heart rate and blood flow delivery to the working muscle resulted in an increased rate pressure product. This cost of exercise places a higher demand on the heart and would be a serious concern in modern society.

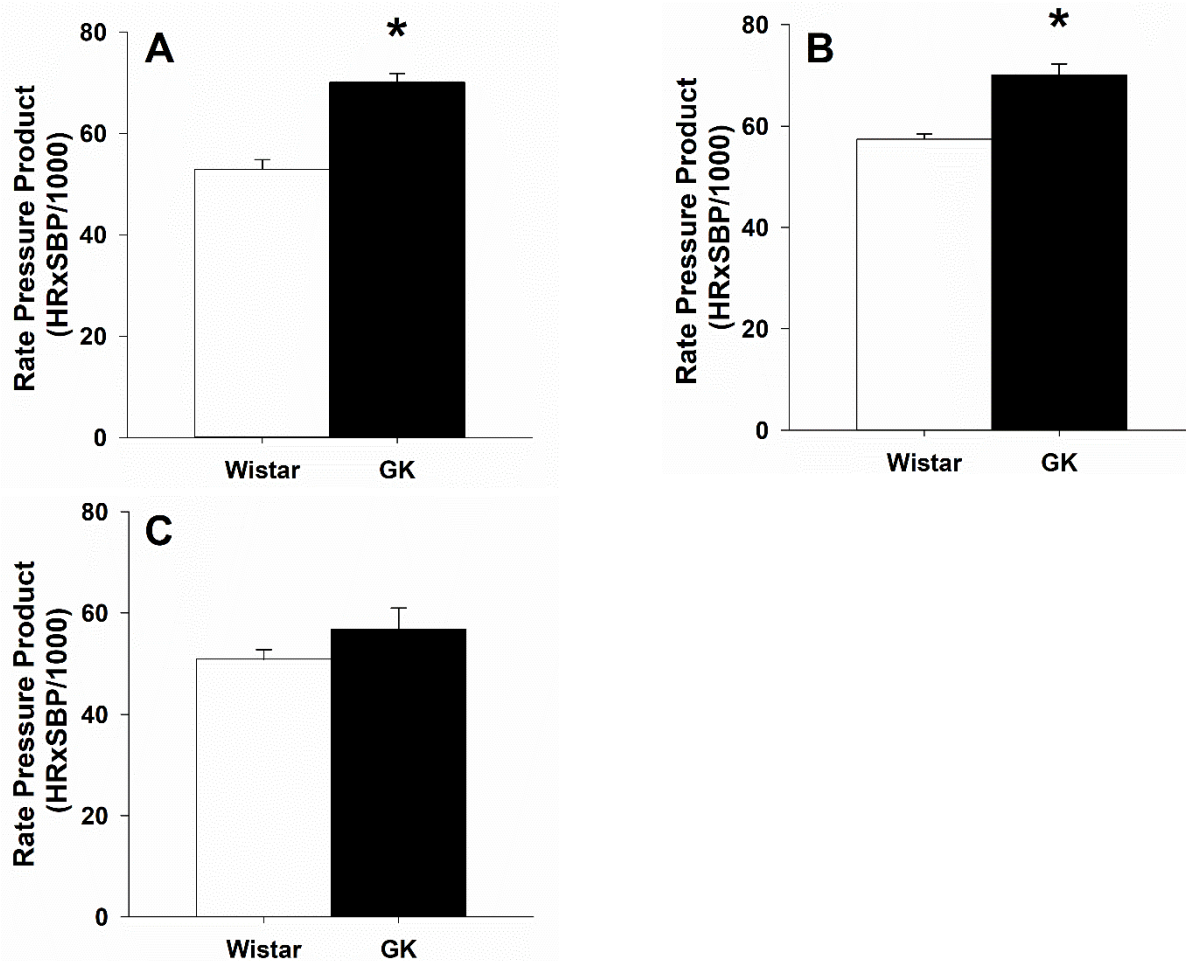


Figure 28. Mean \pm SE rate pressure product for Wistar and GK rats. Rate pressure product was significantly elevated in GK rats during running to exhaustion (A) and graded exercise (B) but not different during stress test (C) ($P=0.34$). (* $P<0.05$, two-tailed t-test).

6.3.6 Additional negative consequences of the “hypertension advantage”

Increased cardiovascular reactivity, a marker for cardiovascular disease, was documented in the GK type 2 diabetic rats (Figure 29). Specifically, a psychological stressor [restraint stress (228)] was used to test cardiovascular reactivity in genetic GK type 2 diabetic rats and Wistar control rats. Restraint stress challenges the cardiovascular

system with a mental stressor and documents an emotional psychological hemodynamic response. Genetic GK type 2 diabetic rats demonstrated elevated arterial blood pressure response (Figure 29, Panel A) to restraint stress. Exaggerated arterial pressure responses to stress are deleterious to cardiovascular health and are significant cardiovascular disease risk factors. Specifically, an elevated arterial blood pressure response to mental stress is a cardiovascular disease risk factor (60, 369) and high blood pressure reactivity to mental stressors has been linked to an increased incidence of myocardial ischemia and greater risk for untoward cardiac events (193, 195, 237, 342). As an example, white coat hypertension, an elevation in arterial blood pressure from feelings of anxiety in a medical environment, is associated with increased cardiovascular risk (107, 160). Similarly, an elevated arterial blood pressure response to mental arithmetic is associated with increased cardiovascular risk (60).

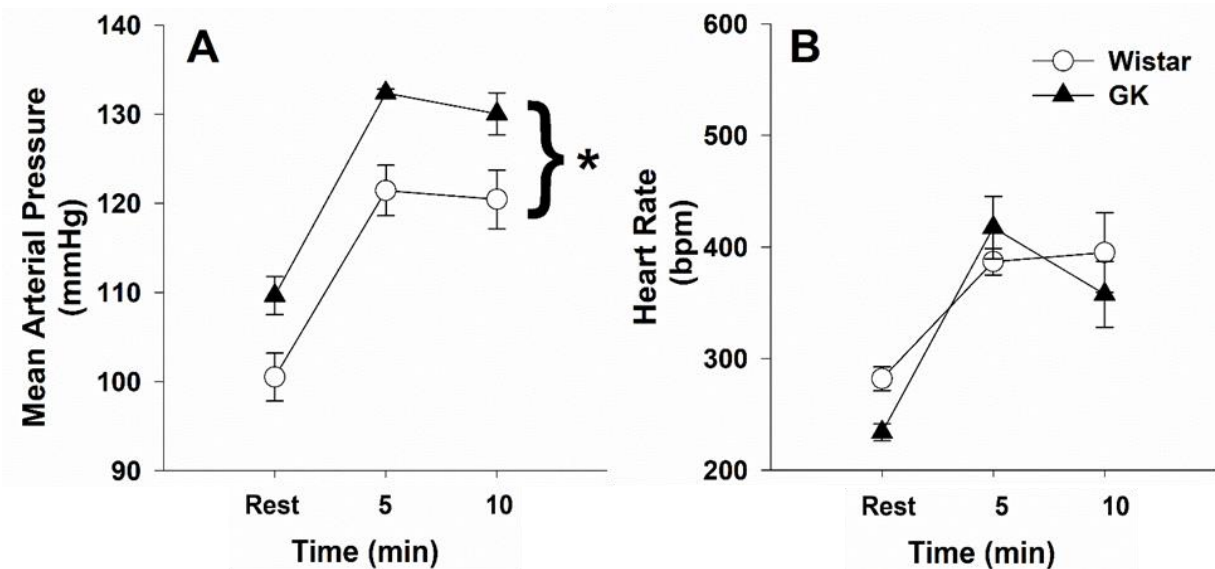


Figure 29. Mean \pm SE mean arterial pressure (A) and heart rate (B) for Wistar and genetic GK type 2 diabetic rats at rest and during restrainer stress challenge. Mean arterial pressure was significantly higher in GK rats (* $P < 0.05$, two-way repeated measures ANOVA).

Other measures of cardiovascular disease risk factors at rest in the GK type 2 diabetic rats included ~14% increased pulse wave velocity compared with Wistar controls indicating reduced vascular compliance. Pulse wave velocity (PWV), an index of aortic compliance and macrovascular disease, was determined at rest by measuring time from the foot of the arterial blood pressure pulse recorded in the arch of the aorta to the foot of the blood flow pulse recorded in the hindlimb (263, 365). PWV provides information about the elastic properties of the arterial system and is defined as the velocity at which the pressure waves, generated by the systolic contraction of the heart, propagate along the arterial tree. The higher PWV corresponds to lower vessel compliance and, therefore, to higher arterial stiffness (32, 41). PWV was increased in GK type 2 diabetic rats compared to Wistar control rats (615.8 ± 16.8 versus 542.5 ± 38.8 cm/s) consistent with arterial stiffness and cardiovascular disease. Individuals with type 2 diabetes are documented to have 20-30% faster PWV and mortality risk is increased by 8% per 1 m/s increase in PWV (83). Taken together, results document enhanced CVD risk factors in animals with genetically-induced type 2 diabetes. This natural selection for hypertension and the resulting increased CVD risk factors occurred during the time in human evolutionary history when the lifespan of most individuals was probably 30–40 years (171), and morbidity and mortality from cardiovascular disorders was limited. Thus, the selection pressure for elevation in arterial blood pressure provided an advantage for hunting and gathering that was greater than the selection pressure exerted by cardiovascular disease in aged individuals (171).

6.4 Discussion: Significance of the Hypothesis

The capacity to enhance a sympathetically driven hypertensive response would be an advantage to hunters and gatherers. Hunters and gatherers evolved under environmental conditions in the hot African savannah that posed a threat of circulatory collapse (171, 229). Specifically, hunters and gatherers were exposed to acute extracellular fluid losses from injury-induced hemorrhage and water and sodium loss via perspiration. Restoring extracellular volume and maintaining blood pressure was difficult especially during a prolonged dry season. This challenge required adaptations that maintained blood volume and blood pressure. Accordingly, we propose the capacity to enhance a sympathetically driven hypertensive response evolved to meet this challenge. However, today, this environmentally and activity triggered phenotypic adaptation contributes to the pathogenesis of hypertension.

6.4.1 Phenotypic similarities of the genetic GK type 2 diabetic rats and exercise training

The primary purpose of the cardiovascular system is to supply tissues with adequate blood flow and oxygen delivery to match metabolic demand and support aerobic respiration. In skeletal muscle, especially during whole body dynamic exercise, the limitation to aerobic respiration is adequate supply of oxygen. As reviewed by Bassett and Howley (2000), the limit to metabolic demand as determined by measuring the maximal oxygen consumption ($\dot{V}O_2\text{Max}$) is related to one of four mechanisms that play a role in oxygen dynamics: 1) pulmonary diffusing capacity, 2) cardiac output, 3) O_2 carrying capacity, or 4) skeletal muscle uptake (19). In subjects with normal lung function

and blood hemoglobin, the limitation to $\dot{V}O_2\text{Max}$ is inadequate cardiac output to perfuse all active tissue (11, 79, 118, 184, 318, 387). Thus the most significant adaptation improving oxygen delivery is increased maximal cardiac output in trained athletes (94, 139). Aerobic exercise training results in an elevated cardiac output by several mechanisms including an increase in heart size (286, 324), contractility (100, 139), and blood volume (72, 73). Interestingly, the genetic GK type 2 diabetic rats in the present work showed similar functional adaptations. Specifically, the genetic GK type 2 diabetic rats presented with increased heart mass to body mass ratio (0.28 ± 0.01 versus 0.20 ± 0.01 %, $P < 0.05$ two-tailed t-test) and increased heart rates during exercise (Figure 25, Panel B; Figure 26, Panel B) suggesting increased cardiac output. Furthermore, while blood volume was not measured in these animals, the mechanisms resulting in hypertension (Figure 23) closely resemble mechanisms increasing blood volume following exercise training. Exercise training increases blood volume, in part, via increased sympathetic nervous activity activating the renin-angiotensin aldosterone system (RAAS) that results in increased sodium reabsorption and renal water retention (73). Similarly, increased sympathetic activity associated with hypertension directly stimulates the RAAS and increases water retention thus expanding blood volume (171). Further adaptations to aerobic exercise training that permit increased oxygen delivery include alterations to vessel structure, number, and reactivity to increase perfusion capacity to the musculature (92, 162). Although previous studies in the GK rat demonstrate altered vascular structure, number and reactivity (59, 110, 125), at the exercise intensities invoked in the current work perfusion to exercising muscle was elevated (Figure 25, Panel C; Figure 26, Panel D) suggesting adequate vessel responses.

Taken together, the cardiovascular adaptations in the GK rat closely resemble adaptations to endurance exercise training and support increases in treadmill exercise performance (Figure 24).

6.4.2 Cardiac vagal activity is strongly associated with exercise capacity

Endurance exercise training is well established to alter autonomic nervous system activity, resulting in an apparent increase in cardiac parasympathetic tone. In fact, resting bradycardia is a well-established consequence of exercise training (29, 88, 95, 120). In this context, the resting heart rate in elite endurance athletes is low due to exceptionally high parasympathetic vagal tone in these select individuals (52, 335). Thus, resting vagal activity directly relates with exercise training (27, 84, 285). Importantly, the genetic GK type 2 diabetic rats had a lower resting heart rate (Figure 26, Panel B) and higher parasympathetic tone (Figure 27, Panel A).

Parasympathetic tone and heart rate recovery have recently been identified as the greatest predictors of exercise capacity (124, 231). Specifically, Machhada and colleagues (2017) determined the role of parasympathetic control of the heart on exercise capacity by targeting dorsal vagal preganglionic neurons [vagal projections modulating ventricular function (230)] in rats using a reversible inhibitor (231). Before inhibition, experimental and control groups had similar exercise capacities determined by shock grid-motivated treadmill running to exhaustion. On a separate day, after inhibiting dorsal vagal preganglionic neurons, exercise capacity was reduced by 80% compared to baseline. Furthermore, on a separate day, exercise capacity returned to baseline levels

after reversal of inhibition. These data document that vagal activity plays a direct role in enhancing exercise performance.

Interestingly, the GK rat demonstrates similar phenotypes in vagal activity. Specifically, GK rats showed increased vagal activity as determined from reduced resting heart rate (Figure 26, Panel B), increased parasympathetic tonus (Figure 27, Panel A), and increased heart rate recovery (Figure 27, Panel B). Each of these independent measures of increased vagal activity demonstrate increased parasympathetic control of the heart and agree with increased exercise capacity in the GK rat.

6.4.3 Genetic determinants of cardiac vagal tone

Evolutionary conservation of diabetes and hypertension is evident in the literature. Similarly, a high degree of cardiac vagal activity is determined by genetics (124). Although vagal activity increases with exercise training, it was also shown that approximately 60% of HRR is determined by genetics. This was determined by studying 225+ sets of twins and comparing maximum exercise capacity and HRR (273). In accordance with the studies performed with twins, two separate studies using genome-wide association studies (GWAS) identified several independent genes that directly relate to HRR and increased vagal activity (308, 381). The genetic contribution to vagal activity is particularly interesting as in the current context. Specifically, the genetically developed GK rats are genetically predisposed to diabetes, hypertension, and increased parasympathetic activity. The role of each of these factors in improving exercise capacity and characteristics intrinsic to survival for hunters and gatherers suggest they may be inherited in concert.

6.4.4 Summary

The genetic GK type 2 diabetic rats have high sympathetic activity, are hypertensive and have significant cardiovascular disease risk factors. *Thus type 2 diabetes is destructive to health and a major public health concern!* However, if type 2 diabetes is a major public health crisis, why have the genetic variants for diabetes not been removed from the genome by natural selection? We hypothesize that insulin resistance, a predisposition to type 2 diabetes, and the associated elevation in sympathetic nervous system activity and arterial blood pressure provided an advantage to humans who lived as hunter-gatherers by enhancing exercise capacity. In fact, the genetic GK type 2 diabetic rats run longer and farther than their genetic controls. Importantly, this hypertension exercise advantage evolved at a cost in that these diabetic animals also had higher rate-pressure products and pulse wave velocity than their genetic controls. However, this natural selection for hypertension occurred during the time in human evolutionary history when the lifespan of most individuals was probably 30–40 years, and morbidity and mortality from cardiovascular disorders was limited (171). Thus, the selection pressure for elevation in sympathetic nervous system activity and blood pressure provided an advantage for hunting and gathering that would be greater than the selection pressure exerted by the manifestations of cardiovascular disease in aged individuals (171). It must be noted that in modern day hunter-gatherer civilizations where food is less scarce this is not apparent and their increased activity permits longer lifespans and reduced risk for cardiovascular disease in contrast with the proposed evolutionary hypothesis (306).

**CHAPTER 7: REDUCED SKELETAL MUSCLE BLOOD FLOW
MEASURED BY MR ANGIOGRAPHY IN THE GOTO-KAKIZAKI RAT
MODEL OF TYPE 2 DIABETES**

7.1 Abstract

Type 2 diabetes (T2D) is characterized by hyperglycemia and insulin resistance and is directly linked with increased risk for blindness, cardiovascular disease, and premature death totaling over \$327 billion in US medical costs. Skeletal muscle can be responsible for up to 80% of glucose uptake and this is driven by muscle respiration that requires sufficient skeletal muscle perfusion. Muscle respiratory impairments have been reported in T2D but the role of blood flow delivery is not well understood. In the current study, the Goto-Kakizaki (GK) rat model of T2D was used to quantify blood flow to contracting muscle across a broad range of contractile workloads. GK rats showed reduced maximal delivery rates and reduced total blood flow to the muscle compared with Wistar controls. However, the reduction in blood flow did not cause any deficit in muscle force production. Maintained force production in the GK rat was likely permitted since the GK rat showed similar changes in blood flow in response to contraction but with a downward shift in absolute flow. Reduced blood flow delivery but no reduction in force suggests oxygen extraction increased to maintain muscle $\dot{V}O_2$ and is consistent with recent work in the GK rat. Taken together, these results suggest that reported deficiencies in T2D skeletal muscle may be attributed to deficient blood flow delivery.

7.2 Introduction

The worldwide prevalence of diabetes has exceeded 422 million (418) and 85-95% of these individuals are type 2 diabetics (T2D) (54, 371). T2D is characterized by hyperglycemia and insulin resistance (10) and its severity directly relates with reduced quality of life (113, 402). Individuals with diabetes are at increased risk of cardiovascular disease (85, 96, 199, 344) including macrovascular (202, 305) and microvascular (17, 182) complications that are strong predictors of poor quality of life (402) and contribute to reduced activity of daily living and premature death (10, 67, 113, 402). Quality of life can be reduced by vascular disease since activities of daily living and glucose disposal rely on sufficient skeletal muscle blood flow delivery (19, 182).

Muscle respiration is determined by the number and function of mitochondria within the tissue and not oxygen delivery/blood flow in healthy individuals during small muscle mass exercise such as plantar flexion (39, 116, 135, 243). However, muscle respiration requires sufficient oxygen delivery ($\dot{Q}O_2$) to support oxygen utilization ($\dot{V}O_2$) by the mitochondria and reductions in oxygen could reduce respiration (189, 245). This has been shown using parallel measures of femoral blood flow, muscle metabolism, and muscle oxygenation by doppler ultrasound, phosphorus magnetic resonance spectroscopy (^{31}P MRS), and near-infrared spectroscopy (NIRS) respectively (245). Blood flow to working gastrocnemius muscle was restricted stepwise using an inflatable cuff over the thigh and using these measures blood flow reductions greater than 25% showed a linear reduction in muscle respiration (245). Although this study showed a direct effect of blood flow restriction on muscle respiration this was only shown at greater than 25% occlusion. The complete experiment to determine when reductions in $\dot{Q}O_2$ limit muscle

$\dot{V}O_2$ has not been performed in health and disease (298, 300) but reductions in blood flow response to muscle contraction have been suggested in type 2 diabetes (337, 346, 406). Determining whether cardiovascular $\dot{Q}O_2$ or muscle mitochondrial $\dot{V}O_2$ limit muscle respiration and metabolism in type 2 diabetes is crucial for diagnostic and prognostic indices but also in development of therapeutic interventions.

The limit for maximal muscle respiration is influenced by physical inactivity and obesity due to changes in mitochondrial number (38, 147, 372) and the majority of individuals with type 2 diabetes present with obesity [87.5% overweight or obese (54)] and sedentary lifestyle [40.8% <10 min of moderate physical activity per week (54)]. The Goto-Kakizaki (GK) rat model of type 2 diabetes permits study of the direct effect of the disease on muscle respiration since the GK rat is physically active (221) and not obese (6). Lewis et al (2019) showed compromised muscle metabolism from increased PCr hydrolysis during high intensity contractions in the GK rat measured by ^{31}P MRS and proposed this was due to reduced muscle oxygen supply (220). Previous work in the GK rat has shown reduced oxygen delivery during rest (281) and contraction (110, 282). Padilla and colleagues showed 40% reduced muscle oxygen supply at rest and during contraction measured from microvascular oxygen pressures (282) and this was explained by reduced blood flow measured by reduced red blood cell flux (281). However, in these works oxygen delivery was only determined at one metabolic load above rest and experiments to match those reported in Lewis et al. (2019) would offer a greater quantitative understanding to any limitations of muscle metabolism in the type 2 diabetic GK rat (220).

The present work quantified blood flow delivery to skeletal muscle contracting at stimulations within and above the capacity for respiration in the type 2 diabetic Goto-Kakizaki rat and its Wistar control. Stimulation protocols mirrored previously reported measures of GK muscle metabolism during sciatic nerve stimulation of hindlimb muscles. Quantification of blood flow to the lower limb showed reduced flow in the diabetic GK rat and results suggest that limitations to muscle metabolism in the type 2 diabetic metabolic condition may be due to reduced oxygen delivery.

7.3 Methods

7.3.1 Animals

Male type 2 diabetic Goto-Kakizaki rats (n=7) were obtained from Taconic Farm (Taconic Farm, Germantown, NY) and studied at 16-17 weeks of age. Male Wistar rats (n=7) obtained from Charles River Laboratories (Wilmington, MA) were used as age-matched controls. Animals were housed three per cage in a temperature- and humidity-controlled room and provided food (NIH-31M: 23% calories from protein, 18% calories from fat, 59% calories from carbohydrate) and water *ad libitum*. Animals were maintained on a 12:12-h light-dark cycle. All procedures were approved by the Michigan State University Institutional Animal Care and Use Committee and complied with The American Physiological Society's "Guiding Principles in the Care and Use of Animals".

7.3.2 Experimental Setup

Animals were fasted overnight (12-h) and on the day of experiment were initially anesthetized with 4% Isoflurane mixed in 100% O₂ (1 L/min) for ~3 minutes and maintained throughout experimental protocol at 1.5 - 2.5%. Animals were weighed and blood glucose measured (Contour Blood Glucose Monitoring System; Bayer HealthCare LLC) by tail vein puncture before being prepared for *in situ* stimulation of the triceps surae (gastrocnemius, plantaris, soleus) muscle group using bipolar platinum electrodes implanted on the sciatic nerve as described previously (129, 176, 220, 251). Rats were fixed with a tungsten pin through the head of the left tibial bone (Figure 30A) into a custom knee holder and Achilles tendon was ligated proximal to the calcaneus process then tied to an isometric force transducer. The force transducer had provisions for adjustment of muscle length and allowed for the muscle to be adjusted to optimal length (L_0) determined from length-tension relation in response to supramaximal twitch stimuli (2-10V, 2 ms duration) using a Grass stimulator S48 (Grass technologies, Warwick, RI, USA). Twitch stimulation in this manner ensures all fibers are recruited (8, 360) and avoids force summation permitting a broad range of contractile intensities for study.

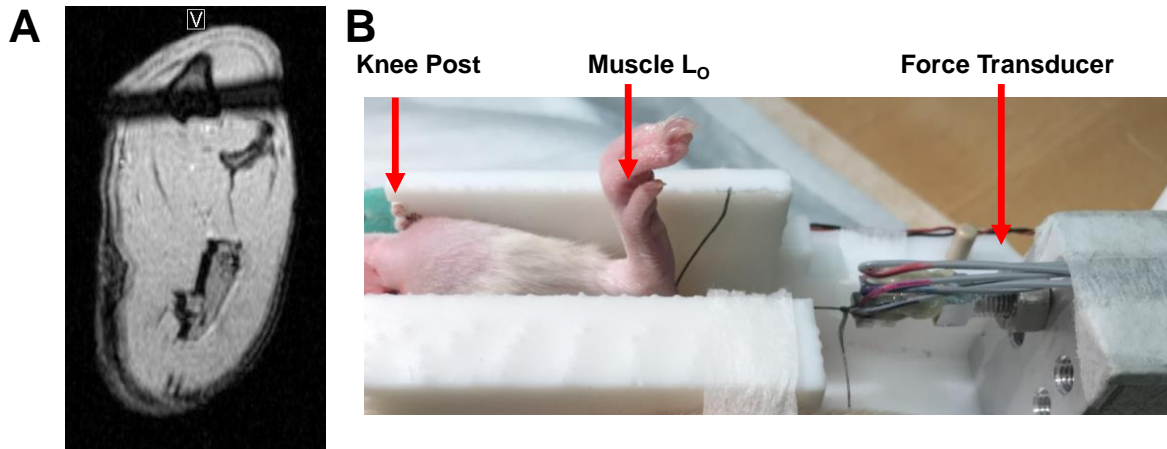


Figure 30. Experimental Setup. A) T1 image demonstrating the tungsten pin passing through the head of the tibial bone. B) Rat leg fixed in place with knee posts and custom force transducer to permit measure of muscle function at L_0 .

Animals were placed in a transmit/receive quadrature volume resonator (112/086, Bruker, Germany) with the triceps surae muscle group at the isocenter of a 7T preclinical scanner (BioSpec 70/30, horizontal bore, Bruker, Germany) housed in the Department of Physiology. A receive-only proton (^1H) surface coil (2 cm diameter, Bruker, Germany) was positioned over the inner thigh of the animal immediately above the knee to center on the popliteal vessels. Respiration and temperature were continuously monitored using the MR compatible Model 1030 monitoring and gating system (SA Instruments Inc., Stony Brook, NY, USA) and maintained at 30-50 breaths per minute and 37°C respectively.

7.3.3 T1 Flash Sequence

Prior to extensive stimulation, T1 Flash images of the lower limb were acquired in the axial plane encompassing the length from knee to ankle. Sequence parameters were: repetition time (TR), 400 ms; echo time (TE), 3.5 ms; 30-35 slices (1 mm thick)

contiguous, FOV 3.50 x 6.26 cm, 256 x 256 acquisition matrix, in-plane resolution 137 x 245 μm , and 4 signal averages (total acquisition time = 4.5 min). For two animals (one Wistar, one GK) acquisition was extended for cleaner images (8 signal averages, total acquisition time was 9 min). Maximal cross-sectional area of the triceps surae was determined by manual selection of the region of interest ensuring only muscle was selected and avoiding inclusion of bone area using “image display and processing” software (Bruker BioSpin MRI GmbH, Errlingen, Germany).

7.3.4 Phase Contrast Angiography

A ^1H surface coil was placed over the bifurcation of the popliteal vessels above the split to posterior and anterior tibialis (Figure 31A,B) and the bifurcation was positioned at the isocenter of the magnet. A standard two-dimensional time of flight sequence (2D_TOF, 30 contiguous axial gradient echo images, slice thickness = 0.5 mm, TE/TR = 3.1/12 ms, flip angle = 80° , matrix = 256 x 256, FOV = 35 x 30 mm, 2 averages, total acquisition time 2 min 28 s) was used to identify popliteal vein location for measures of blood flow. Phase contrast velocity map images (Figure 31C,D) were obtained orthogonal to the popliteal vein ~3 mm above bifurcation to posterior and anterior tibialis vessels to quantify blood flow in the absence of turbulent flow (TE/TR = 3.9/15 ms, Flip angle = 20° , matrix size = 256 x 256, FOV = 3.5 x 3.5 cm, slice thickness = 0.8 mm, 2 averages, total acquisition time = 16.36 s). The flow encoding gradient was applied in parallel with the popliteal vein and velocity thresholds for automated phase adjustments were set to closely outmatch blood velocity and maximize signal/noise throughout experimentation (6 – 40 cm/s, during lowest resting flow and highest stimulation flow respectively) (254).

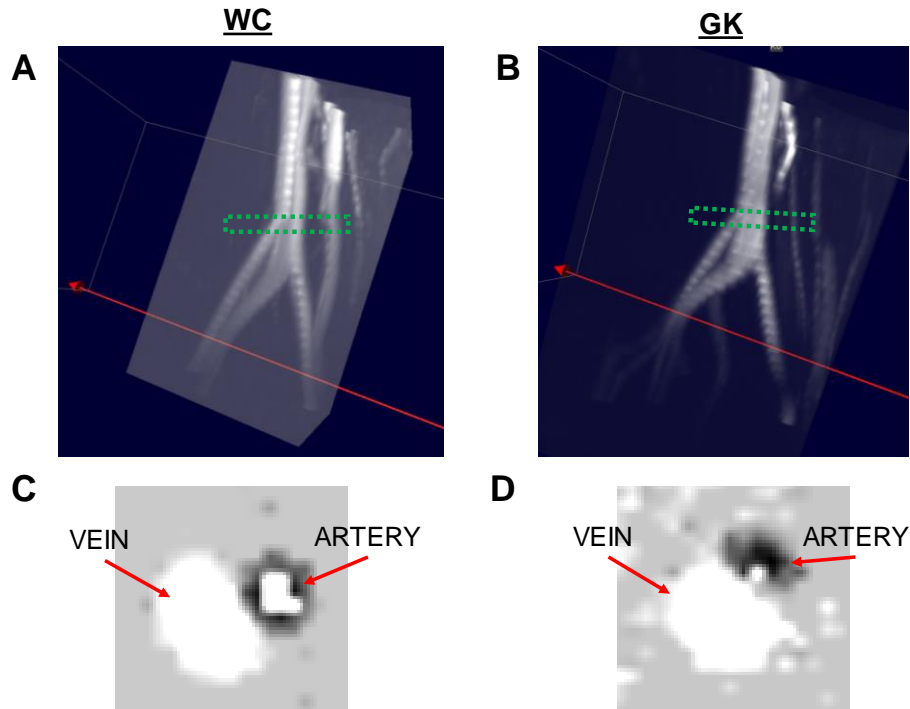


Figure 31. Representative images for the popliteal vessel angiogram and velocity map. A,B) High resolution time of flight images for Wistar control (WC) and Goto-Kakizaki (GK) rats depicting where the imaging acquisition plane (green rectangle) was placed for the velocity map (C,D) used for flow analysis.

Blood flow was measured continuously before (2 min 28 s, rest), intermittently during (10 s between acquisitions) 4 min 48 s of isometric twitch contractions elicited at 0.25, 0.5, 0.75, 1, 2, and 4 Hz frequencies of stimulation in random order and throughout 20 min 34 s of post-contraction recovery. Contractile frequencies were chosen to stimulate within (0.25 – 1 Hz) and above (2, 4 Hz) the reported muscle aerobic capacity for rat skeletal muscle [1 Hz twitch stimulation, (155, 220)]. During stimulation, force production was continuously recorded (WinDaq Data Acquisition Software, DATAQ Instruments Inc., Akron, OH, USA) utilizing an analog to digital external converter (960 Hz sampling rate, DATAQ Instruments Inc., Akron, OH, USA). Following experimentation, animals were

humanely euthanized by an overdose of anesthesia and thoracotomy and hearts were removed, exsanguinated and weighed.

7.3.5 Data Analysis

Blood flow quantification. The popliteal vein region of interest was manually outlined at the edge of the vessel and volume of blood flow (ml/min/100g muscle) was calculated from the product of mean blood flow velocity (cm/min) and vessel area (cm²) across the region of interest for each time point. Post-contraction recovery of blood flow was fit to a mono-exponential curve (22, 47, 214) computed by least squares regression algorithm (MATLAB curve fitting toolbox, Mathworks Inc, Natick, MA, USA). Total blood delivered (ml/100g muscle) in response to a contractile frequency was determined by taking the area under the curve from the start of contraction to $3 \times \tau$ post-contraction computed by trapezoidal numerical integration (MATLAB).

Mechanical performance. Individual twitch peak force (g) and tension-time integral (TTI, g*s) were quantified using the *eventanalysis* algorithm (167) which runs in MATLAB. Twitch peak force and TTI were normalized for muscle cross sectional area to account for differences in size of muscle (64).

7.3.6 Statistics

All data are presented as Mean \pm SE. Comparisons of group means for blood flow measures were performed using SigmaPlot by two-tailed Repeated Measures ANOVA. Comparison of all other group means were performed using two-tailed Student's t-test. All comparisons were performed at the $p < 0.05$ level of significance.

7.4 Results

7.4.1 Animal Characteristics

Type 2 diabetic GK rats were hyperglycemic with twice as high fasting blood glucose compared to Wistar control rats (Table 7). Body mass, muscle mass, and muscle cross sectional area (CSA) were each decreased in GK versus Wistar control rats but not different when normalized to body mass. Heart mass normalized to body mass was increased in the GK rat suggestive of cardiac hypertrophy compared with Wistar control rats. Representative T1 Images of muscle cross-sections are presented in Figure 32. Muscle cross sectional area and muscle mass showed a direct relationship with an R² of 0.90 (Figure 33).

	Wistar	GK
FBG (mg/dL)	102 ± 9	194 ± 13*
Body mass (g)	449 ± 5	347 ± 7*
Triceps surae Muscle Mass (g)	2.76 ± 0.08	1.96 ± 0.03*
TS CSA (cm ²)	1.38 ± 0.02	1.01 ± 0.03*
Total Muscle Mass (g)	4.67 ± 0.15	3.41 ± 0.09*
TMM/BM (%)	1.04 ± 0.03	0.98 ± 0.02
Total CSA (cm ²)	2.47 ± 0.02	1.97 ± 0.08*
Total CSA/BM (%)	0.55 ± 0.02	0.57 ± 0.03
Heart Mass (g)	1.06 ± 0.03	1.00 ± 0.03*
HM/BM (%)	0.24 ± 0.01	0.28 ± 0.01*

Values are Mean ± SE. *=p<0.001 compared to Wistar controls. FBG, fasting blood glucose; CSA, cross sectional area

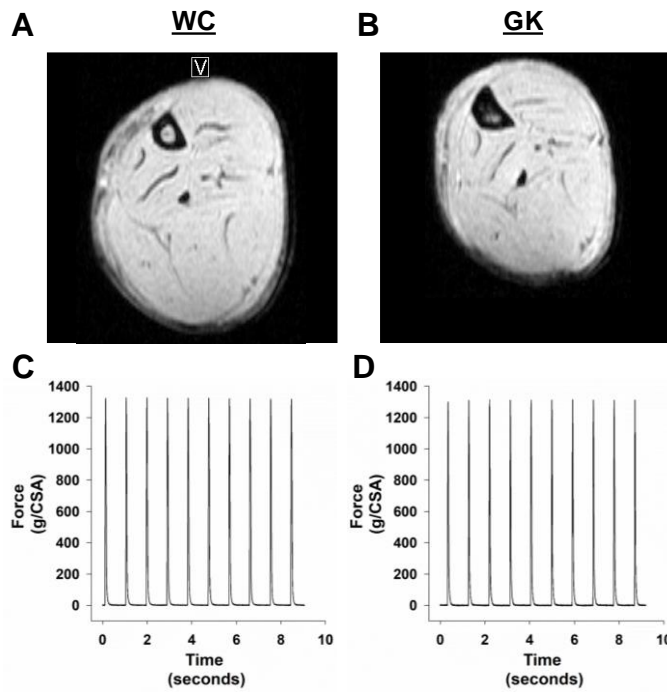


Figure 32. Representative muscle cross-sectional areas (CSA) and muscle twitch force production. A,B) T1 Images for Wistar control (WC) and Goto-Kakizaki rat hindlimb and (C,D) respective force traces per cross sectional area.

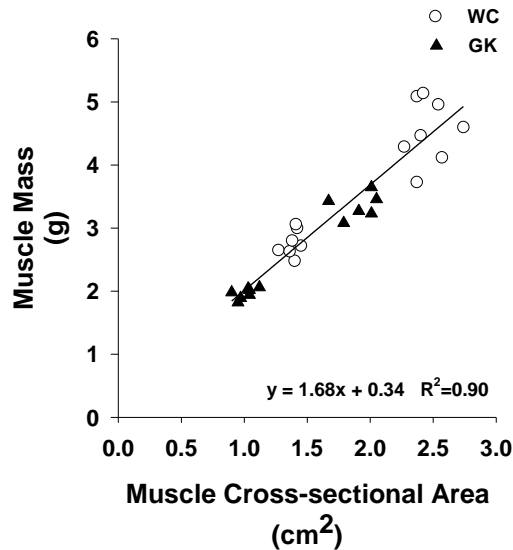


Figure 33. Muscle cross-sectional area demonstrated a direct relationship to muscle mass. Each individual rat was plotted for its respective muscle mass and cross-sectional area for the triceps surae muscle group alone (two left clusters) and entire hindlimb (two right clusters) and fit to a line of regression.

7.4.2 Muscle Performance

Muscle force production and twitch characteristics normalized to muscle cross sectional area are summarized in Table 8. Representative twitches are presented in Figure 32C,D. Wistar control and GK rats had similar peak force and tension time integral for every intensity of stimulation. End twitch force production was not different between animals. Fatigue was not different between animals when end twitch force production was compared to initial twitch force production but was slightly increased in Wistar control rats when compared to maximal twitch force production for 0.5- and 0.75 Hz.

Table 8. Muscle twitch performance							
		Stimulation Frequency (Hz)					
		0.25	0.5	0.75	1.0	2.0	4.0
Initial Twitch (g/cm ²)	<i>Wistar</i>	1175 ± 125	1228 ± 119	1215 ± 113	1162 ± 119	1132 ± 105	1069 ± 95
	<i>GK</i>	1252 ± 48	1193 ± 87	1183 ± 81	1165 ± 79	1121 ± 60	974 ± 102
Max Twitch (g/cm ²)	<i>Wistar</i>	1258 ± 123	1316 ± 109	1314 ± 101	1305 ± 98	1265 ± 87	1172 ± 94
	<i>GK</i>	1310 ± 54	1307 ± 66	1326 ± 64	1331 ± 61	1316 ± 55	1285 ± 66
End Twitch (g/cm ²)	<i>Wistar</i>	1252 ± 123	1263 ± 112	1170 ± 94	1078 ± 80	826 ± 56	500 ± 28
	<i>GK</i>	1294 ± 52	1296 ± 64	1282 ± 55	1176 ± 61	872 ± 43	593 ± 40
%Initial	<i>Wistar</i>	107 ± 1	104 ± 3	98 ± 5	96 ± 7	75 ± 5	48.5 ± 4
	<i>GK</i>	104 ± 2	110 ± 4	110 ± 5	102 ± 6	79 ± 4	64 ± 6
%Max	<i>Wistar</i>	100 ± 0.1	96 ± 1	89 ± 3	83 ± 3	66 ± 3	44 ± 2
	<i>GK</i>	99 ± 0.5	99 ± 0.4*	97 ± 1*	88 ± 2	66 ± 2	46 ± 1
TTI (g*s/ cm ²)	<i>Wistar</i>	58.5 ± 5.2	69.1 ± 4.5	70.1 ± 3.7	66.6 ± 3.7	67.8 ± 4.7	62.9 ± 5.0
	<i>GK</i>	65.9 ± 3.4	68.4 ± 5.0	71.8 ± 6.3	74.4 ± 5.7	74.6 ± 5.3	65.8 ± 3.7
SUMTTI (g*s/cm ²)	<i>Wistar</i>	4144 ± 365	9832 ± 664	15118 ± 921	19382 ± 1244	33571 ± 2323	50765 ± 5319
	<i>GK</i>	4320 ± 242	9406 ± 708	15347 ± 1352	21130 ± 1869	33946 ± 1995	52914 ± 3017

Values are Mean ± SE. * = p < 0.05 compared to Wistar controls. TTI, tension time integral;

7.4.3 Blood Flow Response to Contractions

Blood flow during contraction and recovery for 0.25 (Panel A), 0.5 (Panel B), 0.75 (Panel C), 1 (Panel D), 2 (Panel E), and 4 Hz (Panel F) twitch frequencies are presented in Figure 34. Blood flow increased during contraction and recovered monoexponentially post-contraction in both Wistar control and diabetic GK rats and the magnitude of flow increased with increased intensity of stimulation. Post-contraction recovery is summarized in Table 9 demonstrating no differences in time constant of recovery. Resting flow was higher in Wistar control rats versus GK rats (68.7 ± 3.8 vs. 35.7 ± 9.6 , $p < 0.05$).

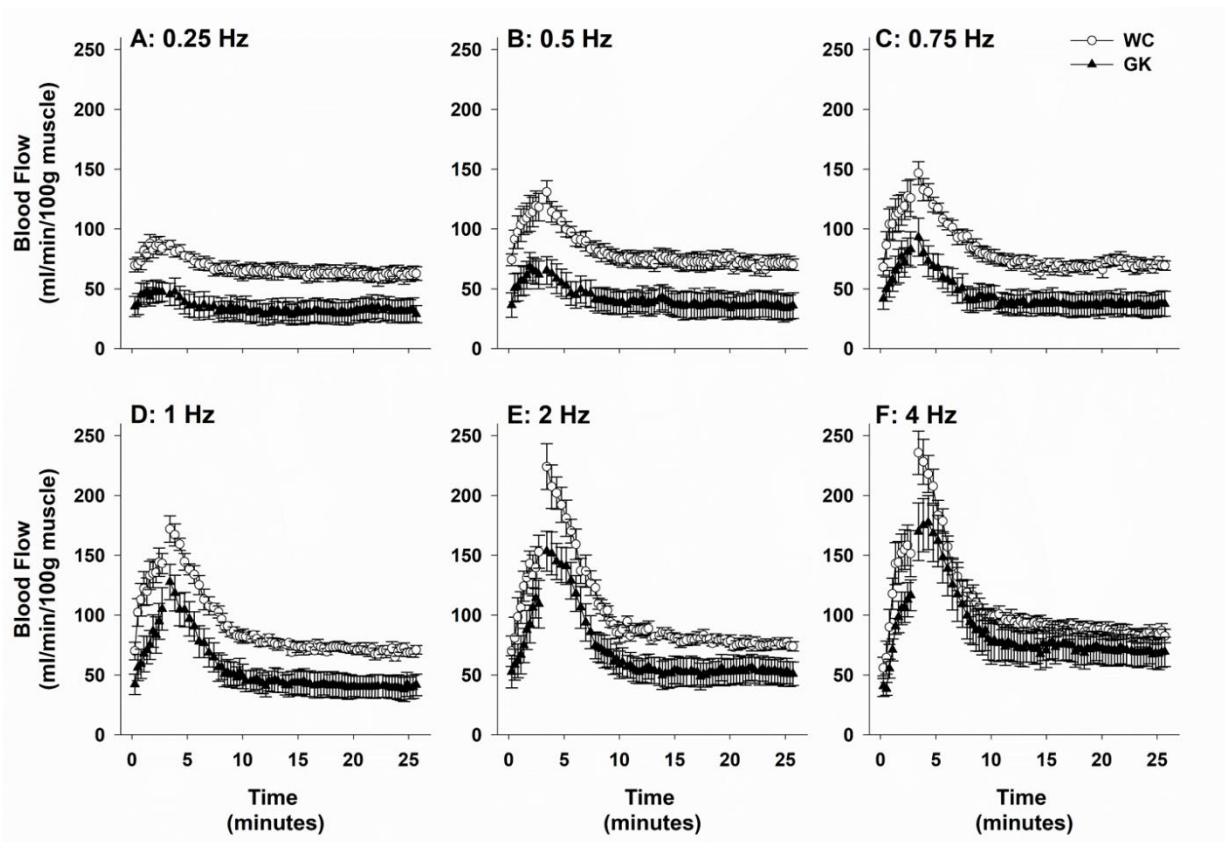


Figure 34. Mean \pm SE muscle blood flow responses during and following contraction. Wistar controls (WC, white circles) demonstrated elevated blood flow compared to Goto-Kakizaki rats (GK, black triangles) during every contraction tested.

Table 9. Post-contractile Recovery		
Stimulation (Hz)	Recovery Time Constant (s)	
	Wistar	GK
0.25	122 ± 17	90 ± 22
0.5	108 ± 11	108 ± 20
0.75	120 ± 7	93 ± 15
1	129 ± 16	116 ± 11
2	136 ± 20	119 ± 17
4	125 ± 16	122 ± 16
Blood flow recovery post-contraction was fit to a mono-exponential curve. Time constants represent where 67% of the recovery has occurred and therefore longer time constants equate with slower recovery. Values are Mean ± SE.		

Maximal blood flow during contraction (Panel A), maximal blood flow post-contraction (Panel B) and total blood delivered (Panel C) are presented in Figure 35. Wistar control rats showed higher maximal blood flow during and post-contraction compared with diabetic GK rats for every frequency of stimulation. Wistar control rats also presented increased total flow delivered for each stimulation compared to GK rats. Together these demonstrate reduced blood flow in the diabetic GK rat compared with Wistar controls in response to every metabolic challenge.

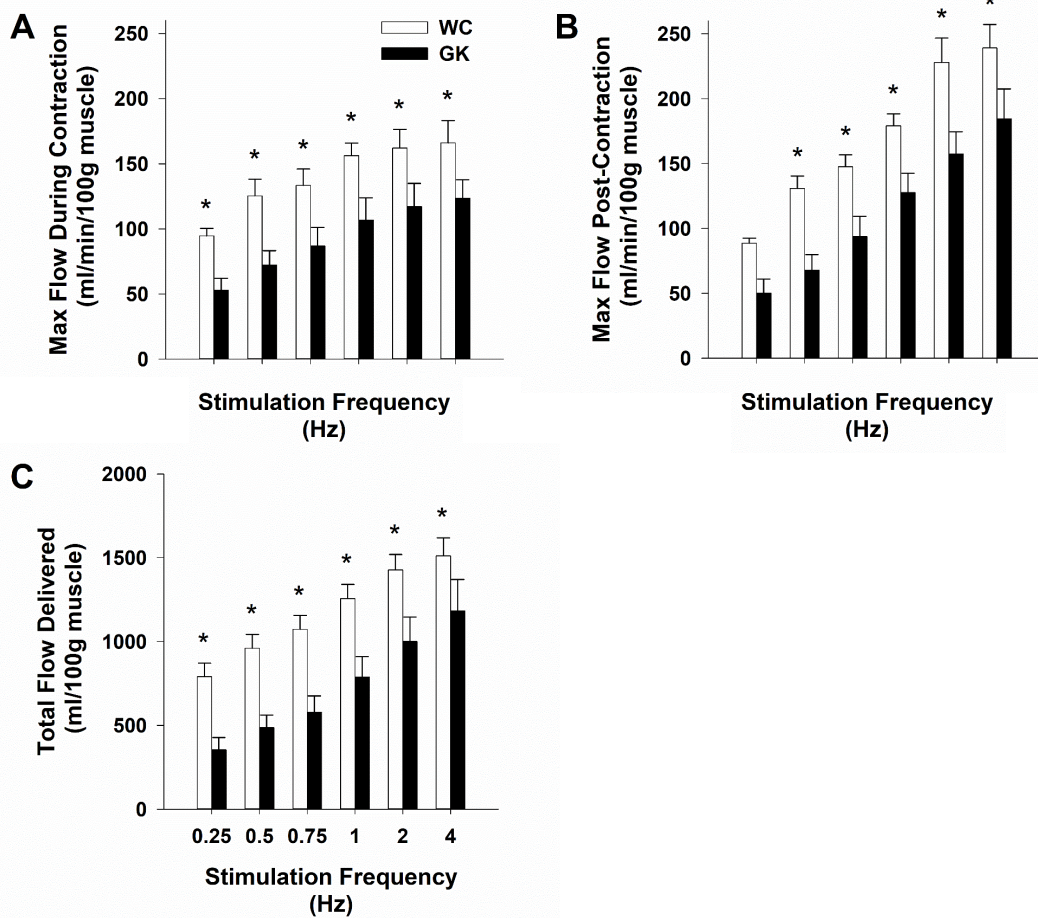


Figure 35. Mean \pm SE maximal blood flow and total blood flow delivered during and post contraction. Maximal blood flow was higher in the Wistar controls (WC, white bars) versus Goto-Kakizaki (GK, black bars) rats for every stimulation intensity both during contraction (A) and immediately post-contraction (B). This coincided with increased total blood flow delivered (C). * $p < 0.05$

Total blood delivered compared to total force produced during contractions is presented in Figure 36. As intensity of stimulation increased, more force was produced, and more blood was delivered for both Wistar control and GK rats. There was no difference in total force produced between animals, but total blood delivered was significantly lower per force produced in the GK rat. The relationship between increased force production and blood flow delivered was not different between animals suggesting the response or change in blood flow for a given demand was not different.

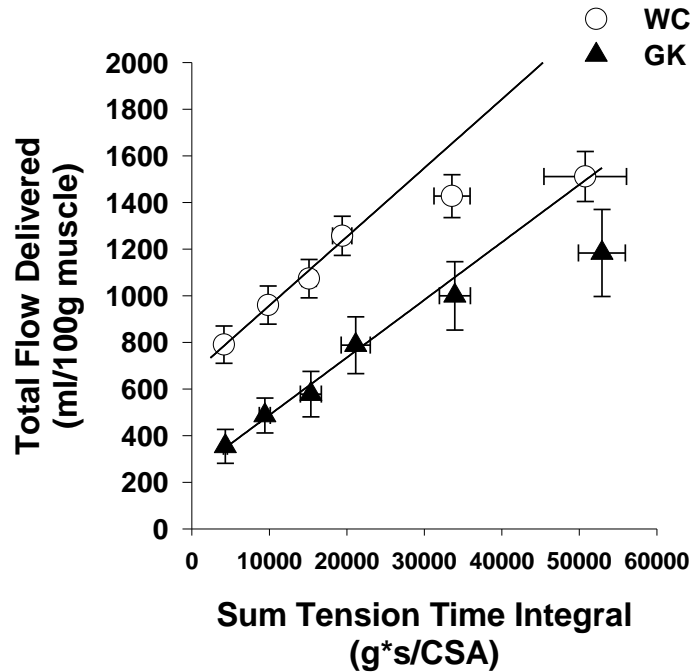


Figure 36. Total flow delivered per work performed. Total flow was reduced in the GK rat for every metabolic demand tested. Lines of regression were fit from 0.25 – 1 Hz since 2 and 4 Hz were nonlinear due to muscle fatigue. This was expected since blood flow response is more closely related to metabolic demand than mechanical contraction (126) and metabolic demand declines during fatigue. Values are presented as Mean \pm SE.

7.5 Discussion

The present study quantified the relationship between blood flow and contracting skeletal muscle in the GK rat model of type 2 diabetes and their Wistar controls. Intensities of stimulation tested a broad range of metabolic demands within and above the range that muscle performance can be sustained by aerobic metabolism. Maximal rate and total blood flow delivery were reduced at every contractile intensity in the diabetic GK compared with Wistar control rats. Although absolute blood flow was reduced, *changes* in flow in response to metabolic demand were not different and permitted similar muscle

force production. Together these observations support reduced oxygen delivery to working muscle in the type 2 diabetic GK rat and suggest reduced matching of muscle oxygen supply ($\dot{Q}O_2$) to utilization ($\dot{V}O_2$).

Reduced skeletal muscle blood flow is in agreement with previous studies in the Goto-Kakizaki rat demonstrating reduced oxygen supply at rest (281) and during elevated contractile intensities (110, 282). The present study expands upon these findings by measuring force production during contractile intensities ranging from within (0.25 – 1 Hz) to above (2 – 4 Hz) the reported range that aerobic respiration can support muscle force production (155, 220). Blood flow measured at the level of the popliteal vessel in the present study includes blood delivery to the entire lower limb including skin and bone and thus does not directly indicate blood supply to the contracting muscle. However, skin perfusion is largely dependent on thermoregulation that is mostly absent under Isoflurane anesthesia and reductions in supply are supported by previous studies by Poole and colleagues (281, 282). Red blood cell flux in the skeletal muscle microvasculature was less than half in diabetic GK rats versus Wistar controls at rest quantified using intravital microscopy and a similar result was shown in the present study with ~50% reduced resting blood flow measured at the popliteal level. When paired with measures of interstitial PO_2 using phosphorescence quenching techniques the authors concluded oxygen delivery was reduced by nearly 75% (281). Together, these results support the measures of reduced bulk flow delivery in the present study representative of reduced muscle delivery. Although blood flow was reduced at each intensity of stimulation, rate of fatigue was not different suggesting that $\dot{V}O_2$ was not impaired. This is supported by previous work in the GK rat demonstrating reduced blood flow during sciatic nerve

stimulation at 1 Hz contractile intensity but similar $\dot{V}O_2$ due to increased oxygen extraction (110) in accordance with Fick's law [$\dot{V}O_2 = QO_2 \times (Ca_{O_2} - Cv_{O_2})$].

Reduced matching of $\dot{Q}O_2$ to $\dot{V}O_2$ can reduce muscle metabolic performance by causing increased O_2 extraction, increased phosphocreatine (PCr) hydrolysis, and reduced sensitivity to the metabolites that drive aerobic respiration [ADP, inorganic phosphate (Pi) (31, 170, 382)] without reducing $\dot{V}O_2$ (71, 138, 189, 299, 407, 408). This was shown through a series of studies by Hogan and colleagues demonstrating the role of oxygen availability on muscle metabolism utilizing ^{31}P MRS (133–136). Muscle oxygen availability was altered by changing the fraction of inspired oxygen (FIO_2) and muscle metabolic performance was determined from measures of PCr, Pi, and ADP. When oxygen availability in arterial blood was decreased, PCr hydrolysis increased and sensitivity to Pi and ADP reduced during contraction despite similar $\dot{V}O_2$ (136). Although blood flow was reduced in the GK rat in the present study, $\dot{V}O_2$ between animals was likely similar since force production was not different and this could have resulted in increased PCr hydrolysis and reduced sensitivity to ADP and Pi. Increased PCr hydrolysis during intense contractions and reduced ADP sensitivity for every contractile intensity was recently reported by Lewis et al (2019) in the diabetic GK rat (220) and this can be entirely explained by reduced oxygen delivery from reduced blood flow measured in the present study.

Blood flow recovery post-contraction recovered more slowly than reported PCr recovery time constants (220, 223) indicating that $\dot{Q}O_2$ off-kinetics do not limit PCr recovery (22, 23, 246). Behnke and colleagues (2009) quantified muscle $\dot{V}O_2$ in rat spinotrapezius muscle from microvascular PO_2 (22) and blood flow (23) recovery

following 1 Hz contractions. Results demonstrated that blood flow recovered $\sim 1.6X$ more slowly than $\dot{V}O_2$ and thus microvascular PO_2 was sustained by elevated $\dot{Q}O_2/\dot{V}O_2$ matching. A similar result is shown in the present work when comparing to PCr recovery using an identical setup supporting that $\dot{V}O_2$ was not limited during recovery (220). Changes in PCr and $\dot{V}O_2$ are closely related when measured during and following contraction (234, 327, 329). Rossiter et al. (2002) quantified PCr dynamics concurrent pulmonary $\dot{V}O_2$ and showed that time constants to steady-state were similar both during and following moderate and high intensity exercise in human quadriceps muscles. Further, when plotted as a percent of initial PCr hydrolysis nearly mirrored pulmonary $\dot{V}O_2$ showing the direct relationship between the kinetic changes in PCr and $\dot{V}O_2$ (329) and this result supports direct comparison between PCr and $\dot{V}O_2$ relative to $\dot{Q}O_2$ in the present study.

There are several mechanisms that could have resulted in reduced blood flow in the diabetic GK rat including reduced cardiac output, peripheral vascular dysfunction, or changes in vessel structure. If cardiac output was reduced it would result in reduced perfusion pressure and blunted blood flow to peripheral muscles. However, previous work using intra-arterial telemetry showed hypertension and suggested increased cardiac output in the GK rat measured from increased heart rate, heart mass, and rate pressure product during metabolic challenges (222) consistent with increased heart mass measured in the present study. Isoflurane anesthetic has been shown to directly reduce cardiac function in a dose-dependent manner (310). In the present study animals were similarly sedated by monitoring respiration and previous work in our lab showed no difference in the effect of Isoflurane on cardiovascular function or resting blood flow in GK

versus Wistar rats (37 ± 3 vs. 52 ± 4 awake (unpublished observations), 36 ± 10 vs. 69 ± 4 anesthetized) in agreement with previous work in the diabetic ZDF rat (48).

Blood flow regulation during small muscle mass contraction is suggested to be more sensitive to peripheral vascular function as opposed to the importance of cardiac function during whole body exercise (414). As such, reduced hindlimb blood flow could be caused by reduced popliteal vessel reactivity or reduced functional dilation impairing the path for flow delivery. Frisbee and colleagues showed that higher acetylcholine was required for similar dilation in GK arterioles compared to controls (110). Acetylcholine causes vasodilation from endothelium-released nitric oxide and thus reduced vasodilation indicates reduced NO release. The authors confirmed reduced NO presence measured from amperometric NO sensors in isolated abdominal aortas and concluded reduced vessel reactivity from endothelium impairments in the diabetic GK rat since antioxidant treatment to improve NO release improved arteriolar responses. Reduced reactivity from reduced NO bioavailability could have reduced vasodilation to contracting muscle and resulted in reduced blood flow in the present study.

Reductions in blood flow in the GK rat could also be explained by structural alterations in vessel size or microvessel density. In the present work, GK popliteal artery cross sectional area was significantly reduced compared to Wistar control when quantified from velocity map acquisitions at rest (0.0045 vs. $.0075$ cm^2 , $p < 0.01$) and normalized to body mass (0.013 vs. 0.017 cm^2/kg , $p < 0.05$) or muscle mass ($.0013$ vs. $.0016$ cm^2/g , $p < 0.05$). Microvessel density was reported ~15% reduced in GK rat gastrocnemius muscles quantified from formalin fixed muscle sections incubated with *Griffonia simplicifolia* and quantified using fluorescence microscopy (110). Reduced

vessel size or microvessel density could have resulted in increased vascular resistance (VR) and diminished blood flow delivery since VR and blood flow are inversely related [$Flow = \frac{\Delta P}{VR}$, where ΔP is the driving pressure (MAP)].

The absolute blood flow was reduced in the GK rat compared to Wistar controls, but the *response* in blood flow delivery to contraction was not different suggesting that reductions in flow were not caused by impaired myogenic responses to contraction (Figure 36). During muscle contraction, vascular signals including NO, K⁺, adenosine, and others are released and cause increased oxygen delivery to working muscle [for review see Joyner and Casey (173)]. Similar *changes* in blood flow delivery suggest that these mechanisms are not deficient in the diabetic GK rat and are in qualitative agreement with previous work reporting similar vascular responses to myogenic vasodilators (110). Frisbee and colleagues demonstrated similar arteriolar dilation in response to a broad range of adenosine and nitroprusside challenges in vessels isolated from GK skeletal muscle compared to controls. Similar dilatory response to vasodilators suggests that the vessel is not dysfunctional so long as the vasodilators are sufficiently released. These data are consistent with similar changes in blood flow in the present study and previous work showing a greater stimuli required for vasodilatory release from reduced acetylcholine reactivity (110).

7.5.1 Conclusions

Type 2 diabetes reports vast cardiovascular impairments (58, 154, 200, 222) and the present study demonstrates reduced blood flow delivery to working muscle in the non-obese, non-sedentary Goto-Kakizaki rat model of type 2 diabetes. Reductions in flow did

not limit muscle performance and this is likely due to increased oxygen extraction maintaining $\dot{V}O_2$ (Fick's Law) as demonstrated by Frisbee and colleagues in the GK rat (110). However, reduced $\dot{Q}O_2$ matching of $\dot{V}O_2$ likely resulted in increased PCr hydrolysis and reduced ADP sensitivity as shown previously in the GK rat (220). Together, these suggest that the limitation to muscle respiration in the GK rat is oxygen delivery to the respiring mitochondria. Future studies measuring ^{31}P MRS in conjunction with direct measures of oxygen supply and uptake are necessary to confirm this hypothesis and apply to human populations. Determining the limitations to muscle metabolism in diabetes is crucial for the development of pharmacologic and therapeutic intervention strategies.

CHAPTER 8: GENERAL SUMMARIES/CONCLUSIONS AND DISCUSSION

8.1 Summary

The work presented here challenges the dogmatic view of skeletal muscle mitochondrial dysfunction in type 2 diabetes that is pervasive in the biomedical literature. In **Chapter 1**, a critical analysis of the literature suggests that reports of mitochondrial dysfunction are *not* inherent to type 2 diabetes but may actually be the result of incomplete experimental design where controls for differences in lifestyle including obesity and sedentary lifestyles were absent. This insight led to the postulate of the central question of this dissertation presented in **Chapter 2** asking whether mitochondria are dysfunctional or not and further determining the limitation to muscle metabolism and performance in type 2 diabetes.

In **Chapter 3**, a top-down computational model was developed to define the regulation of mitochondrial ATP production and the limitations to skeletal muscle respiration. Results demonstrated that mitochondrial ATP production can be mostly explained by the feedback of ATP hydrolysis products (ADP, Pi) and redox status (NADH/NAD⁺). As metabolic workload increased, hydrolysis products increased, redox was more oxidized, and respiration increased until ATP demand was matched. When comparing with experimental *in vivo* mitochondrial function measured by ³¹PMRS in health and disease the model showed it could be applied to determine whether mitochondria themselves or their substrate supply limits mitochondrial respiration. When applied to human studies of type 2 diabetes (225, 288, 378) the model suggested that mitochondria were not dysfunctional but deficits were the result of reduced mitochondrial number or oxygen limitations to the mitochondria. To test this hypothesis experiments

must be carefully designed and mitochondrial function must be quantified both *in vivo* and *in vitro*.

Chapter 4 quantified skeletal muscle mitochondrial function *in vivo* during low and high intensity muscle contractions and in the isolated organelle itself *in vitro* in the non-obese, non-sedentary type 2 diabetic Goto-Kakizaki rat (220). Results demonstrated different energetic steady states from measures of PCr during high intensity contractions. GK rats hydrolyzed more PCr than their Wistar controls but this divergence was not due to dysfunctional mitochondria since no difference was seen when isolated from the muscle nor during low intensities of stimulation measured by ³¹PMRS *in vivo*. Application of findings from **Chapter 3** supported that the observed energetic differences were likely the result of physiologic changes within the muscle bed not inherent to mitochondrial function. Mitochondrial oxidative phosphorylation requires both mitochondrial oxygen utilization and oxygen supply to the mitochondria and therefore oxygen supply was targeted as a potential site for dysregulation (111).

Muscle blood flow delivery carries oxygen to the working muscle and its regulation during exercise requires integration of both feedback to and function by the cardiovascular system that is sensitive to changes at the muscle bed (173). For this reason, the cardiovascular system was thoroughly studied in **Chapters 5 and 6** using chronic intra-arterial telemetry instrumentation placed within the descending aorta of Wistar control and diabetic GK rats. In **Chapter 5**, rats demonstrated similar daily activity and there was no deficit in treadmill performances at low workloads (221) and this result was consistent with observations of no mitochondrial impairment during low workload stimulations in **Chapter 4**. However, despite normal treadmill performance, diabetic rats

presented with a multitude of pathologic markers for cardiovascular disease (CVD). **Chapter 6** showed numerous CVD risk factors during rest, exercise, and mental stressors and these associated with a harder working heart measured from the rate pressure product (222). Exaggerated cardiovascular responses were satisfactory for perfusion to maintain low workload, whole-body exercise however results suggested that if pushed to higher intensities these exaggerated responses would plateau and no longer be able to satisfy oxygen demands. Unfortunately, despite extensive stimuli including electric shock, animals refused to maintain treadmill pace faster than 10 m/min and high metabolic demands as can be imposed by sciatic nerve stimulation and maximal muscle recruitment could not be tested. Therefore, experiments were designed to invoke small muscle mass contraction that has been suggested to rely more on peripheral vascular function as opposed to cardiovascular responses (414).

Chapter 7 presents an *in vivo* study of muscle blood flow supply during contraction and is a direct comparator to the experimental design from **Chapter 4**. Results demonstrated that blood flow was reduced for every contractile intensity in the small triceps surae muscle mass. When directly compared with **Chapter 4** reduced blood flow did not result in differing PCr contractile steady states at low workloads, however was consistent with reduced ADP sensitivity resulting from reduced blood flow. The limitation to muscle metabolism in healthy conditions is determined by the number and function of the mitochondria (111, 135, 243) but whether this is true in diseases such as diabetes is not known (111). Evidence of reduced blood flow herein suggests that the limitation to muscle metabolism in diabetes is determined by oxygen supply and not the mitochondria

and both must be considered when determining the limitation to muscle metabolism in disease conditions.

Taken together, the present work shows that skeletal muscle mitochondrial dysfunction is *not* inherently linked to the type 2 diabetic metabolic condition in the Goto-Kakizaki rat. Accounting for the effects of obesity and inactivity, results suggest that reported mitochondrial deficits in human T2D are likely due to mitochondrial number and explains parallel improvements in mitochondrial function and glycemic control following exercise training increases in mitochondrial number (186, 247, 378). Further, when challenged at high workloads increases in PCr hydrolysis in the diabetic condition suggested that muscle metabolism is limited by oxygen supply to the mitochondria and not the organelle itself. Blood flow reductions have been reported in some instances of individuals with type 2 diabetes (337, 406) but not all (350) and this work highlights the importance of measuring physiological systems from an integrative perspective. Concurrent measures of ³¹PMRS, oxygen supply, and oxygen utilization must be performed to concisely determine if muscle metabolism is deficient in type 2 diabetes and to guide pharmacological and therapeutic interventions to combat the disease. The present work suggests that interventions must target vascular function as opposed to the canonical targeting of mitochondrial dysfunction (121, 269).

8.2 Future Applications

Obesity, physical inactivity, and CVD risk factors vary between health and disease and can impact muscle respiration such that reductions are the result of reduced

mitochondrial fractional volume or oxygen limitations (71, 111, 208, 283). Vascular limitations have been well documented in type 2 diabetes (108, 110, 111, 217, 222, 316, 406). To account for these variables the ideal experiment to determine the limitation to muscle metabolism and any potential mitochondrial role in a range of human pathologies requires quantification of four contributors to aerobic respiration: 1) mitochondrial fractional volume, 2) ATP demand, 3) ATP production, and 4) oxygen supply. The effects of oxygen limitations on mitochondrial ATP production were described by Connett et al. by compiling a large body of previous work and published in 1990 (71). A modified figure from this work is presented here and describes the integration of each component in the ideal experiment (Figure 37).

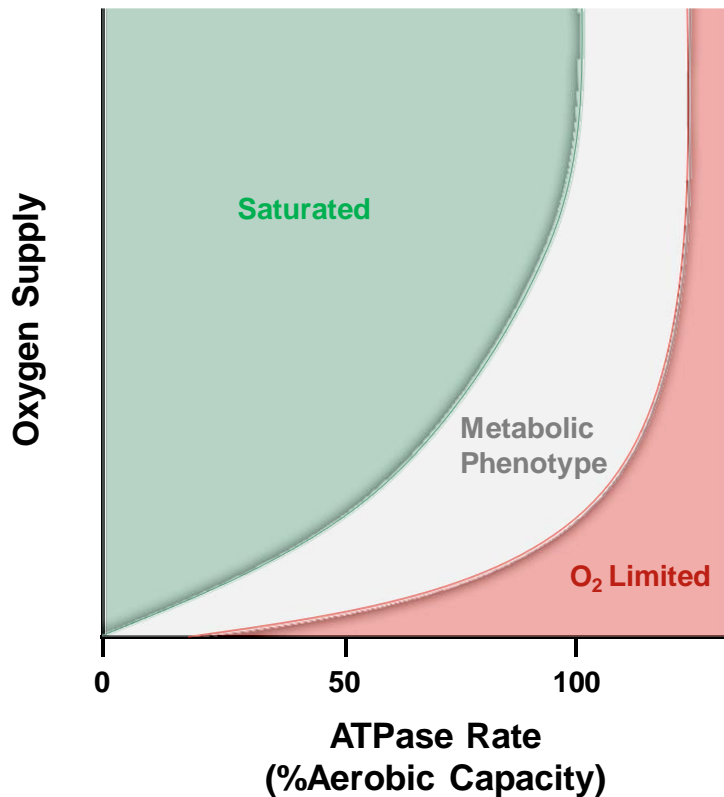


Figure 37. Theoretical description of the critical point for limitations to mitochondrial respiration. Modified from Connett et al. (71) this qualitatively shows the limitations to mitochondrial respiration. The green “saturated” zone represents where oxygen is in excess and reductions at low workloads will not affect mitochondrial function. If oxygen supply is decreased into the “metabolic phenotype” zone, mitochondrial respiration will not decline but at the expense of increased oxygen extraction and decreased phosphate potential. Finally, in the extreme or “O₂ limited” zone, oxygen supply will limit mitochondrial respiration and result in a first-order dependence on oxygen that could be misinterpreted as mitochondrial dysfunction.

Under normal circumstances ATP production is a function of ATP demand because the metabolic biproducts (ADP, Pi) of ATP hydrolysis drive mitochondrial respiration (**Chapter 3**). ATP demand is described along the x-axis of Figure 37 with increasing ATPase rates requiring increased supply of oxygen and is presented as a percent of the aerobic capacity dictated by muscle MOP capacity. On the y-axis of Figure 37 is a relative indication of oxygen supply to respiring mitochondria. Within the green

“Saturated” zone, mitochondrial respiration is not limited by oxygen supply and any reductions will not cause any changes in ATP production permitting they remain within this zone. This occurs because in saturating conditions, oxygen is not a controller of respiration, but only acts as a substrate in support of respiration (238). In other words, oxygen does not drive mitochondrial ATP production like metabolic byproducts in this zone but is simply utilized during respiration. For example, an individual in the early stages of developing peripheral arterial disease, oxygen supply to working muscle may be reduced due to reduced blood flow. However, no metabolic limitation (e.g. exercise intolerance) would occur so long as oxygen supply has not past beyond this theoretical threshold defined by the boundary between the green and grey zones. This boundary was empirically demonstrated by Rowell and colleagues in healthy individuals by altering arterial oxygen content (331). Rowell et al. showed no deficit in muscle mechanical performance during arterial hypoxemia despite likely reductions in cellular PO_2 suggesting subjects did not fall out of the green “Saturated” zone. This concept may contribute to the difficulty in early diagnosis of PAD where patients symptoms only become evident after permanent damage has taken place (390).

If oxygen supply is limited enough for a given ATPase rate to fall within the grey “Metabolic Phenotype” zone, ATP production would not be limited but would result in a reduced phosphorylation potential. This means that more ADP would be present and more PCr would be hydrolyzed within this zone as a result of the reduced oxygen availability. Thus, although ATP production is not limited, this condition will present with a reduction in ADP sensitivity and mimic the result observed from changes in mitochondrial fractional volume (93). Integrating the results presented in **Chapters 4** and

7, this is where the diabetic GK rat would fall since it presents with reduced apparent ADP sensitivity and increased PCr hydrolysis that likely results from reduced oxygen supply. Finally, if oxygen supply were limited enough to fall within the red “O₂ limited” zone ATP production would become oxygen dependent. This would present *in vivo* with increased PCr hydrolysis *and* slowed PCr recovery time constant but *without* any mitochondrial dysfunction.

Application of this conceptual framework demonstrates why therapeutic techniques that increase mitochondrial fractional volume shift the sensitivity to ADP by changing the oxygen consumed per mitochondria (93). In patients with COPD arterial oxygen supply limits muscle performance (353) and rarely can alveolar oxygen exchange be salvaged to improve this condition. However, exercise training has been shown to reduce lactate production and ventilation in COPD patients as a result of increased mitochondrial fractional volume (53) shifting these individuals closer to the green “Saturated” zone. Figure 38 illustrates some examples of different metabolic conditions and where their limitations to aerobic respiration may fall. Note that the boundary conditions between the grey and red zones define a critical point where mitochondrial function becomes oxygen dependent. This critical point will differ depending on the disease pathology and the inherent state of fitness of the subject.

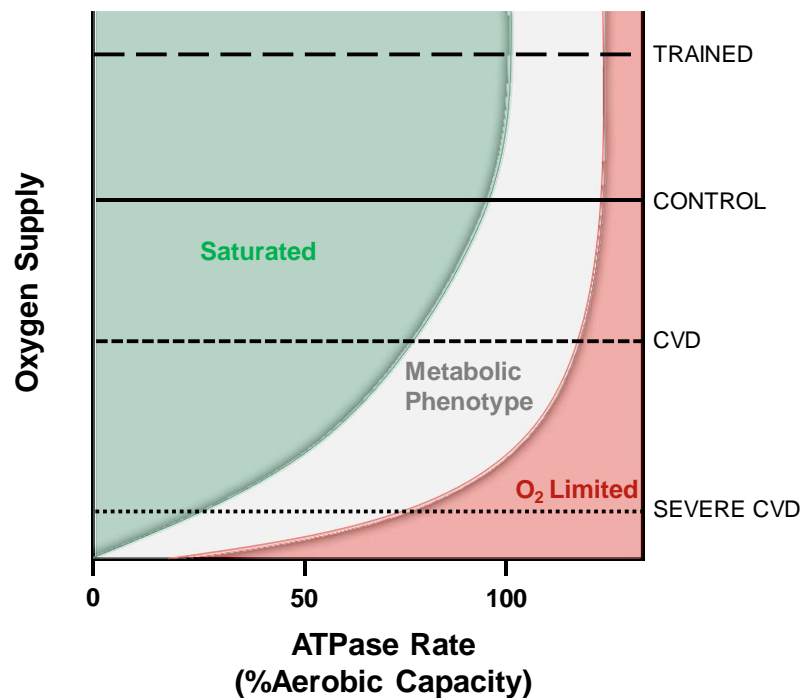


Figure 38. The critical point that limits muscle aerobic respiration varies between metabolic conditions. Within the control condition, oxygen is not limiting until the aerobic capacity is nearly reached and glycolysis affects measures of MOP capacity inherent to mitochondrial function. As cardiovascular disease (CVD) develops such as in the GK rat presented herein, oxygen supply to muscle is reduced and results in a metabolic phenotype (reduced phosphate potential) at lower workloads that may develop into complete oxygen limitations in severe CVD. For simplicity here, severe CVD includes any disease presenting poor oxygen delivery including PAD, heart failure, COPD, and others. In contrast, exercise training increases mitochondrial fractional volume as well as oxygen delivering capacity and thus falls within a zone where oxygen saturation persists at higher workloads.

The critical point where aerobic respiration becomes limited by oxygen supply was demonstrated many years ago by Stainsby et al. in 1964 using a canine gastrocnemius-plantaris muscle *in situ* (361). In this study, muscle $\dot{V}O_2$ was chronically measured while also systematically reducing either blood flow or arterial oxygen content. Utilizing this technique, Stainsby et al. demonstrated that $\dot{V}O_2$ remains unaltered in contracting skeletal muscle until oxygen supply is limited by either reduction in blood flow or by reduction in oxygen content at the same blood flow rates. A similar experiment was designed utilizing

the concept in Figure 37 by Lanza and colleagues in resting muscle (208). In this work, ^{31}P MRS was utilized to determine the critical point for ATP production prior to, during, and after inflatable cuff occlusion and measuring oxygen limitations by ^1H measures of myoglobin desaturation (164, 317). Work in contracting muscle has been performed by McCully and colleagues (245) measuring maximal respiration by ^{31}P MRS and blood flow by doppler ultrasound. Blood flow was restricted in a stepwise fashion by cuff occlusion and the resulting changes in mitochondrial ATP production rates due to these reductions in blood flow were quantified. While these experiments were performed with another goal these authors illustrated an experimental design that can be used to define the critical point in human subjects subjected to modest workloads.

Cree-Green and colleagues showed that oxygen could be limiting MOP capacity in type 2 diabetes patients utilizing ^{31}P MRS (81). PCr dynamics were measured following cessation of contraction with and without oxygen supplementation by changing oxygen concentrations of inspired air (FIO_2). When breathing normal air ($\sim 21\% \text{O}_2$), diabetics demonstrated reduced MOP capacity compared to controls and this reduction was alleviated when breathing $100\% \text{O}_2$ (82). This technique was previously demonstrated by Sunoo et al. in rats (364) and Richardson, Haseler, Hogan and colleagues in humans to change arterial oxygen content and alter phosphorus dynamics (133–136, 146). Depending on the imposed workload and state of physical fitness of the subject, changes in phosphorus dynamics were used to identify the limitation to aerobic respiration. In fact, this series of studies demonstrated limitations that fall within each zone of Figure 37 after reductions in oxygen supply showed: 1) no influence on phosphorus dynamics (134, 135), 2) altered ADP sensitivity (136, 146), and 3) slowed PCr recovery (133, 134). These

conditions would fall within the “Saturated”, “Metabolic Phenotype”, and “O₂ limited” zones respectively.

Determining where the critical point falls for healthy individuals and type 2 diabetic patients requires a sophisticated experimental design to delineate the limitation to muscle metabolic performance. This concept has been described by Poole and colleagues as the theoretical “tipping point” where oxygen supply becomes limiting to mitochondrial respiration (298, 300) . Although oxygen limitations in diabetes have been suggested it has not been *quantitatively* determined if oxygen is in fact limiting ATP production. This must be performed by concurrent measurement of mitochondrial fractional volume, ATP production, ATP demand, and oxygen supply to respiring muscle. To illustrate this point we present an example of such an experiment in Figure 39 where a rat has been studied by magnetic resonance to measure ATP production and demand by ³¹P MRS together with measures of blood flow using ¹H based phase contrast angiography. In Panels D-F, as contractile intensity increases towards the aerobic capacity of rat hindlimb [~1 Hz twitch stimulation, (155)] ATP demand (initial rate of PCr hydrolysis) increases and a steady-state PCr is reached during contraction (ATP production=ATP demand). In Panels A-C, blood flow (indicative of oxygen supply) increases in a reciprocal fashion as expected in a healthy rat. Utilizing this experimental design within disease conditions such as type 2 diabetes would allow a quantitative understanding of any changes in oxygen delivery compared to healthy animals and where the “tipping point” may fall as contractile intensity is increased. As work intensity increases, the “tipping point” is approached and the reduced blood flow would cause increased PCr hydrolysis and reduced ADP sensitivity. Once the “tipping point” is surpassed ATP production would no longer be able

to match ATP consumption, a PCr steady state would not be reached, and PCr recovery time would increase. The limitation to this experimental design however is that it does not quantify O₂ specifically at the level of the muscular bed. This has been vastly improved by getting closer to the blood:myocyte exchange of oxygen by Poole and colleagues utilizing phosphorescence quenching (145). Other measures of oxygen supply [for review, see Sanjay et al. (262)] are improving non-invasive quantification but at present such measures have not been developed concomitant ³¹PMRS.

8.3 Final Conclusions

Based on the body of work presented within this dissertation, the data suggests that in type 2 diabetes if any deficit in MOP is observed *in vivo* it is likely the result of vascular deficiencies provided there is proper matching of control subjects with their diabetic counterparts regarding lean body mass and daily activity levels. Further, integration of these results shows that experiments must be carefully designed to quantitatively determine the limitation to muscle metabolism in disease conditions and to guide intervention strategies. Once these techniques are improved, their application will vastly improve the understanding of diseases presenting with exercise intolerance and impaired activity of daily living. Cogent understanding will improve pharmacological and therapeutic interventions towards the ultimate goal of improving quality of life in these patients.

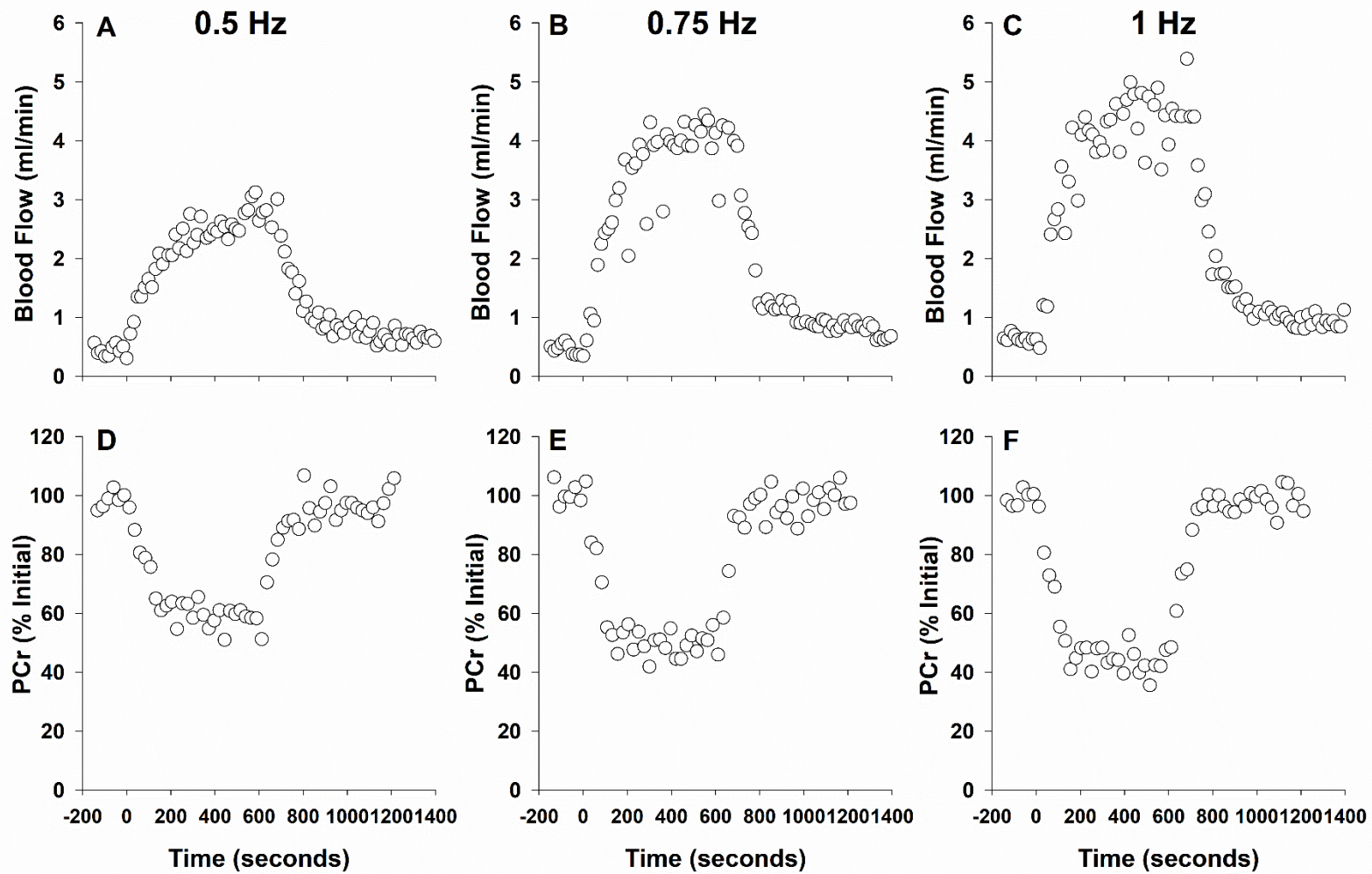


Figure 39. Experimental design measuring blood flow delivery and phosphorus energetics concurrently. As contractile intensity increases, blood flow to the muscle increases (A-C) and more PCr is hydrolyzed (D-F).

REFERENCES

REFERENCES

1. **Abdul-Ghani MA, DeFronzo RA.** Mitochondrial dysfunction, insulin resistance, and type 2 diabetes mellitus. *Curr Diab Rep* 8: 173, 2008.
2. **Abdul-Ghani MA, Jani R, Chavez A, Molina-Carrion M, Tripathy D, Defronzo RA.** Mitochondrial reactive oxygen species generation in obese non-diabetic and type 2 diabetic participants. *Diabetologia* 52: 574–582, 2009.
3. **Adami A, Cao R, Porszasz J, Casaburi R, Rossiter HB.** Reproducibility of NIRS assessment of muscle oxidative capacity in smokers with and without COPD. *Respiratory Physiology & Neurobiology* 235: 18–26, 2017.
4. **Adams GR, Foley JM, Meyer RA.** Muscle buffer capacity estimated from pH changes during rest-to-work transitions. *Journal of Applied Physiology* 69: 968–972, 1990.
5. **Affourtit C, Quinlan CL, Brand MD.** Measurement of Proton Leak and Electron Leak in Isolated Mitochondria. In: *Mitochondrial Bioenergetics*, edited by Palmeira CM, Moreno AJ. Humana Press, p. 165–182.
6. **Akash MS, Rehman K, Chen S.** Goto-Kakizaki rats: its suitability as non-obese diabetic animal model for spontaneous type 2 diabetes mellitus. *Curr Diabetes Rev* 9: 387–396, 2013.
7. **Alameddine A, Fajloun Z, Bourreau J, Gauquelin-Koch G, Yuan M, Gauguier D, Derbre S, Ayer A, Custaud MA, Navasiolava N.** The cardiovascular effects of salidroside in the Goto-Kakizaki diabetic rat model. *J Physiol Pharmacol* 66: 249–257, 2015.
8. **Ameredes BT, Brechue WF, Stainsby WN.** Mechanical and metabolic determination of VO₂ and fatigue during repetitive isometric contractions in situ. *J Appl Physiol* 84: 1909–1916, 1998.
9. **American Diabetes Association.** Report of the Expert Committee on the Diagnosis and Classification of Diabetes Mellitus. *Diabetes Care* 26: s5–s20, 2003.
10. **American Diabetes Association.** Diagnosis and Classification of Diabetes Mellitus. *Diabetes Care* 34: S62–S69, 2011.
11. **Andersen P, Saltin B.** Maximal perfusion of skeletal muscle in man. *J Physiol* 366: 233–249, 1985.
12. **Anderson EJ, Lustig ME, Boyle KE, Woodlief TL, Kane DA, Lin C-T, Price JW, Kang L, Rabinovitch PS, Szeto HH, Houmard JA, Cortright RN, Wasserman DH, Neuffer PD.** Mitochondrial H₂O₂ emission and cellular redox state

link excess fat intake to insulin resistance in both rodents and humans. *J Clin Invest* 119: 573–581, 2009.

13. **Bajpeyi S, Pasarica M, Conley KE, Newcomer BR, Jubrias SA, Gamboa C, Murray K, Sereda O, Sparks LM, Smith SR.** Pioglitazone-induced improvements in insulin sensitivity occur without concomitant changes in muscle mitochondrial function. *Metab Clin Exp* 69: 24–32, 2017.
14. **Balaban RS.** The role of Ca²⁺ signaling in the coordination of mitochondrial ATP production with cardiac work. *Biochimica et Biophysica Acta (BBA) - Bioenergetics* 1787: 1334–1341, 2009.
15. **Baller D, Bretschneider HJ, Hellige G.** A critical look at currently used indirect indices of myocardial oxygen consumption. *Basic Res Cardiol* 76: 163–181, 1981.
16. **Barbato JC, Koch LG, Darvish A, Cicila GT, Metting PJ, Britton SL.** Spectrum of aerobic endurance running performance in eleven inbred strains of rats. *J Appl Physiol* 85: 530–536, 1998.
17. **Barrett EJ, Liu Z, Khamaisi M, King GL, Klein R, Klein BEK, Hughes TM, Craft S, Freedman BI, Bowden DW, Vinik AI, Casellini CM.** Diabetic Microvascular Disease: An Endocrine Society Scientific Statement. *None* 102: 4343–4410, 2017.
18. **Barroso I.** Genetics of Type 2 diabetes. *Diabetic Medicine* 22: 517–535, 2005.
19. **Bassett DR, Howley ET.** Limiting factors for maximum oxygen uptake and determinants of endurance performance. *Med Sci Sports Exerc* 32: 70–84, 2000.
20. **Bauer TA, Reusch JEB, Levi M, Regensteiner JG.** Skeletal muscle deoxygenation after the onset of moderate exercise suggests slowed microvascular blood flow kinetics in type 2 diabetes. *Diabetes Care* 30: 2880–2885, 2007.
21. **Bazil JN, Beard DA, Vinnakota KC.** Catalytic Coupling of Oxidative Phosphorylation, ATP Demand, and Reactive Oxygen Species Generation. *Biophys J* 110: 962–971, 2016.
22. **Behnke BJ, Ferreira LF, McDonough PJ, Musch TI, Poole DC.** Recovery dynamics of skeletal muscle oxygen uptake during the exercise off-transient. *Respiratory Physiology & Neurobiology* 168: 254–260, 2009.
23. **Behnke BJ, Kindig CA, Musch TI, Koga S, Poole DC.** Dynamics of microvascular oxygen pressure across the rest-exercise transition in rat skeletal muscle. *Respiration Physiology* 126: 53–63, 2001.
24. **Beilby J.** Definition of Metabolic Syndrome: Report of the National Heart, Lung, and Blood Institute/American Heart Association Conference on Scientific Issues Related to Definition. *Clin Biochem Rev* 25: 195–198, 2004.

25. **Berg HE, Dudley GA, Hather B, Tesch PA.** Work capacity and metabolic and morphologic characteristics of the human quadriceps muscle in response to unloading. *Clinical Physiology* 13: 337–347, 1993.
26. **Bhambhani Y, Mactavish J, Warren S, Thompson WR, Webborn A, Bressan E, De Mello MT, Tweedy S, Malone L, Frojd K, Van De Vliet P, Vanlandewijck Y.** Boosting in athletes with high-level spinal cord injury: knowledge, incidence and attitudes of athletes in paralympic sport. *Disabil Rehabil* 32: 2172–2190, 2010.
27. **Bhati P, Shenoy S, Hussain ME.** Exercise training and cardiac autonomic function in type 2 diabetes mellitus: A systematic review. *Diabetes & Metabolic Syndrome: Clinical Research & Reviews* 12: 69–78, 2018.
28. **Billings LK, Florez JC.** The genetics of type 2 diabetes: what have we learned from GWAS? *Annals of the New York Academy of Sciences* 1212: 59–77, 2010.
29. **Billman GE, Schwartz PJ, Stone HL.** The effects of daily exercise on susceptibility to sudden cardiac death. *Circulation* 69: 1182–1189, 1984.
30. **Biscetti F, Straface G, Arena V, Stigliano E, Pecorini G, Rizzo P, De Angelis G, Iuliano L, Ghirlanda G, Flex A.** Pioglitazone enhances collateral blood flow in ischemic hindlimb of diabetic mice through an Akt-dependent VEGF-mediated mechanism, regardless of PPARgamma stimulation. *Cardiovasc Diabetol* 8: 49, 2009.
31. **Bishop PD, Atkinson DE.** Adenine nucleotide control of the rate of oxygen uptake by rat heart mitochondria over a 15- to 20-fold range. *Archives of Biochemistry and Biophysics* 230: 335–344, 1984.
32. **Blacher J, Asmar R, Djane S, London GM, Safar ME.** Aortic Pulse Wave Velocity as a Marker of Cardiovascular Risk in Hypertensive Patients. *Hypertension* 33: 1111–1117, 1999.
33. **Blei ML, Conley KE, Kushmerick MJ.** Separate measures of ATP utilization and recovery in human skeletal muscle. *J Physiol* 465: 203–222, 1993.
34. **Blei ML, Conley KE, Odderson IB, Esselman PC, Kushmerick MJ.** Individual variation in contractile cost and recovery in a human skeletal muscle. *Proc Natl Acad Sci USA* 90: 7396–7400, 1993.
35. **Bonen A, Holloway GP, Tandon NN, Han X-X, McFarlan J, Glatz JFC, Luiken JJFP.** Cardiac and skeletal muscle fatty acid transport and transporters and triacylglycerol and fatty acid oxidation in lean and Zucker diabetic fatty rats. *American Journal of Physiology - Regulatory, Integrative and Comparative Physiology* 297: R1202–R1212, 2009.
36. **Bonnard C, Durand A, Peyrol S, Chanseaume E, Chauvin M-A, Morio B, Vidal H, Rieusset J.** Mitochondrial dysfunction results from oxidative stress in the

skeletal muscle of diet-induced insulin-resistant mice. *J Clin Invest* 118: 789–800, 2008.

37. **Booth FW, Roberts CK, Laye MJ.** Lack of exercise is a major cause of chronic diseases. *Compr Physiol* 2: 1143–1211, 2012.
38. **Booth FW, Roberts CK, Thyfault JP, Rueggsegger GN, Toedebusch RG.** Role of Inactivity in Chronic Diseases: Evolutionary Insight and Pathophysiological Mechanisms. *Physiological Reviews* 97: 1351–1402, 2017.
39. **Boushel R, Gnaiger E, Calbet JAL, Gonzalez-Alonso J, Wright-Paradis C, Sondergaard H, Ara I, Helge JW, Saltin B.** Muscle mitochondrial capacity exceeds maximal oxygen delivery in humans. *Mitochondrion* 11: 303–307, 2011.
40. **Boushel R, Gnaiger E, Schjerling P, Skovbro M, Kraunsøe R, Dela F.** Patients with type 2 diabetes have normal mitochondrial function in skeletal muscle. *Diabetologia* 50: 790–796, 2007.
41. **Boutouyrie P.** Determinants of pulse wave velocity in healthy people and in the presence of cardiovascular risk factors: ‘establishing normal and reference values.’ *Eur Heart J* 31: 2338–2350, 2010.
42. **Brand MD, Nicholls DG.** Assessing mitochondrial dysfunction in cells. *Biochem J* 435: 297–312, 2011.
43. **Bratic I, Trifunovic A.** Mitochondrial energy metabolism and ageing. *Biochimica et Biophysica Acta (BBA) - Bioenergetics* 1797: 961–967, 2010.
44. **Brookes PS, Yoon Y, Robotham JL, Anders MW, Sheu S-S.** Calcium, ATP, and ROS: a mitochondrial love-hate triangle. *American Journal of Physiology-Cell Physiology* 287: C817–C833, 2004.
45. **Brooks GA.** Importance of the “crossover” concept in exercise metabolism. *Clin Exp Pharmacol Physiol* 24: 889–895, 1997.
46. **Brownlee M.** Biochemistry and molecular cell biology of diabetic complications. *Nature* 414: 813–820, 2001.
47. **Buck AKW, Elder CP, Donahue MJ, Damon BM.** Matching of postcontraction perfusion to oxygen consumption across submaximal contraction intensities in exercising humans. *Journal of Applied Physiology* 119: 280–289, 2015.
48. **Bussey CT, de Leeuw AE, Lamberts RR.** Increased haemodynamic adrenergic load with isoflurane anaesthesia in type 2 diabetic and obese rats in vivo. *Cardiovasc Diabetol* 13: 161, 2014.
49. **Caballero AE.** Metabolic and vascular abnormalities in subjects at risk for type 2 diabetes: the early start of a dangerous situation. *Arch Med Res* 36: 241–249, 2005.

50. **Carnethon MR, Jacobs DR, Sidney S, Liu K, CARDIA study.** Influence of autonomic nervous system dysfunction on the development of type 2 diabetes: the CARDIA study. *Diabetes Care* 26: 3035–3041, 2003.
51. **Carraro F, Klein S, Rosenblatt JI, Wolfe RR.** Effect of dichloroacetate on lactate concentration in exercising humans. *Journal of Applied Physiology* 66: 591–597, 1989.
52. **Carter JB, Banister EW, Blaber AP.** Effect of endurance exercise on autonomic control of heart rate. *Sports Med* 33: 33–46, 2003.
53. **Casaburi R, Patessio A, Ioli F, Zanaboni S, Donner CF, Wasserman K.** Reductions in Exercise Lactic Acidosis and Ventilation as a Result of Exercise Training in Patients with Obstructive Lung Disease. *American Review of Respiratory Disease* 143: 9–18, 1991.
54. **CDC.** National Diabetes Statistics Report | Data & Statistics | Diabetes | CDC [Online]. 2018. <https://www.cdc.gov/diabetes/data/statistics/statistics-report.html> [22 Jan. 2019].
55. **Challiss RA, Vranic M, Radda GK.** Bioenergetic changes during contraction and recovery in diabetic rat skeletal muscle. *Am J Physiol* 256: E129-137, 1989.
56. **Chance B, Leigh JS, Clark BJ, Maris J, Kent J, Nioka S, Smith D.** Control of oxidative metabolism and oxygen delivery in human skeletal muscle: a steady-state analysis of the work/energy cost transfer function. *Proc Natl Acad Sci U S A* 82: 8384–8388, 1985.
57. **Chandler MP, DiCarlo SE.** Acute exercise and gender alter cardiac autonomic tonus differently in hypertensive and normotensive rats. *Am J Physiol* 274: R510-516, 1998.
58. **Chantler PD, Frisbee JC.** Arterial Function in Cardio-Metabolic Diseases: From the Microcirculation to the Large Conduits. *Progress in Cardiovascular Diseases* 57: 489–496, 2015.
59. **Chen YC, Inagaki T, Fujii Y, Schwenke DO, Tsuchimochi H, Edgley AJ, Umetani K, Zhang Y, Kelly DJ, Yoshimoto M, Nagai H, Evans RG, Kuwahira I, Shirai M, Pearson JT.** Chronic intermittent hypoxia accelerates coronary microcirculatory dysfunction in insulin-resistant Goto-Kakizaki rats. *Am J Physiol Regul Integr Comp Physiol* 311: R426-439, 2016.
60. **Chida Y, Steptoe A.** Greater cardiovascular responses to laboratory mental stress are associated with poor subsequent cardiovascular risk status: a meta-analysis of prospective evidence. *Hypertension* 55: 1026–1032, 2010.
61. **Christensen NJ, Galbo H.** Sympathetic Nervous Activity During Exercise. *Annual Review of Physiology* 45: 139–153, 1983.

62. **Chung S, Nelson MD, Hamaoka T, Jacobs RA, Pearson J, Subudhi AW, Jenkins NT, Bartlett MF, Fitzgerald LF, Miehm JD, Kent JA, Lucero AA, Rowlands DS, Stoner L, McCully KK, Call J, Rodriguez-Miguel P, Harris RA, Porcelli S, Rasica L, Marzorati M, Quaresima V, Ryan TE, Vernillo G, Millet GP, Malatesta D, Millet GY, Zuo L, Chuang C-C.** Commentaries on Viewpoint: Principles, insights, and potential pitfalls of the noninvasive determination of muscle oxidative capacity by near-infrared spectroscopy. *J Appl Physiol* 124: 249–255, 2018.
63. **Cieslar JH, Dobson GP.** Free [ADP] and Aerobic Muscle Work Follow at Least Second Order Kinetics in Rat Gastrocnemius *in Vivo*. *Journal of Biological Chemistry* 275: 6129–6134, 2000.
64. **Close RI.** Dynamic properties of mammalian skeletal muscles. *Physiol Rev* 52: 129–197, 1972.
65. **Coggan AR, Coyle EF.** Metabolism and performance following carbohydrate ingestion late in exercise. *Med Sci Sports Exerc* 21: 59–65, 1989.
66. **Colagiuri S, Brand Miller J.** The 'carnivore connection'--evolutionary aspects of insulin resistance. *Eur J Clin Nutr* 56 Suppl 1: S30-35, 2002.
67. **Colberg SR, Sigal RJ, Yardley JE, Riddell MC, Dunstan DW, Dempsey PC, Horton ES, Castorino K, Tate DF.** Physical Activity/Exercise and Diabetes: A Position Statement of the American Diabetes Association. *Diabetes Care* 39: 2065–2079, 2016.
68. **Collins HL, DiCarlo SE.** Acute exercise reduces the response to colon distension in T(5) spinal rats. *Am J Physiol Heart Circ Physiol* 282: H1566-1570, 2002.
69. **Collins HL, DiCarlo SE.** TENS attenuates response to colon distension in paraplegic and quadriplegic rats. *Am J Physiol Heart Circ Physiol* 283: H1734-1739, 2002.
70. **Connett RJ.** Analysis of metabolic control: new insights using scaled creatine kinase model. *American Journal of Physiology-Regulatory, Integrative and Comparative Physiology* 254: R949–R959, 1988.
71. **Connett RJ, Honig CR, Gayeski TE, Brooks GA.** Defining hypoxia: a systems view of VO₂, glycolysis, energetics, and intracellular PO₂. *J Appl Physiol* 68: 833–842, 1990.
72. **Convertino VA, Brock PJ, Keil LC, Bernauer EM, Greenleaf JE.** Exercise training-induced hypervolemia: role of plasma albumin, renin, and vasopressin. *J Appl Physiol Respir Environ Exerc Physiol* 48: 665–669, 1980.

73. **Convertino VA, Keil LC, Bernauer EM, Greenleaf JE.** Plasma volume, osmolality, vasopressin, and renin activity during graded exercise in man. *J Appl Physiol Respir Environ Exerc Physiol* 50: 123–128, 1981.
74. **Coote JH.** Recovery of heart rate following intense dynamic exercise. *Experimental Physiology* 95: 431–440, 2010.
75. **Copp SW, Hageman KS, Behnke BJ, Poole DC, Musch TI.** Effects of Type II diabetes on exercising skeletal muscle blood flow in the rat. *Journal of Applied Physiology* 109: 1347–1353, 2010.
76. **Corpeleijn E, Saris WHM, Blaak EE.** Metabolic flexibility in the development of insulin resistance and type 2 diabetes: effects of lifestyle. *Obes Rev* 10: 178–193, 2009.
77. **Coutinho M, Gerstein HC, Wang Y, Yusuf S.** The relationship between glucose and incident cardiovascular events. A metaregression analysis of published data from 20 studies of 95,783 individuals followed for 12.4 years. *Diabetes Care* 22: 233–240, 1999.
78. **Coyle EF, Coggan AR, Hemmert MK, Ivy JL.** Muscle glycogen utilization during prolonged strenuous exercise when fed carbohydrate. *Journal of Applied Physiology* 61: 165–172, 1986.
79. **Coyle EF, Martin WH, Sinacore DR, Joyner MJ, Hagberg JM, Holloszy JO.** Time course of loss of adaptations after stopping prolonged intense endurance training. *J Appl Physiol Respir Environ Exerc Physiol* 57: 1857–1864, 1984.
80. **Credeur DP, Reynolds LJ, Holwerda SW, Vranish JR, Young BE, Wang J, Thyfault JP, Fadel PJ.** Influence of physical inactivity on arterial compliance during a glucose challenge. *Experimental Physiology* 103: 483–494, 2018.
81. **Cree-Green M, Gupta A, Coe GV, Baumgartner AD, Pyle L, Reusch JEB, Brown MS, Newcomer BR, Nadeau KJ.** Insulin resistance in type 2 diabetes youth relates to serum free fatty acids and muscle mitochondrial dysfunction. *J Diabetes Complicat* 31: 141–148, 2017.
82. **Cree-Green M, Scalzo RL, Harrall K, Newcomer BR, Schauer IE, Huebschmann AG, McMillin S, Brown MS, Orlicky D, Knaub L, Nadeau KJ, McClatchey PM, Bauer TA, Regensteiner JG, Reusch JEB.** Supplemental Oxygen Improves In Vivo Mitochondrial Oxidative Phosphorylation Flux in Sedentary Obese Adults With Type 2 Diabetes. *Diabetes* 67: 1369–1379, 2018.
83. **Cruickshank K.** Aortic Pulse-Wave Velocity and Its Relationship to Mortality in Diabetes and Glucose Intolerance: An Integrated Index of Vascular Function? *Circulation* 106: 2085–2090, 2002.

84. **Daanen HAM, Lamberts RP, Kallen VL, Jin A, Van Meeteren NLU.** A Systematic Review on Heart-Rate Recovery to Monitor Changes in Training Status in Athletes. *International Journal of Sports Physiology and Performance* 7: 251–260, 2012.
85. **Davidson JA, Parkin CG.** Is Hyperglycemia a Causal Factor in Cardiovascular Disease?: Does proving this relationship really matter? Yes. *Diabetes Care* 32: S331–S333, 2009.
86. **De Feyter HM, Lenaers E, Houten SM, Schrauwen P, Hesselink MK, Wanders RJA, Nicolay K, Prompers JJ.** Increased intramyocellular lipid content but normal skeletal muscle mitochondrial oxidative capacity throughout the pathogenesis of type 2 diabetes. *FASEB J* 22: 3947–3955, 2008.
87. **De Feyter HM, van den Broek NMA, Praet SFE, Nicolay K, van Loon LJC, Prompers JJ.** Early or advanced stage type 2 diabetes is not accompanied by in vivo skeletal muscle mitochondrial dysfunction. *Eur J Endocrinol* 158: 643–653, 2008.
88. **De Meersman RE.** Respiratory sinus arrhythmia alteration following training in endurance athletes. *Eur J Appl Physiol Occup Physiol* 64: 434–436, 1992.
89. **DeFronzo RA, Tripathy D.** Skeletal Muscle Insulin Resistance Is the Primary Defect in Type 2 Diabetes. *Diabetes Care* 32: S157–S163, 2009.
90. **Delp MD, Duan C.** Composition and size of type I, IIA, IID/X, and IIB fibers and citrate synthase activity of rat muscle. *Journal of Applied Physiology* 80: 261–270, 1996.
91. **Díaz A, López-Gruoso R, Gambini J, Monleón D, Mas-Bargues C, Abdelaziz KM, Viña J, Borrás C.** Sex Differences in Age-Associated Type 2 Diabetes in Rats—Role of Estrogens and Oxidative Stress. *Oxid Med Cell Longev* 2019, 2019.
92. **Dinenno FA, Tanaka H, Monahan KD, Clevenger CM, Eskurza I, DeSouza CA, Seals DR.** Regular endurance exercise induces expansive arterial remodelling in the trained limbs of healthy men. *J Physiol (Lond)* 534: 287–295, 2001.
93. **Dudley GA, Tullson PC, Terjung RL.** Influence of mitochondrial content on the sensitivity of respiratory control. *J Biol Chem* 262: 9109–9114, 1987.
94. **Eklom B, Hermansen L.** Cardiac output in athletes. *Journal of Applied Physiology* 25: 619–625, 1968.
95. **Eklom B, Kilbom A, Soltysiak J.** Physical training, bradycardia, and autonomic nervous system. *Scand J Clin Lab Invest* 32: 251–256, 1973.
96. **Emerging Risk Factors Collaboration, Sarwar N, Gao P, Seshasai SRK, Gobin R, Kaptoge S, Di Angelantonio E, Ingelsson E, Lawlor DA, Selvin E,**

- Stampfer M, Stehouwer CDA, Lewington S, Pennells L, Thompson A, Sattar N, White IR, Ray KK, Danesh J.** Diabetes mellitus, fasting blood glucose concentration, and risk of vascular disease: a collaborative meta-analysis of 102 prospective studies. *Lancet* 375: 2215–2222, 2010.
97. **Fang ZY, Sharman J, Prins JB, Marwick TH.** Determinants of Exercise Capacity in Patients With Type 2 Diabetes. *Diabetes Care* 28: 1643–1648, 2005.
98. **Fealy CE, Mulya A, Axelrod CL, Kirwan JP.** Mitochondrial dynamics in skeletal muscle insulin resistance and type 2 diabetes. *Translational Research* 202: 69–82, 2018.
99. **Ferguson SK, Hirai DM, Copp SW, Holdsworth CT, Allen JD, Jones AM, Musch TI, Poole DC.** Impact of dietary nitrate supplementation via beetroot juice on exercising muscle vascular control in rats. *J Physiol* 591: 547–557, 2013.
100. **Fernandes AA, Faria T de O, Ribeiro RF, Costa GP, Marchezini B, Silveira EA, Angeli JK, Stefanon I, Vassallo DV, Lizardo JH.** A single resistance exercise session improves myocardial contractility in spontaneously hypertensive rats. *Braz J Med Biol Res* 48: 813–821, 2015.
101. **Fisher-Wellman KH, Davidson MT, Narowski TM, Lin C-T, Koves TR, Muoio DM.** Mitochondrial Diagnostics: A Multiplexed Assay Platform for Comprehensive Assessment of Mitochondrial Energy Fluxes. *Cell Reports* 24: 3593-3606.e10, 2018.
102. **Fitts RH, Booth FW, Winder WW, Holloszy JO.** Skeletal muscle respiratory capacity, endurance, and glycogen utilization. *Am J Physiol* 228: 1029–1033, 1975.
103. **Fitzpatrick R, Taylor JL, McCloskey DI.** Effects of arterial perfusion pressure on force production in working human hand muscles. *The Journal of Physiology* 495: 885–891, 1996.
104. **Foley JM, Meyer RA.** Energy cost of twitch and tetanic contractions of rat muscle estimated in situ by gated ³¹P NMR. *NMR Biomed* 6: 32–38, 1993.
105. **Forbes SC, Paganini AT, Slade JM, Towse TF, Meyer RA.** Phosphocreatine recovery kinetics following low- and high-intensity exercise in human triceps surae and rat posterior hindlimb muscles. *Am J Physiol Regul Integr Comp Physiol* 296: R161-170, 2009.
106. **Frachetti KJ, Goldfine AB.** Bariatric surgery for diabetes management. *Curr Opin Endocrinol Diabetes Obes* 16: 119–124, 2009.
107. **Franklin SS, Thijs L, Hansen TW, O'Brien E, Staessen JA.** White-coat hypertension: new insights from recent studies. *Hypertension* 62: 982–987, 2013.

108. **Frisbee JC.** Impaired skeletal muscle perfusion in obese Zucker rats. *American Journal of Physiology - Regulatory, Integrative and Comparative Physiology* 285: R1124–R1134, 2003.
109. **Frisbee JC, Delp MD.** Vascular function in the metabolic syndrome and the effects on skeletal muscle perfusion: lessons from the obese Zucker rat. *Essays Biochem* 42: 145–161, 2006.
110. **Frisbee JC, Lewis MT, Kasper JD, Chantler PD, Wiseman RW.** Type 2 diabetes mellitus in the Goto-Kakizaki rat impairs microvascular function and contributes to premature skeletal muscle fatigue. *Journal of Applied Physiology* 126: 626–637, 2018.
111. **Frisbee JC, Lewis MT, Wiseman RW.** Skeletal muscle performance in metabolic disease: microvascular or mitochondrial limitation or both? *Microcirculation* (November 24, 2018). doi: 10.1111/micc.12517.
112. **Fu Q, Levine BD.** Exercise and the autonomic nervous system. *Handb Clin Neurol* 117: 147–160, 2013.
113. **Gebremedhin T, Workicho A, Angaw DA.** Health-related quality of life and its associated factors among adult patients with type II diabetes attending Mizan Tepi University Teaching Hospital, Southwest Ethiopia. *BMJ Open Diabetes Research and Care* 7: e000577, 2019.
114. **Gee CM, West CR, Krassioukov AV.** Boosting in Elite Athletes with Spinal Cord Injury: A Critical Review of Physiology and Testing Procedures. *Sports Med* 45: 1133–1142, 2015.
115. **Giannesini B, Izquierdo M, Le Fur Y, Cozzone PJ, Fingerle J, Himber J, Künnecke B, Von Kienlin M, Bendahan D.** New experimental setup for studying strictly noninvasively skeletal muscle function in rat using ¹H-magnetic resonance (MR) imaging and ³¹P-MR spectroscopy. *Magn Reson Med* 54: 1058–1064, 2005.
116. **Gifford JR, Garten RS, Nelson AD, Trinity JD, Layec G, Witman MAH, Weavil JC, Mangum T, Hart C, Etheredge C, Jessop J, Bledsoe A, Morgan DE, Wray DW, Rossman MJ, Richardson RS.** Symmorphosis and skeletal muscle : in vivo and in vitro measures reveal differing constraints in the exercise-trained and untrained human. *The Journal of Physiology* 594: 1741–1751, 2016.
117. **Glancy B, Balaban RS.** Role of mitochondrial Ca²⁺ in the regulation of cellular energetics. *Biochemistry* 51: 2959–2973, 2012.
118. **Gledhill N.** Blood doping and related issues: a brief review. *Med Sci Sports Exerc* 14: 183–189, 1982.

119. **Gobel FL, Norstrom LA, Nelson RR, Jorgensen CR, Wang Y.** The rate-pressure product as an index of myocardial oxygen consumption during exercise in patients with angina pectoris. *Circulation* 57: 549–556, 1978.
120. **Goldsmith RL, Bigger JT, Steinman RC, Fleiss JL.** Comparison of 24-hour parasympathetic activity in endurance-trained and untrained young men. *J Am Coll Cardiol* 20: 552–558, 1992.
121. **Gonzalez-Franquesa A, Patti M-E.** Insulin Resistance and Mitochondrial Dysfunction. *Adv Exp Med Biol* 982: 465–520, 2017.
122. **Goodwin ML, Harris JE, Hernández A, Gladden LB.** Blood Lactate Measurements and Analysis during Exercise: A Guide for Clinicians. *J Diabetes Sci Technol* 1: 558–569, 2007.
123. **Goto Y, Kakizaki M, Masaki N.** Spontaneous Diabetes Produced by Selective Breeding of Normal Wistar Rats. *Proceedings of the Japan Academy* 51: 80–85, 1975.
124. **Gourine AV, Ackland GL.** Cardiac Vagus and Exercise. *Physiology* 34: 71–80, 2018.
125. **Grönros J, Jung C, Lundberg JO, Cerrato R, Ostenson C-G, Pernow J.** Arginase inhibition restores in vivo coronary microvascular function in type 2 diabetic rats. *Am J Physiol Heart Circ Physiol* 300: H1174-1181, 2011.
126. **Hamann JJ, Kluess HA, Buckwalter JB, Clifford PS.** Blood flow response to muscle contractions is more closely related to metabolic rate than contractile work. *J Appl Physiol* 98: 2096–2100, 2005.
127. **Hamaoka T, McCully KK, Quaresima V, Yamamoto K, Chance B.** Near-infrared spectroscopy/imaging for monitoring muscle oxygenation and oxidative metabolism in healthy and diseased humans. *JBO* 12: 062105, 2007.
128. **Hamman RF, Wing RR, Edelstein SL, Lachin JM, Bray GA, Delahanty L, Hoskin M, Kriska AM, Mayer-Davis EJ, Pi-Sunyer X, Regensteiner J, Venditti B, Wylie-Rosett J.** Effect of Weight Loss With Lifestyle Intervention on Risk of Diabetes. *Diabetes Care* 29: 2102–2107, 2006.
129. **Hancock CR, Brault JJ, Wiseman RW, Terjung RL, Meyer RA.** ³¹P-NMR observation of free ADP during fatiguing, repetitive contractions of murine skeletal muscle lacking AK1. *Am J Physiol, Cell Physiol* 288: C1298-1304, 2005.
130. **Harkema SJ, Meyer RA.** Effect of acidosis on control of respiration in skeletal muscle. *Am J Physiol* 272: C491-500, 1997.
131. **Hart CR, Lanza IR.** Mitochondrial ADP Sensitivity and Transport: New Insights Into Diet-Induced Mitochondrial Impairments. *Diabetes* 67: 2152–2153, 2018.

132. **Hart CR, Layec G, Trinity JD, Le Fur Y, Gifford JR, Clifton HL, Richardson RS.** Oxygen availability and skeletal muscle oxidative capacity in patients with peripheral arterial disease: Implications from in vivo and in vitro assessments. *Am. J. Physiol. Heart Circ. Physiol.* (22 2018). doi: 10.1152/ajpheart.00641.2017.
133. **Haseler LJ, Hogan MC, Richardson RS.** Skeletal muscle phosphocreatine recovery in exercise-trained humans is dependent on O₂ availability. *Journal of Applied Physiology* 86: 2013–2018, 1999.
134. **Haseler LJ, Lin A, Hoff J, Richardson RS.** Oxygen availability and PCr recovery rate in untrained human calf muscle: evidence of metabolic limitation in normoxia. *American Journal of Physiology-Regulatory, Integrative and Comparative Physiology* 293: R2046–R2051, 2007.
135. **Haseler LJ, Lin AP, Richardson RS.** Skeletal muscle oxidative metabolism in sedentary humans: 31P-MRS assessment of O₂ supply and demand limitations. *Journal of Applied Physiology* 97: 1077–1081, 2004.
136. **Haseler LJ, Richardson RS, Videen JS, Hogan MC.** Phosphocreatine hydrolysis during submaximal exercise: the effect of F I O₂. *Journal of Applied Physiology* 85: 1457–1463, 1998.
137. **Heath GW, Gavin JR, Hinderliter JM, Hagberg JM, Bloomfield SA, Holloszy JO.** Effects of exercise and lack of exercise on glucose tolerance and insulin sensitivity. *J Appl Physiol Respir Environ Exerc Physiol* 55: 512–517, 1983.
138. **Heinonen I, Koga S, Kalliokoski KK, Musch TI, Poole DC.** Heterogeneity of Muscle Blood Flow and Metabolism: Influence of Exercise, Aging and Disease States. *Exerc Sport Sci Rev* 43: 117–124, 2015.
139. **Hellsten Y, Nyberg M.** Cardiovascular Adaptations to Exercise Training. In: *Comprehensive Physiology*, edited by Terjung R. John Wiley & Sons, Inc., p. 1–32.
140. **Henriksson J, Reitman JS.** Time course of changes in human skeletal muscle succinate dehydrogenase and cytochrome oxidase activities and maximal oxygen uptake with physical activity and inactivity. *Acta Physiol Scand* 99: 91–97, 1977.
141. **Heo J-W, No M-H, Park D-H, Kang J-H, Seo DY, Han J, Neuffer PD, Kwak H-B.** Effects of exercise on obesity-induced mitochondrial dysfunction in skeletal muscle. *Korean J Physiol Pharmacol* 21: 567–577, 2017.
142. **Hey-Mogensen M, Højlund K, Vind BF, Wang L, Dela F, Beck-Nielsen H, Fernström M, Sahlin K.** Effect of physical training on mitochondrial respiration and reactive oxygen species release in skeletal muscle in patients with obesity and type 2 diabetes. *Diabetologia* 53: 1976–1985, 2010.

143. **Hikida RS, Gollnick PD, Dudley GA, Convertino VA, Buchanan P.** Structural and metabolic characteristics of human skeletal muscle following 30 days of simulated microgravity. *Aviat Space Environ Med* 60: 664–670, 1989.
144. **Hill AV, Allsopp CE, Kwiatkowski D, Anstey NM, Twumasi P, Rowe PA, Bennett S, Brewster D, McMichael AJ, Greenwood BM.** Common west African HLA antigens are associated with protection from severe malaria. *Nature* 352: 595–600, 1991.
145. **Hirai DM, Colburn TD, Craig JC, Hotta K, Kano Y, Musch TI, Poole DC.** Skeletal muscle interstitial O₂ pressures: bridging the gap between the capillary and myocyte. *Microcirculation* 26: e12497, 2019.
146. **Hogan MC, Richardson RS, Haseler LJ.** Human muscle performance and PCr hydrolysis with varied inspired oxygen fractions: a ³¹P-MRS study. *Journal of Applied Physiology* 86: 1367–1373, 1999.
147. **Holloszy JO.** Biochemical Adaptations in Muscle. Effects of exercise on mitochondrial oxygen uptake and respiratory enzyme activity in skeletal muscle. *J Biol Chem* 242: 2278–2282, 1967.
148. **Holloszy JO.** Regulation of Mitochondrial Biogenesis and GLUT4 Expression by Exercise. In: *Comprehensive Physiology*. American Cancer Society, p. 921–940.
149. **Holloszy JO, Coyle EF.** Adaptations of skeletal muscle to endurance exercise and their metabolic consequences. *J Appl Physiol Respir Environ Exerc Physiol* 56: 831–838, 1984.
150. **Holloszy JO, Kohrt WM.** Regulation of carbohydrate and fat metabolism during and after exercise. *Annu Rev Nutr* 16: 121–138, 1996.
151. **Holloszy JO, Oscai LB, Don IJ, Molé PA.** Mitochondrial citric acid cycle and related enzymes: adaptive response to exercise. *Biochem Biophys Res Commun* 40: 1368–1373, 1970.
152. **Holloszy JO, Schultz J, Kusnierkiewicz J, Hagberg JM, Ehsani AA.** Effects of Exercise on Glucose Tolerance and Insulin Resistance. *Acta Medica Scandinavica* 220: 55–65, 1986.
153. **Holloway GP, Gurd BJ, Snook LA, Lally J, Bonen A.** Compensatory Increases in Nuclear PGC1 α Protein Are Primarily Associated With Subsarcolemmal Mitochondrial Adaptations in ZDF Rats. *Diabetes* 59: 819–828, 2010.
154. **Hölscher ME, Bode C, Bugger H.** Diabetic Cardiomyopathy: Does the Type of Diabetes Matter? *Int J Mol Sci* 17, 2016.
155. **Hood DA, Gorski J, Terjung RL.** Oxygen cost of twitch and tetanic isometric contractions of rat skeletal muscle. *Am J Physiol* 250: E449–456, 1986.

156. **Hopman MT, Dueck C, Monroe M, Philips WT, Skinner JS.** Limits to maximal performance in individuals with spinal cord injury. *Int J Sports Med* 19: 98–103, 1998.
157. **Hoppeler H, Howald H, Conley K, Lindstedt SL, Claassen H, Vock P, Weibel ER.** Endurance training in humans: aerobic capacity and structure of skeletal muscle. *Journal of Applied Physiology* 59: 320–327, 1985.
158. **Howlett RA, Hogan MC.** Dichloroacetate accelerates the fall in intracellular Po₂ at onset of contractions in *Xenopus* single muscle fibers. *American Journal of Physiology-Regulatory, Integrative and Comparative Physiology* 284: R481–R485, 2003.
159. **Howlett RA, Parolin ML, Dyck DJ, Hultman E, Jones NL, Heigenhauser GJ, Spriet LL.** Regulation of skeletal muscle glycogen phosphorylase and PDH at varying exercise power outputs. *Am J Physiol* 275: R418-425, 1998.
160. **Huang Y, Huang W, Mai W, Cai X, An D, Liu Z, Huang H, Zeng J, Hu Y, Xu D.** White-coat hypertension is a risk factor for cardiovascular diseases and total mortality. *J Hypertens* 35: 677–688, 2017.
161. **Hue L, Taegtmeyer H.** The Randle cycle revisited: a new head for an old hat. *Am J Physiol Endocrinol Metab* 297: E578-591, 2009.
162. **Huonker M, Schmid A, Schmidt-Trucksass A, Grathwohl D, Keul J.** Size and blood flow of central and peripheral arteries in highly trained able-bodied and disabled athletes. *J Appl Physiol* 95: 685–691, 2003.
163. **Hurley B, Goldberg AP, Hagberg JM.** John O. Holloszy: An Enduring Legacy in Exercise Physiology, Aging, and Muscle Research. *J Gerontol A Biol Sci Med Sci* 74: 588–589, 2019.
164. **I. Bertinini, Luchinat C.** *NMR Paramagnetic Molecules in Biological Systems.* Menlo Park, CA: The Benjamin-Cummings Publishing Co., 1986.
165. **Inoguchi T, Li P, Umeda F, Yu HY, Kakimoto M, Imamura M, Aoki T, Etoh T, Hashimoto T, Naruse M, Sano H, Utsumi H, Nawata H.** High glucose level and free fatty acid stimulate reactive oxygen species production through protein kinase C--dependent activation of NAD(P)H oxidase in cultured vascular cells. *Diabetes* 49: 1939–1945, 2000.
166. **Intensive blood.** -glucose control with sulphonylureas or insulin compared with conventional treatment and risk of complications in patients with type 2 diabetes (UKPDS 33). UK Prospective Diabetes Study (UKPDS) Group. *Lancet* 352: 837–853, 1998.

167. **Jayaraman RC, Latourette MT, Siebert JE, Wiseman RW.** A rapid algorithm for processing digital physiologic signals: Application to skeletal muscle contractions. *Biomedical Signal Processing and Control* 1: 307–313, 2006.
168. **Jeneson JA, Westerhoff HV, Brown TR, Van Echteld CJ, Berger R.** Quasi-linear relationship between Gibbs free energy of ATP hydrolysis and power output in human forearm muscle. *Am J Physiol* 268: C1474-1484, 1995.
169. **Jeneson JA, Wiseman RW, Kushmerick MJ.** Non-invasive quantitative ³¹P MRS assay of mitochondrial function in skeletal muscle in situ. *Mol Cell Biochem* 174: 17–22, 1997.
170. **Jeneson JA, Wiseman RW, Westerhoff HV, Kushmerick MJ.** The signal transduction function for oxidative phosphorylation is at least second order in ADP. *J Biol Chem* 271: 27995–27998, 1996.
171. **Johnson AK, Xue B.** Central nervous system neuroplasticity and the sensitization of hypertension. *Nature Reviews Nephrology* 14: 750, 2018.
172. **Jørgensen W, Jelnes P, Rud KA, Hansen LL, Grunnet N, Quistorff B.** Progression of type 2 diabetes in GK rats affects muscle and liver mitochondria differently: pronounced reduction of complex II flux is observed in liver only. *American Journal of Physiology - Endocrinology and Metabolism* 303: E515–E523, 2012.
173. **Joyner MJ, Casey DP.** Regulation of increased blood flow (hyperemia) to muscles during exercise: a hierarchy of competing physiological needs. *Physiol Rev* 95: 549–601, 2015.
174. **Jubrias SA, Crowther GJ, Shankland EG, Gronka RK, Conley KE.** Acidosis inhibits oxidative phosphorylation in contracting human skeletal muscle in vivo. *J Physiol* 553: 589–599, 2003.
175. **Kasper JD.** The Role and Regulation of Pyruvate Dehydrogenase in Skeletal Muscle Bioenergetics and Type 2 Diabetes [Online]. Michigan State University: 2018.
<https://search.proquest.com/docview/2160629814/abstract/E22EE85BB4B4730PQ/1> [10 Jun. 2019].
176. **Kasper JD, Meyer RA, Beard DA, Wiseman RW.** Effects of altered Pyruvate Dehydrogenase Activity on contracting skeletal muscle bioenergetics. *Am J Physiol Regul Integr Comp Physiol* 316: R76–R86, 2018.
177. **Katzmarzyk PT.** Physical Activity, Sedentary Behavior, and Health: Paradigm Paralysis or Paradigm Shift? *Diabetes* 59: 2717–2725, 2010.

178. **Katzmarzyk PT, Church TS, Craig CL, Bouchard C.** Sitting time and mortality from all causes, cardiovascular disease, and cancer. *Med Sci Sports Exerc* 41: 998–1005, 2009.
179. **Kelley DE, He J, Menshikova EV, Ritov VB.** Dysfunction of Mitochondria in Human Skeletal Muscle in Type 2 Diabetes. *Diabetes* 51: 2944–2950, 2002.
180. **Kemp GJ.** Quantifying Skeletal Muscle Mitochondrial Function *In Vivo* by ³¹P Magnetic Resonance Spectroscopy. In: *Mitochondrial Dysfunction Caused by Drugs and Environmental Toxicants*, edited by Will Y, Dykens JA. John Wiley & Sons, Inc., p. 443–456.
181. **Kenny HC, Rudwill F, Breen L, Salanova M, Blottner D, Heise T, Heer M, Blanc S, O’Gorman DJ.** Bed rest and resistive vibration exercise unveil novel links between skeletal muscle mitochondrial function and insulin resistance. *Diabetologia* 60: 1491–1501, 2017.
182. **Keske MA, Premilovac D, Bradley EA, Dwyer RM, Richards SM, Rattigan S.** Muscle microvascular blood flow responses in insulin resistance and ageing. *J Physiol* 594: 2223–2231, 2016.
183. **Kim J, Wei Y, Sowers JR.** Role of Mitochondrial Dysfunction in Insulin Resistance. *Circ Res* 102: 401–414, 2008.
184. **Knight DR, Poole DC, Schaffartzik W, Guy HJ, Prediletto R, Hogan MC, Wagner PD.** Relationship between body and leg VO₂ during maximal cycle ergometry. *J Appl Physiol* 73: 1114–1121, 1992.
185. **Knight DR, Schaffartzik W, Poole DC, Hogan MC, Bebout DE, Wagner PD.** Effects of hyperoxia on maximal leg O₂ supply and utilization in men. *Journal of Applied Physiology* 75: 2586–2594, 1993.
186. **Knowler WC, Barrett-Connor E, Fowler SE, Hamman RF, Lachin JM, Walker EA, Nathan DM, Diabetes Prevention Program Research Group.** Reduction in the incidence of type 2 diabetes with lifestyle intervention or metformin. *N Engl J Med* 346: 393–403, 2002.
187. **Koch LG, Britton SL, Barbato JC, Rodenbaugh DW, DiCarlo SE.** Phenotypic differences in cardiovascular regulation in inbred rat models of aerobic capacity. *Physiol Genomics* 1: 63–69, 1999.
188. **Koebmann BJ, Westerhoff HV, Snoep JL, Nilsson D, Jensen PR.** The Glycolytic Flux in *Escherichia coli* Is Controlled by the Demand for ATP. *Journal of Bacteriology* 184: 3909–3916, 2002.
189. **Koga S, Rossiter HB, Heinonen I, Musch TI, Poole DC.** Dynamic Heterogeneity of Exercising Muscle Blood Flow and O₂ Utilization: *Medicine & Science in Sports & Exercise* 46: 860–876, 2014.

190. **Kohn MC, Achs MJ, Garfinkel D.** Computer simulation of metabolism in pyruvate-perfused rat heart. III. Pyruvate dehydrogenase. *Am J Physiol* 237: R167-173, 1979.
191. **Konopka AR, Asante A, Lanza IR, Robinson MM, Johnson ML, Man CD, Cobelli C, Amols MH, Irving BA, Nair KS.** Defects in Mitochondrial Efficiency and H₂O₂ Emissions in Obese Women Are Restored to a Lean Phenotype With Aerobic Exercise Training. *Diabetes* 64: 2104–2115, 2015.
192. **Korzeniewski B, Rossiter HB.** Each-step activation of oxidative phosphorylation is necessary to explain muscle metabolic kinetic responses to exercise and recovery in humans. *The Journal of Physiology* 593: 5255–5268, 2015.
193. **Krantz DS, Santiago HT, Kop WJ, Bairey Merz CN, Rozanski A, Gottdiener JS.** Prognostic value of mental stress testing in coronary artery disease. *Am J Cardiol* 84: 1292–1297, 1999.
194. **Krassioukov A.** Autonomic dysreflexia: current evidence related to unstable arterial blood pressure control among athletes with spinal cord injury. *Clin J Sport Med* 22: 39–45, 2012.
195. **Kupper N, Denollet J, Widdershoven J, Kop WJ.** Cardiovascular reactivity to mental stress and mortality in patients with heart failure. *JACC Heart Fail* 3: 373–382, 2015.
196. **Kushmerick MJ, Meyer RA.** Chemical changes in rat leg muscle by phosphorus nuclear magnetic resonance. *American Journal of Physiology-Cell Physiology* 248: C542–C549, 1985.
197. **Kushmerick MJ, Moerland TS, Wiseman RW.** Mammalian skeletal muscle fibers distinguished by contents of phosphocreatine, ATP, and Pi. *PNAS* 89: 7521–7525, 1992.
198. **Kuzmiak-Glancy S, Willis WT.** Skeletal muscle fuel selection occurs at the mitochondrial level. *J Exp Biol* 217: 1993–2003, 2014.
199. **Laakso M.** Hyperglycemia and cardiovascular disease in type 2 diabetes. *Diabetes* 48: 937–942, 1999.
200. **Laakso M.** Cardiovascular disease in type 2 diabetes: challenge for treatment and prevention. *J Intern Med* 249: 225–235, 2001.
201. **Laakso M.** Cardiovascular Disease in Type 2 Diabetes From Population to Man to Mechanisms: The Kelly West Award Lecture 2008. *Diabetes Care* 33: 442–449, 2010.
202. **Laakso M, Lehto S.** Epidemiology of risk factors for cardiovascular disease in diabetes and impaired glucose tolerance. *Atherosclerosis* 137 Suppl: S65-73, 1998.

203. **Lai N, Kummitha C, Hoppel C.** Defects in skeletal muscle subsarcolemmal mitochondria in a non-obese model of type 2 diabetes mellitus. *PLOS ONE* 12: e0183978, 2017.
204. **LaMonte MJ, Eisenman PA, Adams TD, Shultz BB, Ainsworth BE, Yanowitz FG.** Cardiorespiratory Fitness and Coronary Heart Disease Risk Factors: The LDS Hospital Fitness Institute Cohort. *Circulation* 102: 1623–1628, 2000.
205. **Lanza IR, Nair KS.** Muscle mitochondrial changes with aging and exercise. *Am J Clin Nutr* 89: 467S-471S, 2009.
206. **Lanza IR, Nair KS.** Mitochondrial Metabolic Function Assessed In Vivo and In Vitro. *Curr Opin Clin Nutr Metab Care* 13: 511–517, 2010.
207. **Lanza IR, Short DK, Short KR, Raghavakaimal S, Basu R, Joyner MJ, McConnell JP, Nair KS.** Endurance exercise as a countermeasure for aging. *Diabetes* 57: 2933–2942, 2008.
208. **Lanza IR, Tevald MA, Befroy DE, Kent-Braun JA.** Intracellular energetics and critical PO₂ in resting ischemic human skeletal muscle in vivo. *Am J Physiol Regul Integr Comp Physiol* 299: R1415-1422, 2010.
209. **Larsen S, Ara I, Rabøl R, Andersen JL, Boushel R, Dela F, Helge JW.** Are substrate use during exercise and mitochondrial respiratory capacity decreased in arm and leg muscle in type 2 diabetes? *Diabetologia* 52: 1400–1408, 2009.
210. **Larsen S, Nielsen J, Hansen CN, Nielsen LB, Wibrand F, Stride N, Schroder HD, Boushel R, Helge JW, Dela F, Hey-Mogensen M.** Biomarkers of mitochondrial content in skeletal muscle of healthy young human subjects. *J Physiol (Lond)* 590: 3349–3360, 2012.
211. **Larson-Meyer DE, Newcomer BR, Hunter GR, Joanisse DR, Weinsier RL, Bamman MM.** Relation between in vivo and in vitro measurements of skeletal muscle oxidative metabolism. *Muscle Nerve* 24: 1665–1676, 2001.
212. **Larsson Y, Persson B, Sterky G, Thorén C.** Functional adaptation to rigorous training and exercise in diabetic and nondiabetic adolescents. *Journal of Applied Physiology* 19: 629–635, 1964.
213. **Lawson JW, Veech RL.** Effects of pH and free Mg²⁺ on the Keq of the creatine kinase reaction and other phosphate hydrolyses and phosphate transfer reactions. *J Biol Chem* 254: 6528–6537, 1979.
214. **Layec G, Hart CR, Trinity JD, Kwon O-S, Rossman MJ, Broxterman RM, Le Fur Y, Jeong E-K, Richardson RS.** Oxygen delivery and the restoration of the muscle energetic balance following exercise: implications for delayed muscle recovery in patients with COPD. *Am J Physiol Endocrinol Metab* 313: E94–E104, 2017.

215. **Layec G, Malucelli E, Le Fur Y, Manners D, Yashiro K, Testa C, Cozzone PJ, Iotti S, Bendahan D.** Effects of exercise-induced intracellular acidosis on the phosphocreatine recovery kinetics: a ³¹P MRS study in three muscle groups in humans. *NMR Biomed* 26: 1403–1411, 2013.
216. **Lemaster K, Jackson D, Goldman D, Frisbee JC.** Insidious incrementalism: The silent failure of the microcirculation with increasing peripheral vascular disease risk. *Microcirculation* 24: e12332, [date unknown].
217. **Lemaster KA, Frisbee SJ, Dubois L, Tzemos N, Wu F, Lewis MT, Wiseman RW, Frisbee JC.** Chronic atorvastatin and exercise can partially reverse established skeletal muscle microvasculopathy in metabolic syndrome. *American Journal of Physiology-Heart and Circulatory Physiology* 315: H855–H870, 2018.
218. **Lenaers E, De Feyter HM, Hoeks J, Schrauwen P, Schaart G, Nabben M, Nicolay K, Prompers JJ, Hesselink MKC.** Adaptations in mitochondrial function parallel, but fail to rescue, the transition to severe hyperglycemia and hyperinsulinemia: a study in Zucker diabetic fatty rats. *Obesity (Silver Spring)* 18: 1100–1107, 2010.
219. **Lerner E, Shug AL, Elson C, Shrago E.** Reversible Inhibition of Adenine Nucleotide Translocation by Long Chain Fatty Acyl Coenzyme A Esters in Liver Mitochondria of Diabetic and Hibernating Animals. *J Biol Chem* 247: 1513–1519, 1972.
220. **Lewis MT, Kasper JD, Bazil JN, Frisbee JC, Wiseman RW.** Skeletal muscle energetics are compromised only during high-intensity contractions in the Goto-Kakizaki rat model of type 2 diabetes. *American Journal of Physiology-Regulatory, Integrative and Comparative Physiology* 317: R356–R368, 2019.
221. **Lewis MT, Lujan HL, Tonson A, Wiseman RW, DiCarlo SE.** Obesity and inactivity, not hyperglycemia, cause exercise intolerance in individuals with type 2 diabetes: Solving the obesity and inactivity versus hyperglycemia causality dilemma. *Medical Hypotheses* 123: 110–114, 2019.
222. **Lewis MT, Lujan HL, Wiseman RW, DiCarlo SE.** The Hypertension Advantage and Natural Selection: Since Type 2 Diabetes Associates with Co-morbidities and Premature Death, Why have the Genetic Variants Remained in the Human Genome? *Medical Hypotheses* (May 20, 2019). doi: 10.1016/j.mehy.2019.109237.
223. **Liu Y, Mei X, Li J, Lai N, Yu X.** Mitochondrial function assessed by ³¹P MRS and BOLD MRI in non-obese type 2 diabetic rats. *Physiol Rep* 4, 2016.
224. **Loimaala A, Huikuri HV, Kööbi T, Rinne M, Nenonen A, Vuori I.** Exercise training improves baroreflex sensitivity in type 2 diabetes. *Diabetes* 52: 1837–1842, 2003.

225. **Lowell BB, Shulman GI.** Mitochondrial dysfunction and type 2 diabetes. *Science* 307: 384–387, 2005.
226. **Ludzki A, Paglialunga S, Smith BK, Herbst EAF, Allison MK, Heigenhauser GJ, Neufer PD, Holloway GP.** Rapid Repression of ADP Transport by Palmitoyl-CoA Is Attenuated by Exercise Training in Humans: A Potential Mechanism to Decrease Oxidative Stress and Improve Skeletal Muscle Insulin Signaling. *Diabetes* 64: 2769–2779, 2015.
227. **Lujan HL, Rivers JP, DiCarlo SE.** Complex and interacting influences of the autonomic nervous system on cardiac electrophysiology in conscious mice. *Auton Neurosci* 201: 24–31, 2016.
228. **Lujan HL, Tonson A, Wiseman RW, DiCarlo SE.** Chronic, complete cervical 6–7 cord transection: distinct autonomic and cardiac deficits. *Journal of Applied Physiology* 124: 1471–1482, 2018.
229. **MacGregor GA, Wardener HE de.** *Salt, Diet and Health.* Cambridge University Press, 1998.
230. **Machhada A, Marina N, Korsak A, Stuckey DJ, Lythgoe MF, Gourine AV.** Origins of the vagal drive controlling left ventricular contractility. *The Journal of Physiology* 594: 4017–4030, 2016.
231. **Machhada A, Trapp S, Marina N, Stephens RCM, Whittle J, Lythgoe MF, Kasparov S, Ackland GL, Gourine AV.** Vagal determinants of exercise capacity. *Nature Communications* 8: 15097, 2017.
232. **Macia M, Pecchi E, Desrois M, Lan C, Vilmen C, Portha B, Bernard M, Bendahan D, Giannesini B.** Exercise training impacts exercise tolerance and bioenergetics in gastrocnemius muscle of non-obese type-2 diabetic Goto-Kakizaki rat in vivo. *Biochimie* 148: 36–45, 2018.
233. **Macia M, Pecchi E, Vilmen C, Desrois M, Lan C, Portha B, Bernard M, Bendahan D, Giannesini B.** Insulin Resistance Is Not Associated with an Impaired Mitochondrial Function in Contracting Gastrocnemius Muscle of Goto-Kakizaki Diabetic Rats In Vivo. *PLoS ONE* 10: e0129579, 2015.
234. **Mahler M.** First-Order Kinetics of Muscle Oxygen Consumption, and an Equivalent Proportionality Between $\dot{V}O_2$ and Phosphorylcreatine Level Implications for the Control of Respiration. *THE JOURNAL OF GENERAL PHYSIOLOGY* 86: 31, 1985.
235. **Malyala S, Zhang Y, Strubbe JO, Bazil JN.** Calcium phosphate precipitation inhibits mitochondrial energy metabolism. *PLoS Comput Biol* 15: e1006719, 2019.

236. **Manson JE, Skerrett PJ, Greenland P, VanItallie TB.** The escalating pandemics of obesity and sedentary lifestyle. A call to action for clinicians. *Arch Intern Med* 164: 249–258, 2004.
237. **Manuck SB, Olsson G, Hjemdahl P, Rehnqvist N.** Does cardiovascular reactivity to mental stress have prognostic value in postinfarction patients? A pilot study. *Psychosom Med* 54: 102–108, 1992.
238. **Marcinek DJ, Ciesielski WA, Conley KE, Schenkman KA.** Oxygen regulation and limitation to cellular respiration in mouse skeletal muscle in vivo. *Am J Physiol Heart Circ Physiol* 285: H1900-1908, 2003.
239. **Martin IK, Katz A, Wahren J.** Splanchnic and muscle metabolism during exercise in NIDDM patients. *American Journal of Physiology-Endocrinology and Metabolism* 269: E583–E590, 1995.
240. **Matthews DR, Hosker JP, Rudenski AS, Naylor BA, Treacher DF, Turner RC.** Homeostasis model assessment: insulin resistance and beta-cell function from fasting plasma glucose and insulin concentrations in man. *Diabetologia* 28: 412–419, 1985.
241. **Mazzeo F, Santamaria S, Iavarone A.** “Boosting” in Paralympic athletes with spinal cord injury: doping without drugs. *Funct Neurol* 30: 91–98, 2015.
242. **McAllister A, Allison SP, Randle PJ.** Effects of dichloroacetate on the metabolism of glucose, pyruvate, acetate, 3-hydroxybutyrate and palmitate in rat diaphragm and heart muscle in vitro and on extraction of glucose, lactate, pyruvate and free fatty acids by dog heart in vivo. *Biochemical Journal* 134: 1067–1081, 1973.
243. **McAllister RM, Terjung RL.** Acute inhibition of respiratory capacity of muscle reduces peak oxygen consumption. *Am J Physiol* 259: C889-896, 1990.
244. **McCully KK, Fielding RA, Evans WJ, Leigh JS, Posner JD.** Relationships between in vivo and in vitro measurements of metabolism in young and old human calf muscles. *J Appl Physiol* 75: 813–819, 1993.
245. **McCully KK, Smith S, Rajaei S, Leigh JS, Natelson BH.** Muscle metabolism with blood flow restriction in chronic fatigue syndrome. *J Appl Physiol* 96: 871–878, 2004.
246. **McDonough P, Behnke BJ, Kindig CA, Poole DC.** Rat muscle microvascular PO₂ kinetics during the exercise off-transient. *Exp Physiol* 86: 349–356, 2001.
247. **Meex RCR, Schrauwen-Hinderling VB, Moonen-Kornips E, Schaart G, Mensink M, Phielix E, van de Weijer T, Sels J-P, Schrauwen P, Hesselink MKC.** Restoration of muscle mitochondrial function and metabolic flexibility in type 2

diabetes by exercise training is paralleled by increased myocellular fat storage and improved insulin sensitivity. *Diabetes* 59: 572–579, 2010.

248. **Mensah GA, Mokdad AH, Ford E, Narayan KMV, Giles WH, Vinicor F, Deedwania PC.** Obesity, metabolic syndrome, and type 2 diabetes: emerging epidemics and their cardiovascular implications. *Cardiology Clinics* 22: 485–504, 2004.
249. **Meyer RA.** A linear model of muscle respiration explains monoexponential phosphocreatine changes. *Am J Physiol* 254: C548-553, 1988.
250. **Meyer RA.** Linear dependence of muscle phosphocreatine kinetics on total creatine content. *American Journal of Physiology - Cell Physiology* 257: C1149–C1157, 1989.
251. **Meyer RA, Brown TR, Krilowicz BL, Kushmerick MJ.** Phosphagen and intracellular pH changes during contraction of creatine-depleted rat muscle. *American Journal of Physiology-Cell Physiology* 250: C264–C274, 1986.
252. **Meyer RA, Foley JM.** Testing models of respiratory control in skeletal muscle. *Med Sci Sports Exerc* 26: 52–57, 1994.
253. **Meyer RA, Foley JM.** Cellular Processes Integrating the Metabolic Response to Exercise. In: *Comprehensive Physiology*. American Cancer Society, p. 841–869.
254. **Meyer RA, Foley JM, Harkema SJ, Sierra A, Potchen EJ.** Magnetic resonance measurement of blood flow in peripheral vessels after acute exercise. *Magnetic Resonance Imaging* 11: 1085–1092, 1993.
255. **Meyer RA, Sweeney HL, Kushmerick MJ.** A simple analysis of the “phosphocreatine shuttle.” *Am J Physiol* 246: C365-377, 1984.
256. **Meyer RA Wiseman, Robert W.** Chapter 13: The Metabolic Systems: Control of ATP Synthesis in Skeletal Muscle. In: *ACSM's Advanced Exercise Physiology*. Lippincott Williams & Wilkins, Baltimore, MD, 2011.
257. **Middleton B.** 3-Ketoacyl-CoA thiolases of mammalian tissues. *Meth Enzymol* 35: 128–136, 1975.
258. **Mikus CR, Oberlin DJ, Libla J, Boyle LJ, Thyfault JP.** Glycaemic control is improved by 7 days of aerobic exercise training in patients with type 2 diabetes. *Diabetologia* 55: 1417–1423, 2012.
259. **Miller JC, Colagiuri S.** The carnivore connection: dietary carbohydrate in the evolution of NIDDM. *Diabetologia* 37: 1280–1286, 1994.

260. **Miotto PM, LeBlanc PJ, Holloway GP.** High-Fat Diet Causes Mitochondrial Dysfunction as a Result of Impaired ADP Sensitivity. *Diabetes* 67: 2199–2205, 2018.
261. **Miralles F, Portha B.** Early development of beta-cells is impaired in the GK rat model of type 2 diabetes. *Diabetes* 50 Suppl 1: S84-88, 2001.
262. **Misra S, Shishehbor MH, Takahashi EA, Aronow HD, Brewster LP, Bunte MC, Kim ESH, Lindner JR, Rich K, American Heart Association Council on Peripheral Vascular Disease; Council on Clinical Cardiology; and Council on Cardiovascular and Stroke Nursing.** Perfusion Assessment in Critical Limb Ischemia: Principles for Understanding and the Development of Evidence and Evaluation of Devices: A Scientific Statement From the American Heart Association. *Circulation* (August 12, 2019). doi: 10.1161/CIR.0000000000000708.
263. **Mitchell GF, Pfeffer MA, Finn PV, Pfeffer JM.** Comparison of techniques for measuring pulse-wave velocity in the rat. *J Appl Physiol* 82: 203–210, 1997.
264. **Mitchell P.** Coupling of phosphorylation to electron and hydrogen transfer by a chemi-osmotic type of mechanism. *Nature* 191: 144–148, 1961.
265. **Mlinac ME, Feng MC.** Assessment of Activities of Daily Living, Self-Care, and Independence. *Arch Clin Neuropsychol* 31: 506–516, 2016.
266. **Mogensen M, Sahlin K, Fernström M, Glintborg D, Vind BF, Beck-Nielsen H, Højlund K.** Mitochondrial Respiration Is Decreased in Skeletal Muscle of Patients With Type 2 Diabetes. *Diabetes* 56: 1592–1599, 2007.
267. **Mogensen M, Vind BF, Højlund K, Beck-Nielsen H, Sahlin K.** Maximal lipid oxidation in patients with type 2 diabetes is normal and shows an adequate increase in response to aerobic training. *Diabetes, Obesity and Metabolism* 11: 874–883, 2009.
268. **Mohler ER, Lech G, Supple GE, Wang H, Chance B.** Impaired Exercise-Induced Blood Volume in Type 2 Diabetes With or Without Peripheral Arterial Disease Measured by Continuous-Wave Near-Infrared Spectroscopy. *Diabetes Care* 29: 1856–1859, 2006.
269. **Montgomery MK, Turner N.** Mitochondrial dysfunction and insulin resistance: an update. *Endocr Connect* 4: R1–R15, 2014.
270. **Mootha VK, Lindgren CM, Eriksson K-F, Subramanian A, Sihag S, Lehar J, Puigserver P, Carlsson E, Ridderstråle M, Laurila E, Houstis N, Daly MJ, Patterson N, Mesirov JP, Golub TR, Tamayo P, Spiegelman B, Lander ES, Hirschhorn JN, Altshuler D, Groop LC.** PGC-1 α -responsive genes involved in oxidative phosphorylation are coordinately downregulated in human diabetes. *Nat Genet* 34: 267–273, 2003.

271. **Morrison PR, Montgomery JA, Wong TS, Booth FW.** Cytochrome c protein-synthesis rates and mRNA contents during atrophy and recovery in skeletal muscle. *Biochem J* 241: 257–263, 1987.
272. **Myers J.** Exercise and Cardiovascular Health. *Circulation* 107: e2–e5, 2003.
273. **Nederend I, Schutte NM, Bartels M, ten Harkel ADJ, de Geus EJC.** Heritability of heart rate recovery and vagal rebound after exercise. *Eur J Appl Physiol* 116: 2167–2176, 2016.
274. **Neel JV.** Diabetes Mellitus: A “Thrifty” Genotype Rendered Detrimental by “Progress”? *Am J Hum Genet* 14: 353–362, 1962.
275. **Neel JV, Weder AB, Julius S.** Type II Diabetes, Essential Hypertension, and Obesity as “Syndromes of Impaired Genetic Homeostasis”: The “Thrifty Genotype” Hypothesis Enters the 21st Century. *Perspectives in Biology and Medicine* 42: 44–74, 1998.
276. **Nicholls DG, Ferguson SJ.** *Bioenergetics*. 4th ed. Amsterdam, The Netherlands: Academic Press, 2013.
277. **Nie J, Xue B, Sukumaran S, Jusko WJ, DuBois DC, Almon RR.** Differential Muscle Gene Expression as a Function of Disease Progression in Goto-Kakizaki Diabetic Rats. *Mol Cell Endocrinol* 338: 10–17, 2011.
278. **Onat A, Ceyhan K, Erer B, Başar O, Uysal O, Sansoy V.** Systolic, diastolic, and pulse pressures as coronary risk factors in a population with low cholesterol levels: a prospective 10-year evaluation. *Clin Cardiol* 26: 91–97, 2003.
279. **Orozco LJ, Buchleitner AM, Gimenez-Perez G, Roqué I Figuls M, Richter B, Mauricio D.** Exercise or exercise and diet for preventing type 2 diabetes mellitus. *Cochrane Database Syst Rev* : CD003054, 2008.
280. **Ouriel K.** Peripheral arterial disease. *Lancet* 358: 1257–1264, 2001.
281. **Padilla DJ, McDonough P, Behnke BJ, Kano Y, Hageman KS, Musch TI, Poole DC.** Effects of Type II diabetes on capillary hemodynamics in skeletal muscle. *American Journal of Physiology - Heart and Circulatory Physiology* 291: H2439–H2444, 2006.
282. **Padilla DJ, McDonough P, Behnke BJ, Kano Y, Hageman KS, Musch TI, Poole DC.** Effects of Type II diabetes on muscle microvascular oxygen pressures. *Respir Physiol Neurobiol* 156: 187–195, 2007.
283. **Paganini AT, Foley JM, Meyer RA.** Linear dependence of muscle phosphocreatine kinetics on oxidative capacity. *Am J Physiol* 272: C501-510, 1997.

284. **Patti ME, Butte AJ, Crunkhorn S, Cusi K, Berria R, Kashyap S, Miyazaki Y, Kohane I, Costello M, Saccone R, Landaker EJ, Goldfine AB, Mun E, DeFronzo R, Finlayson J, Kahn CR, Mandarino LJ.** Coordinated reduction of genes of oxidative metabolism in humans with insulin resistance and diabetes: Potential role of PGC1 and NRF1. *PNAS* 100: 8466–8471, 2003.
285. **Pearson MJ, Smart NA.** Exercise therapy and autonomic function in heart failure patients: a systematic review and meta-analysis. *Heart Fail Rev* 23: 91–108, 2018.
286. **Pelliccia A, Maron BJ, Spataro A, Proschan MA, Spirito P.** The upper limit of physiologic cardiac hypertrophy in highly trained elite athletes. *N Engl J Med* 324: 295–301, 1991.
287. **Perry CGR, Kane DA, Lanza IR, Neuffer PD.** Methods for Assessing Mitochondrial Function in Diabetes. *Diabetes* 62: 1041–1053, 2013.
288. **Petersen KF, Befroy D, Dufour S, Dziura J, Ariyan C, Rothman DL, DiPietro L, Cline GW, Shulman GI.** Mitochondrial Dysfunction in the Elderly: Possible Role in Insulin Resistance. *Science* 300: 1140–1142, 2003.
289. **Peterson RG, Shaw WN, Neel M-A, Little LA, Eichberg J.** Zucker Diabetic Fatty Rat as a Model for Non-insulin-dependent Diabetes Mellitus. *ILAR J* 32: 16–19, 1990.
290. **Phielix E, Mensink M.** Type 2 diabetes mellitus and skeletal muscle metabolic function. *Physiol Behav* 94: 252–258, 2008.
291. **Phielix E, Schrauwen-Hinderling VB, Mensink M, Lenaers E, Meex R, Hoeks J, Kooi ME, Moonen-Kornips E, Sels J-P, Hesselink MKC, Schrauwen P.** Lower intrinsic ADP-stimulated mitochondrial respiration underlies in vivo mitochondrial dysfunction in muscle of male type 2 diabetic patients. *Diabetes* 57: 2943–2949, 2008.
292. **Phillips WT, Kiratli BJ, Sarkarati M, Weraarchakul G, Myers J, Franklin BA, Parkash I, Froelicher V.** Effect of spinal cord injury on the heart and cardiovascular fitness. *Curr Probl Cardiol* 23: 641–716, 1998.
293. **Picot J, Jones J, Colquitt JL, Gospodarevskaya E, Loveman E, Baxter L, Clegg AJ.** The clinical effectiveness and cost-effectiveness of bariatric (weight loss) surgery for obesity: a systematic review and economic evaluation. *Health Technol Assess* 13: 1–190, 215–357, iii–iv, 2009.
294. **Pipinos II, Judge AR, Zhu Z, Selsby JT, Swanson SA, Johannig JM, Baxter BT, Lynch TG, Dodd SL.** Mitochondrial defects and oxidative damage in patients with peripheral arterial disease. *Free Radical Biology and Medicine* 41: 262–269, 2006.

295. **Pistrosch F, Natali A, Hanefeld M.** Is Hyperglycemia a Cardiovascular Risk Factor? *Diabetes Care* 34: S128–S131, 2011.
296. **Poitras VJ, Bentley RF, Hopkins-Rosseel DH, LaHaye SA, Tschakovsky ME.** Lack of independent effect of type 2 diabetes beyond characteristic comorbidities and medications on small muscle mass exercising muscle blood flow and exercise tolerance. *Physiol Rep* 3, 2015.
297. **Poitras VJ, Hudson RW, Tschakovsky ME.** Exercise intolerance in Type 2 diabetes: is there a cardiovascular contribution? *J Appl Physiol* 124: 1117–1139, 2018.
298. **Poole DC, Copp SW, Hirai DM, Musch TI.** Dynamics of muscle microcirculatory and blood-myocyte O₂ flux during contractions: Dynamics of muscle microcirculatory O₂ flux. *Acta Physiologica* 202: 293–310, 2011.
299. **Poole DC, Ferreira LF, Behnke BJ, Barstow TJ, Jones AM.** The final frontier: oxygen flux into muscle at exercise onset. *Exerc Sport Sci Rev* 35: 166–173, 2007.
300. **Poole DC, Jones AM.** Oxygen Uptake Kinetics [Online]. In: *Comprehensive Physiology*. John Wiley & Sons, Inc. <http://onlinelibrary.wiley.com/doi/10.1002/cphy.c100072/abstract> [3 Mar. 2017].
301. **Poole DC, Richardson RS, Haykowsky MJ, Hirai DM, Musch TI.** Exercise limitations in heart failure with reduced and preserved ejection fraction. *J Appl Physiol* 124: 208–224, 2018.
302. **Portha B, Giroix M-H, Turrel-Cuzin C, Le-Stunff H, Movassat J.** The GK Rat: A Prototype for the Study of Non-overweight Type 2 Diabetes. In: *Animal Models in Diabetes Research*, edited by Joost H-G, Al-Hasani H, Schürmann A. Humana Press, p. 125–159.
303. **Pörtner HO, Heisler N, Grieshaber MK.** Anaerobiosis and acid-base status in marine invertebrates: a theoretical analysis of proton generation by anaerobic metabolism. *J Comp Physiol B* 155: 1–12, 1984.
304. **Praet SFE, De Feyter HMM, Jonkers R a. M, Nicolay K, van Pul C, Kuipers H, van Loon LJC, Prompers JJ.** 31P MR spectroscopy and in vitro markers of oxidative capacity in type 2 diabetes patients. *MAGMA* 19: 321–331, 2006.
305. **Pyörälä K, Laakso M, Uusitupa M.** Diabetes and atherosclerosis: an epidemiologic view. *Diabetes Metab Rev* 3: 463–524, 1987.
306. **Raichlen DA, Pontzer H, Harris JA, Mabulla AZP, Marlowe FW, Josh Snodgrass J, Eick G, Colette Berbesque J, Sancilio A, Wood BM.** Physical activity patterns and biomarkers of cardiovascular disease risk in hunter-gatherers. *Am J Hum Biol* 29, 2017.

307. **Raina Elley C, Kenealy T.** Lifestyle interventions reduced the long-term risk of diabetes in adults with impaired glucose tolerance. *Evid Based Med* 13: 173, 2008.
308. **Ramírez J, Duijvenboden S van, Ntalla I, Mifsud B, Warren HR, Tzani E, Orini M, Tinker A, Lambiase PD, Munroe PB.** Thirty loci identified for heart rate response to exercise and recovery implicate autonomic nervous system. *Nature Communications* 9: 1947, 2018.
309. **Randle PJ, Garland PB, Hales CN, Newsholme EA.** The glucose fatty-acid cycle. Its role in insulin sensitivity and the metabolic disturbances of diabetes mellitus. *Lancet* 1: 785–789, 1963.
310. **Redfors B, Shao Y, Omerovic E.** Influence of anesthetic agent, depth of anesthesia and body temperature on cardiovascular functional parameters in the rat. *Lab Anim* 48: 6–14, 2014.
311. **Regensteiner JG.** Type 2 diabetes mellitus and cardiovascular exercise performance. *Rev Endocr Metab Disord* 5: 269–276, 2004.
312. **Regensteiner JG, Bauer TA, Reusch JE, Brandenburg SL, Sippel JM, Vogelsong AM, Smith S, Wolfel EE, Eckel RH, Hiatt WR.** Abnormal oxygen uptake kinetic responses in women with type II diabetes mellitus. *J Appl Physiol* 85: 310–317, 1998.
313. **Regensteiner JG, Sippel J, McFarling ET, Wolfel EE, Hiatt WR.** Effects of non-insulin-dependent diabetes on oxygen consumption during treadmill exercise. *Med Sci Sports Exerc* 27: 875–881, 1995.
314. **Reusch JEB, Bridenstine M, Regensteiner JG.** Type 2 diabetes mellitus and exercise impairment. *Rev Endocr Metab Disord* 14: 77–86, 2013.
315. **Reynolds LJ, Credeur DP, Holwerda SW, Leidy HJ, Fadel PJ, Thyfault JP.** Acute inactivity impairs glycemic control but not blood flow to glucose ingestion. *Med Sci Sports Exerc* 47: 1087–1094, 2015.
316. **Rhee SY, Kim YS.** Peripheral Arterial Disease in Patients with Type 2 Diabetes Mellitus. *Diabetes Metab J* 39: 283–290, 2015.
317. **Richardson RS, Noyszewski EA, Kendrick KF, Leigh JS, Wagner PD.** Myoglobin O₂ desaturation during exercise. Evidence of limited O₂ transport. *J Clin Invest* 96: 1916–1926, 1995.
318. **Richardson RS, Poole DC, Knight DR, Kurdak SS, Hogan MC, Grassi B, Johnson EC, Kendrick KF, Erickson BK, Wagner PD.** High muscle blood flow in man: is maximal O₂ extraction compromised? *Journal of Applied Physiology* 75: 1911–1916, 1993.

319. **Richardson RS, Wary C, Wray DW, Hoff J, Rossiter H, Layec G, Carlier PG.** MRS evidence of adequate O₂ supply in human skeletal muscle at the onset of exercise. *Med Sci Sports Exerc* 47: 2299–2307, 2015.
320. **Richter EA, Hargreaves M.** Exercise, GLUT4, and Skeletal Muscle Glucose Uptake. *Physiological Reviews* 93: 993–1017, 2013.
321. **Ritov VB, Menshikova EV, He J, Ferrell RE, Goodpaster BH, Kelley DE.** Deficiency of subsarcolemmal mitochondria in obesity and type 2 diabetes. *Diabetes* 54: 8–14, 2005.
322. **Roberts PA, Loxham SJG, Poucher SM, Constantin-Teodosiu D, Greenhaff PL.** The acetyl group deficit at the onset of contraction in ischaemic canine skeletal muscle. *J Physiol (Lond)* 544: 591–602, 2002.
323. **Robinson S, Edwards HT, Dill DB.** New Records in Human Power. *Science* 85: 409–410, 1937.
324. **Roeske WR, O'Rourke RA, Klein A, Leopold G, Karliner JS.** Noninvasive evaluation of ventricular hypertrophy in professional athletes. *Circulation* 53: 286–291, 1976.
325. **Roman BB, Meyer RA, Wiseman RW.** Phosphocreatine kinetics at the onset of contractions in skeletal muscle of MM creatine kinase knockout mice. *Am J Physiol, Cell Physiol* 283: C1776-1783, 2002.
326. **Roos A, Boron WF.** Intracellular pH. *Physiol Rev* 61: 296–434, 1981.
327. **Rossiter HB, Ward SA, Howe FA, Kowalchuk JM, Griffiths JR, Whipp BJ.** Dynamics of intramuscular ³¹P-MRS P(i) peak splitting and the slow components of PCr and O₂ uptake during exercise. *J Appl Physiol* 93: 2059–2069, 2002.
328. **Rossiter HB, Ward SA, Howe FA, Wood DM, Kowalchuk JM, Griffiths JR, Whipp BJ.** Effects of dichloroacetate on VO₂ and intramuscular ³¹P metabolite kinetics during high-intensity exercise in humans. *J Appl Physiol* 95: 1105–1115, 2003.
329. **Rossiter HB, Ward SA, Kowalchuk JM, Howe FA, Griffiths JR, Whipp BJ.** Dynamic asymmetry of phosphocreatine concentration and O₂ uptake between the on- and off-transients of moderate- and high-intensity exercise in humans. *The Journal of Physiology* 541: 991–1002, 2002.
330. **Rowell LB.** Human cardiovascular adjustments to exercise and thermal stress. *Physiol Rev* 54: 75–159, 1974.
331. **Rowell LB, Saltin B, Kiens B, Christensen NJ.** Is peak quadriceps blood flow in humans even higher during exercise with hypoxemia? *Am J Physiol* 251: H1038-1044, 1986.

332. **Rowley WR, Bezold C, Arikan Y, Byrne E, Krohe S.** Diabetes 2030: Insights from Yesterday, Today, and Future Trends. *Popul Health Manag* 20: 6–12, 2017.
333. **Russo D, Morrone LF, Brancaccio S, Napolitano P, Salvatore E, Spadola R, Imbriaco M, Russo CV, Andreucci VE.** Pulse Pressure and Presence of Coronary Artery Calcification. *CJASN* 4: 316–322, 2009.
334. **Ryan TE, Southern WM, Reynolds MA, McCully KK.** A cross-validation of near-infrared spectroscopy measurements of skeletal muscle oxidative capacity with phosphorus magnetic resonance spectroscopy. *Journal of Applied Physiology* 115: 1757–1766, 2013.
335. **Sacknoff DM, Gleim GW, Stachenfeld N, Coplan NL.** Effect of athletic training on heart rate variability. *Am Heart J* 127: 1275–1278, 1994.
336. **Sahlin K.** Muscle glucose metabolism during exercise. *Ann Med* 22: 85–89, 1990.
337. **Sanchez OA, Copenhaver EA, Chance MA, Fowler MJ, Towse TF, Kent-Braun JA, Damon BM.** Postmaximal contraction blood volume responses are blunted in obese and type 2 diabetic subjects in a muscle-specific manner. *Am J Physiol Heart Circ Physiol* 301: H418-427, 2011.
338. **Scheuermann-Freestone M, Madsen PL, Manners D, Blamire AM, Buckingham RE, Styles P, Radda GK, Neubauer S, Clarke K.** Abnormal Cardiac and Skeletal Muscle Energy Metabolism in Patients With Type 2 Diabetes. *Circulation* 107: 3040–3046, 2003.
339. **Schiaffino S, Reggiani C.** Fiber Types in Mammalian Skeletal Muscles. *Physiological Reviews* 91: 1447–1531, 2011.
340. **Schrauwen-Hinderling VB, Kooi ME, Hesselink MKC, Jeneson J a. L, Backes WH, van Echteld CJA, van Engelshoven JMA, Mensink M, Schrauwen P.** Impaired in vivo mitochondrial function but similar intramyocellular lipid content in patients with type 2 diabetes mellitus and BMI-matched control subjects. *Diabetologia* 50: 113–120, 2007.
341. **Schulman AP, del Genio F, Sinha N, Rubino F.** “Metabolic” surgery for treatment of type 2 diabetes mellitus. *Endocr Pract* 15: 624–631, 2009.
342. **Schwartz AR, Gerin W, Davidson KW, Pickering TG, Brosschot JF, Thayer JF, Christenfeld N, Linden W.** Toward a causal model of cardiovascular responses to stress and the development of cardiovascular disease. *Psychosom Med* 65: 22–35, 2003.
343. **Scott LJ, Mohlke KL, Bonnycastle LL, Willer CJ, Li Y, Duren WL, Erdos MR, Stringham HM, Chines PS, Jackson AU, Prokunina-Olsson L, Ding C-J, Swift AJ, Narisu N, Hu T, Pruijm R, Xiao R, Li X-Y, Conneely KN, Riebow NL, Sprau**

- AG, Tong M, White PP, Hetrick KN, Barnhart MW, Bark CW, Goldstein JL, Watkins L, Xiang F, Saramies J, Buchanan TA, Watanabe RM, Valle TT, Kinnunen L, Abecasis GR, Pugh EW, Doheny KF, Bergman RN, Tuomilehto J, Collins FS, Boehnke M.** A Genome-Wide Association Study of Type 2 Diabetes in Finns Detects Multiple Susceptibility Variants. *Science* 316: 1341–1345, 2007.
344. **Selvin E, Marinopoulos S, Berkenblit G, Rami T, Brancati FL, Powe NR, Golden SH.** Meta-Analysis: Glycosylated Hemoglobin and Cardiovascular Disease in Diabetes Mellitus. *Annals of Internal Medicine* 141: 421, 2004.
345. **Sena CM, Barosa C, Nunes E, Seïça R, Jones JG.** Sources of endogenous glucose production in the Goto-Kakizaki diabetic rat. *Diabetes Metab* 33: 296–302, 2007.
346. **Senefeld JW, Limberg JK, Lukaszewicz KM, Hunter SK.** Exercise-induced hyperemia is associated with knee extensor fatigability in adults with type 2 diabetes. *J Appl Physiol* 126: 658–667, 2019.
347. **Sesso HD, Stampfer MJ, Rosner B, Hennekens CH, Gaziano JM, Manson JE, Glynn RJ.** Systolic and Diastolic Blood Pressure, Pulse Pressure, and Mean Arterial Pressure as Predictors of Cardiovascular Disease Risk in Men. *Hypertension* 36: 801–807, 2000.
348. **Shiota M, Printz RL.** Diabetes in Zucker Diabetic Fatty Rat [Online]. In: *Animal Models in Diabetes Research*, edited by Joost H-G, Al-Hasani H, Schürmann A. Humana Press, p. 103–123. http://dx.doi.org/10.1007/978-1-62703-068-7_8.
349. **Shulman GI.** Ectopic Fat in Insulin Resistance, Dyslipidemia, and Cardiometabolic Disease. *New England Journal of Medicine* 371: 1131–1141, 2014.
350. **Slade JM, Towse TF, Gossain VV, Meyer RA.** Peripheral microvascular response to muscle contraction is unaltered by early diabetes but decreases with age. *J Appl Physiol* 111: 1361–1371, 2011.
351. **Smyth S, Heron A.** Diabetes and obesity: the twin epidemics. *Nat Med* 12: 75–80, 2006.
352. **Snader CE, Marwick TH, Pashkow FJ, Harvey SA, Thomas JD, Lauer MS.** Importance of estimated functional capacity as a predictor of all-cause mortality among patients referred for exercise thallium single-photon emission computed tomography: report of 3,400 patients from a single center. *J Am Coll Cardiol* 30: 641–648, 1997.
353. **Soguel Schenkel N, Burdet L, de Muralto B, Fitting JW.** Oxygen saturation during daily activities in chronic obstructive pulmonary disease. *Eur Respir J* 9: 2584–2589, 1996.

354. **Sparks LM, Gemmink A, Phielix E, Bosma M, Schaart G, Moonen-Kornips E, Jörgensen JA, Nascimento EBM, Hesselink MKC, Schrauwen P, Hoeks J.** ANT1-mediated fatty acid-induced uncoupling as a target for improving myocellular insulin sensitivity. *Diabetologia* 59: 1030–1039, 2016.
355. **Spinazzi M, Casarin A, Pertegato V, Salviati L, Angelini C.** Assessment of mitochondrial respiratory chain enzymatic activities on tissues and cultured cells. *Nat Protoc* 7: 1235–1246, 2012.
356. **Spires J, Gladden LB, Grassi B, Goodwin ML, Saidel GM, Lai N.** Distinguishing the effects of convective and diffusive O₂ delivery on $\dot{V}O_2$ on-kinetics in skeletal muscle contracting at moderate intensity. *American Journal of Physiology-Regulatory, Integrative and Comparative Physiology* 305: R512–R521, 2013.
357. **Squire W, Trapp G.** Using Complex Variables to Estimate Derivatives of Real Functions. *SIAM Rev* 40: 110–112, 1998.
358. **Srere PA.** [1] Citrate synthase: [EC 4.1.3.7. Citrate oxaloacetate-lyase (CoA-acetylating)]. In: *Methods in Enzymology*. Academic Press, p. 3–11.
359. **Srinivasan K, Ramarao P.** Animal models in type 2 diabetes research: An overview. *Indian Journal of Medical Research* 125: 451–72, 2007.
360. **Stainsby WN, Barclay JK.** Relation of load, rest length, work, and shortening to oxygen uptake by in situ dog semitendinosus. *Am J Physiol* 221: 1238–1242, 1971.
361. **Stainsby WN, Otis AB.** BLOOD FLOW, BLOOD OXYGEN TENSION, OXYGEN UPTAKE, AND OXYGEN TRANSPORT IN SKELETAL MUSCLE. *Am J Physiol* 206: 858–866, 1964.
362. **Stanford KI, Goodyear LJ.** Exercise and type 2 diabetes: molecular mechanisms regulating glucose uptake in skeletal muscle. *Advances in Physiology Education* 38: 308–314, 2014.
363. **Stephens JA, Taylor A.** Fatigue of maintained voluntary muscle contraction in man. *J Physiol (Lond)* 220: 1–18, 1972.
364. **Sunoo S, Asano K, Mitsumori F.** ³¹P nuclear magnetic resonance study on changes in phosphocreatine and the intracellular pH in rat skeletal muscle during exercise at various inspired oxygen contents. *Eur J Appl Physiol Occup Physiol* 74: 305–310, 1996.
365. **Tan I, Butlin M, Liu YY, Ng K, Avolio AP.** Heart rate dependence of aortic pulse wave velocity at different arterial pressures in rats. *Hypertension* 60: 528–533, 2012.

366. **Timmons JA, Norrbom J, Schéele C, Thonberg H, Wahlestedt C, Tesch P.** Expression profiling following local muscle inactivity in humans provides new perspective on diabetes-related genes. *Genomics* 87: 165–172, 2006.
367. **Timmons JA, Poucher SM, Constantin-Teodosiu D, Macdonald IA, Greenhaff PL.** Metabolic responses from rest to steady state determine contractile function in ischemic skeletal muscle. *American Journal of Physiology - Endocrinology and Metabolism* 273: E233–E238, 1997.
368. **Toledo FGS, Menshikova EV, Ritov VB, Azuma K, Radikova Z, DeLany J, Kelley DE.** Effects of Physical Activity and Weight Loss on Skeletal Muscle Mitochondria and Relationship With Glucose Control in Type 2 Diabetes. *Diabetes* 56: 2142–2147, 2007.
369. **Treiber FA, Kamarck T, Schneiderman N, Sheffield D, Kapuku G, Taylor T.** Cardiovascular reactivity and development of preclinical and clinical disease states. *Psychosom Med* 65: 46–62, 2003.
370. **Truglio-Londrigan M, Lewenson SB.** *Public Health Nursing: Practicing Population-Based Care*. 2 edition. Burlington, Mass: Jones & Bartlett Learning, 2012.
371. **Tuomilehto J.** The Emerging Global Epidemic of Type 1 Diabetes. *Curr Diab Rep* 13: 795–804, 2013.
372. **Turner N, Bruce CR, Beale SM, Hoehn KL, So T, Rolph MS, Cooney GJ.** Excess Lipid Availability Increases Mitochondrial Fatty Acid Oxidative Capacity in Muscle. *Diabetes* 56: 2085–2092, 2007.
373. **Ugur-Altun B, Altun A, Tatli E, Tugrul A.** Factors related to exercise capacity in asymptomatic middle-aged type 2 diabetic patients. *Diabetes Res Clin Pract* 67: 130–136, 2005.
374. **van Bree BWJ, Lenaers E, Nabben M, Briedé JJ, Jörgensen JA, Schaart G, Schrauwen P, Hoeks J, Hesselink MKC.** A genistein-enriched diet neither improves skeletal muscle oxidative capacity nor prevents the transition towards advanced insulin resistance in ZDF rats. *Sci Rep* 6: 22854, 2016.
375. **van den Broek NMA, De Feyter HMML, Graaf L de, Nicolay K, Prompers JJ.** Intersubject differences in the effect of acidosis on phosphocreatine recovery kinetics in muscle after exercise are due to differences in proton efflux rates. *American Journal of Physiology-Cell Physiology* 293: C228–C237, 2007.
376. **van Eunen K, Simons SMJ, Gerding A, Bleeker A, den Besten G, Touw CML, Houten SM, Groen BK, Krab K, Reijngoud D-J, Bakker BM.** Biochemical competition makes fatty-acid β -oxidation vulnerable to substrate overload. *PLoS Comput Biol* 9: e1003186, 2013.

377. **van Loon LJC, Greenhaff PL, Constantin-Teodosiu D, Saris WHM, Wagenmakers AJM.** The effects of increasing exercise intensity on muscle fuel utilisation in humans. *The Journal of Physiology* 536: 295–304, 2001.
378. **van Tienen FHJ, Praet SFE, de Feyter HM, van den Broek NM, Lindsey PJ, Schoonderwoerd KGC, de Coo IFM, Nicolay K, Prompers JJ, Smeets HJM, van Loon LJC.** Physical Activity Is the Key Determinant of Skeletal Muscle Mitochondrial Function in Type 2 Diabetes. *The Journal of Clinical Endocrinology & Metabolism* 97: 3261–3269, 2012.
379. **Vanderwall C, Randall Clark R, Eickhoff J, Carrel AL.** BMI is a poor predictor of adiposity in young overweight and obese children. *BMC Pediatr* 17, 2017.
380. **Vanhamme, van den Boogaart A, Van Huffel S.** Improved method for accurate and efficient quantification of MRS data with use of prior knowledge. *J Magn Reson* 129: 35–43, 1997.
381. **Verweij N, Vegte YJ van de, Harst P van der.** Genetic study links components of the autonomous nervous system to heart-rate profile during exercise. *Nature Communications* 9: 898, 2018.
382. **Vinnakota KC, Bazil JN, Van den Bergh F, Wiseman RW, Beard DA.** Feedback Regulation and Time Hierarchy of Oxidative Phosphorylation in Cardiac Mitochondria. *Biophys J* 110: 972–980, 2016.
383. **Vinnakota KC, Singhal A, Van den Bergh F, Bagher-Oskouei M, Wiseman RW, Beard DA.** Open-Loop Control of Oxidative Phosphorylation in Skeletal and Cardiac Muscle Mitochondria by Ca²⁺. *Biophys J* 110: 954–961, 2016.
384. **Vondra K, Rath R, Bass A, Slabochová Z, Teisinger J, Vítek V.** Enzyme activities in quadriceps femoris muscle of obese diabetic male patients. *Diabetologia* 13: 527–529, 1977.
385. **Vos T.** Global, regional, and national incidence, prevalence, and years lived with disability for 310 diseases and injuries, 1990–2015: a systematic analysis for the Global Burden of Disease Study 2015. *Lancet* 388: 1545–1602, 2016.
386. **Vranish JR, Young BE, Stephens BY, Kaur J, Padilla J, Fadel PJ.** Brief periods of inactivity reduce leg microvascular, but not macrovascular, function in healthy young men. *Exp Physiol* 103: 1425–1434, 2018.
387. **Wagner PD.** Determinants of Maximal Oxygen Transport and Utilization. *Annual Review of Physiology* 58: 21–50, 1996.
388. **Wahl MP, Scalzo RL, Regensteiner JG, Reusch JEB.** Mechanisms of Aerobic Exercise Impairment in Diabetes: A Narrative Review. *Front Endocrinol (Lausanne)* 9, 2018.

389. **Wahren J, Felig P, Hagenfeldt L.** Physical exercise and fuel homeostasis in diabetes mellitus. *Diabetologia* 14: 213–222, 1978.
390. **Walker CM, Bunch FT, Cavros NG, Dippel EJ.** Multidisciplinary approach to the diagnosis and management of patients with peripheral arterial disease. *Clin Interv Aging* 10: 1147–1153, 2015.
391. **Walsh B, Tiivel T, Tonkonogi M, Sahlin K.** Increased concentrations of P(i) and lactic acid reduce creatine-stimulated respiration in muscle fibers. *J Appl Physiol* 92: 2273–2276, 2002.
392. **Walter G, Vandenborne K, McCully KK, Leigh JS.** Noninvasive measurement of phosphocreatine recovery kinetics in single human muscles. *Am J Physiol* 272: C525-534, 1997.
393. **Wanders RJ, Westerhoff HV.** Sigmoidal relation between mitochondrial respiration and $\log ([ATP]/[ADP])_{out}$ under conditions of extramitochondrial ATP utilization. Implications for the control and thermodynamics of oxidative phosphorylation. *Biochemistry* 27: 7832–7840, 1988.
394. **Wang J, Wang H, Liu J, Ma J.** [The association between body mass index, waist circumference with body fat percent, and abdominal fat rate in overweight and obese pupils]. *Zhonghua Yu Fang Yi Xue Za Zhi* 47: 603–607, 2013.
395. **Wasserman DH.** Four grams of glucose. *Am J Physiol Endocrinol Metab* 296: E11–E21, 2009.
396. **Watt IN, Montgomery MG, Runswick MJ, Leslie AGW, Walker JE.** Bioenergetic cost of making an adenosine triphosphate molecule in animal mitochondria. *Proc Natl Acad Sci USA* 107: 16823–16827, 2010.
397. **Webborn AD.** “Boosting” performance in disability sport. *Br J Sports Med* 33: 74–75, 1999.
398. **Weibel ER.** *The pathway for oxygen: structure and function in the mammalian respiratory system.* Cambridge: Harvard university press, 1984.
399. **Wessels B, Ciapaite J, Broek NMA van den, Nicolay K, Prompers JJ.** Metformin Impairs Mitochondrial Function in Skeletal Muscle of Both Lean and Diabetic Rats in a Dose-Dependent Manner. *PLOS ONE* 9: e100525, 2014.
400. **Wessels B, Ciapaite J, van den Broek NMA, Houten SM, Nicolay K, Prompers JJ.** Pioglitazone treatment restores in vivo muscle oxidative capacity in a rat model of diabetes. *Diabetes Obes Metab* 17: 52–60, 2015.
401. **West AM, Anderson JD, Epstein FH, Meyer CH, Hagspiel KD, Berr SS, Harthun NL, Weltman AL, Annex BH, Kramer CM.** Percutaneous intervention in

peripheral artery disease improves calf muscle phosphocreatine recovery kinetics: A pilot study. *Vasc Med* 17: 3–9, 2012.

402. **Wexler DJ, Grant RW, Wittenberg E, Bosch JL, Cagliero E, Delahanty L, Blais MA, Meigs JB.** Correlates of health-related quality of life in type 2 diabetes. *Diabetologia* 49: 1489–1497, 2006.
403. **Whipp BJ, Wasserman K.** Oxygen uptake kinetics for various intensities of constant-load work. *Journal of Applied Physiology* 33: 351–356, 1972.
404. **WHO.** | Diabetes [Online]. 2013. <https://web.archive.org/web/20130826174444/http://www.who.int/mediacentre/factsheets/fs312/en/> [11 Jun. 2018].
405. **Widhalm K, Schönegger K.** BMI: does it really reflect body fat mass? *J Pediatr* 134: 522–523, 1999.
406. **Wilkerson DP, Poole DC, Jones AM, Fulford J, Mawson DM, Ball CI, Shore AC.** Older type 2 diabetic males do not exhibit abnormal pulmonary oxygen uptake and muscle oxygen utilization dynamics during submaximal cycling exercise. *Am J Physiol Regul Integr Comp Physiol* 300: R685-692, 2011.
407. **Wilson DF, Erecińska M, Drown C, Silver IA.** Effect of oxygen tension on cellular energetics. *Am J Physiol* 233: C135-140, 1977.
408. **Wilson DF, Erecińska M, Drown C, Silver IA.** The oxygen dependence of cellular energy metabolism. *Archives of Biochemistry and Biophysics* 195: 485–493, 1979.
409. **Wiseman RW, Ellington WR, Rosanske RC.** Effects of extracellular pH and D-lactate efflux on regulation of intracellular pH during isotonic contractions in a molluscan muscle: A 31p-nuclear magnetic resonance study. *Journal of Experimental Zoology* 252: 228–236, 1989.
410. **Wiseman RW, Jeneson J a. L.** Noninvasive Assessment of Mitochondrial Function Using Nuclear Magnetic Resonance Spectroscopy. In: *Drug-Induced Mitochondrial Dysfunction*. Wiley-Blackwell, 2008, p. 555–574.
411. **Wiseman RW, Kushmerick MJ.** Creatine Kinase Equilibration Follows Solution Thermodynamics in Skeletal Muscle. 31P NMR STUDIES USING CREATINE ANALOGS. *J Biol Chem* 270: 12428–12438, 1995.
412. **Wiseman RW, Moerland TS, Chase PB, Stuppard R, Kushmerick MJ.** High-performance liquid chromatographic assays for free and phosphorylated derivatives of the creatine analogues beta-guanidopropionic acid and 1-carboxy-methyl-2-iminoimidazolidine (cyclocreatine). *Anal Biochem* 204: 383–389, 1992.

413. **Wollenman LC, Vander Ploeg MR, Miller ML, Zhang Y, Bazil JN.** The effect of respiration buffer composition on mitochondrial metabolism and function. *PLoS ONE* 12: e0187523, 2017.
414. **Wray DW, Amann M, Richardson RS.** Peripheral vascular function, oxygen delivery and utilization: the impact of oxidative stress in aging and heart failure with reduced ejection fraction. *Heart Fail Rev* 22: 149–166, 2017.
415. **Wright JR, McCloskey DI, Fitzpatrick RC.** Effects of muscle perfusion pressure on fatigue and systemic arterial pressure in human subjects. *Journal of Applied Physiology* 86: 845–851, 1999.
416. **Wright JR, McCloskey DI, Fitzpatrick RC.** Effects of systemic arterial blood pressure on the contractile force of a human hand muscle. *Journal of Applied Physiology* 88: 1390–1396, 2000.
417. **Wu F, Zhang J, Beard DA.** Experimentally observed phenomena on cardiac energetics in heart failure emerge from simulations of cardiac metabolism. *Proc Natl Acad Sci USA* 106: 7143–7148, 2009.
418. **Zhou B, Lu Y, Hajifathalian K, Bentham J, Cesare MD, Danaei G, Bixby H, Cowan MJ, Ali MK, Taddei C, Lo WC, Reis-Santos B, Stevens GA, Riley LM, Miranda JJ, Bjerregaard P, Rivera JA, Fouad HM, Ma G, Mbanya JC, McGarvey ST, Mohan V, Onat A, Pilav A, Ramachandran A, Romdhane HB, Paciorek CJ, Bennett JE, Ezzati M, Abdeen ZA, Kadir KA, Abu-Rmeileh NM, Acosta-Cazares B, Adams R, Aekplakorn W, Aguilar-Salinas CA, Agyemang C, Ahmadvand A, Al-Othman AR, Alkerwi A, Amouyel P, Amuzu A, Andersen LB, Anderssen SA, Anjana RM, Aounallah-Skhiri H, Aris T, Arlappa N, Arveiler D, Assah FK, Avdicová M, Azizi F, Balakrishna N, Bandosz P, Barbagallo CM, Barceló A, Batieha AM, Baur LA, Romdhane HB, Benet M, Bernabe-Ortiz A, Bharadwaj S, Bhargava SK, Bi Y, Bjerregaard P, Bjertness E, Bjertness MB, Björkelund C, Blokstra A, Bo S, Boehm BO, Boissonnet CP, Bovet P, Brajkovich I, Breckenkamp J, Brenner H, Brewster LM, Brian GR, Bruno G, Bugge A, León AC de, Can G, Cândido AP, Capuano V, Carlsson AC, Carvalho MJ, Casanueva FF, Casas JP, Caserta CA, Castetbon K, Chamukuttan S, Chaturvedi N, Chen CJ, Chen F, Chen S, Cheng CY, Chetrit A, Chiou ST, Cho Y, Chudek J, Cifkova R, Claessens F, Concin H, Cooper C, Cooper R, Costanzo S, Cottel D, Cowell C, Crujeiras AB, D'Arrigo G, Dallongeville J, Dankner R, Dauchet L, Gaetano G de, Henauw SD, Deepa M, Dehghan A, Deschamps V, Dhana K, Castelnuovo AD, Djalalinia S, Doua K, Drygas W, Du Y, Dzerve V, Egbagbe EE, Eggertsen R, Ati JE, Elosua R, Erasmus RT, Erem C, Ergor G, Eriksen L, Peña JE la, Fall CH, Farzadfar F, Felix-Redondo FJ, Ferguson TS, Fernández-Bergés D, Ferrari M, Ferreccio C, Feskens EJ, Finn JD, Föger B, Foo LH, Forslund AS, Fouad HM, Francis DK, Mdo CF, Franco OH, Frontera G, Furusawa T, Gaciong Z, Garnett SP, Gaspoz JM, Gasull M, Gates L, Geleijnse JM, Ghasemian A, Ghimire A, Giampaoli S, Gianfagna F, Giovannelli J, Giwerzman A, Gross MG, Rivas JG, Gorbea MB, Gottrand F, Grafnetter D, Grodzicki T, Grøntved A, Gruden G, Gu**

D, Guan OP, Guerrero R, Guessous I, Guimaraes AL, Gutierrez L, Hambleton IR, Hardy R, Kumar RH, Hata J, He J, Heidemann C, Herrala S, Hihtaniemi IT, Ho SY, Ho SC, Hofman A, Hormiga CM, Horta BL, Houti L, Howitt C, Htay TT, Htet AS, Htike MM, Hu Y, Hussieni AS, Huybrechts I, Hwalla N, Iacoviello L, Iannone AG, Ibrahim MM, Ikeda N, Ikram MA, Irazola VE, Islam M, Iwasaki M, Jacobs JM, Jafar T, Jamil KM, Jasienska G, Jiang CQ, Jonas JB, Joshi P, Kafatos A, Kalter-Leibovici O, Kasaeian A, Katz J, Kaur P, Kavousi M, Keinänen-Kiukaanniemi S, Kelishadi R, Kengne AP, Kersting M, Khader YS, Khalili D, Khang YH, Kiechl S, Kim J, Kolsteren P, Korrovits P, Kratzer W, Kromhout D, Kujala UM, Kula K, Kyobutungi C, Laatikainen T, Lachat C, Laid Y, Lam TH, Landrove O, Lanska V, Lappas G, Laxmaiah A, Leclercq C, Lee J, Lee J, Lehtimäki T, Lekhraj R, León-Muñoz LM, Li Y, Lim WY, Lima-Costa MF, Lin HH, Lin X, Lissner L, Lorbeer R, Lozano JE, Luksiene D, Lundqvist A, Lytsy P, Ma G, Machado-Coelho GL, Machi S, Maggi S, Magliano DJ, Makdisse M, Rao KM, Manios Y, Manzato E, Margozzini P, Marques-Vidal P, Martorell R, Masoodi SR, Mathiesen EB, Matsha TE, Mbanya JC, McFarlane SR, McGarvey ST, McLachlan S, McNulty BA, Mediene-Benchekor S, Meirhaeghe A, Menezes AM, Merat S, Meshram II, Mi J, Miquel JF, Miranda JJ, Mohamed MK, Mohammad K, Mohammadifard N, Mohan V, Yusoff MM, Møller NC, Molnár D, Mondo CK, Morejon A, Moreno LA, Morgan K, Moschonis G, Mossakowska M, Mostafa A, Mota J, Motta J, Mu TT, Muiesan ML, Müller-Nurasyid M, Mursu J, Nagel G, Námešná J, Nang EE, NangThetia VB, Navarrete-Muñoz EM, Ndiaye NC, Nenko I, Nervi F, Nguyen ND, Nguyen QN, Nieto-Martínez RE, Ning G, Ninomiya T, Noale M, Noto D, Nsour MA, Ochoa-Avilés AM, Oh K, Onat A, Ordunez P, Osmond C, Otero JA, Owusu-Dabo E, Pahomova E, Palmieri L, Panda-Jonas S, Panza F, Parsaeian M, Peixoto SV, Pelletier C, Peltonen M, Peters A, Peykari N, Pham ST, Pilav A, Pitakaka F, Piwonska A, Piwonski J, Plans-Rubió P, Porta M, Portegies ML, Poustchi H, Pradeepa R, Price JF, Punab M, Qasrawi RF, Qorbani M, Radisauskas R, Rahman M, Raitakari O, Rao SR, Ramachandran A, Ramke J, Ramos R, Rampal S, Rathmann W, Redon J, Reganit PF, Rigo F, Robinson SM, Robitaille C, Rodríguez-Artalejo F, Mdel CR-P, Rodríguez-Villamizar LA, Rojas-Martinez R, Ronkainen K, Rosengren A, Rubinstein A, Rui O, Ruiz-Betancourt BS, Horimoto RR, Rutkowski M, Sabanayagam C, Sachdev HS, Saidi O, Sakarya S, Salanave B, Salonen JT, Salvetti M, Sánchez-Abanto J, Santos D, Santos R dos, Santos R, Saramies JL, Sardinha LB, Sarrafzadegan N, Saum KU, Scazufca M, Schargrodsky H, Scheidt-Nave C, Sein AA, Sharma SK, Shaw JE, Shibuya K, Shin Y, Shiri R, Siantar R, Sibai AM, Simon M, Simons J, Simons LA, Sjostrom M, Slowikowska-Hilczer J, Slusarczyk P, Smeeth L, Snijder MB, So HK, Sobngwi E, Söderberg S, Solfrizzi V, Sonestedt E, Soumare A, Staessen JA, Stathopoulou MG, Steene-Johannessen J, Stehle P, Stein AD, Stessman J, Stöckl D, Stokwiszewski J, Stronks K, Strufaldi MW, Sun CA, Sundström J, Sung YT, Suriyawongpaisal P, Sy RG, Tai ES, Tamosiunas A, Tang L, Tarawneh M, Tarqui-Mamani CB, Taylor A, Theobald H, Thijs L, Thuesen BH, Tolonen HK, Tolstrup JS, Topbas M, Torrent M, Traissac P, Trinh OT, Tulloch-Reid MK, Tuomainen TP, Turley ML, Tzourio C, Ueda P, Ukoli FA, Ulmer H,

Uusitalo HM, Valdivia G, Valvi D, Rossem L van, Valkengoed I van, Vanderschueren D, Vanuzzo D, Vega T, Velasquez-Melendez G, Veronesi G, Verschuren WM, Verstraeten R, Viet L, Vioque J, Virtanen JK, Visvikis-Siest S, Viswanathan B, Vollenweider P, Voutilainen S, Vrijheid M, Wade AN, Wagner A, Walton J, Mohamud WW, Wang F, Wang MD, Wang Q, Wang YX, Wannamethee SG, Weerasekera D, Whincup PH, Widhalm K, Wiecek A, Wijga AH, Wilks RJ, Willeit J, Wilsgaard T, Wojtyniak B, Wong TY, Woo J, Woodward M, Wu FC, Wu SL, Xu H, Yan W, Yang X, Ye X, Yoshihara A, Younger-Coleman NO, Zambon S, Zargar AH, Zdrojewski T, Zhao W, Zheng Y, Cisneros JZ.
Worldwide trends in diabetes since 1980: a pooled analysis of 751 population-based studies with 4·4 million participants. *The Lancet* 387: 1513–1530, 2016.